CROSS-LAYER MODELING AND OPTIMIZATION OF NEXT-GENERATION INTERNET NETWORKS

A DISSERTATION

SUBMITTED TO THE DEPARTMENT OF

COMPUTER ARCHITECTURE

OF UNIVERSITAT POLITÈCNICA DE CATALUNYA

IN PARTIAL FULFILLMENT OF THE REQUIREMENTS

FOR THE DEGREE OF

DOCTOR OF PHILOSOPHY

Oscar Pedrola Escribà

September 2012

I certify that I have read this dissertation and that, in my opinion, it is fully adequate in scope and quality as a dissertation for the degree of Doctor of Philosophy.

_____

(Davide Careglio)   Principal Co-Advisor

I certify that I have read this dissertation and that, in my opinion, it is fully adequate in scope and quality as a dissertation for the degree of Doctor of Philosophy.

_____

(Josep Solé Pareta)   Principal Co-Advisor

Summary

Scaling traditional telecommunication networks so that they are able to cope with the volume of future traffic demands and the stringent European Commission (EC) regulations on emissions would entail unaffordable investments. For this very reason, the design of an innovative ultra-high bandwidth power-efficient network architecture is nowadays a bold topic within the research community. So far, the independent evolution of network layers has resulted in isolated, and hence, far-from-optimal contributions, which eventually have lead to the issues today's networks are facing such as inefficient energy strategy, limited network scalability and flexibility, reduced network manageability and increased overall network and customer services costs. Consequently, there is currently large consensus among network operators and the research community that cross-layer interaction and coordination is fundamental for the proper architectural design of next-generation Internet networks.

This thesis actively contributes to the this goal by addressing the modeling, optimization and performance analysis of a set of potential technologies to be deployed in future cross-layer network architectures. By applying a transversal design approach (i.e., joint consideration of several network layers), we aim for achieving the maximization of the integration of the different network layers involved in each specific problem. To this end, Part I provides a comprehensive evaluation of optical transport networks (OTNs) based on layer 2 (L2) sub-wavelength switching (SWS) technologies, also taking into consideration the impact of physical layer impairments (PLIs) (L0 phenomena). Indeed, the recent and relevant advances in optical technologies have dramatically increased the impact that PLIs have on the optical signal quality, particularly in the context of SWS networks. Then, in Part II, we present a set of case studies where we show that the application of operations research (OR) methodologies in the desing/planning stage of future cross-layer Internet network architectures leads to the successful joint optimization of key network metrics such as cost, resources usage and energy consumption. OR can definitely play an important role by allowing network designers/architects to obtain good near-optimal solutions to real-sized problems within practical running times.

Introduction

Internet data traffic has been growing at a very fast pace for many years, even in recent adverse economic conditions such as the 2000 dot-com bubble and the current international crisis, and it is highly likely that this growth will inevitably continue in the future. Indeed, in an attempt to overcome the current economic situation, there is significant support for the expansion of public information infrastructure, leading to even higher growth. In addition, and according to the EC's commitment to reduce the overall emissions, energy efficiency is currently a major concern for network operators as energy consumption in backbone core networks is scaling with traffic volume [1]. To top it all, the unpredictable traffic patterns of emerging bandwidth-hungry services and applications, make it crucial to enable flexible bandwidth management in next-generation transport networks.

Scaling traditional network infrastructures, so that they are able to cope with all these factors, is however not a viable option as it would entail substantial investments in all of the network tiers, leading to increased total cost of ownership (TCO) (i.e., those costs involving both capital and operational expenditures (CAPEX and OPEX)). Indeed, current network architectures have been designed to handle current traffic demands, but they are inadequate to cope with future traffic volumes. Although it is hard to generalize the network structure of many different countries and operators, it is possible to identify some common issues:

- Too many network tiers with electronic interfaces between them. Networks can typically have access, aggregation, metro, outer core and inner core tiers.

- Too many IP routers. All electronic interfaces are costly and power-consuming, in particular due to deep packet inspection (DPI) of the data.

- Too many nodes. The large number of nodes is often based on legacy technologies.

All these features go against network operators goals, which are currently facing strong pressure to deliver high quality of service (QoS) and rising bandwidth for services such as video and mobile broadband, whilst, at the same time, containing costs.

For this very reason, one of the main concerns in the telecommunications industry is the development of a new network architecture to be deployed in the next years. Such a network will have to

meet the key requirements that are expected from innovative ultra-high bandwidth networks. These requirements mainly refer to the maximization of the integration between the IP/packet, optical transport and control layers. Traditionally, the scientific community has progressively divided into groups working on the upper network layers, that is, layer 3 (L3)(IP routing) and up, and those dealing with the transport layer, that is, L1/L2 lambda switching capable technologies such as wavelength switched optical networks (WSON)[2]-L1 and optical burst switching (OBS)[3]-L2 as well as the so-called physical layer (L0), which deals with the physical impairments found in the optical domain. This independent evolution has resulted in isolated, and hence, far-from-optimal contributions, which eventually have lead to the issues today's networks are facing such as inefficient energy strategy, limited network scalability and flexibility, reduced network manageability and increased overall network and customer services costs.

Consequently, there is currently large consensus among network operators and the research community that cross-layer (i.e., among the different network layers) interaction and coordination is fundamental for the proper architectural design of next-generation Internet networks. A layered approach is therefore needed to enhance each area of network performance, thereby helping to deal better with the whole variety of possible phenomena in an overall efficient way and benefiting from the advantages of the solution adopted in each particular layer.

Within the *FP7 STRONGEST* project [4], we focus on the design and demonstration of an evolutionary ultra-high (Petabit) capacity multi-layer transport network, based on optimized integration of optical and packet nodes, and equipped with a multi-domain, multi-technology control plane, overcoming the problems of current networks that still provide limited scalability, are not cost-effective and do not properly guarantee end-to-end quality of service (QoS). The key features such a network must be able to offer are:

- High scalability and flexibility.

- Guaranteed end-to-end performance and survivability.

- Increased energy efficiency.

- Reduced TCO.

Challenges toward next-generation networks

New applications, an increased number of users and a higher bandwidth usage per user will lead to massive core bandwidth growth. In this scenario, the following question arises: *How can that amount of information be transported?* In addressing such a fundamental question, the research community is concerned about three main facts:

- In 2020, the bandwidth required will be two orders of magnitude higher.

- Transport network equipment must use less electrical power than today.

- Transport network cost will have to rise sub-linearly with bandwidth to allow users to afford it.

Motivations

To address these issues and in an attempt to move toward next-generation network architectures, this thesis focuses on the modeling, optimization and performance analysis of a set of potential technologies to be deployed in future cross-layer network architectures. By applying a transversal design approach (i.e., joint consideration of several network layers), we aim for achieving the maximization of the integration of the different network layers involved in each specific problem.

Currently, the internet engineering task force (IETF) is putting a lot of effort into the definition of a new L1 switching technology based on WSON [2], which relies on the current ITU-T DWDM rigid frequency grid (50GHz) [5]. Since WSONs include wavelength selective devices such as tunable lasers and reconfigurable add/drop multiplexers (ROADMs), a more efficient and dynamic network operation can be obtained when compared to legacy networks based on SONET/SDH (synchronous optical network/synchronous digital hierarchy) over static point-to-point dense wavelength division multiplexing (DWDM). In multi-layer IP/MPLS-over-WSON networks there exists the need for a substantial amount of grooming functionality in order to efficiently carry the IP traffic. Grooming implies electronic processing, which in turn means energy consumption, and therefore, both CAPEX and OPEX costs are involved. For this very reason, the planning/dimensioning of such networks is a problem that needs to be carefully engineered as it eventually determines the network TCO.

Moving forward, however, and given the dramatic increase in the use of new disruptive bandwidth intensive services and applications, network operators foresee the emergence of a mismatch between the client layer and current rigid-grid, (DWDM)-based optical layer. This issue will result in a highly inefficient use of the network capacity, and consequently, in multi-layer networks requiring a large amount of highly expensive, power-consuming IP/MPLS equipments to be installed for aggregation (at the edge) and grooming (at intermediate nodes) purposes. In an attempt to counter this problem, the flexgrid technology [6], [7], which divides the available optical spectrum into a set of frequency slots (FSs) of a fixed finer spectral width, is currently regarded as a future, viable and highly efficient replacement for WSONs. As of now, several candidate slot with sizes are being considered, namely 25GHz, 12.5GHz and 6.25GHz. It is therefore crucial to determine, based on the expected IP traffic evolution, the appropriate slot size for future multi-layer networks based on flexgrid technology.

Concurrently, recent network measurements predict that an important part of the network traffic will be highly dynamic and characterized by short-lived, small granularity flows [8]. Under these circumstances, it is crucial for next-generation optical transport networks (OTNs) to engage highly

agile optical transport technologies that include sub-wavelength switching (SWS) like optical packet or burst switching (OPS/OBS)[3]. By leveraging recent advances in nanosecond-range photonic devices such as fast tunable lasers and fast switching elements ([9], [10]), future OTNs supporting dynamic SWS can flexibly accommodate diverse traffic conditions with better efficiency [11].

Most probably the transport architecture of the future Internet will consist of hybridized network entities (or nodes) capable of performing, for example, both flow/burst/packet and circuit traffic accommodation. This future network architecture will be application/service-aware driven, that is, network operations and resources assignment will be performed in accordance to the specific traffic requirements of the different services and applications [12]. To this end, the physical layer needs to evolve from a bit transport medium to an intelligent service aware carrier [13].

Thesis contributions and structure

Regarding the evolution of OTNs, the contributions of this thesis are multifold. It is divided into two parts, and a total of 8 chapters as detailed next.

Part I provides a comprehensive set of cross-layer analysis which assume SWS-based L2 technologies. Specifically, each chapter tackles, from different angles, the issue that the presence of the physical layer impairments (PLIs) (i.e., L0 phenomena) represents for the optical signal quality. It is a fact that PLIs severely limit the reach and capacity of optical systems, and hence, their consideration in the design and evaluation of future SWS network architectures has become unavoidable. To this end, the works presented in Part I deal with the cross-layer integration of L2 and L0 of the network with the aim of optimizing a set of network performance metrics such as cost, energy, and packet loss performance.

The structure, content and scientific contribution of the different chapters are provided next:

- Chapter 1 proposes a novel transmission mode for OBS networks, that is, the quasi-synchronous (QS) transmission. We provide a comprehensive performance overview of the QS-OBS network and compare its performance with that of the well-known synchronous and asynchronous transmission modes. In this chapter, L0 phenomena are taken into account in the form of pulse time deviation factors. The contents of this chapter have been published in [14] and [15]. This work was partially done within the framework of an 11-months M.Sc. internship at the laboratoire de télécommunications (TCOM) at École Polytechnique Fédérale de Laussane (EPFL), Switzerland.

- Chapter 2 presents the modeling and preliminary performance evaluation of a translucent SWS network architecture. We provide a SWS node architecture and perform a power budget and noise analysis to determine its feasibility. In this thesis, we use the optical signal to noise ratio (OSNR) as the signal quality performance indicator of the degradation due to PLIs (L0

phenomena). Afterwards, a couple of preliminary regenerator placement algorithms are used to evaluate the network performance, and to confirm that the impact of PLIs is effectively mitigated. The contents of this chapter have been published in [16], [17], and [18]. This work has been done in collaboration with the National Institute of Telecommunications (NIT), Poland.

- Chapter 3 provides both an optimal and heuristic mixed integer linear programming (MILP) formulations to solve the complex routing and regenerator placement and dimensioning (RRPD) problem found in SWS networks. Furthermore, a set of heuristic algorithms are provided. The performance of all these algorithms is evaluated over a broad range of continental-scale and nation-wide backbone topologies. The contents of this chapter have been published in [19] and [20]. This work was done in collaboration with the National Institute of Telecommunications (NIT), Poland.

- Chapter 4 is entirely devoted to analyzing the cost feasibility of deploying future translucent OTNs based on nodes which rely on all-optical wavelength converter (WC) sharing configurations. The contents of this chapter have been published in [21], and are currently under review in [22]. This work was done in collaboration with the National Institute of Telecommunications (NIT), Poland, and the Lightwave Research Laboratory (LRL) at Columbia University (US).

- Chapter 5 tackles the issue of dynamically changing PLIs in the network by proposing a novel cross-layer networking approach which includes real-time impairment awareness. Through real-time monitoring of physical layer parameters (in this case OSNR), we show through simulations that it is possible to achieve greater energy efficiency and optimized network performance. The contents of this chapter have been published in [23], and an extension including an experimental validation will be submitted to [24] by the end of September 2012. This work was done within the framework of a 10-months Ph.D internship (FPU mobility grant) in the LRL lab. at Columbia University, US.

Part II applies operational research (OR) methodologies to solve a variety of complex cross-layer (i.e., multi-layer) network optimization problems which are currently identified as open issues among network operators. The common goal in these works has been the optimization of resources utilization whilst, at the same time, minimizing network TCO. Hence, we show that OR methods allow for the design cost-effective, power-efficient network solutions.

The structure, content and scientific contribution of the different chapters are provided next:

- Chapter 6 deals with the survivable multi-layer IP/MPLS-over-WSON (L3 over L1) network optimization problem. Minimizing the required IP/MPLS equipment to accommodate the requested traffic demands is crucial to cost-effective cross-layer architectures. Furthermore, to guarantee stringent survivability levels, we propose a novel lightpath restoration approach

which provides substantial cost savings with respect to the overlay (redundant) approach. Efficient metaheuristic methods are specifically tailored to tackle this problem. In this chapter, the impact of L0 phenomena is, to some extent, taken into consideration by considering 1000 km maximum lightpath distance. The contents of this chapter have been published in [25]. This study as well as the one presented in Chapter 7, were done in collaboration with Telefónica I+D, Spain, within the framework of the FP7 STRONGEST project [4].

- Chapter 7 analyzes the impact of the frequency grid (i.e., slot width) on the CAPEX required to deploy a multi-layer IP/MPLS-over-Flexgrid (L3 over L1). Again, the minimization of the equipment deployed at L3 (IP/MPLS) is crucial to minimize network TCO. In this study, we develop a GRASP algorithm to evaluate, using a realistic evolution of the network traffic demands, which slot width will better suit future cross-layer networks based on Flexgrid technology. In this analysis, L0 phenomena are considered by assuming bit-rate dependent optical signal reach. The contents of this chapter have been published in [26], and [27]

- Chapter 8 builds on top of Chapter 3 by developing a set of enhanced metaheuristic hybridizations to solve the complex RPD problem characteristic of SWS networks. RPD aims at minimizing the number of costly, power-consuming optical-electrical-optical (O/E/O) signal regenerators. The contents of this chapter have been published in [28]. This work was done in collaboration with the NIT (Poland) and LRL at Columbia University (US).

Acknowledgments

Contents

List of Tables

List of Figures

Part I

Cross-Layer Network Modeling for Future Sub-Wavelength Switching Optical Transport Networks

Introduction

With the advent of ultra high bandwidth access systems such as the passive optical networks (xPON) and the next generation mobile networks (i.e., long term evolution (LTE) and 4G), we are forced to move into the next phase of broadband backbone technologies. Indeed, multi-industry initiatives have already started the definition of new business models with the aim of accelerating mass adoption of new devices and services such as video streaming/conferencing, high-definition TV, and video on demand.

In this scenario, and after becoming a real networking layer, optical technology and ultra high-bandwidth dense wavelength division multiplexing (DWDM)-powered optical transport networks (OTNs) in particular, are the prevailing communications infrastructure poised to support the delivery of such emerging bandwidth-hungry applications and services in a cost-effective, energy-efficient way.

In order to be able to better cope with current traffic demands, legacy OTNs have evolved over the last years from synchronous optical network/synchronous digital hierarchy (SONET/SDH) over static point-to-point DWDM links toward wavelength-switched optical networks (WSONs)[2]. By cleverly dealing with the wavelength and space domains, WSONs enable dynamical network reconfiguration and allow for efficient network operation.

So far, OTNs have been classified into three major network architectures based on the amount of electrical 3R (i.e., re-amplifying, re-shaping, re-timing of the signal) (a.k.a optical/electrical/optical (O/E/O)) regenerators they require: (i) Transparent networks, where the data signal remains in the optical domain for the entire end-to-end path. In this approach, there is no need for electrical 3R regenerator devices as it is assumed either an ideal physical layer or availability of all-optical 3R regenerators [29]; (ii) Opaque networks, where the data signal undergoes an electrical 3R regeneration at every node along its path [30]; (iii) Translucent networks, where O/E/O regenerations are only allowed at selected points in the network [31].

Undoubtedly, the ultimate objective is to achieve full optical transparency involving all-optical switching and end-to-end optical path provisioning. In fact, such an objective is strongly supported by the continuous and tremendous advances in optical technologies which are nowadays fostering the deployment of fully transparent OTNs. Concurrently, however, these advances have brought to light the serious impact that layer 0 (L0) phenomena, that is, the physical layer impairments

(PLIs) have on the optical end-to-end signal quality of transmission (QoT) [31]. Indeed, PLIs severely limit the reach and capacity of optical systems, and consequently, hamper the deployment of transparent optical networks, at least until all-optical 3R regeneration devices become mature enough to be considered as a viable solution [32]. For this very reason, translucent OTNs, which combine features of both opaque and transparent networks, allowing signal regeneration only at selected nodes [31], have emerged as potential yet feasible candidates for bridging the gap between opaque and transparent networks.

However, for translucent optical networks to be a competitive solution, they should be designed in such a way that both the cost and power consumption is minimized. Both constraints are clearly related to the number of electrical 3R regenerators deployed across the network, and therefore, their number must be reduced as much as possible. For this very reason, the definition of algorithms for routing and regenerator placement (RRP) (see e.g., [33]) is essential to the success of translucent architectures. Specifically, these techniques are aimed at minimizing the number of regenerators deployed in the network by finding their optimal location.

Due to the maturity of the technology that wavelength switched optical networks (WSONs) require (e.g., reconfigurable optical add-drop multiplexers (ROADMs) and optical cross-connects (OXCs)), translucent WSONs have been the first to receive the attention from the research community. Indeed, protocol extensions and requirements to take into account the presence of PLIs in WSONs are currently under development within IETF [34].

In light of recent measurements, however, network operators now forecast a highly dynamic data traffic scenario characterized by short-lived, small granularity (i.e., occupying small portions of a wavelength) flows [8]. In this context, and due to their inflexibility and coarse granularity, WSONs would result in a highly bandwidth-inefficient approach. For this very reason, it has now become crucial for next-generation OTNs to engage highly agile optical transport technologies that include sub-wavelength switching (SWS) [3]. By leveraging recent advances in nanosecond-range photonic devices such as fast tunable lasers and fast switching elements ([9], [10]), future OTNs supporting dynamic SWS can flexibly accommodate diverse traffic conditions with better efficiency [11]. Indeed, technologies like optical packet switching (OPS) and optical burst switching (OBS) [3], which were initially proposed ten years ago, are re-gaining much of the research interest together with more recent proposals such as optical data-unit switching (ODS) [35] and optical flow switching (OFS) [36].

In short, SWS technologies introduce optical switching in the time domain as a means to further improve the utilization of network resources, and consequently, the use of any network resource (e.g., a wavelength in a link, wavelength converters and electrical 3R regenerators in a node) is subject to the so-called statistical multiplexing concept whereby resources are accessible according to their timely availability (i.e., there is a fair competition for the use of resources among all packets/bursts/flows in the network).

Without loss of generality, in this thesis we assume a layer 2 (L2) optical transport technology based on OBS [3]. In an OBS network, edge nodes are in charge of assembling client input packets coming from different sources (e.g., IP packet, Ethernet or SDH frames) into outgoing bigger data containers called bursts which, once ready, are launched optically into the network. Similarly, edge nodes are also responsible for disassembling incoming bursts into original client packets. For each outgoing burst, an edge node emits a separate control information called burst control packet (BCP) which is transmitted out-of-band and delivered to the core nodes with some offset-time prior to the burst. The offset-time provides the necessary time budget to reserve resources along the way from the ingress node to an egress node. Such reservation consists of a wavelength which is booked on-the-fly and can be reused afterwards by any other burst (i.e., the resources are therefore shared among all nodes and subject to statistical multiplexing). Core nodes and their corresponding control units are responsible for reading, processing, and updating the BCPs and for switching individual bursts accordingly. In OBS, core nodes are generally assumed to be wavelength conversion capable.

In our analysis, we assume that each OBS node is both an edge and a core buffer-less node capable of generating packets destined to any other nodes. We consider the offset time emulated OBS network architecture (E-OBS) [37] which compensates the offset-time of bursts at every hop. Moreover, we assume the one-way just-in-time (JIT) [38] resources reservation protocol together with the last available unscheduled channel (LAUC) scheduling algorithm also known as Horizon [39]. For the sake of simplicity, however, we neglect the switching and processing times, and therefore, the choice of both the resources reservation protocol and the scheduling algorithm does not have any impact on the performance results obtained.

Under these circumstances, given the fact that we completely avoid dealing with the offset-time, the most distinctive feature of OBS networks, all the studies and results provided in this part of the thesis (Part I) as well as Chapter 8 can be generalized to a generic SWS network scenario. It must be mentioned, however, that the QS-OBS study provided in Chapter 1 lacks technical interest if small packet sizes (i.e., close to an OPS scenario) are considered. Note that given the dimensions of the drift/skew time deviations as well as that of the required guard-time, OPS-like packet sizes would result in strong performance degradation, as in such a case even very small packet misalignments do adversely affect network performance. We refer the reader to Chapter 1 for more details on this issue.

It is for these reasons that we believe that the different SWS studies provided in this thesis are applicable to any of the aforementioned SWS technologies. Hence, the OBS consideration will be made explicit only when strictly necessary, and accordingly, we use the terms *SWS* and *packet* generically to refer, respectively, to the switching paradigm under which the OTN is operating and the optical data unit of such an infrastructure (i.e., packets/bursts/flows).

The focus of this part of the thesis is therefore set on the study and analysis of SWS OTNs.

To be precise, we first propose in Chapter 1 a novel operation mode for OBS networks, the quasi-synchronous (QS) transmission which accounts for the time-deviation/synchronization impact that PLIs (L0 phenomena) have on the OBS transmission system. We assess the QS-OBS network performance by comparing it with that of the well-known asynchronous and synchronous transmission modes. Then, Chapter 2, incorporates the impact of PLIs into the offline design/planning phase of a SWS OTN, thereby leading to the modeling of a translucent SWS (T-SWS) network architecture. Then, Chapter 3 is specifically devoted to assessing the complex routing and regenerator placement and dimensioning (RRPD) problem. Afterwards, Chapter 4, analyzes the feasibility of deploying future SWS OTNs relying on nodes which consider wavelength converter sharing configurations. Finally, Chapter 5 tackles the issue of dynamically changing PLIs in the network by proposing a novel cross-layer networking approach which includes real-time impairment awareness. This chapter represents an structural and operational enhancement over the networking paradigm proposed in Chapters 2 and 3.

For the sake of clarity, and unless given differently, in this thesis we use the term *regenerator* implicitly to refer to the electrical 3R regenerator, that is, the optical signal undergoes an optical-electrical-optical (O/E/O) conversion in order to be regenerated.

Chapter 1

A novel operation mode for OBS networks: The Quasi-Synchronous transmission

1.1 Introduction and motivation

Two main features distinguish Optical Burst Switching (OBS) [40] from other optical switching technologies: the transmission of large data bursts, which are aggregated at the edge of the network, and the possibility to establish a path dynamically and on-the-fly (i.e., without acknowledgment of the availability of transmission resources). Because of the absence of optical buffering capabilities, the main challenge of OBS is to deal with high burst losses that arise due to the contention of bursts transmitted in the network.

To mitigate the burst contention problem, there have been proposed solutions based on deflection (or alternative) routing. All these methods allow re-routing contending bursts from primary to alternative routes and, by this means, alleviating congestion on bottleneck links and achieving dynamic load balancing in the network. In this thesis, we consider the so-called offset time-Emulated OBS (E-OBS) network architecture [37], which facilitates the application of alternative routing since routing decision can be taken freely inside the network without constraints on the length of routing path.

In principle, the transmission of optical bursts is asynchronous in an OBS network. That means that bursts are not aligned with each other, and thus, they arrive at a core switching node in casual instances of time. Performance improvements can be achieved if synchronous operation is applied: in fact, in such a case, contention may only occur between entire data units and better transmission resource utilization can be obtained with simple contention resolution mechanisms

[41]. Such synchronous operation was proposed in the past to the optical packet switching (OPS) networks (see e.g., [42]), and although it has not been widely considered in OBS networks, still some relevant studies can be found in the literature (see e.g., [43],[44],[45],[46] and [47]). Besides, in [14], we verified that with the utilization of effective deflection routing techniques, the performance gain of the synchronous operation with respect to the asynchronous one is brought to a very motivating extent. However, all these studies consider that synchronization of data bursts is achieved by means of an input stage at each core node which involves the use of additional hardware elements such as incremental fiber delay blocks and switching devices. All these components and the increased control complexity that they entail lead to a bulky and complex structure whose viability has not been demonstrated yet.

In this direction, we proposed a novel operation mode for OBS networks, the quasi-synchronous (QS) operation, with the aim of reaching performance benefits close to those obtained with perfect synchronization while keeping a moderate hardware complexity. In the QS OBS scenario, we do not have the need for any intricate synchronization device. Contrarily, we assume both that network links are designed such that the resulting propagation delays correspond to a multiple of a given fixed time slot duration and that bursts are released only at the beginning of such time slots. In addition, to take into account that perfect synchronization is practically impossible, we accept the presence of some time deviation. The existence of this time variation between the actual arrival of bursts and the beginning of time slots causes that the bursts are not perfectly aligned at the core switching nodes. For that, we refer to the QS operation.

Specifically, we model the time deviation of the QS transmission mode as a superposition of two different sources, denoted as drift and skew respectively. We consider the drift as an irretrievable error due to structural inaccuracy of the different devices constituting an OBS node and to the physical impairments that may change the propagation time characteristics of the different channels of a fibre. In contrast, we consider the skew as the consequence of not having well-aligned hardware clock information amongst all network edge nodes. The skew is, hence, a retrievable time deviation error and, for that reason, we propose a method to bound its value to a range where there is no (or negligible) performance degradation.

The contribution of this chapter is twofold. First, we present the details of the QS scheme highlighting its architectural benefits compared to the synchronous and asynchronous cases. In particular, we provide a detailed performance study (through both analytic and simulation model) both to analyze the effects of the presence of the drifts and skews and to find out a set of values that highlights the performance of the QS scheme. Second, we compare the performance of the asynchronous, synchronous and QS operation modes with the support of different deflection routing algorithms.

The rest of this chapter is organized as follows. In Section 1.2, we provide complete information on the analyzed network scenarios. In Section 1.3, we first present in detail the analytic models for

all the OBS transmission modes considered. Afterwards, we validate by simulation the models with special emphasis on our novel analytic model for the QS operation in OBS networks. Then, in Section 1.4, we focus on the key parameters in the QS-OBS network and provide values for them that are in accordance with real OBS network scenarios. In Section 1.5, we present the re-synchronization mechanism that we propose with the purpose of maintaining such quasi-synchronization at edge nodes. Section 1.6 presents an overall comparison between the synchronous, asynchronous and our QS schemes under different deflection routing algorithms. Finally, the conclusions are presented in Section 1.7.

1.2 OBS network scenarios

In this study, we consider an E-OBS network scenario [37]: core switching nodes are enhanced with a pool of fibre delay coils that is inserted into the data path at the input port of the node. In conventional OBS (C-OBS) architectures, the processing offset time is provided at the edge node by delaying the transmission of a burst with respect to its control packet. In E-OBS, on the contrary, the offset times are provided by means of these fibre delay coils at each core node. Thus, both the burst and control packet can be sent together from the edge node, avoiding several problems that result from the offset time variation inside the network, a feature that is inherent to C-OBS. For instance, concerning routing management, it is advantageous to provide offset times at each core node since routing decisions can be taken freely inside the network without any constraints on the length of the path. Contrarily, in C-OBS, the maximal length of routing path is related to the offset which, once introduced at the edge node, decreases at each hop.

In general, the transmission of optical data in the network can be either asynchronous or synchronous. Although both approaches have been studied extensively in the context of OPS networks, the research on OBS still concerns mostly the asynchronous approach.

1.2.1 Asynchronous OBS

In asynchronous OBS networks, optical bursts are released from edge nodes at arbitrary (random) instances of time and they are not aligned when they arrive at core switching nodes (see Figure 1.1A). Accordingly, the switching operation is performed asynchronously. The advantage of this approach is the simplification of the burstification process and the low complexity of switching nodes.

1.2.2 Synchronous OBS

The idea of synchronous, or time-slotted, transmission in optical networks has been considered mainly in the context of OPS networks. In case of a synchronous OBS scenario, optical bursts are aligned and transmitted synchronously at the beginning of a fixed-duration time slot (see Figure

1.1B). The main advantage of the synchronous approach, with respect to the asynchronous approach, is the improvement of the overall burst loss performance. In synchronous OBS networks, since bursts traveling over different length links may still arrive at a core node at different instances of time, their synchronization is achieved by means of a specialized node input interface. For example, in [45], a time-slotted OBS architecture called time-sliced OBS which performs the switching in the time domain rather than in the wavelength one is proposed. Such operation is achieved by means of a two-block stage: a) a synchronizer consisting of variable delay lines which require feedback control information from the node controller; b) an optical time slot interchanger (OTSI) consisting of optical crossbars and delay lines. However, as the authors conclude, there is still the need to undertake substantial additional work in order to prove the viability of this solution. Besides [45], no further works address such time-slotted OBS solution.

On the other hand, in [47] and [48], a variant of the time-slotted OBS operation is proposed under the name of time-synchronized OBS (SynOBS). The authors assume that the length of both bursts and slots is fixed as we do in our QS-OBS. In SynOBS, synchronization is performed by means of time slot synchronizers and wavelength delay variation compensators. The synchronizers consist of cascaded variable-length delay lines, also known as tunable delay lines, and a number of 2x2 switching devices. Their duty is to synchronize incoming data bursts from different input ports. Examples of such a mechanism can be found in [49]. The compensators, by contrast, are used to balance the different speeds at which wavelengths travel in a fiber. Assuming that the impact of delay variations among wavelengths can be neglected, these devices may be implemented with fixed-length delay lines. This is not, however, the case with tunable delay lines, whose design entails a rather complex control and structure. Note that the node controller is in charge of dynamically adjusting the delays applied to data streams from different input ports so that they all become synchronized. Furthermore, in the 2x2 switches, high switching speeds (i.e., in the nanosecond range) are essential, and hence, semiconductor optical amplifier (SOA) switches are required. Both the cost that this structure entails (i.e., substantial extra hardware is necessary) and the impact that the added physical layer impairments have on the optical signal (i.e., SOA amplifiers also bring out some non-desirable effects such as power consumption, noise and nonlinearity) must be thoroughly evaluated before this solution can be considered viable.

On the contrary, in our QS-OBS network operating under the E-OBS control architecture there is no need for such extra hardware. In E-OBS, pools of fixed-length delay coils are used at each core node to provide bursts with enough time to compensate the processing and switching times (i.e., what electrical memories do at edge nodes in C-OBS). This provided time depends on the length of the delay coil exclusively and cannot be tuned; it is fixed and defined in the design phase of the network (we refer to [37] for more details). In addition, this pool of delay coils can act as a dispersion compensation unit to mitigate the chromatic dispersion.
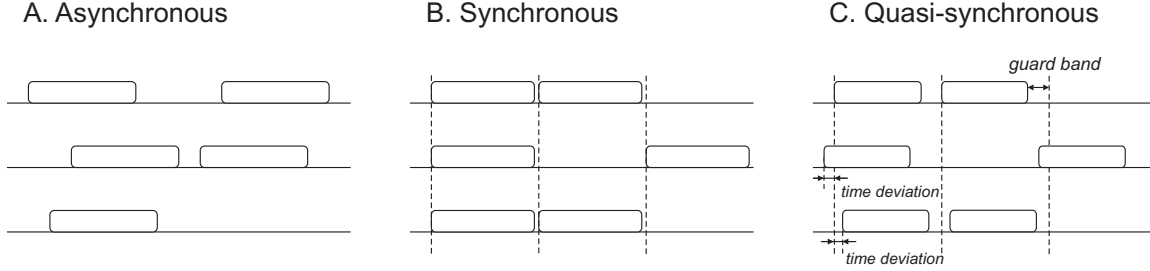
Figure 1.1: OBS transmission modes.

1.2.3 Quasi-Synchronous OBS

In the QS scenario, there are no synchronization devices; the network links are designed so that the resulting propagation delays correspond to a multiple of the slot size; the edge nodes are synchronized with each other and release data bursts at the beginning of time slots.

Since it is impossible to have all edge nodes perfectly synchronized, we assume that there exist some skew amongst their clocks. Moreover, we consider the presence of a local drift which counts for the devices inaccuracies and physical impairments. A possible representation of this scenario is shown in Figure 1.2, where we model the drift as a Normal random variable and the skew as a Uniform random variable. Therefore, and due to the effect of both the drift and the skew, bursts arriving at core nodes are not perfectly aligned (see Figure 1.1C) with the consequence of having performance degradation compared to the perfectly synchronized case.

In order to prevent the overlapping of de-synchronized bursts and given that both sources of time deviation are independent, we propose two separate solutions for their adjustment. The problem can, therefore, be split into two different parts.

On the one hand, to correct the effect of the skew, we present in Section 1.5 a re-synchronization mechanism adapted to OBS networks. The basis of our mechanism was proposed in the past in [50] for distributing well-aligned hardware clock throughout the physical extent of a synchronous processor. Its scope is to bound the skew effect to a range of values that guarantees good performance results.

On the other hand, to overcome the problem posed by the drift present at the instant of burst departure, we introduce a guard band between the bursts so that they do not occupy the slots completely. This guard-time should be large enough to maintain (as much as possible) the burst alignment as in the case of synchronous operation but not too large in order to not decrease excessively the bandwidth utilization. As a consequence, the duration of the guard-time results in a clear trade-off between utilization and performance. Notice that, in any mode of operation (i.e., asynchronous, synchronous and QS), a time margin must be included between every two consecutive bursts to allow for switching the bursts in intermediate nodes (both to process the information and to physically reconfigure the switches). Let us denote this margin as basic guard-time. Since such

basic guard-time is required indifferently and affects equally any mode of operation, we neglect it in all scenarios considered in this study for the sake of simplicity. Nonetheless, we do consider that this basic guard-time has a fixed value only in the synchronous approach because its input node interfaces can re-align the bursts perfectly. In the asynchronous and QS cases, by contrast, such basic guard-time is not necessarily maintained constant since burst arrivals may be affected by time variations and, as a result of this, the basic guard-time may be either increased or reduced. Such variations is what we define as drift. For this very reason, in the QS operation mode, we propose and evaluate the use of an additional guard-time whose purpose is to minimize the impact of the drifts on the network performance. Hereinafter in this chapter, we only consider, if not explicitly stated, the additional guard-time, and thus, we will shorten it to guard-time.

Note that, on the contrary to OPS networks, where optical packets have small size and even their small misalignment might result in a serious degradation of performance, in OBS there is possibly a higher margin for de-synchronization of burst transmission owing to much larger burst durations and, as a result, much larger guard bands. For these reasons, we expect that the results obtained with the QS operation should be somewhere between the asynchronous and synchronous cases.

In the next section, we present an analytic model of the drift deviation and study its impact on the node and network behavior. For the sake of simplicity, the analytic model presented relies on exponentially distributed drifts. Analytic and simulation results comparing the performance of the QS scheme with that of both the synchronous and asynchronous schemes are also provided. Afterwards, in Section 1.4 we make use of a more realistic model of the drifts (i.e., gaussian-distributed drifts may fall on either side of the node clock pulse) and provide practical values for the time slot, guard-time and drift so that in subsequent sections the QS-OBS network performance can be effectively evaluated.

1.3 Evaluation of the drift impact

To evaluate the impact of the drift on the performance of the QS operation mode, we present a detailed performance study (through both analytic and simulation model) of the three different OBS transmission modes considered in this chapter, namely asynchronous, synchronous and QS. Firstly, we consider a single OBS node with W wavelengths in its output port p. Then, we extend the models to a network scenario using the reduced-load fixed point approximation proposed in [51]. It is worth pointing out that both the analytic and simulation studies presented in this section are independent from the time slot size. Hence, all drifts and guard-time values are given as a percentage of the time slot size. An analysis assuming absolute values for drifts (and consequently also absolute values for the time slot and guard-time) will be later presented in Section 1.4.
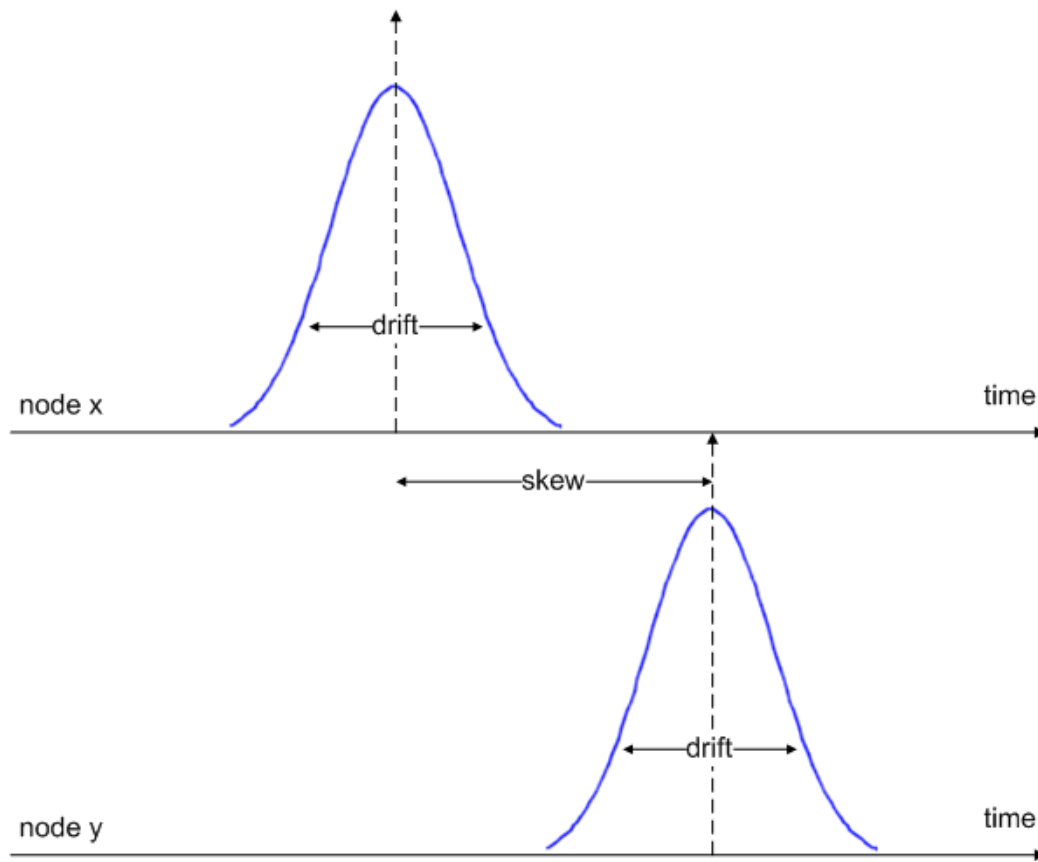
Figure 1.2: Time deviation sources in the QS-OBS network.

1.3.1 Analytic models

We present the asynchronous, synchronous and QS analytic models, with special emphasis on our single-wavelength QS model. For the sake of mathematical tractability, let us assume in our analysis that burst arrivals can be modeled as a Poisson process with parameter λ. We consider fixed burst size in all cases. For simplicity, we assume the service time μ of bursts to be equal to 1, and consequently, the traffic intensity ρ be equal to $\rho = \lambda/\mu = \lambda$. Note that, whilst in the synchronous case the burst size is equal to the slot size, in the QS case it is decreased by the guard-time value used. In the next subsections we introduce the analytic models corresponding to each of the operation modes considered.

Asynchronous loss model

Since we are considering Poisson burst arrivals, it is well-known (see e.g., [52]) that an output port p can be modeled as an W-server loss system, and thus, its blocking probability (Pb_{ASYN}) under traffic intensity ρ, is given by the following Erlang-B formula:

$$Pb_{ASYN}(\rho, W) = E(\rho, W) = \frac{\rho^W/W!}{\sum\limits_{i=0}^{W} \rho^i/i!} \tag{1.1}$$

Synchronous loss model

Under synchronous operation, bursts are only released at the exact instant of the slot start time. Due to the fact that the number of burst arrivals at each slot is Poisson distributed, we can model the probability of having exactly k burst arrivals during a slot N_j as follows:

$$P(k \text{ arrivals}) = P(N_j = k) = \frac{\lambda^k}{k!}e^{-\lambda} \tag{1.2}$$

Notice that assuming a perfectly synchronized scenario, burst loss can only occur when within a slot time the number of burst arrivals is higher than the number of available wavelengths at p (i.e., higher than W). Hence, we can analytically model the synchronous blocking probability (Pb_{SYNC}) as follows [53]:

$$Pb_{SYNC}(\rho, W) = \frac{1}{\rho} \sum_{i=W+1}^{\infty} P(N_j = i)(i - W) \tag{1.3}$$

Each of the three terms in the formula models a different factor. Whilst $P(N_j = i)$ represents the probability of an event to happen, $(i - W)$ counts the number of bursts undergoing such event. Eventually, $\frac{1}{\rho}$ acts as a traffic normalization factor. Indeed, as long as $\rho < 1$, it corresponds to the server utilization or occupation rate. For example, this factor is responsible for capturing the impact
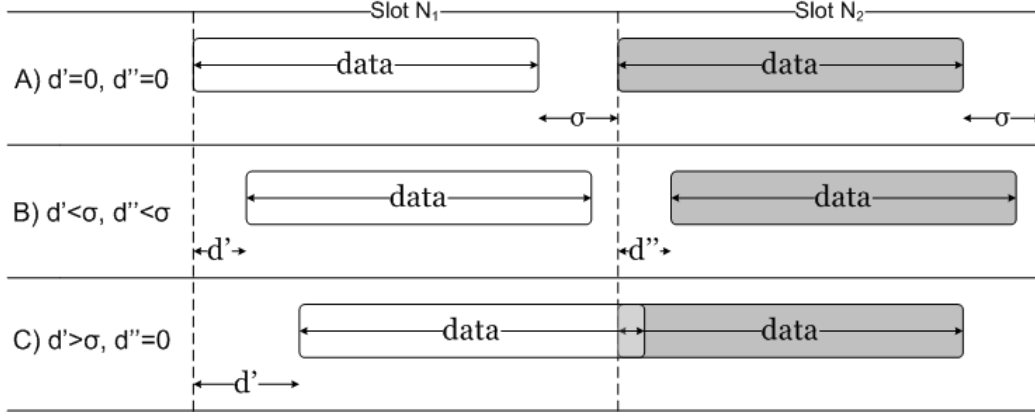
Figure 1.3: Exponential drifts collision scenario.

that a reduction in the service time of bursts would have on the loss probability.

Quasi-synchronous loss model

In this section, we present our single-wavelength analytic model for the QS operation. In the QS scenario each edge node generates bursts with a certain time deviation. This deviation can be modeled as a superposition of a skew and a drift. In this section, we only model the presence of the drift. Although modeling the drift as a Normal random variable is a more realistic option, in our model, we assume, for the sake of simplicity, that drifts follow an exponential distribution with parameter α. We also consider the presence of a guard-time of value σ at the end of bursts.

Under QS network operation, burst loss can be caused by two different factors. The first loss factor is the consequence of a drift-based collision (i.e., a collision between two bursts that overlap in two consecutive slots due to incompatible drift values (see e.g., Figure 1.3C). In the cases represented in Figures 1.3A and 1.3B there is no possibility for a drift-based collision to occur. Notice that in the case 1.3B, the condition $d' < \sigma$ is enough to guarantee that there is not a drift-based collision between slots N_1 and N_2; however, by adding the condition $d'' < \sigma$ we also prevent a possible drift-based collision with the next slot (i.e., N_3). The second loss factor results from an overflow-based collision (i.e., the arrival of more bursts than wavelengths available at p during one time slot). To model the drift-based collisions, we consider arrivals in two consecutive time-slots, namely slot N_1 and slot N_2 in Figure 1.3. Since arrivals are modeled using a Poisson process, we are able to estimate the probability of arrivals in two consecutive time slots as a simple product thanks to the independence between time intervals. To ease the mathematical development, we split the computation QS blocking probability (Pb_{QS}) into two components depending on the number of arrivals in the first slot, giving the following structure:

$$Pb_{QS}(\rho, 1) = P_{QS0} + P_{QS1} \tag{1.4}$$

where P_{QS0} refers to the case where there are no burst arrivals in the first slot N_1, and P_{QS1} refers to the case where there is a positive number of arrivals at N_1. Note that P_{QS0} corresponds to a synchronous loss model in a single-wavelength scenario.

As aforementioned, in the QS operation mode, there are two different classes of burst loss, namely drift-based collisions and overflow collisions. It is important to notice that, in a perfectly synchronized scenario, where only overflow collisions exist, burst $W + 1$ and any subsequent arrivals are lost with a probability equal to 1 because no more than W wavelengths are available. However, in the QS mode, it is not true at all since earlier arrivals may be lost due to drift-based collisions. In our analytic model, we take this fact into account, and the term B_r accounts for such reduced probabilities. Eventually, the formulation for the two components in equation (1.4) corresponds to:

$$P_{QS0} = P(N_1 = 0)Pb_{SYNC}(\rho, 1) = \frac{P(N_1 = 0)}{\rho} \sum_{l=2}^{\infty} P(N_2 = l)(l - 1) \tag{1.5}$$

$$P_{QS1} = \frac{1}{\rho} \sum_{k=1}^{\infty} P(N_1 = k) \sum_{l=1}^{\infty} P(N_2 = l) \left(\sum_{n=1}^{l} A_n + \sum_{r=1}^{l-1} B_r \right) \tag{1.6}$$

where k and l refer to the number of burst arrivals at slot N_1 and slot N_2 respectively. Besides, A_n represents the burst loss probability caused by drift-based collisions for the burst arrival number n at slot N_2 and B_r denotes the burst loss probability caused by overflow-based collisions for the burst arrival number $r + 1$ at slot N_2 (i.e., notice that the first burst arrival cannot be lost due to overflow). Since B_r values are dependent on those of A_n, we are able to derive them as follows:

$$B_r = 1 - \overline{B_r} \tag{1.7}$$

$$\overline{B_r} = (1 - A_{r+1}) \prod_{i=1}^{r} A_i \tag{1.8}$$

In Equation (1.8) we can observe that the burst arrival $r + 1$ at slot N_2 will not be lost due to overflow if and only if all the preceding arrivals have been lost due to drift-based collisions ($\prod_{i=1}^{r} A_i$) and it is not lost owing to its own drift $(1 - A_{r+1})$. Hence, our goal in this study is to analytically model A_n.

If we take a look at Figure 1.3, we observe that a collision will occur if and only if the drifts corresponding to two consecutive reservations fulfil the following condition:

$$d' > d'' + \sigma \tag{1.9}$$

Our objective is to find an analytic model for the calculation of the burst loss probability taking into account losses that are the direct consequence of the cases where condition (1.9) is fulfilled.

Let us start by considering the random variables Z and U that correspond to d' and d'' respectively. Since we consider a single-wavelength scenario, our interest lies in the minimum drift value (i.e., the first burst arrivals at each slot). Then, Z is equal to $\min < d'_1, d'_2, ..., d'_k >$, where $d'_1, d'_2, ..., d'_k$ form an increasing sequence of exponentially distributed drifts at slot N_1. Likewise, U is equal to $\min < d''_1, d''_2, ..., d''_l >$, where $d''_1, d''_2, ..., d''_l$ form an increasing sequence of exponentially distributed drifts at slot N_2. Note that the smaller the drift, the earlier the arrival.

First of all, we find the cumulative distribution function of the Z random variable.

$$
\begin{aligned}
F_Z(z) &= P(Z < z) = P(\min(d'_1, d'_2, ..., d'_k) \leq z) = \\
&= 1 - P(\min(d'_1, d'_2, ..., d'_k) > z) = \\
&= 1 - P(\{d'_1 > z\} \cap \{d'_2 > z\} \cap ... \cap \{d'_k > z\}) = \\
&= 1 - P(d'_1 > z)^k = 1 - [1 - F_D(z)]^k
\end{aligned}
\tag{1.10}
$$

where $F_D(x)$ is the cumulative distribution function of an exponential random variable D with parameter α and which corresponds to:

$$
F_D(x) = 1 - e^{-\alpha x} \ \forall \ x \in [0, \infty)
\tag{1.11}
$$

then,

$$
F_Z(z) = 1 - [1 - (1 - e^{\alpha z})]^k = 1 - e^{-\alpha k z} \ \forall \ z \in [0, \infty), k \in \mathbb{N}
\tag{1.12}
$$

Note that Z is an exponential distribution with parameter αk.

Hereinafter, we assume that d'_k and d''_l are equally distributed with parameter α. Therefore, if Z is exponential with parameter αk, U is also exponential with parameter αl.

The term $P(Z > U + \sigma)$ refers to the probability that the first burst to arrive at slot N_2 is lost as a result of a drift-based collision. Then,

$$
P(Z > U + \sigma) = P(Z > U + \sigma | Z > \sigma)P(Z > \sigma)
\tag{1.13}
$$

and if we apply the memoryless property of the exponential distribution, we have that:

$$
P(Z > U + \sigma | Z > \sigma) = P(Z > U)
\tag{1.14}
$$

hence,

$$
P(Z > U + \sigma) = P(Z > U)P(Z > \sigma)
\tag{1.15}
$$

The first term is derived as follows:

$$P(Z > U) = \int_0^\infty \int_0^x (\alpha k e^{-\alpha k x} \alpha l e^{-\alpha l y}) dy dx = \frac{l}{l+k} \tag{1.16}$$

and the second term corresponds to:

$$P(Z > \sigma) = 1 - P(Z < \sigma) = 1 - F_Z(\sigma) = e^{-\alpha k \sigma} \tag{1.17}$$

thus, we finally have:

$$P(Z > U + \sigma) = e^{-\alpha k \sigma} \frac{l}{l+k} \tag{1.18}$$

Note that the above expression can only be applied when we compute the drift-loss probability for the first burst arrival in the second slot. For all successive new arrivals $n \in [2, \infty)$, we must take into account their arrival times which consist of the arrival time of the first burst (i.e., $U + \sigma$) plus the distance between two consecutive drifts (i.e., $d_n'' - d_{n-1}''$) times the number of arrivals after the first one (i.e., $n - 1$). Thus, we propose the following formulation:

$$
\begin{aligned}
P(Z \quad > \quad & (n-1)(d_n'' - d_{n-1}'') + U + \sigma) = \\
= \quad & P(Z > (n-1)(d_n'' - d_{n-1}'') + U + \sigma | Z > \sigma) P(Z > \sigma)
\end{aligned}
\tag{1.19}
$$

Again, if we recursively apply the memoryless property of the exponential distribution, we obtain the following:

$$
\begin{aligned}
P(Z \quad > \quad & (n-1)(d_n'' - d_{n-1}'') + U + \sigma | Z > \sigma) = \\
= \quad & P(Z > (n-1)(d_n'' - d_{n-1}'') + U) = \\
= \quad & P(Z > (n-1)(d_n'' - d_{n-1}'') + U | Z > U) P(Z > U)
\end{aligned}
\tag{1.20}
$$

$$
\begin{aligned}
P(Z \quad > \quad & (n-1)(d_n'' - d_{n-1}'') + U | Z > U) = \\
= \quad & P(Z > (n-1)(d_n'' - d_{n-1}'')) = \\
= \quad & P(\frac{Z}{(n-1)} > (d_n'' - d_{n-1}''))
\end{aligned}
\tag{1.21}
$$

Hence, we eventually have that:

$$
\begin{aligned}
P(Z &> (n-1)(d_n'' - d_{n-1}'') + U + \sigma) = \\
&= P(\frac{Z}{(n-1)} > (d_n'' - d_{n-1}''))P(Z > U)P(Z > \sigma)
\end{aligned}
\tag{1.22}
$$

Now the objective is to obtain a valid expression for $P(\frac{Z}{(n-1)} > (d_n'' - d_{n-1}''))$. We define two new random variables, namely Q and T, that correspond to:

$$
Q = \frac{Z}{(n-1)}
\tag{1.23}
$$

$$
T = d_n'' - d_{n-1}'' = X - Y
\tag{1.24}
$$

It is easy to note that Q is an exponential random variable with parameter $\alpha k(n-1)$. However, in order to compute the probability $P(Q > T)$, we have to derive the density function of T, which corresponds to the subtraction of two exponential and independent random variables with the same parameter. Since the sequence is in increasing order we must take into account the constraint $X > Y$. $F_T(t)$ is defined as:

$$
F_T(t) = P(T \le t) = P(X - Y \le t)
\tag{1.25}
$$

Now, let us define the boundaries of the region to integer taking into account the constraint $X > Y$. The region is, therefore, defined by these two inequalities:

$$
(a)\ x \le y + t; (b)\ x > y
\tag{1.26}
$$

Hence,

$$
\begin{aligned}
F_T(t) &= \int_0^\infty \int_y^{y+t} f_{XY}(x,y)dxdy = \int_0^\infty \int_y^{y+t} \alpha^2 e^{-(x+y)}dxdy = \\
&= \frac{1}{2}(1 - e^{-\alpha t})
\end{aligned}
\tag{1.27}
$$

The density function $f_T(t)$ is obtained through the derivation of $F_T(t)$.

$$
f_T(t) = \frac{dF_T(t)}{dt} = \frac{\alpha}{2}e^{-\alpha t} \ \forall\ t \in [0, \infty)
\tag{1.28}
$$

Therefore, now it is possible to compute the probability $P(Q > T)$ for the arrival number n, as follows:

$$P(Q > T)_n = \int\limits_{0}^{\infty} \int\limits_{0}^{x} (\alpha k(n-1)e^{-\alpha k(n-1)x} \frac{\alpha}{2} e^{-\alpha y}) dy dx =$$
$$= \frac{1}{2(k(n-1)+1)} \ \forall \ k \in \mathbb{N} \tag{1.29}$$

Summarizing, to compute the drift-loss probability for the arrival number $n \in [2, \infty)$ in the second slot, we apply the following formula:

$$P(Z > (n-1)(d_n'' - d_{n-1}'') + U + \sigma) =$$
$$= P(Z > \sigma)P(Z > U)P(Q > T)_n \tag{1.30}$$

Finally, we can define the A_n values as follows:

$$A_n = \left\{ \begin{array}{ll} e^{-\alpha k \sigma} \frac{l}{l+k}, & n = 1 \\ e^{-\alpha k \sigma} \frac{l}{l+k} \frac{1}{2(k(n-1)+1)}, & otherwise \end{array} \right\} \tag{1.31}$$

A boundary condition can be inferred from this model. If $\alpha = 0$ (i.e., there is no drift at edge nodes), then $A_n = 0$ and $B_r = 1$. Therefore, $Pb_{QS} = Pb_{SYNC}$ (i.e., the QS loss model becomes a synchronous loss model). Besides, it is easy to observe that for a large number k of arrivals at slot N_1, A_n will tend to a low probability value. In contrast, for a small number k of arrivals, A_n will tend to a high probability value. The same can be inferred from the number l of arrivals at slot N_2. Notice that the higher the number of arrivals, the smaller the drift of the first burst arrival.

1.3.2 Analytic models validation

In order to validate the analytic models, we compare their numerical results with those obtained through simulations.

Single OBS node

We first consider a scenario composed by an isolated single OBS node with only one wavelength in its output port p. In this chapter, we assume, if not differently mentioned, the simulation scenario as described in Appendix A as well as the following considerations: (1) the NSFNET network topology;(2) all network links have equal length and the resulting propagation delays correspond to a multiple of the slot size; (3) a single-path shortest-path routing algorithm is used.

In Figures 1.4, and 1.5, we present the simulation and numerical results obtained using the QS model with guard-time values ranging from approximately $\sigma = 0.033\%$ to a 33% of the slot size.

The drifts follow an exponential distribution with a parameter α such that $E(D) = \frac{1}{\alpha} \approx 0.77\%$ and $E(D) \approx 5\%$ of the slot size respectively in each figure. Besides, the asynchronous and synchronous cases are used as benchmark references. As can be observed in both figures, all simulation results perfectly match those obtained through the analytic expressions presented before. It is interesting to notice that whilst a negligible value of the guard-time results in a performance close to that of the asynchronous operation, gradual increments of the guard-time display performances that tend towards that of the perfectly synchronized case. However, as stated earlier, we cannot increase as much as we want the value of the guard-time, since it will result in a performance degradation due to the overload cost that we should pay; indeed, in order to maintain a constant load when decreasing the size of the burst (i.e., increasing the guard-time), the number of bursts launched into the network is increased. As a direct consequence of these results, it is clear that finding an optimal value for the guard-time is of major importance in this problem. Although the derived analytic model only concerns a single-wavelength scenario, it allows to gain of a valuable insight into the evaluation of the QS operation in OBS networks.

OBS network

Taking advantage of the analytic model presented, we can gain more insight in the QS operation by analyzing its behavior in a network scale. In order to obtain the network-wide burst loss probability we apply the reduced-load fixed point approximation [51] model. It assumes that blocking events occur independently from link to link along any route r, where $r = (l_1, ..., l_{k-n}, ..., l_k)$ is an ordered set of links which connect a source node to a destination node. It also assumes that the routes are predefined by means of using, for example, a shortest-path algorithm, and thus, the load assigned to each network link can be obtained. Then, considering a vector of stationary link blocking probabilities, the reduced offered load resulting from blocking can be approximated, i.e., for any route r that crosses link l_{k-n}, the load it offers to link l_{k-n} is reduced by blocking events occurred in its preceding links, that is, links $l_1, ..., l_{k-n-1}$. In order to obtain a solution for the vector of link blocking probabilities, the authors of [51] make use of a successive substitution procedure for which convergence is guaranteed.

In our models, we compute the loss probability in each network link using either the Erlang-B loss formula (1.1) (asynchronous case), the synchronous loss formula (1.3) (synchronous case) or the QS loss formula (1.4) (quasi-synchronous case). Note that, in the QS case, arrivals are still Poisson distributed since the drifts also follow an exponential distribution. Thus, the reduced-load fixed point approximation can also be applied in this case.

Due to the fact that our analytic model is only valid for a single-wavelength scenario, we consider links equipped with only one single channel. We present the results in Figure 1.6(a) for a drift equal to a 0.77% of the slot size and guard-time values ranging from approximately $\sigma = 0.033\%$ to 3.33% of the slot size, and in Figure 1.6(b) for a drift equal to a 5% of the slot size and guard-time values
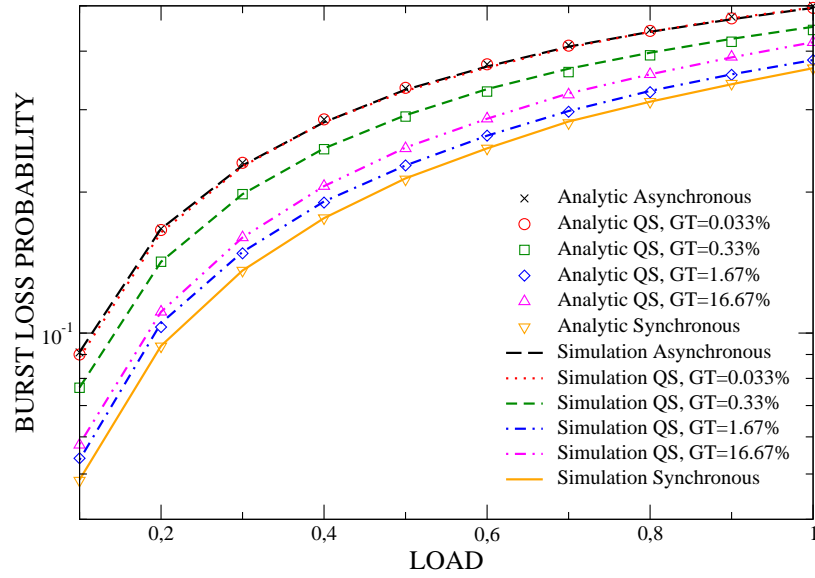
Figure 1.4: Single node validation with 0.77% drift.
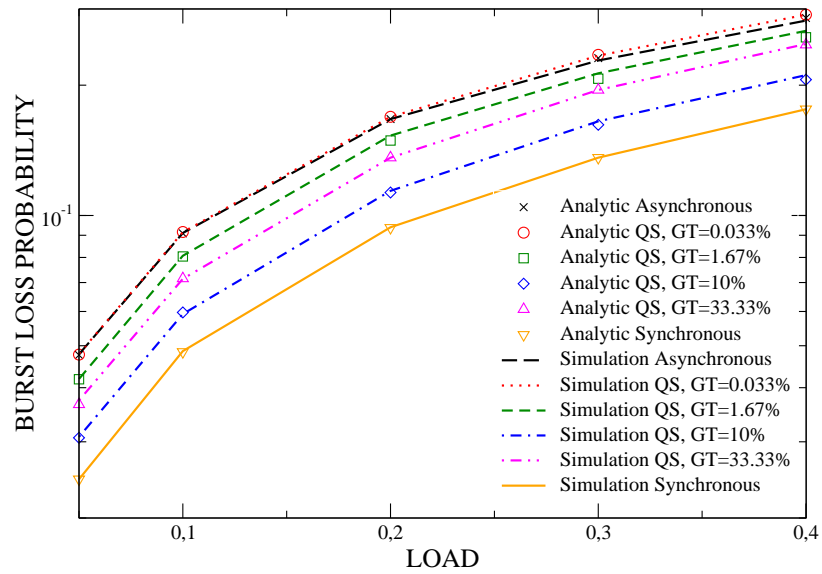
Figure 1.5: Single node validation with 5% drift.

ranging from $\sigma = 0.033\%$ to 13.33% of the slot size. Note that, as a consequence of having only one channel in each link, we have to consider a very light loaded scenario in order to be able to plot significant values of the loss probability. We observe, in both figures, a similar behavior than that obtained with the isolated OBS node. Consequently, with the use of an optimal value of the guard-time we expect that the performance displayed by the QS operation will achieve results close to those obtained with perfect synchronization.

1.4   Time slot and guard-time dimensioning

The aim of this section is the dimensioning of the two main defining parameters of the QS-OBS network, namely the time slot size and the guard-time. Both parameters are of crucial importance in the design of the QS-OBS network, and hence, impact seriously on the network performance. They not only must be carefully engineered in order to obtain good network performance results, but also must be dimensioned so that they are in accordance with the presence of the drift phenomenon in the considered OBS network scenarios. For this purpose, we first provide a reasonable model for the drifts, and second, we perform a simulation study to evaluate the impact that both the time slot and guard-time size have on the QS-OBS network performance.

1.4.1   Drift model

As mentioned in Section 1.2, we consider that the best way to model the drifts that may arise in a real OBS network is by making use of a gaussian-distributed random variable (see Figure 1.2). Specifically, we consider that drifts follow a Normal distribution denoted by $N(0, \xi^2)$, where ξ corresponds to the standard deviation of the random variable expressed in μs. Hence, we are assuming that 68% of the drifts values fall within the region $[-\xi\mu s, \xi\mu s]$, 95% of them $\in [-2\xi\mu s, 2\xi\mu s]$ and 99.7% $\in [-3\xi\mu s, 3\xi\mu s]$.

We consider that in real OBS network scenarios drifts are the result of the contribution of several inaccuracies. On the one hand, there are the contributions of the inevitable structural inaccuracy of the devices constituting an OBS node which may introduce random time differences between two identical bursts (e.g., control pulse activating the lasers, inaccurate wavelength conversion, delayed processing time, etc.). On the other hand, the physical impairments of the fibers may change the propagation time characteristics of the different channels (recall that a burst can change randomly the wavelength along its path to solve a contention); nonetheless, considering that a signal cannot usually remain in the optical domain more than $1500km$ before requiring a full regeneration, the effect of the wavelength walk-off can be considered to be limited to approximately $1\mu s$ [54]. In summary, it is reasonable to model the drift phenomenon as a gaussian distribution, where the majority of the bursts experienced a drift within a given region while scattered events can fall in any zone.
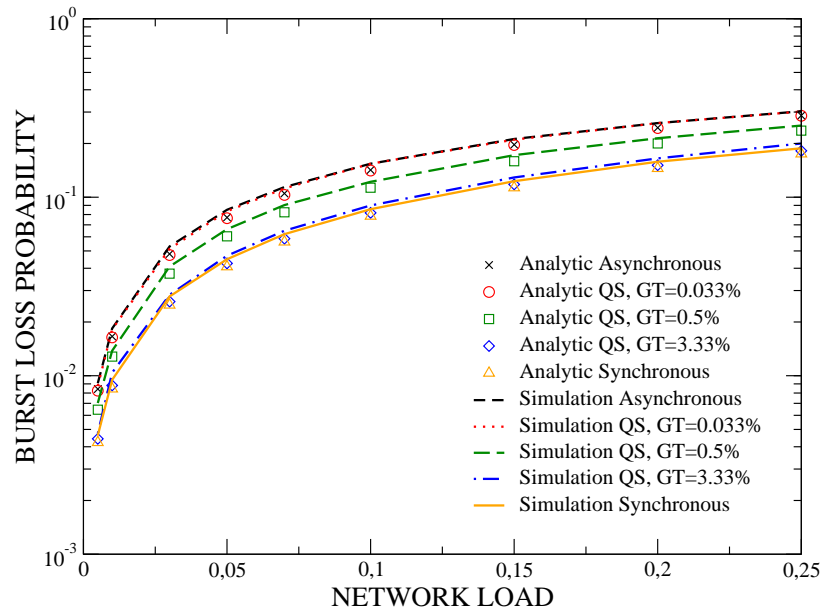
(a)
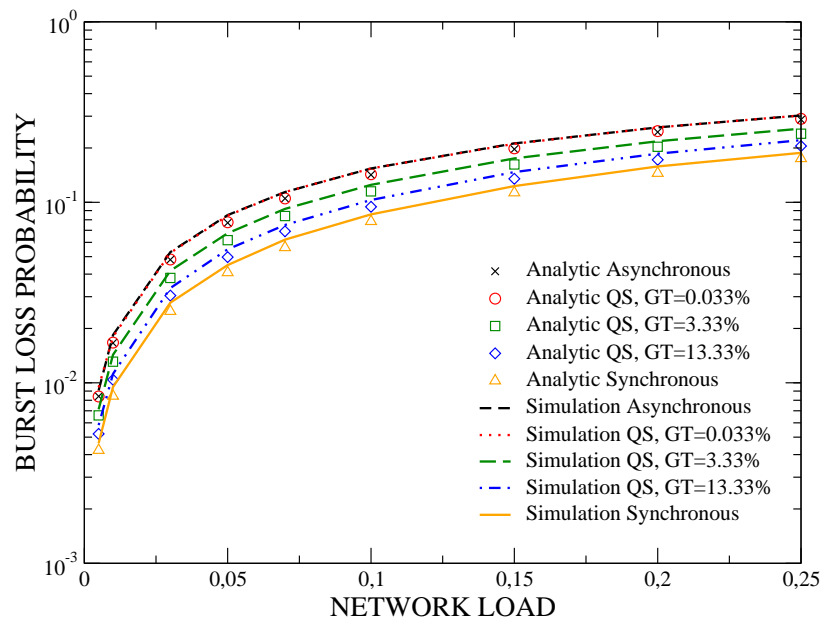
(b)

Figure 1.6: NSFNET analytic results with a drift equal to (a) 0.77%, and (b) 5%.

1.4.2 Evaluation of the time slot size

In the QS-OBS network both the time slot and guard-time size have strong influence on network performance results. Indeed, intuitively, one can remark that the larger the time slot, the smaller the influence of the (absolute) drift. Thus, whilst for the guard-time a trade-off between burst overlapping reduction and bandwidth utilization must be evaluated, for the time slot only a very large size would provide the optimality. However, the time slot size cannot be freely selected since other factors inherent to OBS networks must be taken into account. Indeed, the burst assembly algorithm performance as well as the basic guard-time already mentioned in Section 1.2 impact on the time slot dimensioning directly. Notice that, the burst assembly time is limited and large time slots may lead to inefficient resource utilization due to the incapacity of the burst assembler to produce large bursts in time. On the other hand, since the basic guard-time is required between every two consecutive time slots, a small time slot size would also compromise resource utilization. An evaluation of the optimal time slot size for the SynOBS network which takes into consideration the issue of both the burst assembly and the basic guard-time can be found in [55]. Since our main objective is to evaluate the impact that both the drifts and skews have on the QS-OBS network, the evaluation of both the burst assembly process and the basic guard-time is left out of the scope of this thesis. However, their consideration when determining the time slot size is certainly a subject for further research in the QS-OBS network.

In particular, here we assess the impact that the selection of the time slot size has on the overall QS-OBS network performance, in terms of the overall burst loss probability, considering several guard-time values. In order to do so, we conduct a series of simulations on the NSFNET network topology considering links are equipped with 16 wavelengths each and the load is set to $\rho = 0.5$. We assume two different drift scenarios, namely $\xi = 0.3\mu s$ (see Figure 1.7(a)) and $\xi = 0.9\mu s$ (see Figure 1.7(b)). The time slot sizes considered range from $5\mu s$ to $100\mu s$, and the guard-time values from 0% to 5% of the time slot size. The asynchronous and synchronous cases are used as performance references again. From the results obtained in both figures, it is easy to note that both factors together define a clear trade-off between drift correction (i.e., higher slot sizes benefit from larger guard-times) and resource utilization (i.e, larger guard-times increase the number of packets injected into the network). Whilst larger time slots require smaller guard-times to minimize the drift effect, smaller time slots struggle to reduce the drift impact unsuccessfully. Indeed, in such cases, no clear minimum is observed regardless of the guard-time value used, particularly in Fig. 1.7(b).

Hereinafter in this chapter, we consider a time slot value of $30\mu s$ (a maximum burst size value of $0.3Mb$ considering $10Gb/s$ links) since we assume that it provides a fair trade-off between the performance achieved and the requirements it imposes on both the burst assembler and the system (i.e., basic guard-time issue).

24
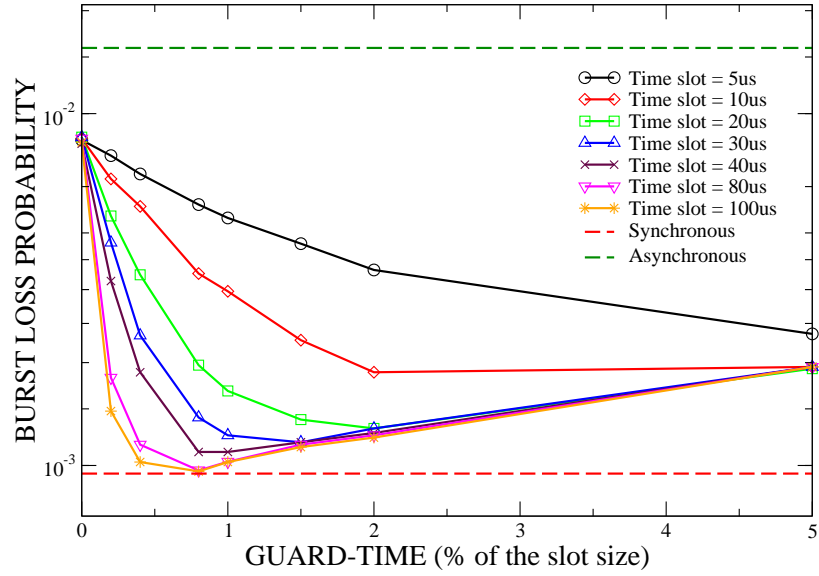
(a)
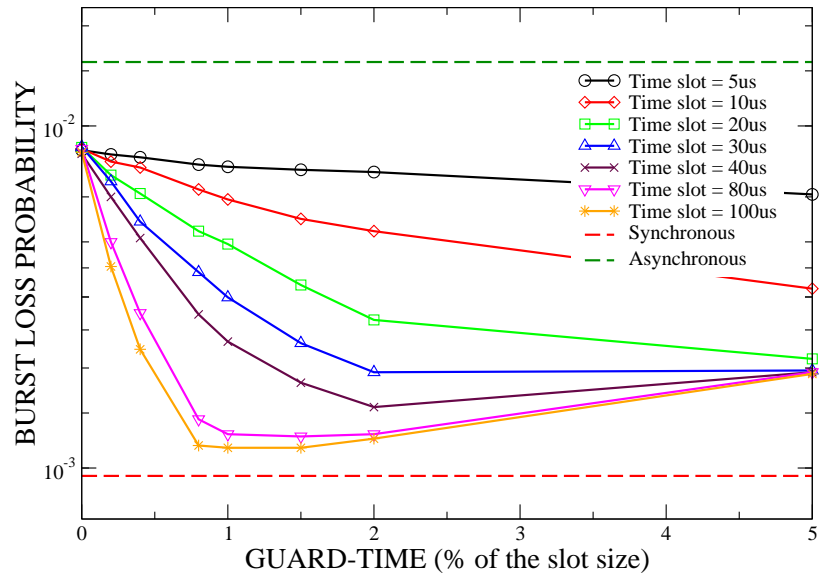
(b)

Figure 1.7: Time slot and guard-time evaluation for drifts generated by (a) $\xi = 0.3\mu s$, and (b) $\xi = 0.9\mu s$.

1.4.3 Optimal guard-time

In Section 1.3.2, we realized that a key factor for achieving the desired performance in the QS operation is the finding of an optimal value for the guard-time. This guard-time results in a clear trade-off between the reduction of the number of drift-based collisions (i.e., the increase of the guard-time reduces the probability of fulfilling condition (1.9)) and the increase of the number of overflow-based collisions (i.e., to maintain a constant load, a higher number of packets has to be injected into the network). To analyze the optimal value for the guard-time, we conduct several simulations in both the SIMPLE [56] (a network that consists of 6 nodes and 8 bidirectional links) and the NSFNET network topologies. In particular, we run a set of simulations in both networks considering a $30\mu s$ time slot and links equipped with $8, 16$ and 32 wavelengths. The results for the NSFNET network topology are presented in Fig. 1.8 under two different load scenarios, namely $\rho = 0.5$ and $\rho = 0.6$.

Figure 1.8 clarifies the concept of the guard-time trade-off aforementioned. It is easy to observe that the value of the guard-time cannot be freely increased since it implies strong performance degradation. It is also relevant the fact that by considering a higher drift, the minimum point moves to higher guard-time values (right hand side of the figure). From all the results obtained, we can conclude that under scenarios falling inside the typical OBS operating range (i.e., scenarios such that the network-wide burst loss probability $\in [10^{-3}, 10^{-6}]$), there exist an optimal range for the selection of the guard-time. Despite the fact that we present the results for ξ values up to $3\mu s$ (recall that ξ represents the standard deviation of the gaussian distributed drift model), we assume that this value, as mentioned in Section 1.4.1, should not exceed the $0.9\mu s$. Taking this fact into account, we plot in the figure the optimal range for the guard-time. We observed in further analysis not included here, that in such range the optimal value for the guard-time do not depend neither on the topology nor on the number of wavelengths or the load. It is interesting to see that in such optimal range there are only insignificant differences in the performance obtained. For these reasons, we select a guard-time value of $0.5\mu s$ (i.e., 1.67% of the slot size for a $30\mu s$ time slot) which implies a reduction of the fixed burst size to $0.295Mb$. Hereinafter in this chapter, we consider the $0.5\mu s$ guard-time as the optimal value for all $\xi \in [0.3\mu s, \ 1.5\mu s]$. Notice that the optimal guard-time range can also be spotted in Figures 1.7(a) and 1.7(b).

1.5 Evaluation of the skew impact

Reaching a perfect synchronization at the edge nodes, so that all have the same clock information all the time, is practically impossible. Therefore, we assume that there exist some skew amongst their clocks. In the next subsections, we first evaluate which is the impact of the skew in the performance of the QS operation, and later, we propose a novel scheme to reduce the negative impact of such skew.
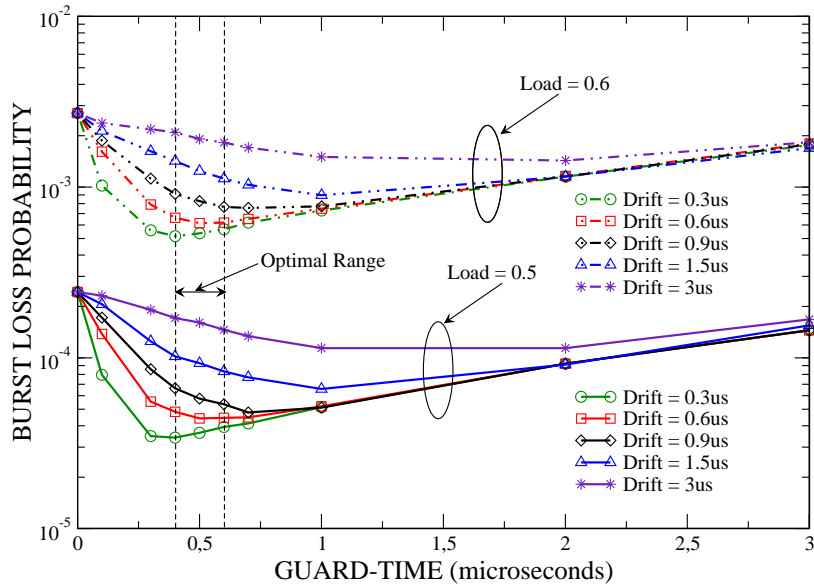
Figure 1.8: Optimal guard-time study.

1.5.1 Performance degradation due to skew

In order to evaluate the skew impact, we consider that each edge node has a clock information with a certain time deviation from their network counterparts. In particular, we assume that this time deviation can be considered constant in time within the $\mu s - ms$ scales (i.e., it changes at a larger time scale). In our model, we consider that (at a given time) each node has its own skew value; thus, we assign to each node a value generated according to a Uniform random distribution that can be defined as $U(0, \varphi)$, where φ represents the maximum skew value expressed in μs.

To evaluate the degradation introduced by the skew, we present in Figures 1.9(a) and 1.9(b) the results obtained under QS operation making use of the guard-time value obtained in Section 1.4.3, that is, a guard-time equal to $0.5\mu s$ (i.e., a burst size of $0.295Mb$ in a time slot of $30\mu s$). We consider drifts with ξ values ranging from $0\mu s$ to $0.9\mu s$. In the cases at hand, we assume links equipped with 16 wavelengths each and a network load equal to $\rho = 0.4$ and $\rho = 0.7$ respectively in each figure. In the x-axis we plot values of φ ranging from 0 to 15 μs (i.e., 50% of the slot size). Whilst the left y-axis displays the performance degradation in terms of the network-wide burst loss probability, the right y-axis gives a percentage figure that is computed according to the following formula:

$$Degradation[\%] = \frac{BLP_\varphi - BLP_{\varphi=0}}{BLP_{\varphi=0}} * 100 \tag{1.32}$$

where BLP_φ corresponds to the network-wide burst loss probability for a particular φ. For the sake of readability, in the Figures we only plot the performance degradation of the $0.6\mu s$ drift case.

27

As was to be expected, the performance of the QS operation is strongly worsened as a consequence of the presence of the skew. However, we noticed that there exist a region of interest for values of φ up to approximately $0.9\mu s$ of the slot size (referred to as safe region in both figures) where no degradation is observed (i.e., the performance obtained remains nearly flat) and up to $1.8\mu s$ for a 25% degradation. Therefore, our objective is to devise a solution able to permanently guarantee that the skew present in the network falls within that safe region or, at least, within acceptable performance levels (e.g., $1.8\mu s$ region).

1.5.2 Skew re-synchronization mechanism

In our study, we assume that the skew values may vary slowly and not faster than in minutes scale. In fact, external factors such as changes in temperature or a voltage drift could cause transitions in the skew values. Therefore, we must also guarantee that the devised mechanism achieves its objective within a time scale that is not affected by possible skew transitions within such high-order scales. In consequence, aside from reaching the re-synchronization of the network, this mechanism also has to achieve it within an acceptable convergence time (e.g., within the milliseconds scale).

We propose a novel re-synchronization mechanism adapted to OBS networks. The basis of this technique is an averaging scheme proposed in [50] for distributing well-aligned hardware clock throughout the physical extent of a synchronous processor. In fact, the averaging scheme, with minor variation, is used by many computer networks to maintain coherent notions of absolute time. The goal of this scheme is that all skew values converge to a common value. For our purposes, this final value is not significant and it is only the final uniformity that matters. In this simple scheme, the skew of each local clock is driven towards the average skew of its topological neighbors (i.e., nodes that are directly connected by a physical link to a particular node). In this way, when all nodes have the same skew, all driving forces are zero and a stationary point is reached. It is clear that, in order to execute this mechanism inside a network, an exchange of information is needed. To convey such information inside an OBS network, we take advantage of the burst control packets (BCPs). It is worth pointing out that contention between BCPs is generally neglected in OBS networks, and thus, the performance of the mechanism is not dependent on the load.

To explain our OBS-averaging scheme, let us first define L_x as the local clock reference at node x and $RTT_{y,x}$ as the round trip time between neighbor nodes y and x (we assume each node computes the RTT to its neighbors by sending periodic pings through the control channel). Node x includes the time information L_x in each of its BCPs. A node y is able to compute its current clock skew relative to node x as:

$$\delta(y,x) = L_y - \frac{RTT_{y,x}}{2} - L_x \tag{1.33}$$

The exact skew can be determined if all values in (1.33) are exact. However, some uncertainties
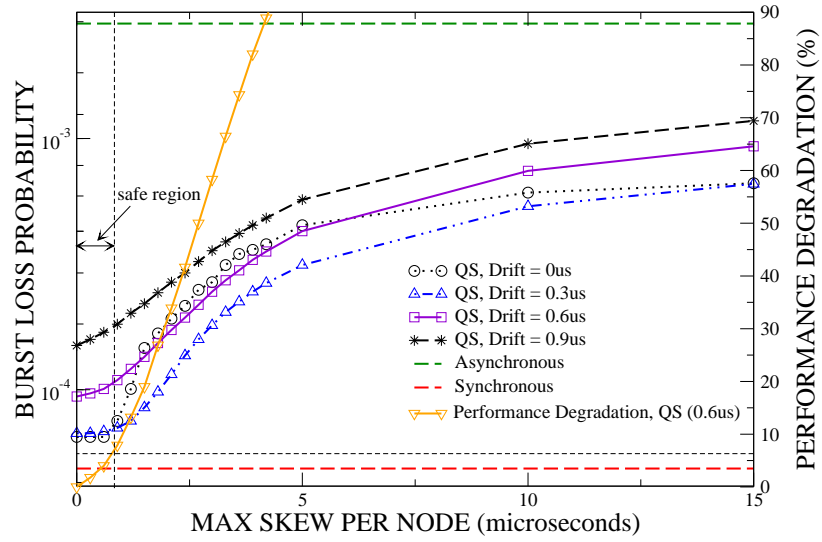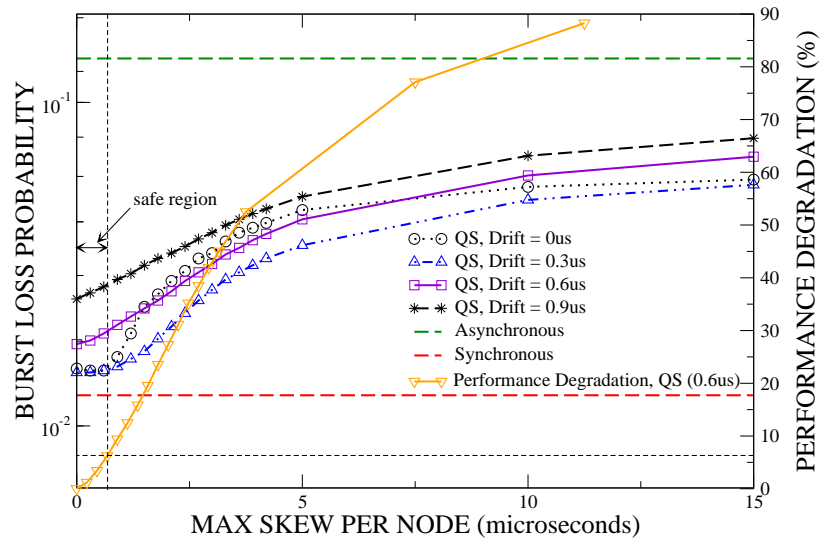
Figure 1.9: Skew impact on the QS-OBS network performance under a load of (a) 0.4, and (b) 0.7.

could be present, for instance, due to possible variations of the node processing time. This could introduce evaluation errors, and therefore, affect the synchronization process. Nevertheless, in Section 1.5.1, we show that a region of $0.9\mu s$ or even of $1.8\mu s$ is acceptable in the skew synchronization; thus, uncertainties causing errors that fall within such region do not impact negatively the entire process.

Once the network operation is started, each node x includes in every BCP it generates the following tuple:

$$< L_x, ID_x > \tag{1.34}$$

where ID_x is a unique identifier that is assigned to each different value of L_x, that is, every time L_x is updated, a new and different unique ID_x is assigned to L_x. This stamp is used to prevent a node from updating its local clock before it has updated clock information from all of its neighbors.

Figure 1.10 clarifies how the identifier is used. At any time node A receives a BCP coming from any of its neighbors, it extracts the carried tuple and updates the information concerning this neighbor. To store this information, node A maintains two databases with information related to each of the nodes constituting its set of topological neighbors $K = \{n_1, n_2, ..., n_{|K|}\}$, or in this particular example, $K = \{B, C, D\}$. The first one (upper left-hand side) stores the unique identifiers that are being received. The value of a unique stamp is updated if and only if the newly received value differs from the stored one. Accordingly, once an update of any identifier is performed, its corresponding time information is also updated in the second database (upper right-hand side). For the sake of clarity, we have not depicted how node A sends its ID_A to nodes B, C and D.

Hence, node A cannot update neither its L_A nor its ID_A until it has updated information from all of its neighbors. As shown in Figure 1.10, once A has a new identifier for all of its neighbors, it proceeds to update its local clock information according to the information stored in the time database (i.e., clock skews). Note that we illustrate an update on the identifier by replacing ID_A with ID'_A. In order to update L_A, node A performs the following two steps:

1. Skew average computation: $\triangle_A = \frac{1}{|K|} \sum\limits_{i=1}^{|K|} \delta(A, n_i)$

2. Local clock update: $L_A = L_A + \triangle_A$

In the event of a node not sending any control packet, which will prevent the mechanism to continue working properly (i.e., notice that nodes do not update their local clocks until they receive information from all neighboring nodes), our mechanism makes use of an additional time-out reference to avoid such a deadlock state and trigger an automatical re-start of the re-synchronization mechanism without taking that particular node into consideration.

In order to analyze the convergence properties of the mechanism, in this particular experiment, we consider the real length of the NSFNET network links. Hence, we have both correct information
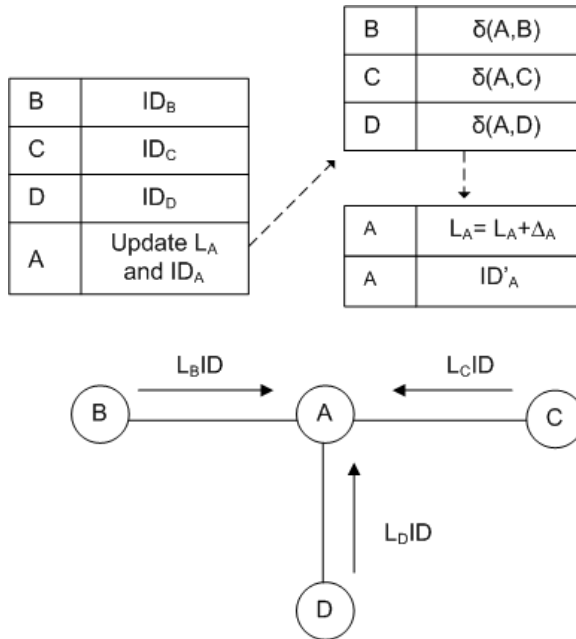
Figure 1.10: Unique identifer usage in the re-synchronization mechanism.

on propagation delays and a valid estimation of the convergence time. To point out that it is the uniformity that matters and not the final stationary point, we present in Figures 1.11 and 1.12 the results obtained using two different uniform distributions for the skew, namely $U(0, 10)$ and $U(0, 20)$. In the figures, each line represents the value of the skew in one of the nodes. In this two different cases, the stationary points are found at approximately $4.8\mu s$ and $9.7\mu s$ respectively. In spite of the difference found between them, in both cases a nearly perfect re-synchronization is reached at about $200ms$ after the mechanism is triggered. Note that this implies that the time-out, utilized to prevent that a node not sending any control packet alters the re-synchronization procedure, must be enough larger than this value and can be setup to 10 seconds for example.

As a conclusion, these results show that the skew effect can be completely erased from the network when our re-synchronization mechanism is effectively applied.

1.6 Deflection routing support in a QS-OBS network

In this final section, we present the results of the performance of the QS operation for OBS networks making use of the optimal guard-time value of $0.5\mu s$ (i.e., a burst size of $0.295Mb$) found in Section 1.4.3 and also considering that the skew impact in the network can be bounded to negligible values thanks to the re-synchronization mechanism presented in Section 1.5. However, this time, and in order to improve the performance of the synchronous strategies in front of the asynchronous one,
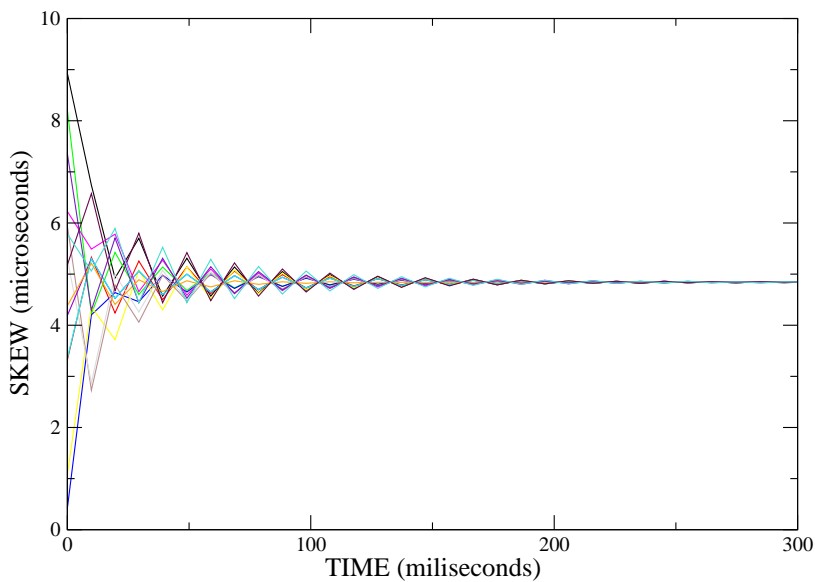
Figure 1.11: Convergence for skew values generated by $U(0, 10)$
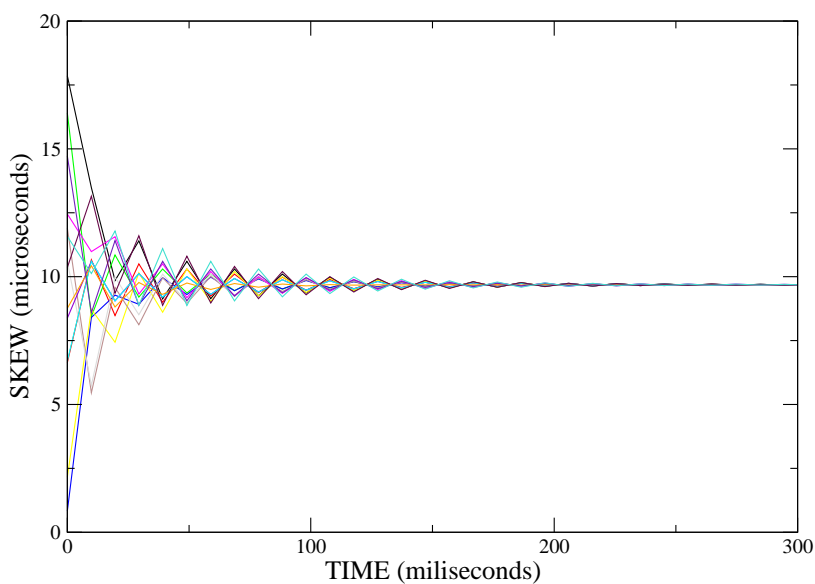
Figure 1.12: Convergence for skew values generated by $U(0, 20)$.

32

we consider routing algorithms that make use of effective deflection routing policies. To be precise, we evaluate the performance of the following deflection techniques: (1) load-based reflection routing algorithm (LBRR)[57](without resource pre-allocation); (2) reflection-based deflection routing (RDR)[58]; (3) multi-topology routing (MTR)[59]; (4) conventional deflection routing (DR)[60]. For comparison purposes, we use a time-to-live (TTL) field in the control packets that limits the number of hops a burst can undertake.

First, we analyze the behavior of the QS operation regarding the number of wavelengths in each link. For this purpose, we consider the LBRR algorithm under both 32 wavelengths (see Fig. 1.13(a)) and 64 wavelengths (see Fig. 1.13(b)) respectively. A reflection routing algorithm allows sending a contending burst towards a neighbor node (reflection neighbor) on the condition that this reflection neighbor, after receiving the burst, will intend to return the burst back or, in other words, reflect it. In this study, we set the maximum number of reflections a burst can undergo to 3. We provide the results for the QS operation under drifts corresponding to three different ξ values, namely $0.3\mu s$, $0.9\mu s$ and $1.5\mu s$. In the plot, the asynchronous and synchronous cases are included as benchmark indicators. As can be seen, even for high values of ξ, such us $1.5\mu s$, the improvement of the QS operation with respect to the asynchronous operation is noticeable in both cases. In fact, as the number of wavelengths increases (see Fig. 1.13(b)), the impact of the drift is substantially lessened (i.e., the more channels are available, the more chances a burst has to find a compatible drift). Therefore, the performance achieved by the QS operation becomes, inside the typical OBS operating range, approximately an order of magnitude, which is a very significant figure. It is also worth mentioning that, with the increase of the number of wavelengths, the performance gain of the synchronous case with respect to the asynchronous one is also significantly improved.

Second, we evaluate the performance of the QS operation with respect to both the asynchronous and synchronous cases considering all the aforementioned deflection routing algorithms. In order to fairly compare the different strategies, the TTL is set to 6 hops more than the shortest-path route. To be precise, since the MTR algorithm applied to the NSFNET network only allows undergoing a maximum of 3 deflections per burst (i.e., MTR divides the NSFNET topology into 4 different layers), we also set the maximum number of reflections a burst can undergo to 3 in the LBRR algorithm (i.e., the aforementioned 6 hops). In this case, the number of wavelengths per link is set to 32 and the load injected into the network to $\rho = 0.65$. This load value has been selected in order to obtain burst loss probability values which fall inside the typical OBS operating range. The results obtained are presented in Table 1.1. We also include the results obtained under shortest-path routing (SPR). In all the five different cases, the performance improvement obtained with the QS operation (considering a drift with $\xi = 0.3\mu s$) is higher than a 77%, and in some cases, approximately an order of magnitude (e.g., LBRR and RDR algorithms). Notice that the benefit is slightly less under the SPR algorithm. It is, hence, possible to achieve significant improvements when the QS transmission mode is used together with effective deflection routing techniques.
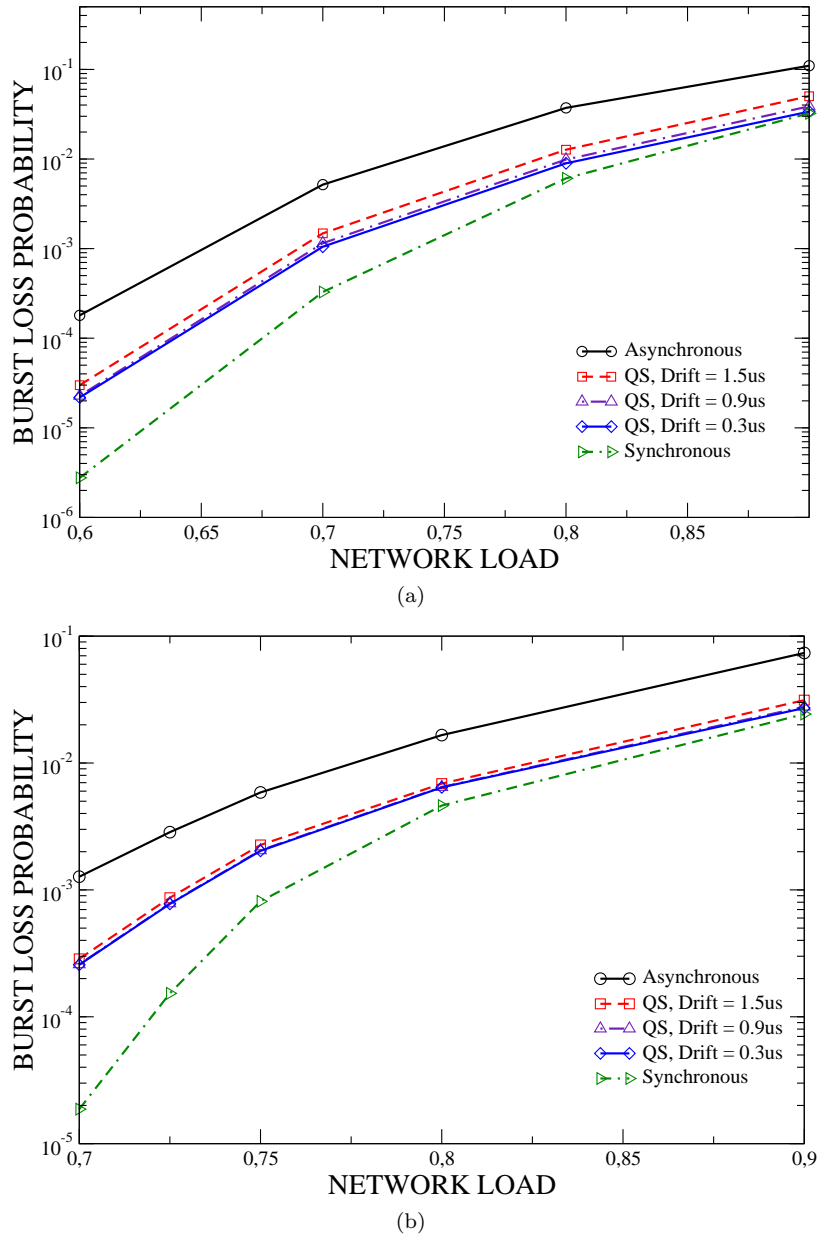
Figure 1.13: QS performance using the LBRR algorithm with (a) 32, and (b) 64 wavelengths.

Routing algorithm	Asynchronous	QS $(0.3\mu s)$	Synchronous
SPR	$6.33 * 10^{-3}$	$1.60 * 10^{-3}$	$1.30 * 10^{-3}$
DR	$7.74 * 10^{-4}$	$1.76 * 10^{-4}$	$2.19 * 10^{-5}$
MTR	$4.08 * 10^{-4}$	$7.94 * 10^{-5}$	$2.82 * 10^{-5}$
LBRR	$1.33 * 10^{-3}$	$1.94 * 10^{-4}$	$3.18 * 10^{-5}$
RDR	$9.37 * 10^{-4}$	$1.45 * 10^{-4}$	$5.57 * 10^{-6}$

Table 1.1: Performance comparison between the asynchronous, synchronous and QS transmission modes.

1.7 Summary

In this chapter, we have proposed the novel QS operation mode for OBS networks aiming to achieve performance results close to those obtained with perfect synchronization. We contrasted the architectural benefits and requirements of the QS scheme with those of the synchronous one. We also showed that with the use of effective deflection routing techniques the performance improvement of the synchronous mode with respect to the asynchronous one is brought to a very interesting range. Therefore, the idea of devising a novel architecture, without the technical requirements imposed by the perfectly synchronized case, such as our QS operation mode, gains momentum.

For this purpose, we considered two different sources of time deviation in our QS-OBS scenario, namely skew and drift. We developed an analytic model to test the performance of the QS operation in both an isolated node and the NSFNET network topology. The model presented is exact for the case that the drifts are exponentially distributed. Through numerical examples and with the use of a more realistic distribution of the drifts, an optimal range for the selection of the optimal guard-time value was found. We also observed that within the region of interest such value is not dependent on any network parameters. In order to correct the skew effect, we proposed an averaging scheme that effectively limits the impact of this time phenomenon. Thanks to this scheme, the performance of the QS operation remains unaffected. Eventually, we performed a set of simulations to study the behavior of the QS approach when deflection routing policies are applied.

The main benefit of the proposed QS transmission mode is the significant improvement attained with respect to the asynchronous mode in terms of the overall burst loss probability. In the specific examples considered in this chapter, improvements as high as an order of magnitude have been observed when the QS transmission mode is used together with effective deflection routing algorithms.

Chapter 2

Modeling of a T-SWS network architecture

2.1 Translucent networks: A step-wise roadmap evolution

Over the last years, optical transport networks (OTNs) have been undergoing an architectural evolution from traditional *opaque* toward *transparent* architectures. The two main driving forces behind such re-definition are, on the one hand, network operators' aim for lowering both capital and operational expenditures (CAPEX/OPEX), and, on the other, several key optical technology breakthroughs, which provided relevant improvements in the main optical signal functions and boosted the implementation of integrated transmission and switching sub-systems at the physical layer [61].

In order to provide the required quality of transmission (QoT) network performance, current opaque network architectures rely on electrical 3R regeneration (hereinafter regeneration) at every node [30], that is, each transmission is a point-to-point connection, and hence, each node is a regenerator site/location with as many regenerators as connections being switched. Such an architecture does nevertheless not represent a scalable model for next-generation OTNs. Indeed, considering both the ultra-fast pace at which traffic is growing, and the fact that the impact of regeneration strongly depends on several data transmission parameters such as the line rate and the modulation format, it is clear that the opaque concept poses serious scalability problems regarding, among others, heat dissipation, power-consumption, physical space, and costs [61]. Obviously, these issues did not scape the attention of network designers/architechts which quickly realized the potential for significant cost, footprint, and power savings by minimizing the number of regenerations required to guarantee proper end-to-end signal QoT performance in OTNs. Consequently, whilst the opaque architecture is bound to succumb to its inherent costly, power-consuming regeneration process, the transparent network approach has gathered great momentum over the last decade.

Transparent optical networks propose a networking paradigm where data signals remain in the optical domain for the entire end-to-end path, thereby eliminating from the network the costly regeneration devices [29]. However, what makes it so attractive is the fact that, in its strictest sense, transparency means that the transmission of optical signals in the network is performed independently of the protocol, bit rate, or the framing structure used. Note that such property does not hold when regenerators are used, as they rely on standardized digital frames and require intelligent control functions to be performed at the electrical domain. Hence, a transparent network is a highly flexible, scalable architecture that can seamlessly support the future novel traffic types and bit-rates associated with the emerging bandwidth-hungry applications and services.

For these very reasons, the deployment of transparent networks is seen as both the natural choice and conceptually ideal for next-generation OTNs; however, as of now its most basic concept can only be supported under the assumption of either an ideal physical layer or availability of all-optical 3R regenerators. First, the assumption of ideal conditions at the physical layer has been widely used in the literature, and it is indeed useful, for example, for the study and development of traffic engineering algorithms. This approach is nevertheless not valid when dealing with network design/planning problems, as QoT signal performance is actually adversely affected by physical layer impairments (PLIs) [31]. Second, despite the fact that all-optical 3R regeneration has been and is the focus of intensive research (see e.g., [62], [63], [64]), it is not mature enough yet, and cannot be considered as a viable/practical solution, at least in the short-medium term [65].

As a matter of fact, it has precisely been the tremendous advances in the field of optical research what has brought to light the serious impact that PLIs have on the signal QoT. Novel optical systems and devices allowing for longer transmission distances, higher bit-rates, and more closely spaced wavelength channels, have dramatically increased the sensitivity to PLIs, which accumulate and severely degrade the optical signal along its way from source to destination [66]. Consequently, PLIs limit optical reach, thereby hampering the deployment of transparent optical networks. To go beyond this optical reach is therefore necessary for the optical signal to undergo regeneration. Note that the optical reach depends on the network equipment considered, with longer reach generally entailing higher equipment cost (e.g., amplification, transmission). Hence, the optical reach results in a trade-off between CAPEX and OPEX savings due to a reduced number of regenerators being deployed, and the CAPEX increase required to achieve longer optical reach [67].

According to this last discussion, the deployment of transparent networks is halted until all-optical 3R regenerators become available. Therefore, to continue moving forward in the evolution, there is the need for an intermediate network architecture able to bridge the gap between the opaque and transparent solutions. As shown in Fig. 2.1, this intermediate step in the evolution of OTNs is called *translucent* network ([31],[33]). Translucent networks combine features of both opaque and transparent networks allowing regeneration only at selected points in the network, that is, in a translucent infrastructure all nodes are not regenerator locations but only a subset of them.
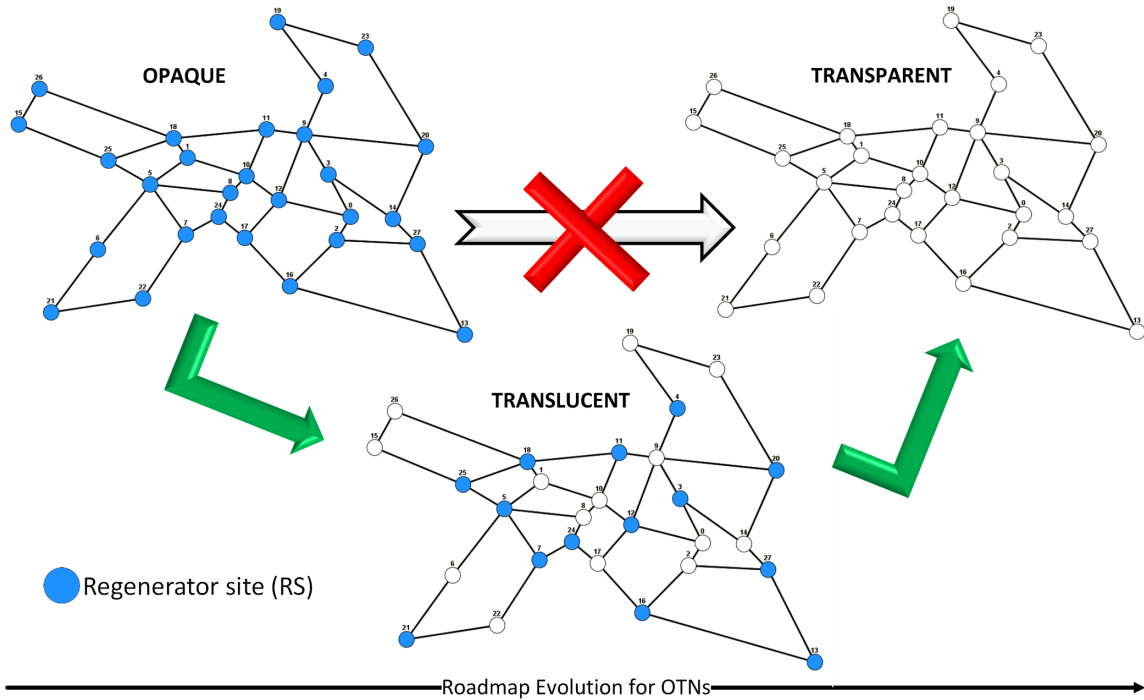
Figure 2.1: A Step-Wise Roadmap Evolution for OTNs

Since regeneration devices are both expensive and power-consuming, translucent networks are really attractive to network operators, which strive for cost-effective, power-efficient architectures, and as a result, the deployment of translucent optical networks is nowadays considered a very promising short term solution to decrease costs and power consumption in OTNs.

2.2 Designing a T-SWS network architecture

The design of a translucent network results in a network planning/dimensioning problem where the identification of the optimal trade-off between network construction costs (i.e., regeneration devices are costly) and service provisioning performance (i.e., a target network QoT performance must be met) is of great importance. For this reason, it is clear that a careful engineering of both the routing problem and techniques to minimize whilst, at the same time, strategically locate regenerators (i.e., decide which nodes are regenerator locations) is crucial to the success of translucent architectures. This scenario gives rise to the regenerator placement (RP) problem ([33], [68]). In addition, recent studies in wavelength switched optical networks (WSONs) have shown that better network performance can be achieved if routing and wavelength assignment (RWA) constraints are incorporated into the RP problem, thus solving the routing and regenerator placement (RRP)

problem. However, both the RP and RWA problems as well as the joint RRP are proven to be *NP*-complete constrained optimization problems [68]. For this reason, and due to the technological maturity of translucent WSONs, heuristic approaches to tackle the joint RRP, under the WSON context, have been the focus of intensive research over the last years (see e.g.,[69], [65], [34], [70], [71]). In fact, a couple of years ago, a standardization activity started within the *common control and measurement plane* (CCAMP) working group [34], which belongs to the *internet engineering task force* (IETF).

In the context of SWS networks, however, this is not the case as, thus far, most of the research efforts on SWSNs have been geared towards evaluating the opaque and transparent architectures. Considering any of these two network scenarios allows one to neglect the impact of PLIs, thereby notably simplifying the design and operation of OBS. Indeed, as long as realistic core node parameters (e.g., node degree, and link and wavelength capacity) are considered, the optical signal degradation between two neighboring core nodes is not an issue [72]. Unfortunately, as discussed in Section 2.1, the high cost of regenerators on the one hand, and the lack of mature optical technology able to perform fully optical 3R regeneration on the other, hamper the deployment of these architectures. As a result, there is no way to neglect the severe impact that PLIs have on the performance of SWS networks, and the design of cost-effective, power-efficient translucent SWS networks has nowadays become a rising challenge for the research community.

Recently, however, as a result of the increasing interest on assessing the effect of the PLIs on optical networks, we find few interesting works that involve the PLI constraint in the evaluation of SWS networks performance. For example, in [73] the authors deal with a OBS scheduling method which incorporates the impairments constraint, and in [74], several impairment-aware algorithms to provide manycasting services in OBS networks are proposed. However, the most interesting work regarding PLIs in SWS networks can be found in [72], and its complementary study [75]. In both papers, the authors present an extensive analysis and evaluation of the design and maximum size and throughput of OBS core nodes. To this end, authors consider the effects of a range of PLIs such as amplifier noise, crosstalk of WDM channels, gain saturation and dynamics. Nonetheless, the authors focus on an opaque SWS network where all nodes are equipped with regenerators, one per each wavelength, which are also responsible for performing wavelength conversion.

Over the next sections, we propose, for the first time to the best of our knowledge, a complete translucent SWS (T-SWS) network architecture which successfully mitigates the impact of PLIs. To this end, we first model and evaluate a feasible (i.e., with commercially available or at most lab trial devices) all-optical SWS network which has regenerators available at selected nodes; secondly, we propose and evaluate two distinct RRP heuristics, which are specifically tailored to suit the requirements of SWS-based networks.

Here it is worth pointing out that the proposed RRP algorithms require QoT estimator to account for the accumulation of the PLIs along the path and, by this means, determine the feasibility of the

path. In the literature, there are two main QoT estimators [76] based on the numerical calculation of the optical signal to noise ratio (OSNR) [77] or on the computation of the Q-factor value either by means of analytical formulas [78] or numerical interpolation and laboratory measurements [79]; both these figure-of-merit have a direct relation to the signal bit-error-rate (BER) [54]. Although in this work any QoT estimator can be used, in this thesis we adopt the OSNR as the main signal QoT performance indicator, and hence, hereinafter in this thesis we refer to QoT_{th} as OSNR_{th}.

2.2.1 T-SWS network model

In this section, we provide extensive details on the proposed translucent SWS network model. First, we specify an all-optical SWS node architecture which incorporates a limited number of shared electrical regenerators. Second, we present the analytic model that we consider for the calculation of the OSNR level. Finally, a power budget and noise analysis of the characteristic signal path between two adjacent SWS nodes are provided.

Node architecture

The node architecture here presented is based on the model proposed in [72], which initially assumes an opaque operation. To be precise, the authors present two semiconductor optical amplifier (SOA)-based node architectures for SWS networks, namely broadcast-and-select (BAS) and tune-and-select (TAS). Both architectures rely on the SOA technology and on wavelength converters performing regeneration as their fundamental switching modules. SOAs acting as switching elements (SW-SOA) bring some interesting advantages such as high on/off ratios and high loss compensation characteristics. Despite this, however, SOA technology also entails some non-desirable effects such as power consumption, noise and nonlinearity that must be taken into account during the node design process. Among these architectures, the authors conclude that TAS is more appropriated for SWS networks because BAS displays some major drawbacks (e.g., high power requirements and large inter channel crosstalk) inherent to its architecture.

In this thesis, we modify the aforementioned opaque TAS SWS core node architecture by replacing each inline electrical wavelength converter with a block consisting of a tunable laser and a wavelength conversion-type SOA (WC-SOA) device. Hence, this modified, generic TAS SWS node architecture (depicted in Fig. 2.2) is able to perform an all-optical switching operation. The node consists of N input/output fibers with M channels each and a limited number R of regenerators available. After the signal is amplified by the Erbium-Doped Fiber Amplifier (EDFA) pre-amplifier at each node input port, it is demultiplexed and passes through a fixed-input and variable-output WC-SOA. Then, the signal is split into $N + 1$ branches, one per each fiber plus an extra branch that allows the access to the regenerator pool, which consists of a set of R fixed receivers, an electrical buffering stage and a set of R lasers emitting in predefined wavelengths (i.e., $\lambda_1, ..., \lambda_R$). The signal is then transported to the output ports of the node following the decisions of the SWS node controller by
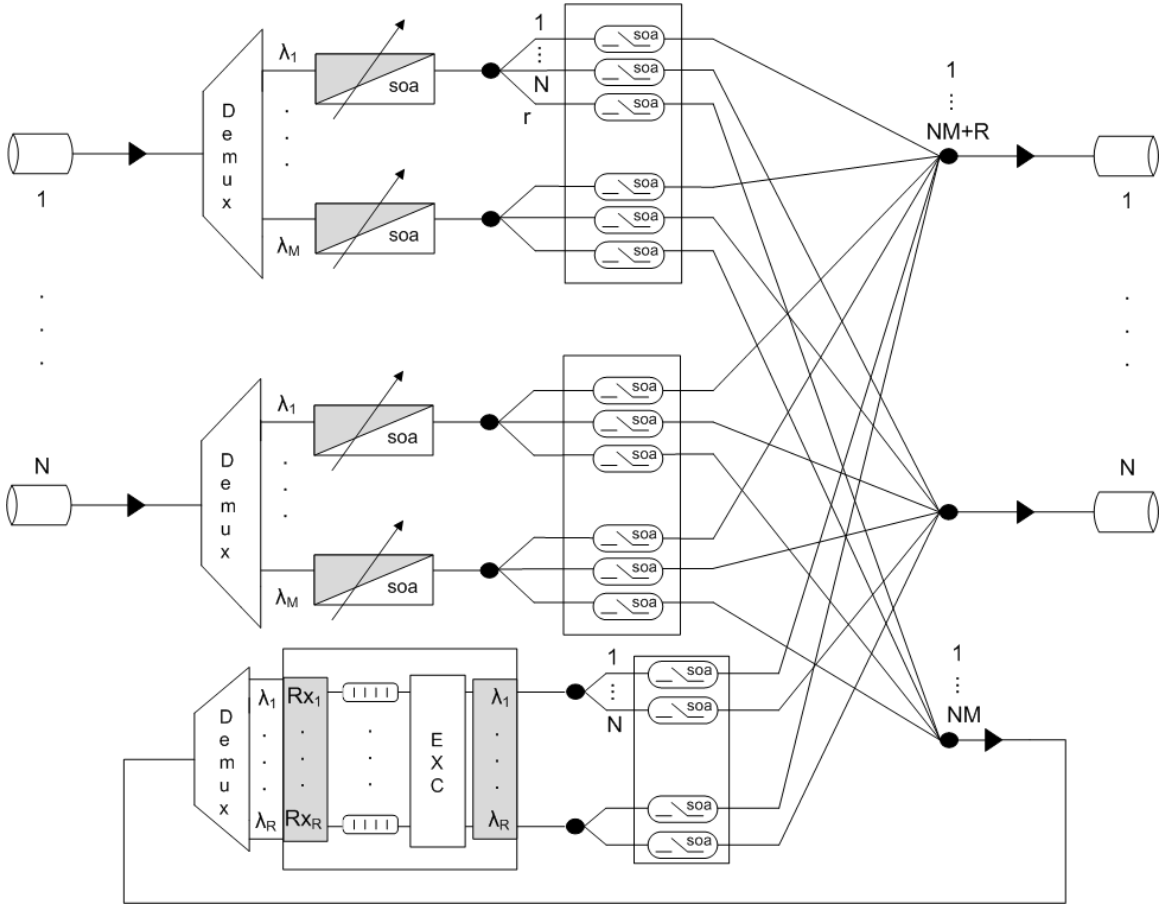
Figure 2.2: T-SWS node architecture

turning the SW-SOAs either ON or OFF. After the combiner stage, an EDFA booster amplifier provides the signal with enough power to cope with the losses of the first fiber span. Note also that, in this case, the combiners behind the SW-SOAs port merge $NM + R$ signals at each output port as a consequence of the presence of the regenerator pool.

It is worth mentioning that since the output of the WC-SOA is handled by the SWS node controller, all wavelengths from all input ports have the same privileges when requesting a regenerator, and thus, fairness in the access to the regenerator pool is provided by this architecture.

In the following sections, we evaluate the performance of the proposed node architecture by means of an OSNR model.

OSNR model

In this OSNR model, the impact of PLIs is captured by considering the power of both the signal and the noise, which are affected by different gains and losses along the path, at the destination

node. This model considers the ASE noise introduced by both the EDFA and SOA amplifiers as well as the splitting and attenuation losses as the significant signal impairment factors [77]. In the literature, OSNR is generally defined as the ratio between the signal channel power and the power of the ASE noise in a specified bandwidth (e.g., $0.1nm$ are usually taken by convention). For instance, for a transparent WSON, an OSNR model is proposed and evaluated in [80], and it is experimentally validated in [77]. Thus, all packets arriving at the destination node with an accumulated OSNR value lower than the predefined quality threshold (i.e., $OSNR_{th}$) cannot be read correctly, and thus, are discarded. Although ASE noise is commonly considered as the most severe impairment limiting the reach and capacity of optical systems, it should be noted that in the context of SWS networks, non-linear impairments mainly arise due to the ultra-fast ON-OFF switching nature of packet rate traffic, which causes the signal power of every single channel to constantly vary. These power variations strongly impact system performances. For example, on the one hand, signal degradations in a packet caused by neighboring packets which co-propagate simultaneously over several common links (e.g., Cross-Phase Modulation (XPM)-induced crosstalk) and, on the other, OSNR degradation due to dynamic power fluctuations generated by gain changes in amplifiers. Indeed, WDM packet channels randomly switched ON and OFF may be a problem when considering amplifier dynamics. This problem was studied in [81], and it was shown that EDFA amplifiers implemented in a simple and all-optical configuration known as optical gain-clamped can reduce output power excursions by effectively limiting gain ripples. In this thesis, non-linear impairments are taken into account by adding an OSNR penalty to $OSNR_{th}$. To be precise, we consider that the OSNR threshold is determined by [77]:

$$OSNR_{th} = OSNR_{min} + OSNR_{pen} \tag{2.1}$$

where $OSNR_{min}$ represents the OSNR tolerance of the receiver, and $OSNR_{pen}$ accounts for the OSNR penalties due to maximum tolerable Polarization Mode Dispersion (PMD), residual Chromatic Dispersion (CD), and all the other non-linearities. We consider that the $OSNR_{pen}$ margin is configured by the network operator according to the transmitted signal bitrate, modulation format, etc. [77]. For the systems for which the impact of non-linear impairments is dominant, either larger values of $OSNR_{pen}$ should be setup, with a possible impact on the network performance (see Chapter 5 for details on this issue and others related to the configuration of $OSNR_{th}$), or more accurate and computationally efficient analytical models to capture dynamic PLIs have to be developed.

To quantify the OSNR degradation along the optical path, we define the optical path OSNR (P_{osnr}) by adapting the model described in [82]. Specifically, the OSNR consists of two main components, namely the link and node OSNR that we denote as L_{osnr} and N_{osnr} respectively. Since a link is composed of several amplifier spans, each ending with an in-line EDFA amplifier, the longer the path the higher the impact of the ASE noise in the OSNR received. Similarly, to minimize the ASE effect caused by the internal node amplifiers, gain values should be designed such that each

node presents an OSNR level as high as possible. We can compute P_{osnr} for an optical end-to-end path traversing k links by using the following equation [82],

$$P_{osnr} = 1/(\sum_{i=1}^{k} \frac{1}{L_{osnr}^i} + \sum_{i=1}^{k} \frac{1}{N_{osnr}^i}), \tag{2.2}$$

where for a link consisting of r amplifier spans, L_{osnr}^i is defined as follows,

$$L_{osnr}^i = 1/(\sum_{j=1}^{r} \frac{1}{AS_{osnr}^j}), \tag{2.3}$$

where AS_{osnr}^j is the amplifier span OSNR, which can be calculated as,

$$AS_{osnr}^j[dB] = P_j[dBm] - QN[dBm] - F_j[dB] - G_j[dB], \tag{2.4}$$

where P_j, QN, F_j, G_j, correspond to the output power after the jth amplifier span, the quantum noise, the noise figure and the gain of the jth amplifier (i.e., either EDFA in-line or pre-amplifier) respectively. The expression that we use to compute N_{osnr} is equal to the one that we have defined for AS_{osnr}, however, due to the presence of several components (e.g., amplifiers, splitters and combiners) in our translucent node, both an equivalent noise and gain figure, namely F_{eq} and G_{eq} respectively, have to be derived.

In the next subsection, we provide specific values for all these figures by considering performance parameter values obtained from datasheets of commercially available or lab trial devices (see e.g., [83], [84], [85]).

Power budget and noise analysis

We consider the power and noise constraints together in order to evaluate the OSNR of a signal that follows the characteristic path between two TAS neighboring nodes depicted in Fig. 2.3. Component specifications are provided in Table 2.1 and the power constraints for this analysis are: the output power of the node (i.e., output of the EDFA booster amplifier) set to 0dBm/channel, and its input power (i.e., input of the EDFA pre-amplifier) set by link losses to -16dBm/channel.

From (2.4) and bearing in mind that the objective is to have a N_{osnr} as high as possible, it can be inferred that both F_{eq} and G_{eq} must be designed so that their resultant values are minimized. For this particular case, the equivalent noise and gain figures of the TAS node are obtained as follows,

$$F_{eq} = F_{wc-soa} + \frac{MF_{sw-soa} - 1}{\frac{G_{wc-soa}}{L_{splitter}}} + \frac{F_{edfa-booster} - 1}{\frac{G_{wc-soa}G_{sw-soa}}{L_{splitter}L_{combiner}}}, \tag{2.5}$$

$$G_{eq} = \frac{G_{wc-soa}G_{sw-soa}G_{edfa-booster}}{L_{splitter}L_{combiner}}. \tag{2.6}$$

Channels (M)	32	
Span length	65km	
Fiber attenuation	0.2dB/km+3dB (cable margin)	
Quantum Noise	-58dBm	
EDFA (pre-amp)	noise figure	5.5dB
	max. gain	20dB
	max. output power	13dBm
	min. input power	-30dBm
EDFA (booster)	noise figure	5.5dB
	max. gain	15dB
	max. output power	18dBm
	min. input power	-15dBm
EDFA (in-line)	noise figure	5.5dB
	max. gain	25dB
	max. output power	18dBm
	min. input power	-25dBm
WC-SOA	noise figure	9dB
	max. gain	16dB
	max. output power	5dBm
	min. input power	-25dBm
SW-SOA	noise figure	10dB
	max. gain	10dB
	max. output power	3dBm
	rise-fall time	500ps
WDM Demux	insertion loss ($M = 32$) (≈ 5.5) dB	
Splitter	insertion loss (0.5-1) dB	
Combiner	insertion loss (1.5-2) dB	

Table 2.1: Parameter values considered
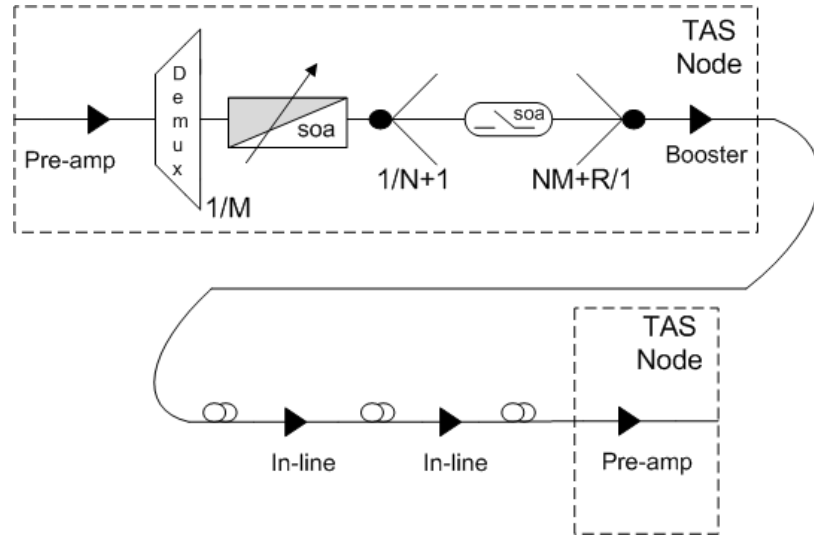
Figure 2.3: Signal path between two TAS OBS core nodes.

The most critical point is the combiner where, in the worst case, the ASE noise power from M SW-SOAs is merged. Both the pre-amplifier and booster EDFAs, and the WC-SOA and SW-SOA have to be used to compensate the internal losses. Their gain values must be carefully designed so that both equivalent figures are minimized and the power constraints are respected. In order to minimize F_{eq}, it can be deduced from (2.5) that, as long as the saturation output power is not reached, it is better to set the gain on the WC-SOA. In this way, the impact of the M ASE powers is reduced. The EDFAs pre-amplifier and booster and SW-SOA gains, by contrast, are kept as low as allowed by the system power requirements. The exact set up for each component depends on the number of input/output ports of each particular node, which eventually define the splitting losses that are to be covered by G_{eq}.

In Fig. 4.6, we show the result of the application of the OSNR model presented considering the optical end-to-end paths of the Pan-European core transport network in three different topology configurations (Large, Basic, and Core), a German backbone topology, and an American backbone network (Usa-Can). See Appendix A for the simulation details. All network paths are computed making use of the routing algorithm presented in Section 2.3. One can observe that, with the exception of the German topology, the length, and thus, the number of amplifier spans, have a strong impact on the received OSNR. In the German network, which is characterized by much shorter links and by a high number of nodes (see Appendix A), by contrast, it is the number of intermediate nodes what has the greater impact on the OSNR figure.

One can note that all paths whose OSNR at the receiving end is below OSNR_{th}, (i.e., beyond the receiver's sensitivity) will require regeneration at some point along their way from source to destination. These paths are the input data for the RRP algorithm used to deploy the required
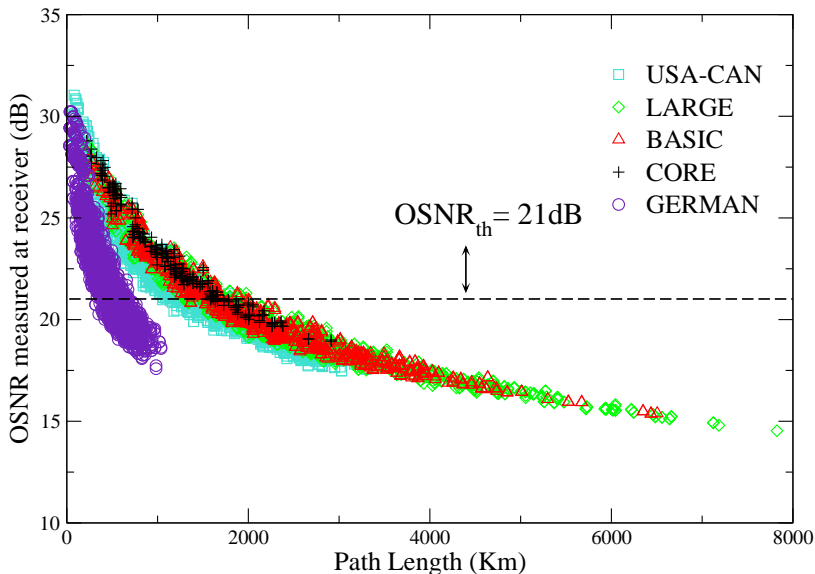
Figure 2.4: OSNR evaluation for some European and American network end-to-end optical paths.

regenerators.

Being the T-SWS network architecture and the network model used to capture the impact of PLI described, the next section is devoted to performing a preliminary performance evaluation through the use of two distinct heuristics for the placement of sparse signal regenerators in the network (i.e., RRP algorithms). Note that the study here presented follows an off-line approach since RRP decisions are taken during the network planning stage. The consideration of a dynamic traffic matrix, by contrast, would result in the evaluation of an on-line problem, and issue which is left out of the scope of this thesis.

2.3 A first approach to RRP in SWS networks

In this section, we focus on the RRP problem in a translucent SWS network. It must be noted that the use of classical RP or RRP algorithms for WSON networks is nevertheless not viable for SWSNs due to their statistical multiplexing nature. Indeed, in contrast to WSONs, where there exists a one-to-one correspondence between a path and a regenerator, in a SWS network, regenerator resources are statistically shared (i.e., according to their timely availability) by all packets requiring regeneration. Indeed, in SWS networks, RRP extends to, what we call, the routing and RP and dimensioning (RRPD) problem. Being the routes to be followed by each flow of packets computed, and the locations for regenerator pools selected (RP), the final dimensioning phase (D) is responsible for calculating the minimum amount of such regenerators so as to meet a pre-defined target QoT

46

network performance. In this first approach, and for the sake of simplicity, we tackle RRPD by proposing a three-step process as described in the following sections.

It is also worth pointing out that since we are addressing an off-line strategy, we can assume that the RRPD algorithm disseminates both the routing and regeneration information to all network nodes so that they are able to determine, for each incoming flow of packets and according to the respective packet headers, the corresponding output port and whether such flow has to be regenerated. We begin by presenting the design assumptions and by introducing the corresponding notation.

2.3.1 Notation

We use $\mathcal{G} = (\mathcal{V}, \mathcal{E})$ to denote the graph of a SWS network; the set of nodes is denoted as $\mathcal{V}$, and the set of unidirectional links is denoted as $\mathcal{E}$. Let d_e denote the length of link e.

Let $\mathcal{P}$ denote the set of predefined candidate paths between source s and termination t nodes, $s, t \in \mathcal{V}$, and $s \neq t$. Each path $p \in \mathcal{P}$ is identified with a subset $p \subseteq \mathcal{E}$. Let $\delta_p = \sum_{e \in p} d_e$ be the length of path p. Let s_p and t_p denote the source and termination nodes of p. Let $\mathcal{V}_p$ denote the set of intermediate nodes, that is, excluding s_p and t_p, on path p.

Let $\mathcal{D}$ denote the set of demands, where each demand corresponds to a pair of source-termination nodes. For each demand $d \in \mathcal{D}$, $h_d \in \mathbb{R}_+$ denotes the volume of packet traffic.

We assume the network operates with explicit source routing. Let $\mathcal{P}_d \subseteq \mathcal{P}$ denote the set of candidate paths supporting demand d; $\mathcal{P} = \bigcup_{d \in D} \mathcal{P}_d$. Each subset $\mathcal{P}_d$ comprises a (small) number of paths, for example, k shortest paths. We consider single-path routing and, accordingly, only one path $p_d \in \mathcal{P}_d$ is selected as the valid path to be followed by all packets belonging to demand d. Let $\mathcal{Q}$ denote the set of valid paths, $\mathcal{Q} = \{p_d, d \in \mathcal{D}\}$.

Let $\mathcal{K}_d$ denote the set of nodes where the regeneration is performed on valid path p_d. Let k_v indicate the number of paths requiring regeneration in node $v \in \mathcal{V}$; note that the value of k_v is subject to changes during the algorithm procedure.

2.3.2 The RRPD framework

As aforementioned, in this preliminary evaluation of the T-SWS architecture we tackle the RRPD problem by decomposing it into three main phases.

The first two phases are the *routing* (R) and the *regenerator placement* (RP). They are sequentially executed and iteratively, for each demand $d \in \mathcal{D}$. The result of this step is the set of valid routing paths $\mathcal{Q}$ and, for each $d \in \mathcal{D}$, the set of nodes $\mathcal{K}_d$ in which the regeneration of an optical packet, when sent on path p_d, has to be performed. Although the order of the iteratively processed demands may result in different solutions, still we observed that the algorithm performance does not vary significantly. Thus, we consider an arbitrary order. The last phase is the *regenerator pool dimensioning* (D). Having found valid paths and regeneration nodes, this step determines the number

of regenerators to be installed in these nodes.

Below we present the details of the algorithm subroutines.

Routing phase

In the routing phase the algorithm makes a decision on the selection of (single) path p_d from the set of candidate paths $\mathcal{P}_d$. We study the performance of two different methods. Whilst in the regenerator grouping-oriented (RG) policy the routing decision is biased toward those paths containing the largest amount of regenerators installed, the link congestion reduction-oriented (LCR) selection is purely based on packet contention minimization. The primary objective of this initial evaluation of the T-SWS architecture is to see whether introducing RP data into the routing problem (as the RG selection does) pays off or not. Note that while the RG selection represents a joint RRP method (as RP decisions do have impact on the subsequent route selections), LCR performs a clear decoupling of the routing and RP problems (i.e., R+RP).

i) *Regenerator Grouping-oriented (RG) selection*

The RG method aims at the selection of paths that tends to group the regenerators in nodes as much as possible. First, it checks if there is a path $p \in \mathcal{P}_d$ such that the OSNR requirements are met; if yes, it selects the shortest one. Otherwise, the algorithm performs the search for the set of paths $\mathcal{P}_d^*$ with the maximal number of regenerators placed so far, that is, $\mathcal{P}_d^* = \left\{ p : \sum_{v \in \mathcal{V}_p} k_v \geq \sum_{v \in \mathcal{V}_q} k_v, p, q \in \mathcal{P}_d \right\}$ and, among those paths, the (arbitrary) selection of the shortest one. Hence, this algorithm is a clear example of a joint RRP method.

ii) *Link Congestion Reduction-oriented (LCR) selection*

The objective of the LCR method is to select paths that lead to the congestion reduction in network links. To achieve it we make use of the Linear Programming (LP)-based multi-path routing algorithm presented in Section 4.2 in [86] (this algorithm will be described in detail in Chapter 3)). Specifically, to find a single path p_d for each demand d, we modify the LP formulation by forcing routing variables to be binary and then solve the resulting Mixed Integer Linear Programming (MILP) problem. Note that since we find a solution for all $d \in \mathcal{D}$ at once, it is enough to run the LCR procedure only once (e.g., at the beginning of the RRP algorithm). As earlier mentioned, LCR represents a R+RP method where both problems are solved independently of each other and in sequence.

Consequently, these two route selection methods result in two RRP algorithms, which we name as the RG and LCR algorithms.

Regenerator placement phase

This phase aims at selecting those regenerator sites which lead to solutions having the smallest possible number of nodes equipped with regenerators. The idea is that, since the access to the regenerators

is subject to statistical multiplexing, grouping regenerators in a small number of regenerator locations/sites instead of spreading them throughout the network (thus having few regenerators in many sites) may increase its effectiveness.

Note that this step is run only if necessary (i.e., whenever path p_d does not meet the OSNR requirements). To this end, the OSNR level of each candidate transparent segment is evaluated (see lines 13 and 19 in Procedure 1). Hence, let $\mathcal{K}_p$ denote the node or set of nodes where the regeneration is performed for path p_d, $d \in \mathcal{D}$. Let $\mathcal{K} = \bigcup_{d \in \mathcal{D}} \mathcal{K}_p$ be the set of all nodes where the regenerators have to be installed for all demand $d \in \mathcal{D}$. Let Ω_p be the set of subpaths of p_d to be processed. Then, Procedure 1 is executed.

Procedure 1 Regenerator Placement Heuristic

INPUT: $\mathcal{D}$
OUTPUT: $\mathcal{K}$
1: $\mathcal{K} \leftarrow \emptyset, \Omega_p \leftarrow \emptyset$
2: **for all** path $d \in \mathcal{D}$ **do**
3:     $\Omega_p \leftarrow \Omega_p \cup \{p_d\}$
4:     $\mathcal{K}_d \leftarrow \emptyset$
5:     $\mathcal{T}_p \leftarrow \mathcal{K} \cap \{\mathcal{V}_p\}$
6:     **if** $\mathcal{T}_p \neq \emptyset$ **then**
7:         Select node $v \in \mathcal{T}_p$ which is closer to the middle of the path (with respect to the number of hops)
8:         $\mathcal{K}_d \leftarrow \mathcal{K}_d \cup \{v\}$
9:         $\Omega_p \leftarrow \Omega_p \cup \{p_{s-v}, p_{v-t}\} \backslash \{p\}$
10:     **end if**
11:     **while** $\Omega_p \neq \emptyset$ **do**
12:         Take the first subpath q from Ω_p
13:         **if** q meets OSNR **then**
14:             $\Omega_p \leftarrow \Omega_p \backslash \{q\}$
15:         **else**
16:             **repeat**
17:                 Let q^* be a clone of q
18:                 Remove the last link (and node) from q^*
19:             **until** q^* meets OSNR
20:             Consider t_{q^*} as the regenerative node,
21:             $\mathcal{K}_d \leftarrow \mathcal{K}_d \cup \{t_{q^*}\}$
22:             $\Omega_p \leftarrow \Omega_p \cup \{q \backslash q^*\}$
23:         **end if**
24:     **end while**
25:     $\mathcal{K} \leftarrow \mathcal{K} \cup \{\mathcal{K}_d\}$
26: **end for**

Procedure 1 iteratively processes each demand $d \in \mathcal{D}$ with the aim of ensuring that the OSNR signal level meets the predefined OSNR_{th} threshold at each node $v \in \mathcal{N}_p$. To provide a regenerator grouping-like behavior, in lines 5-10, the algorithm searches among all the previously processed paths if there are nodes $v \in \mathcal{V}_p$ with regenerators already installed, and if so, it takes the node $v \in \mathcal{V}_p$ that is nearest to the middle of the path (with respect to the number of hops) and selects it as the first regeneration point for path p. Hence, two new subpaths are added to Ω_p. Between line 11 and 24,

the algorithm performs a loop that adds regeneration sites to path p until Ω_p becomes an empty set.

Once Procedure 1 finishes, the set of nodes $\mathcal{K}$ where the regeneration has to be performed for all demand $d \in \lceil$ is obtained. In order to assess the complexity of this algorithm let us focus on the amount of nodes constituting the largest path $p_d \in \mathcal{Q}$. We denote such number as δ (how this value is derived will be detailed in Section 3.1.4). Then, the complexity of the algorithm is given by,

$$O(|\mathcal{D}^o| \, (\frac{(\delta - 1)(\delta - 2)}{2})), \tag{2.7}$$

where $\mathcal{D}^o \subseteq \mathcal{D}$ corresponds to the subset of demands for which the OSNR at the receiving end is below OSNR_{th}, and thus, have to be processed by the RP phase. The second term is the upper bound on the maximum possible number of iterations required to create a feasible path, that is, when a regenerator is required at every node $v \in \mathcal{V}_p$. Such operation is performed once per path $d \in \mathcal{D}^o$, and hence, $|\mathcal{D}^o|$. Note that $\delta \geq 3$ for all path $p \in \mathcal{P}^o$, since all paths with two nodes (just source and destination) are feasible.

Regenerator dimensioning phase

Since we are dealing with a T-SWS network, once we have obtained set $\mathcal{K}$, that is, the locations for each path $p_d \in \mathcal{D}^o$ where the regeneration has to be performed, this last phase (dimensioning), is responsible for determining the minimum amount of such regenerators at each location so as to meet a pre-defined target QoT performance.

To this end, we take the assumption that packets entering node $v \in \mathcal{K}$ and requiring regeneration compete in the access to regeneration resources. The load of such packet traffic is (approximately) given by $\rho_v = \sum_{d \in \mathcal{D}, v \in \mathcal{K}_d} h_d$. In order to determine the number of regenerators required in node v we define a dimensioning function $f(\rho_v, B^{QoT}) : (R^+, R^+) \mapsto \mathbb{Z}^+$, where B^{QoT} represents some target packet blocking probability in the access to regeneration resources. Under the assumption that any packet may access any regenerator in a node (as shown in Section 2.2, the architecture proposed guarantees a fair access to the regenerator pool), we make use of the inverse of the Erlang B-loss function as the dimensioning function f. In the next chapter, in Section 3.1.4, where a formal model to solve the RRPD problem is provided, both the dimensioning function as well as a straightforward way to implement it are provided. Hence, readers are referred to Section 3.1.4 for more details on the dimensioning function (D).

2.4 Results and discussion

In this Section, we present the performance results of the T-SWS network architecture. Specifically, the RG and LCR heuristics are compared against each other as well as against both the opaque and transparent cases, which here are used as benchmarking references. Note that, for the sake of a fair
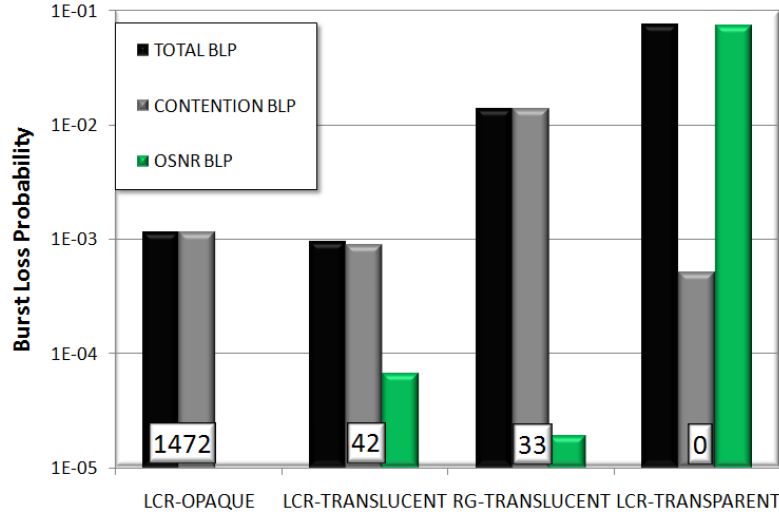
Figure 2.5: Packet Loss Probability due to contention and OSNR comparing the opaque, the transparent and both the RG and LCR translucent solutions considering the Core topology.

comparison, the transparent network used in this study does neither assume an ideal physical layer nor availability of all-optical 3R regeneration.

2.4.1 Scenario

The metric of interest in this study is the overall packet loss probability (PLP). The evaluation is accomplished through a series of simulations which consider the Pan-European Core and Large networks (see Appendix A for the network details) and an OSNR threshold $OSNR_{th} = 20dB$, which consists of an $OSNR_{min} = 19dB$ (see Appendix A for details on this threshold) and an $OSNR_{pen} = 1dB$ so as to account for the signal degradation caused by non-linear impairments. Moreover, B^{QoT} is set to 10^{-3} and $|\mathcal{P}_d| = 2$.

2.4.2 Results

Figure 6.4, shows the results obtained considering the Core topology under four different scenarios, namely an opaque and a transparent network both operating under the MILP routing proposed by the LCR algorithm and a translucent network operating under both the LCR and RG algorithms. Besides, the total number of regenerators placed in each case is shown inside squares. The columns in the figure represent, respectively, the total PLP, the PLP due to packet contention and the PLP due to packets arrived at destination with an accumulated OSNR below the pre-defined receiver threshold, that is, $OSNR_{th}$. In this study, each node generates a total amount of 133Gb/s.

51

The result of the transparent case makes it clear that the impact of the PLIs in an SWS network is quite severe; losses are completely dominated by packets dropped due to OSNR. On the other hand, the opaque solution provides the lowest PLP but requires a vast number of regenerators (1472). It is easy to observe that for the proposed translucent architecture, the PLP of both the LCR and RG strategies are dominated by contentions, which means that OSNR losses are maintained under control thanks to the regenerators placed in the network. Although the RG method requires slightly less regenerators, its routing decisions lead to a poor network performance. The LCR strategy, by contrast, attains the performance of the opaque case, but more importantly, LCR only needs 3 % of the regenerators considered in the opaque solution. In further analysis on the Large topology, similar results were observed. Hence, these results make it clear that given the high contention losses found in bufferless SWS networks, it is much preferable to base routing decisions purely on packet contention minimization as proposed by the LCR algorithm rather than considering RP data, as in the RG selection.

For this reason, hereinafter we only consider the LCR algorithm (i.e., an R+RP approach) for the evaluation of our T-SWS network architecture.

In Fig. 6.5, we depict the PLP performance with respect to the number of regenerators placed in the network. We consider the Core topology and that each node generates 142Gb/s. Both the opaque and transparent cases are plot and used as benchmarking indicators. As it was to be expected, the performance of the translucent topology is clearly bounded by that of both the opaque and transparent network. The LCR heuristic requires 45 regenerators to meet the OSNR requirements. Note that the performance of the translucent network with more than 40 regenerators is slightly better than that of the opaque one (which needs an unfeasible number of regenerators) as in the former, packets undergoing regeneration, make use of electrical buffers at the regenerator pool and, therefore, the contention is slightly reduced.

Eventually, in Fig. 2.6(b), we assess how effective at maintaining OSNR losses under control the LCR strategy is. In this experiment, the Large topology is considered. One can note that, whilst OSNR losses remain nearly flat regardless of the network load, contention losses become dominant as the load increases. The number of regenerators required in each case is displayed in the top x-axis. Again, OSNR losses are slightly decreased as a consequence of the high contention losses.
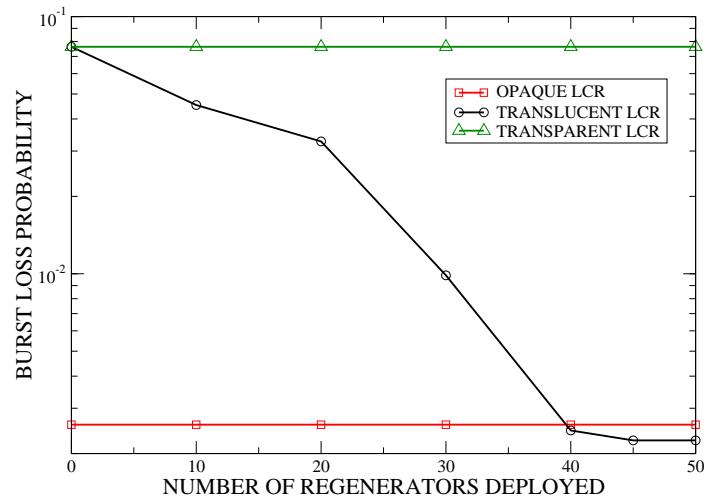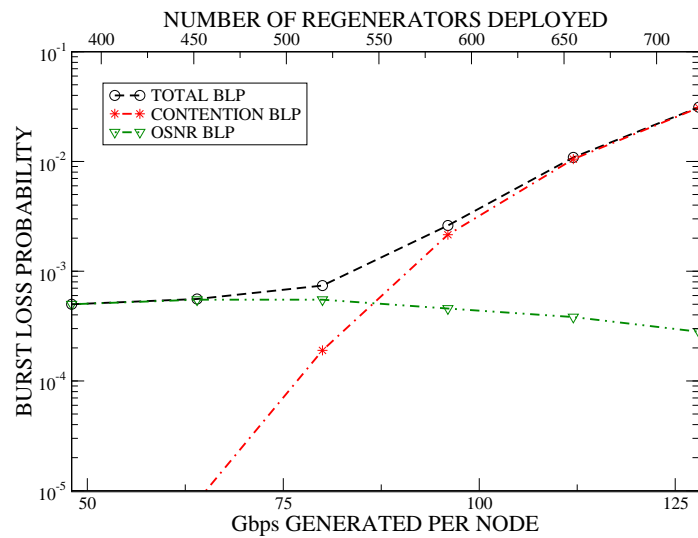
Figure 2.6: (a) PLP of the LCR algorithm as a function of the number of regenerators considering the Core topology. (b) PLP due to contention and OSNR of the LCR algorithm as a function of the offered load considering the Large topology.

2.5 Summary

In this chapter, we have focused on the problem of PLIs in SWS networks. In particular, we have proposed a novel T-SWS network architecture consisting of all-optical TAS nodes equipped with a limited number of regenerators. We have provided an OSNR model to evaluate the impact of the main PLIs (i.e., ASE noise and splitting losses) and illustrated a method to compute a power budget

53

and noise analysis. This model has then been used to carry out a preliminary performance evaluation of the T-SWS network architecture. First, we have pointed out the fact that the use of classical RP or RRP solutions developed for WSONs cannot be used in the context of SWS networks due to their statistical multiplexing nature. To tackle this issue, we have introduced the so-called Routing and Regenerator Placement and Dimensioning (RRPD) problem. Here it is worth stressing the novelty of this solution which incorporates the dimensioning phase (D) that clearly distinguishes it from the RRP problem applied in WSONs. In a first attempt to tackle the complex RRPD, and with the aim of performing a preliminary performance evaluation of the T-SWS network model presented, we have defined two RRP+D heuristics, namely RG (performing joint RRP+D) and LCR (R+RP+D). Performance results indicate that both heuristics successfully maintain negligible packet losses due to intolerable OSNR. Among them, LCR, which follows an R+RP approach and is based on a MILP routing model, attains the performance of the opaque network [72] but requiring a reduced amount of regenerators (e.g., 43 vs. 1472, in the Core topology and 528 vs. 3648, in the Large topology).

Despite both the RG and LCR techniques do not perform an optimal RRPD, they have allowed us to gain a valuable insight into the evaluation of our T-SWS network architecture. For this very reason, the next chapter is entirely devoted to extending the present study to include a formal MILP model for the RRPD problem as well as several compelling heuristic algorithms. Using this enhanced RRPD methods, we aim for a comprehensive assessment of the T-SWS network model provided in this chapter.

Chapter 3

The Routing and Regenerator Placement and Dimensioning problem

As mentioned in Chapter 2, the classical RRP problem found in WSONs is not applicable to T-SWS networks, as the access to signal regenerators is, like any other resource, subject to statistical multiplexing. Hence, it is required the introduction of an additional dimensioning phase which eventually extends the problem to the joint Routing and Regenerator Placement and Dimensioning (RRPD) problem, whose comprehensive description is our primary objective in this chapter.

In this chapter, we show that the joint RRPD problem leads to a very complex formulation, and consequently, to tackle RRPD we propose a *divide and conquer* approach: the routing and RPD subproblems are solved sequentially. To be precise, we provide a mixed integer linear programming (MILP) model for the routing problem (minimizing congestion in network bottleneck links) (LCR algorithm in Chapter 2), and an optimal MILP-based RPD formulation. Furthermore, since RPD results in a complex formulation for which only fairly small problem instances can be solved exactly, we also provide both MILP-based and heuristic RPD algorithms and thoroughly assess their performance.

3.1 Optimal RRPD MILP formulation

In this section, we focus on the modeling of the RRPD problem in a T-SWS network. We begin by presenting the problem definition and its particular design assumptions. In general, our approach to RRPD concerns, respectively, the design of explicit paths to be used to route bursts through the network, and the placement and dimensioning of regenerators at selected nodes on those paths. The

result of this design procedure is a set of routing paths and a subset of regenerative nodes which is specified for each individual path that does not comply with the QoT requirements (i.e., whose OSNR at reception is below OSNR_{th}). It is essential to our approach that a packet, whenever sent on a path, will be regenerated only at the nodes that are specified as regenerative nodes for this path. We also assume that the signal quality of packet headers is always satisfactory as they undergo an O/E/O conversion at each node for processing purposes and a successful transmission must be assured between at least two adjacent nodes. Finally, it is worth recalling that we assume SWS core nodes with full wavelength conversion capability.

3.1.1 RRPD problem definition

We address the RRPD problem by uncoupling the routing formulation from that of the RPD issue, and therefore, we provide a model to tackle the R+RPD problem. Two main reasons support this modeling decision. First, treating both problems together and at a time would definitely make of the problem an extremely complex undertaking, particularly in terms of computation times or even of solving feasibility. Second, and most compelling, is the fact that in SWS networks, routing must be carefully engineered as the main source of performance degradation is the contention between packets that arise due to the lack of optical buffering and the fact that, in general, SWS networks implement a one-way resource reservation scheme. As shown in Chapter 2, if routing decisions are biased towards minimizing the number of regenerators deployed (RG algorithm), burst losses in network links become uncontrollable, thereby further justifying the decoupling of the problems (i.e., R+RPD as in the LCR algorithm).

Hence, given a set of traffic demands, we first find a proper routing that minimizes burst losses due to congestion in bottleneck network links. Then, this routing solution is used as input information to solve the RPD problem. Since in the T-SWS network the access to the regenerator pools is based on statistical multiplexing, the RPD method must deal with both the selection of regeneration nodes and the dimensioning of regenerator pools so that a given target burst loss rate due to QoT non-compliant bursts is satisfied. Thus, the aim of the RPD formulation here proposed is the minimization of the number of regenerators deployed in the network whilst, at the same time, guaranteeing that losses caused by QoT signal degradation are kept well below those caused by contentions in network links.

3.1.2 Global notation

We use $\mathcal{G} = (\mathcal{V}, \mathcal{E})$ to denote the graph of a SWS network; the set of nodes is denoted as $\mathcal{V}$, and the set of unidirectional links is denoted as $\mathcal{E}$. Let $\mathcal{P}$ denote the set of predefined candidate paths between source s and termination t nodes, $s, t \in \mathcal{V}$, and $s \neq t$. Each path $p \in \mathcal{P}$ is identified with a subset of network links, that is, $p \subseteq \mathcal{E}$. Adequately, subset $\mathcal{P}_e \subseteq \mathcal{P}$ denotes all paths that go through link e. Let s_p and t_p denote the source and termination nodes of p. Let $\mathcal{D}$ denote the set of demands, where each demand corresponds to a pair of source-termination nodes. Let $h_d = \lambda_d/\mu$ denote the

average offered burst traffic load for demand $d \in \mathcal{D}$, where λ_d is the average packet arrival rate and μ is the average packet service rate; Let $\mathcal{N}_p$ be the set of all nodes constituting path p. Finally, let $\mathcal{V}_p$ denote the set of intermediate nodes on path p such that $\mathcal{V}_p = \mathcal{N}_p \setminus \{s_p, t_p\}$.

3.1.3   Routing problem

Model assumptions

As commented in Section 2.3 in Chapter 2, the routing model that we consider and the routing algorithm that we apply are similar to the Linear Programming (LP) approach presented in [86]. To be precise, the authors consider a multi-path routing approach (i.e., splittable routing) to solve the routing problem. The objective of this method is to distribute traffic over a set of candidate paths so that to reduce congestion in network bottleneck links. To this end, the network is assumed to apply source based routing, and hence, the source node is able to determine the path that a packet entering the network must follow. Although we take the same routing objective, in our study we consider unsplittable (non-bifurcated) routing and, accordingly, all the traffic offered to demand $d \in D$ is carried over a single path in the network. Note that this approach can be easily converted into a multi-path (i.e., splittable) routing problem by relaxing the routing variables. Nonetheless, we use the unsplittable solution to avoid the problem of out-of-order packet arrival which is inherent in any splittable routing algorithm.

It is also worth noticing that the average packet traffic load (h_d) offered by all path $p \in \mathcal{P}_e$ to a particular link $e \in \mathcal{E}$, will decrease due to both contentions at output ports and at regenerator pools in the preceding links on those paths. This problem was studied in [51], where authors present a reduced link load loss-model for OBS networks based on the *Erlang fixed-point approximation*. This model was later compared with a simplified non-reduced link load loss-model in [87], and it was shown that the accuracy of the non-reduced link load model is very strict for values of the BLP lower than 10^{-2}. Thus, we can assume a non-reduced link load model since this requirement is to be largely met in a properly dimensioned network.

Let $\mathcal{P}_d \subseteq \mathcal{P}$ denote the set of candidate paths supporting demand d; $\mathcal{P} = \bigcup_{d \in D} \mathcal{P}_d$. Each subset $\mathcal{P}_d$ comprises a (small) number of paths, for example, k shortest paths. The selection of path p from set $\mathcal{P}_d$ is performed according to a decision variable x_p. In this study, on the contrary to the assumption taken in [86], variables x_p are forced to be binary. Strictly speaking, a packet flow is routed over path p iff $x_p = 1$. Moreover, there is only one path $p \in \mathcal{P}_d$ such that $x_p = 1$. Hence, these routing constraints can be expressed as:

$$\sum_{p \in \mathcal{P}_d} x_p = 1, \quad \forall d \in \mathcal{D}, \tag{3.1a}$$

$$x_p \in \{0, 1\}, \quad \forall p \in \mathcal{P}, \tag{3.1b}$$

and the traffic ρ_p to path $p \in \mathcal{P}_d$ can be calculated as:

$$\rho_p = x_p h_d = \left\{ \begin{array}{ll} h_d & \text{if } x_p = 1, \\ 0 & \text{otherwise.} \end{array} \right\} \tag{3.2}$$

As a consequence, the problem formulations presented in the next subsection are MILP formulations. Notice that the set of variables x_p (i.e., vector $\mathbf{x} = (x_1, ..., x_{|\mathcal{P}|})$) determines the distribution of the traffic over the network. This vector has to be optimized in order to reduce link congestion and to improve the overall network performance.

Problem formulation

Following the LP algorithm presented in [86], the next two MILP models are sequentially solved to find a solution to the routing problem. First, let variable y represent the average traffic load on the bottleneck link. Then, the first MILP formulation, which aims at minimizing the load on such particular link of the network, can be written as follows:

$$minimize \quad y \tag{RMILP1}$$
$$subject\ to$$
$$\sum_{p \in \mathcal{P}_e} x_p h_d - y \leq 0, \ \forall e \in \mathcal{E} \tag{3.3}$$

and subject to the routing constraints given by (3.1a) and (3.1b).

Despite minimizing the average traffic load on the bottleneck link, many solutions to this problem may exist and most of them exploit unnecessary resources in the network (i.e., solutions that select longer paths). Therefore, the next MILP is solved in order to obtain, between the solutions of RMILP1, the one that entails the minimum increase of the average traffic load offered to the remaining network links. For this purpose, let us denote y^* as an optimal solution of RMILP1, then we solve the following problem:

$$minimize \quad \sum_{e \in \mathcal{E}} \sum_{p \in \mathcal{P}_e} x_p h_d \tag{RMILP2}$$
$$subject\ to$$
$$\sum_{p \in \mathcal{P}_e} x_p h_d \leq y^*, \ \forall e \in \mathcal{E} \tag{3.4}$$

and subject to the routing constraints given by (3.1a) and (3.1b). Note that, in constraint (3.4), we ensure that the maximum average traffic load on the bottleneck link is bounded by the solution of RMILP1.

These MILP models, if sequentially solved, determine the path p that will be in charge of carrying the traffic for each demand d. Hence, only one path $p_d \in \mathcal{P}_d$ is selected as the valid path to be followed by all packets belonging to demand d. Thus, we can now denote $\mathcal{Q}$ as the set of valid paths, $\mathcal{Q} = \{p_d, d \in \mathcal{D}\}$. In the next section, we use $\mathcal{Q}$ as input information to solve the RPD problem.

3.1.4 RPD problem

Model assumptions

Let $\mathcal{P}^o \subseteq \mathcal{Q}$ denote the subset of paths for which the QoT level at receiver t is non-compliant with the quality of signal requirements, and thus, paths $p \in \mathcal{Q}$ requiring regeneration at some node $v \in \mathcal{V}_p$. For each $p \in \mathcal{P}^o$ there may exist many different options on how to build an end-to-end QoT compliant path, composed by its transparent segments, since the node or group of nodes where the regeneration has to be performed might not be a unique solution. Thus, let $\mathcal{S}_p = \{s_1, \ldots, s_{|\mathcal{S}_p|}\}$ denote the set of different options to establish a QoT compliant path for each path $p \in \mathcal{P}^o$, where $s_i \subseteq \mathcal{V}$, $i = 1 \ldots |\mathcal{S}_p|$ and size $|\mathcal{S}_p|$ depends on the length of the transparent segments in path p. Figure 3.1 illustrates this concept by means of an optical path between a source-termination pair $(s - t)$ with two different options to establish a QoT compliant path. To be precise, if s_1 is selected, the optical signal only undergoes regeneration at node v_y, whereas if s_2 is the choice, it is converted to the electrical domain twice (i.e., at nodes v_x and v_z). Hence, $s_1 = \{v_y\}$ and $s_2 = \{v_x, v_z\}$. In this particular case, the transparent segments that make it possible to use both regeneration solutions are segments $[s - v_y]$-$[v_y - t]$ and $[s - v_x]$-$[v_x - v_z]$-$[v_z - t]$. Notice that we could also consider other cases like $s_3 = \{v_x, v_y, v_z\}$, however, we have not depicted all of the options for the sake of clarity. In order to obtain $\mathcal{S}_p$, $p \in \mathcal{P}^o$ (i.e., all possible regeneration options) we make use of the OSNR model presented in Chapter 2. However, it could also be done considering any other valid QoT estimator. In order to find an upper bound on the size of set $\mathcal{S}_p$ we must focus on the number of nodes constituting the largest path in $\mathcal{P}^o$. To this end, let us denote such a number by $\delta = \max\{|\mathcal{N}_p| : p \in \mathcal{P}^o\}$.

Then, an upper bound on the maximum size of set $\mathcal{S}_p, p \in \mathcal{P}^o$ can be written as,

$$\Theta = 2^{(\delta - 2)} - 1. \tag{3.5}$$

We assume that for each path $p \in \mathcal{P}^o$, the selection of the regeneration option s from set $\mathcal{S}_p$ is performed according to a decision variable z_{ps}, which later is referred to as regenerator placement variable, such that the following constraints are fulfilled:

$$\sum_{s \in S_p} z_{ps} = 1, \quad \forall p \in \mathcal{P}^o, \tag{3.6a}$$

$$z_{ps} \in \{0, 1\}, \quad \forall s \in \mathcal{S}_p, \forall p \in \mathcal{P}^o. \tag{3.6b}$$
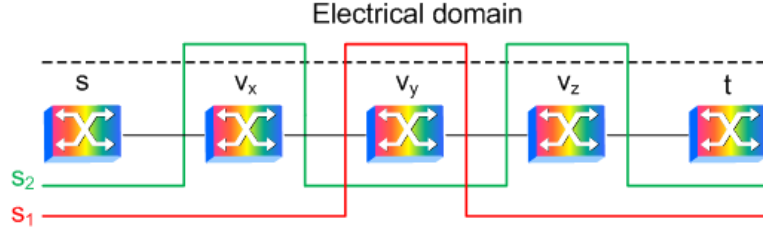
Figure 3.1: Two different valid options to perform the regeneration for a particular source-termination pair.

Let ρ_v^o denote the offered traffic load requiring regeneration at node v. To estimate ρ_v^o (approximately) we add up the traffic load ρ_p offered to each path $p \in \mathcal{P}^o$ that both crosses and undergoes regeneration at node v:

$$\rho_v^o = \sum_{p \in \mathcal{P}^o : \mathcal{V}_p \ni v} \sum_{s \in \mathcal{S}_p : s \ni v} z_{ps} \rho_p. \tag{3.7}$$

Similarly,

$$\rho_v = \sum_{p \in \mathcal{P}^o : \mathcal{V}_p \ni v} \rho_p, \tag{3.8}$$

denotes an estimation of the maximal traffic load that is subject to regeneration at node $v \in \mathcal{V}$.

Eventually, we define a regenerator pool dimensioning function $F_v(\cdot)$, which for a given traffic load ρ_v^o, determines the minimum number of regenerators to be allocated in node v. This number must ensure that a given B^{QoT} is met. Assuming Poisson arrivals and fairness in the access to regenerator pools among packets, such a function is given by the following discontinuous, step-increasing function,

$$F_v(\rho_v^o) = \left\lceil B^{-1}(\rho_v^o, B^{QoT}) \right\rceil, \tag{3.9}$$

where B corresponds to the Erlang B-loss formula which for a given number of regenerators $r \in \mathbb{N}$ available at node v can be calculated as,

$$B(\rho_v^o, r) = \frac{(\rho_v^o)^r / r!}{\sum_{k=0}^{r} (\rho_v^o)^k / k!}, \tag{3.10}$$

and where $B^{-1}(\rho_v^o, B^{QoT})$ is the inverse function of (3.10) extended to the real domain [88], and $\lceil \cdot \rceil$ is the ceiling function. It is worth noticing that the Poisson arrivals which lead to an Erlang formula for the dimensioning of regenerator pools can be replaced with another distribution for which the blocking probability is attainable. Because B^{QoT} is a predetermined parameter, for simplicity of presentation we skipped it from the list of arguments of function $F_v(\cdot)$.
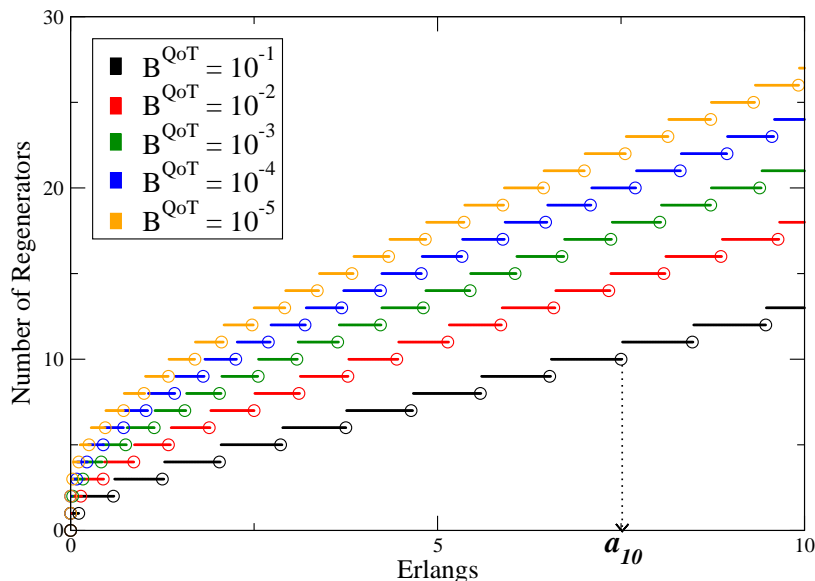
Figure 3.2: Discontinuous step-increasing regenerator pool dimensioning function and (a_r, r) points for some exemplary target burst loss probabilities.

For the purpose of problem formulation, it is convenient to define a_r as the maximal load supported by r regenerators given a B^{QoT}, that is, $a_r = B^{-1}(r, B^{QoT})$. Note that the inverse function $B^{-1}(r, B^{QoT})$ is expressed with respect to r and B^{QoT}, which is not the same as in function (3.9).

Although there is no close formula to compute the inverse of (3.10), we can make use of a line search method (see e.g., [89]) to find the root ρ^* of the function $f(\rho) = B^{QoT} - B(\rho, r)$ so that the value of a_r is approximated by $a_r = \rho^*$ for any index r. Finally, let R denote the number of regenerators required in the most loaded node, that is:

$$R = \max\{F_v(\rho_v) : v \in \mathcal{V}\}. \tag{3.11}$$

Note that we can make use of vector $\mathbf{a} = (a_1, ..., a_R)$ to obtain the Piecewise Linear Approximation (PLA) of $F_v(\cdot)$, which for a single node $v \in \mathcal{V}$, can be expressed as $F_v(\rho_v^o) = \min\{r : a_r > \rho_v^o\}$. The PLA will be of practical interest in the next subsection, where it will allow us to better deal with function $F_v(\cdot)$, and consequently with $B^{-1}(\cdot)$. For the sake of clarity, function $F_v(\rho_{vo})$ is depicted in Fig. 3.2 for some exemplary B^{QoT} values. Note that $B^{-1}(\cdot)$ is a real-valued concave function. Moreover, we also provide points (a_r, r) (represented by circles in the plot) which will eventually help us generate the different $\mathbf{a}$ vectors. The accuracy of the PLA of $F_v(\cdot)$ depends on the precision of the line search algorithm that is used to generate vector $\mathbf{a}$. In our implementation of the line search algorithm the termination criteria is set to $\xi = 10^{-6}$, which guarantees a fine approximation (i.e., $B^{QoT} - B(\rho, r) \leq \xi$).

Eventually, vector **a** will also be used by the methods proposed in Sections 2.3, 3.2 and 3.3 to determine $F_v(\rho_v^o)$ according to Procedure 7 (i.e., to perform the dimensioning phase (D)). Note that Procedure 7 is a polynomial time algorithm of complexity $O(R)$.

Procedure 2 Regenerator Pool Dimensioning

1: $r \leftarrow 0$
2: **while** $\rho_v^o > a_r$ **do**
3:     $r \leftarrow r + 1$
4: **end while**
5: $F_v \leftarrow r$

Problem formulation

Taking into account the network modeling assumptions previously presented, here we present a mathematical formulation for the RPD part of the problem.

The RPD problem can be formulated as a non-convex optimization problem:

$$\underset{\mathbf{z}}{minimize} \quad F = \sum_v F_v(\rho_v^o(\mathbf{z})) \tag{NLP1}$$

$$subject\ to \quad (3.6a)\ \text{and}\ (3.6b) \tag{3.12a}$$

where $F_v(\cdot)$ is the step-increasing regenerator pool dimensioning function defined by (3.9) and $\rho_v^o(\mathbf{z})$ is the function representing the traffic load offered to a regenerator node defined by (3.7). The optimization objective of NLP1 is to minimize the sum of regenerators installed in network nodes. Constraints (3.12a) represent the selection of a QoT compliant path from the options provided for each path requiring regeneration. Eventually, the regenerator placement decision vector $\mathbf{z}$ is defined as $\mathbf{z} = (z_{11} \ldots z_{1|\mathcal{S}_p|}, \ \ldots, \ z_{|\mathcal{P}^o|1} \ldots z_{|\mathcal{P}^o||\mathcal{S}_{|\mathcal{P}^o|}|})$.

The difficulty of formulation NLP1 lays in the fact that there is no close formula to express $F_v(\cdot)$ since no such formula exists for the inverse of the Erlang function $B^{-1}(\cdot)$. A way to solve the problem is to substitute function $F_v(\cdot)$, $v \in \mathcal{V}$ with its piecewise linear approximation and reformulate NLP1 as a MILP problem.

For a single node $v \in \mathcal{V}$, the PLA of $F_v(\cdot)$ can also be expressed by means of the following 0-1 integer programming (IP) formulation:

$$minimize_{\mathbf{u}} \quad F_v = \sum_r u_v^r r \tag{IP1}$$

$$subject\ to \quad u_v^r(a_r - \rho_v^o) \geq 0, \ \forall r \in [1, R], \tag{3.13a}$$

$$\sum_r u_v^r = 1, \tag{3.13b}$$

$$u_v^r \in \{0, 1\}, \ \forall r \in [1, R]. \tag{3.13c}$$

In IP1, decision variables u_v^r have been introduced in order to represent the number of regenerators required in node v. Due to constraint (3.13b), in each node only one variable u_v^r is active (i.e., equal to 1), and the one with minimum r satisfying $a_r \geq \rho_v^o$ is found when solving the problem. Notice that formulation IP1, when solved, gives the same solution as Procedure 7. The shortcoming of IP1 is that since ρ_v^o is dependent on vector $\mathbf{z}$ (i.e., ρ_v^o is a function of $\mathbf{z}$), constraints (3.13a) have quadratic form. To overcome this difficulty, we can consider the following alternative formulation:

$$minimize_{\mathbf{u}} \quad F_v = \sum_r u_v^r r \tag{ILP1}$$

$$subject\ to \quad \sum_r u_v^r a_r \geq \rho_v^o, \tag{3.14a}$$

$$\sum_r u_v^r = 1, \tag{3.14b}$$

$$u_v^r \in \{0, 1\}, \ \forall r. \tag{3.14c}$$

It is easy to note that formulation of ILP1 results directly from IP1; it is enough to add up constraints (3.13a) and use (3.13b) for substituting $\rho_v^o \sum_r u_v^r$ for ρ_v^o.

Eventually, taking into account all network nodes and introducing the regenerator placement decision variables, problem NLP1 can be reformulated as the following MILP problem:

$$\underset{\mathbf{u},\boldsymbol{\rho}^o,\mathbf{z}}{minimize} \quad F = \sum_v \sum_r u_v^r r \tag{MP1}$$

$subject\ to$

$$\sum_r u_v^r a_r - \rho_v^o \geq 0, \quad \forall v \in \mathcal{V}, \tag{3.15a}$$

$$\sum_r u_v^r = 1, \quad \forall v \in \mathcal{V}, \tag{3.15b}$$

$$\sum_{s \in S_p} z_{ps} = 1, \quad \forall p \in \mathcal{P}^o, \tag{3.15c}$$

$$\sum_{p \in \mathcal{P}^o : \mathcal{V}_p \ni v} \sum_{s \in \mathcal{S}_p : s \ni v} z_{ps} \rho_p - \rho_v^o = 0, \ \forall v \in \mathcal{V}, \tag{3.15d}$$

$$u_v^r \in \{0,1\}, \quad \forall r \in [1,R], \forall v \in \mathcal{V}, \tag{3.15e}$$

$$z_{ps} \in \{0,1\}, \quad \forall p \in \mathcal{P}^o, \forall s \in \mathcal{S}_p, \tag{3.15f}$$

$$\rho_v^o \in \mathbb{R}^+, \quad \forall v \in \mathcal{V}. \tag{3.15g}$$

where we consider ρ_v^o to be an auxiliary variable representing the traffic load requiring regeneration offered to node $v \in \mathcal{V}$.

The objective of the optimization problem MP1 is to minimize the total number of regenerators that have to be placed in the network. Constraints (3.15a) and (3.15b) result from the 0-1 representation of the dimensioning function and from the reformulation of IP1 as mentioned before. In particular, the number of regenerators in node $v \in \mathcal{V}$ should be such that the maximum traffic load (given a B^{QoT}) is greater or equal to the offered traffic load ρ_v^o. Constraints (3.15c) are the QoT compliant path selection constraints. Constraints(3.15d) are the traffic load offered to a regenerator node calculation constraints. Eventually, (3.15e), (3.15f), and (3.15g) are the variable range constraints.

MP1 is a well-known Discrete Cost Multicommodity Flow (DCMCF) problem [90]. DCMCF was shown to be an extremely difficult combinatorial problem for which only fairly small instances (in our case, situations where $\mathcal{P}^o$ has a rather small size) can be solved exactly with currently available techniques. Indeed, considering the problem in hand, the total amount of variables can be approximated by $|\mathcal{V}| \cdot R + |\mathcal{P}^o| \cdot \Theta$, where the first term represents the amount of u_v^r variables and the second term is an upper bound on the size of variable vector $\mathbf{z}$. Similarly, the size of the constraint set is $3 \cdot |\mathcal{V}| + |\mathcal{P}^o|$. For example, if the Large network (see Appendix A for network details) is considered, then $\delta = 12$. Now assume that R is set to 100. Hence, the problem size increases to approximately $8 \cdot 10^5$ variables and $9 \cdot 10^2$ constraints, thereby making highly difficult its exact solution. It must also be noted that, as shown in (3.5), the size of set $\mathcal{S}_p$ increases exponentially to the size of the problem instance. In order to limit the problem size, we only consider the K smallest options (with respect to the number of regenerations along the path) to fill $\mathcal{S}_p$, that is, $\mathcal{S}_p = \{s_1, ..., s_K\}$. In the next Section, we propose two relaxed MILP-based methods to solve the

RPD problem.

3.2 MILP-based RPD resolution methods

To overcome the difficulty imposed by the resolution of MP1, in this section, we propose two MILP-based heuristic methods that provide near-optimal solutions to the RPD problem within acceptable computational times. The main idea behind both strategies is to decouple the RPD problem into the RP problem, which is solved first, and the dimensioning phase, thereby solving the so-called RP+D problem. The performance of these methods is later discussed in Section 3.4.

3.2.1 Load-based MILP formulation

The MILP formulation here proposed is focused on the distribution of the traffic load requiring regeneration (i.e., ρ_v^o, $\forall v \in \mathcal{V}$). Hence, this load must be aggregated in such a way that the number of regenerators to be deployed is minimized. After a ρ_v^o solution is obtained for each node $v \in \mathcal{V}$, we take advantage of the regenerator pool dimensioning function detailed in Section 3.1.4 to obtain the number of regenerators required.

Owing to the concave character of the dimensioning function (3.9), it must be noted that it is of our interest to aggregate the traffic requiring regeneration in as few nodes as possible rather than spreading out such load in little amounts over a large number of nodes. Hence, we propose to solve the problem by making use of two MILP models, namely MILP2 and MILP3. These models can be sequentially solved to obtain a sub-optimal solution of MP1.

First, MILP2 aims at minimizing the number of nodes where the regenerators must be installed (i.e., nodes such that $\rho_v^o > 0$), and thus, groups as much as possible the load that requires regeneration. Let $\mathbf{y} = (y_1, ..., y_{|\mathcal{V}|})$ denote a vector of binary decision variables. Each value corresponds to one node and determines if this node is used as regeneration point by some path $p \in \mathcal{P}^o$ ($y_v = 1$) or not ($y_v = 0$).

Then, we solve the following problem:

$$\underset{\boldsymbol{\rho}^o, \mathbf{z}, \mathbf{y}}{minimize} \quad \sum_v y_v \tag{MILP2}$$

$$subject\ to \quad \rho_v y_v \geq \rho_v^o, \quad \forall v \in \mathcal{V}, \tag{3.16a}$$

$$y_v \in \{0, 1\}, \ \forall v \in \mathcal{V}. \tag{3.16b}$$

and subject to constraints (3.6a), (3.6b), (3.15d) and (3.15g).

Although ILP1 minimizes the number of nodes where the regenerations are performed, multiple solutions to this problem may exist and some of them may exploit more regenerations than required,

increasing unnecessarily ρ_v^o at some nodes. Therefore, a second MILP model, that is, MILP3, needs to be formulated with the objective of minimizing the total network load requiring regeneration.

Therefore, let k^* denote an optimal solution of MILP2. Second, we solve the following problem:

$$\underset{\boldsymbol{\rho}^o, \mathbf{z}, \mathbf{y}}{minimize} \quad \sum_v \rho_v^o \qquad \qquad \text{(MILP3)}$$

$$subject\ to \quad \sum_v y_v \le k^*, \qquad \qquad \text{(3.17a)}$$

and subject to constraints (3.6a), (3.6b), (3.15d), (3.15g), (3.16a) and (3.16b).

Due to the simplicity of both formulations, both models are expected to be promptly solved even for large-sized problem instances. Here it is worth mentioning that problems MILP2 and MILP3 as well as routing problems RMILP1 and RMILP2 could have been solved by using a single weighted multi-objective MILP formulation. However, we have considered the sequential approach for both the sake of clarity and to avoid dealing with the weights used in the resulting multi-objective cost functions.

It is also important to note that the sequential resolution of both MILP2 and MILP3, which will hereinafter be cited within the text as MP2/3, provides an optimal solution in terms of the distribution of the traffic and not with respect to the number of regenerators (which is precisely the case of MP1).

3.2.2 Reduced MILP1 (MILP1*)

This method aims at reducing the complexity of MP1 by introducing new constraints to its definition. Specifically, these constraints are the sequentially obtained solutions of both MILP2 and MILP3 as detailed previously in subsection 3.2.1. Although these new constraints are not valid in that they may exclude the optimal solution of MP1, they can be used to achieve good near-optimal solutions within reasonable time limits.

Therefore, let us denote g^*, and again k^*, as the optimal sequentially solved solutions of MILP3 and MILP2 respectively. Then, we reformulate MP1 as follows,

$$\underset{\mathbf{u}, \boldsymbol{\rho}^o, \mathbf{z}}{minimize} \quad F = \sum_v \sum_r u_v^r r \qquad \qquad \text{(R-MP1)}$$

$$subject\ to \quad \sum_v y_v \le k^*, \qquad \qquad \text{(3.18a)}$$

$$\sum_v \rho_v^o \le g^*, \qquad \qquad \text{(3.18b)}$$

and subject to constraints (3.15a), (3.15b), (3.15c), (3.15d), (3.15e), (3.15f), (3.15g), (3.16a) and (3.16b).

In fact, we sequentially solve all three models in order, that is, first MILP2, second MILP3 and finally MP1 including all solutions obtained as constraints for the subsequent problem.

It is worth pointing out that, as long as the scenario considered does not involve optical paths that require a large number of regenerations, constraint (3.18a) is very unlikely to exclude the optimal solution of MP1. Basically, it is due to the fact that the dimensioning function of our problem is (3.9), which favors, to some degree, the grouping-like behavior. Constraint (3.18b), by contrast, is just an heuristic approach to help solve the problem. Notice that (3.18b) does not deal with the distribution of the load but with its minimization, and thus, the optimal solution in terms of the number of regenerators is generally excluded.

Finally these two alternative RRPD methods require the regenerator pool dimensioning phase (D) as described in Section 2.3.2. Recall that a straightforward way to implement this dimensioning function is to make use of vector **a** and Procedure 7, which have been both detailed in Section 3.1.4.

3.3 RPD meta-heuristic algorithms

While Section 3.2 provided two different MILP-based RPD resolution methods, this section presents a set of RPD algorithms which are based on well-known meta-heuristic methods. Specifically, in the following subsections, we propose three different offline meta-heuristic RPD algorithms. For the sake of clarity, we consider an objective function denoted by $g(\cdot)$ which accounts for the calculation of the number of regenerators required. As explained in the last section, this is achieved by calling the dimensioning function detailed in 2.3.2. Although this procedure may be called several times within the RPD heuristics next presented, the solutions of Procedure 7 are pre-computed only once at the very beginning of the algorithm and stored in an ordered array, thereby substantially reducing the time complexity (see details in Section 3.1.4). Hence, we do not include this factor in the complexity analysis of the different heuristic RPD algorithms presented below.

3.3.1 KL Local Search (KLS) algorithm

The KLS algorithm is an heuristic algorithm which is based on the K-L local search technique [91]. In this algorithm, we assume a neighboring solution is achieved by means of a flip operation which consists in a permutation of the regeneration sites for a specific set of demands. The pseudo-code of the KLS algorithm is shown in Procedure 3. Let $\mathcal{R}_z$ be the set of all regeneration vectors that define for each path $p \in \mathcal{P}^o$, the node or set of nodes where the regeneration is performed, that is, $\mathcal{R}_z = \bigcup_{p \in \mathcal{P}^o} \mathbf{z}_p$, where $\mathbf{z}_p = (z_{p1}, ..., z_{p|\mathcal{S}_p|})$. Then, let $\mathcal{R}_o$ be an initial (randomly selected) solution to the problem where constraints (3.6a) (3.6b) are met for each $\mathbf{z}_p$, $p \in \mathcal{P}^o$.

Similarly, let $\mathcal{R}_{tb}$, $\mathcal{R}_i$ and $\mathcal{R}_b$ denote, respectively, the global best solution obtained so far, the best solution of a whole iteration and one of the solutions of the iteration in progress. Moreover, let $\Omega_{\mathcal{R}}$ be the set of valid solutions obtained once loop between lines 5-13 in Procedure 3 is completed.

Procedure 3 KLS Heuristic

INPUT: $\mathcal{P}^o, \mathcal{R}_o, \Omega_{\mathcal{R}} \leftarrow \emptyset$
OUTPUT: $g(\mathcal{R})$
 1: $\mathcal{R}_{tb} \leftarrow \mathcal{R}_o$
 2: $\Omega_{\mathcal{R}} \leftarrow \Omega_{\mathcal{R}} \cup \{\mathcal{R}_o\}$
 3: $\mathcal{R}_b \leftarrow \mathcal{R}_o$
 4: **repeat**
 5:    **for all** path $p \in \mathcal{P}^o$ **do**
 6:       $\mathcal{P}_x \leftarrow \mathcal{P}_o \backslash \{p\}$
 7:       Take $\mathbf{z}_p$ from $\mathcal{R}_b$
 8:       Determine $\mathbf{z}_p^*$ which minimizes $g(\cdot)$ considering, for all path $p \in \mathcal{P}_x$, the option $\mathbf{z}_p$ selected in $\mathcal{R}_b$
 9:       Let $\mathcal{R}_p$ be a new solution
10:       $\mathcal{R}_p \leftarrow \mathcal{R}_b \cup \{\mathbf{z}_p^*\} \backslash \{\mathbf{z}_p\}$
11:       $\Omega_{\mathcal{R}} \leftarrow \Omega_{\mathcal{R}} \cup \{\mathcal{R}_p\}$
12:       $\mathcal{R}_b \leftarrow \mathcal{R}_p$
13:    **end for**
14:    Take $\mathcal{R}_i$ from $\Omega_{\mathcal{R}}$ which minimizes $g(\cdot)$
15:    $\mathcal{R}_b \leftarrow \mathcal{R}_i$
16:    $\Omega_{\mathcal{R}} \leftarrow \mathcal{R}_b$
17:    **if** $g(\mathcal{R}_{tb}) > g(\mathcal{R}_i)$ **then**
18:       $\mathcal{R}_{tb} \leftarrow \mathcal{R}_i$
19:    **end if**
20: **until** $r_{tb} \leq r_i$
21: $\mathcal{R} \leftarrow \mathcal{R}_{tb}$

Between lines 5 and 13, starting from solution $\mathcal{R}_b$, we iteratively take, for each $p \in \mathcal{P}^o$, vector $\mathbf{z}_p \in \mathcal{R}_b$, and then we set it to $\mathbf{z}_p^*$, which is the solution for vector $\mathbf{z}_p$ that minimizes the number of regenerators to be deployed taking into account the current solutions for all other paths, that is, solutions in the current $\mathcal{R}_b$. Once a choice is made for p, then it remains fixed until the loop is initiated again.

It is also worth noticing that in line 12, an update of the current solution is performed even if it entails worsening $\mathcal{R}_b$. Procedure 3 does this in order to increase the probabilities of escaping from the local optima and in the hope that some neighboring solution generated during an iteration will turn out better than the current global best solution $\mathcal{R}_{tb}$.

To evaluate the complexity of this algorithm we use the upper bound on the maximum number of regeneration options Θ as defined in Eq (3.5).

Then, the complexity of Procedure 3 is given by,

$$O(M \cdot |\mathcal{E}| \cdot |\mathcal{P}^o| \cdot \Theta), \tag{3.19}$$

where $M|\mathcal{E}|$ (the number of regenerators required in an opaque SWS network) defines an upper bound on the number of iterations at the worst-case improvement (i.e., one per iteration) of the cost function. $|\mathcal{P}^o|$ accounts for the number of iterations in the *for all* loop in Procedure 3 and the last term represents the maximum number of regeneration options (Θ).

3.3.2 ACO algorithm

In this section, we propose the application of the ant colony optimization (ACO) [92] methodology to solve the RPD problem. ACO was introduced in the early 1990s as a nature-inspired meta-heuristic for solving hard combinatorial optimization problems. In the field of optical networks, ACO algorithms have been used, for example, to solve the problem of RWA (see e.g., [93], [94], [95]). ACO methods try to mimic the behavior of real ants on their task of foraging for food. Initially, an ant explores the area surrounding its nest, and when a food source is found, it evaluates the quantity and quality of its finding. Based on this measurement, the ant on its way back to the nest will deposit more or less quantity of a chemical pheromone, thereby creating a so-called pheromone trail which will subsequently help other ants find the best possible food source. If these other ants also find food, they will reinforce the same trail by depositing more pheromone. However, if the quantity or quality of the food found decreases, pheromone trails will tend to evaporate over time, thereby reducing the trail attractiveness.

In our problem, for each path $p \in \mathcal{P}^o = \{p_1, ..., p_{|\mathcal{P}^o|}\}$, we have a set of possible regeneration options $\mathcal{S}_p = \{s_1, ..., s_{|\mathcal{S}_p|}\}$. Let us define a variable instantiation as the assignment of a regeneration option $s_j \in \mathcal{S}_p$ to a path $p_i \in \mathcal{P}^o$, that is, $p_i = s_j$. Once an assignment for each path is performed, a feasible solution for the RPD problem is obtained. Note that we are dealing with an unconstrained problem, and thus, each path can take any $s \in \mathcal{S}_p$ independently of the decision taken by other paths. Finally, let us also call the combination of a path p_i with a regeneration option s_j a solution component which we denoted by c_i^j. Hence, we define the set of possible solution components for path p_i as $\mathcal{C}_i$. Note that $|\mathcal{C}_i| = |\mathcal{S}_{p_i}|$.

Pheromone model

The pheromone model consists of a pheromone trail parameter $\mathcal{T}_i^j$ for each solution component c_i^j as proposed in [92]. This pheromone trail parameter provides the pheromone value (τ_i^j), and much as in our case τ_i^j is a function of the algorithm iteration (i.e., $\tau_i^j = \tau_i^j(t)$), this dependence will however be made explicit only when necessary. Eventually, we denote the whole set of pheromone trail parameters by $\mathcal{T}$. Given the fact that our interest lies in minimizing the number of regenerators and that this is better achieved if they are aggregated in as few nodes as possible, we consider that the pheromone value τ_i^j for solution component c_i^j depends exclusively on the quantity of pheromone deposited on each regeneration node $v \in s_j$ (recall that s_j consists of the set of nodes where the regeneration for path p_i is performed). Hence, we assume that each node $v \in \mathcal{V}$ has an amount of deposited pheromone equal to φ_v. Note that φ_v is like τ_i^j dependent on the algorithm iteration. Thus, the pheromone value for solution component c_i^j can be obtained as follows,

$$\tau_i^j = \sum\nolimits_{v \in s_j} \varphi_v.$$ (3.20)

Besides, we consider for each solution component c_i^j a desirability factor (i.e., an heuristic infor-
mation) denoted by $\eta(c_i^j)$, which provides a bias towards regeneration options with fewer regeneration
nodes. In this case, the desirability factor is obtained as follows,

$$\eta(c_i^j) = \frac{1}{\sum_{v \in s_j} \sigma}, \tag{3.21}$$

where σ is a user-predefined constant parameter.

The pseudo-code of our ACO RPD algorithm is shown in Procedure 4. First, pheromone values
for all nodes are initialized to a constant predefined parameter, that is, $\varphi_v = k, v \in \mathcal{V}$. Then,
over a number of global iterations, a number of ants are generated to construct, independently, a
solution to the problem by selecting, for each path $p \in \mathcal{P}^o$, a solution component according to a
state transition rule. Hence, each ant performs the complete set of variable instantiations. Since the
order in which paths are processed does have impact on the goodness of the solution, each ant has
a different, randomly generated order for processing the paths in $\mathcal{P}^o$. In our ACO heuristic, we rely
on two different pheromone updates, namely, a local and a global update. Whilst the former tries to
bias the ant towards regeneration options which contain nodes with its own pheromone (i.e., due to
previously processed paths), the latter aims at keeping track of high quality solutions by depositing
more pheromone on nodes belonging to those solutions so that subsequent ants can more easily find
the best trails. The state transition rule and both types of pheromone updates are next described.
It is worth mentioning that some of the mathematical expressions here presented are borrowed from
[92] and [95].

State transition rule

This rule is responsible for selecting the next solution component (regeneration option) in the ant
regenerator allocation process (see line 10 in Procedure 4). To be precise, the transition is based on a
pseudo-random-proportional rule aimed at balancing the exploration and exploitation abilities of the
algorithm. Assuming the ordered set of paths to be processed $\Lambda = \{p_1, ..., p_{|\mathcal{P}^o|}\}$ (see Procedure 4),
the selection of the solution component c_i^j for path p_i is done according to the following rule,

$$c_i^j = \left\{ \begin{array}{ll} \max_{c_i^j \in \mathcal{C}_i} \{\tau_i^j [\eta(c_i^j)]^\beta\} & \text{if } r \leq r_0 \\ Q & \text{if } r > r_0 \end{array} \right\}, \tag{3.22}$$

where $r \sim U(0,1)$, and $r_0 \in [0,1]$ and $\beta \in \mathbb{R}^+$ are user-predefined parameters. While β deter-
mines the relative importance of the heuristic information, r_0 balances between exploitation and
exploration: if $r \leq r_0$, the algorithm favors the solution component with the best compromise be-
tween pheromone and heuristic value, whereas if $r > r_0$ the algorithm explores the space of solutions
by choosing a solution component $c_i^j \in \mathcal{C}_i$ according to an empirical distribution whose probability
mass function is defined by $f_Q(q) = Pr(Q = q) = Pr\{c_i^j \in \mathcal{C}_i : Q(c_i^j) = q\} = p(c_i^j)$, where,

$$p(c_i^j) = \frac{\tau_i^j [\eta(c_i^j)]^\beta}{\sum_{c_i^k \in \mathcal{C}_i} \tau_i^k [\eta(c_i^k)]^\beta}. \tag{3.23}$$

Local update

The modifications on $\varphi_v, v \in \mathcal{V}$ caused by the local pheromone update process only have impact on the trail followed by the ant in progress (see lines 6 and 13 in Procedure 4). The main objective of this rule is to bias the ant towards nodes it has already visited during the construction of the solution with the aim of aggregating regenerators across the network. After selecting each solution component c_i^j, all the nodes contained in s_j update their pheromone values τ_i^j. The updating rule is defined as follows,

$$\varphi_v(t+1) = \varphi_v(t) + \alpha e^{-\psi \Delta_r}, \forall v \in s_j, \tag{3.24}$$

where $\alpha, \psi \in \mathbb{R}^+$ are two more user-specified parameters and $\Delta_r = |s_j| - 1$. Note that when the option selected s_j only contains one regeneration node $\Delta_r = 0$, thereby maximizing the quantity of pheromone deposited by the ant. Moreover, ψ is a decay constant which also controls the amount of deposition.

Global update

After a group of $MaxAnts$ have constructed their respective solutions (stored in Ω_{IT}), a global updating rule is applied to all solution components contained in each $\mathcal{R}_x \in \Omega_{IT}$. The aim of this rule is to guide the next group of ants towards high-quality solution components. To this end, node pheromone values are updated as follows,

$$\varphi_v(t+1) = (1 - \vartheta)\varphi(t) + \vartheta e^{-\phi(g(\mathcal{R}_x) - g(\mathcal{R}_{BEST}))},$$
$$\forall v \in s_j : \Omega_x \ni s_j, \forall \Omega_x \in \Omega_{IT}, \tag{3.25}$$

where $\vartheta, \phi \in \mathbb{R}^+$ are two user-predefined parameters. Note that ϑ controls the speed at which pheromone evaporate and ϕ is another decay factor. Finally, the exponential factor favors the deposit of pheromone on those regeneration nodes belonging to the best solutions obtained by each group of ants. All the parameters required to define the ACO RPD heuristic here presented will be adjusted in Section 3.4.

The worst case complexity of this algorithm is given by,

$$O(GlobItr \cdot MaxAnts \cdot |\mathcal{P}^o| \cdot \Theta), \tag{3.26}$$

where the first three factors represent the *repeat-until* and *for all* loops, and Θ in this case represents the maximum number of solution components that an ant may need to evaluate before applying the state transition rule.

Procedure 4 Ant Colony Optimization(ACO)

INPUT: $\mathcal{P}^o, \mathcal{S}_p \; \forall \; p \in \mathcal{P}^o, GlobItr, MaxAnts$
OUTPUT: $g(\mathcal{R}_{BEST})$
 1: InitializePheromoneValues($\mathcal{T}$)
 2: $\mathcal{R}_{BEST} \leftarrow \emptyset, count \leftarrow 0$
 3: **repeat**
 4:     $\Omega_{IT} \leftarrow \emptyset, ant \leftarrow 0$
 5:     **repeat**
 6:         Local Pheromones $\mathcal{T}_{LOC} \leftarrow \mathcal{T}$
 7:         $\Omega_x \leftarrow \emptyset$
 8:         $\Lambda \leftarrow$ random order of paths in $\mathcal{P}^o$
 9:         **for all** path $p \in \Lambda$ **do**
10:             $c_p^x \leftarrow$ getNextSolutionComponent($\mathcal{T}_{LOC}$)
11:             Take s_x from c_p^x
12:             $\Omega_x \leftarrow \Omega_x \cup \{s_x\}$
13:             UpdateLocalPheromones($c_p^x, \mathcal{T}_{LOC}$)
14:         **end for**
15:         Generate $\mathcal{R}_x$ from Ω_x
16:         **if** $g(\mathcal{R}_x) < g(\mathcal{R}_{BEST})$ **then**
17:             $\mathcal{R}_{BEST} \leftarrow \mathcal{R}_x$
18:         **end if**
19:         $\Omega_{IT} \leftarrow \Omega_{IT} \cup \{\Omega_x\}$
20:         $ant \leftarrow ant + 1$
21:     **until** $ant \geq MaxAnts$
22:     UpdateGlobalPheromones($\Omega_{IT}, \mathcal{T}$)
23:     $count \leftarrow count + 1$
24: **until** $count \geq GlobItr$

3.3.3 BRKGA algorithm

BRKGA is a type of genetic algorithm (GA) which has recently been proposed to effectively solve complex optimization problems, for instance, network related problems such as routing in IP networks and RWA in optical networks [96], [97]. In most cases, this meta-heuristic is characterized by being able to obtain high quality solutions in very short times.

In BRKGA, each individual is an array of n_g genes called *chromosome*. In addition, each gene is assigned a value, called an *allele*, in the real interval $[0, 1]$. Each chromosome encodes a solution of the problem and a *fitness* level (i.e., the objective function value $g(\cdot)$). Like any other GA algorithm, BRKGA evolves a set of p individuals, called a *population*, over a number of generations until a stopping criterion is met (e.g., number of iterations, generations without improvement). The subsequent generations consist of individuals which are created by means of: (1) a mating process (two chromosomes of the current population are combined); (2) a set of high quality chromosomes of the current generation (called elite set p_e) which are copied unchanged; (3) a set of new randomly generated chromosomes (called mutants) p_m, which should help the algorithm escape from local optima.

To produce offspring through the mating process, two chromosomes of the current population (one elite and another non-elite) are selected at random and then combined. The offspring can inherit alleles from both parents (though with a bias defined by the probability of inheriting from the elite parent ρ_e). In order to compute the fitness of each chromosome, a deterministic algorithm, called *decoder*, is used. The decoder is the only problem-dependent part of the BRKGA algorithm, and hence, is the only part that needs to be specifically developed to solve the RPD problem.

The pseudo-code of our decoder algorithm is shown in Procedure 19. In this case, each chromosome contains $n_g = |\mathcal{N}|$ genes (i.e., one per node in the network), and the metric value for each node corresponds to the value of the allele (i.e., the value of the gene). We select the option $s \in \mathcal{S}_p$ which minimizes the cost in terms of that metric. This cost corresponds to the sum of the alleles for all the nodes in a regeneration option (denoted by $c(s)$ in Procedure 19).

Considering a population size $p = n_g = |\mathcal{N}|$ and a maximum number of generations MG, the complexity of the BRKGA is given by,

$$O(MG \cdot |\mathcal{N}| \cdot Proc.19). \tag{3.27}$$

The complexity of the decoder algorithm in Procedure 19 is obtained as follows,

$$Proc.19 = O(|\mathcal{P}^o| \cdot \Theta \cdot (\delta - 2)), \tag{3.28}$$

where each term represents, respectively, $|\mathcal{P}^o|$ the most outer loop (line 5), the maximum number of regeneration options (loop in line 6) and the largest path $p \in \mathcal{P}^o$ having all its intermediate nodes as regeneration sites (loop in line 7).

Procedure 5 BRKGA decoder algorithm

INPUT: $\mathcal{N}, chromo, \mathcal{P}^o, \mathcal{S}_p \; \forall \; p \in \mathcal{P}^o$
OUTPUT: $fitness$
 1: **for all** node $n \in \mathcal{N}$ **do**
 2:     $n.metric \leftarrow chromo.getGene(n)$
 3: **end for**
 4: $\mathcal{R}_x \leftarrow \emptyset$
 5: **for all** path $p \in \mathcal{P}^o$ **do**
 6:     **for all** option $s \in \mathcal{S}_p$ **do**
 7:         **for all** node $n \in s$ **do**
 8:             $c(s) \leftarrow c(s) + n.metric$
 9:         **end for**
10:     **end for**
11:     Select $s \in \mathcal{S}_p$ with minimum $c(s)$ and generate $\mathbf{z}_p$
12:     $\mathcal{R}_x \leftarrow \mathcal{R}_x \cup \{\mathbf{z}_p\}$
13: **end for**
14: $fitness \leftarrow g(\mathcal{R}_x)$

$OSNR_{min}$	$OSNR_{pen}$	Usa-Can	Core	Basic	Large
19dB	1dB	421	18	349	746
19dB	2dB	657	55	462	919

Table 3.1: Number of paths that require regeneration ($|\mathcal{P}^o|$) and OSNR threshold values

3.4 Results and discussion

In this Section, we first present and compare the performance results of all the RRPD resolution methods presented in Sections 3.1, 3.2 and 3.3. Then, we study the performance of the T-SWS network architecture under some of the algorithms presented in order to prove that they are effective at satisfying the QoT requirements.

3.4.1 MILP-based resolution methods comparison

The evaluation has been performed by considering four different network topologies that are detailed in Appendix A. For this experiment, we consider a maximum of $K = 1000$ regeneration options to fill set $\mathcal{S}_p, p \in \mathcal{P}^o$, that is, for the specific network instances considered in this section, all possible regeneration options are added to the problem. Besides, the $OSNR_{th}$ values evaluated are provided in Table 3.1. We consider 1dB and 2dB as additional OSNR penalties (i.e., $OSNR_{pen}$) to account for the signal degradation caused by non-linear impairments (see Appendix A for further details on the OSNR thresholds). Hence, we evaluate our algorithms considering 20dB and 21dB as the system $OSNR_{th}$ thresholds. Note also that $OSNR_{th}$ determines the number of paths that require regeneration (i.e., $|\mathcal{P}_o|$), and hence, the level of complexity that is given to the problem. $|\mathcal{P}_o|$ values are also given in Table 3.1 for each considered network.

We use CPLEX [98] to solve, for each network and scenario, the three MILP RPD models

Scenario	Usa-Can	Core	Basic	Large
OPAQUE	3904	1472	2624	3648
OSNR$_{th}$ = 20dB				
MP1	355	55	497	854
MP2/3	351	56	502	866
R-MP1	344	55	496	860
OSNR$_{th}$ = 21dB				
MP1	634	146	752	1231
MP2/3	652	147	757	1238
R-MP1	646	146	751	1225

Table 3.2: MILP RPD methods comparison

Scenario	Usa-Can	Core	Basic	Large
OSNR$_{th}$ = 20dB				
MP1	(7.61%)	2	(2.91%)	(3.4%)
MP2/3	89	3	9	28
R-MP1	313	3	152	427
OSNR$_{th}$ = 21dB				
MP1	(9.43%)	2	(0.66%)	(2.68%)
MP2/3	57	3	12	36
R-MP1	224	3	751	280

Table 3.3: MILP RPD methods: execution times (seconds) and optimality gaps (%)

presented, namely MILP1 (optimal), MP2/3, and MILP1*. Table 3.2 reports the minimum number of regenerators to be deployed considering $B^{QoT} = 10^{-3}$ and that each node injects 20.8 Erlangs into the network. CPLEX is run with the time limit set to 1 hour. Note that Table 3.2 also provides the number of regenerators required when an opaque network architecture is considered. Finally, Table 3.3 reports the computation times for all the algorithms as well as the optimality gaps (%) for those cases in which optimality is not reached after 1 hour. One can note that MP1 is solved very effectively when small problem instances are considered (i.e., Core). However, and due to its computational complexity, MP1 reports optimality gaps in all the other cases. In contrast, R-MP1 is always solved to optimality and is able to substantially improve the trade-off provided by MP1 for some of the scenarios evaluated. Finally, MP2/3 also reports an overall good trade-off performance, as it is solved very quickly and with an average deviation to the best solution of 1.71%. From the results obtained, it can be concluded that both of the heuristic MILP formulations proposed, that is, R-MP1 and MP2/3, provide satisfactory near-optimal solutions within short running times.

Network	Usa-Can	German	Core	Basic	Large
$|\mathcal{P}_o|$	657	752	55	462	919

Table 3.4: $\mathcal{P}^o$ size values.

p	n_g	MG	ρ_e	p_e	p_m
$|\mathcal{N}|$	$|\mathcal{N}|$	100	0.7	0.2	0.2

Table 3.5: BRKGA parameter values

3.4.2 Meta-heuristic resolution methods comparison

In this section, we compare the performance of our RPD meta-heuristic methods (see Section 2.3 for the LCR algorithm description) with those of the optimal MP1 formulation and the load-based MILP heuristic (MP2/3) (Section 3.2), which here are used as baseline references.

Network scenario and parameter tuning

In this case, the evaluation is performed considering five different network topologies (see details in Appendix A). $|\mathcal{P}_o|$ values are reported in Table 3.4. Note that for these experiments we consider $OSNR_{th} = 21$dB (i.e., 19dB+2dB).

Here we consider a maximum of $K = 25$ options to fill $\mathcal{S}_p$, that is, $\mathcal{S}_p = \{s_1, \ldots, s_K\}$. Since all the RPD methods rely on random parameters to generate their respective solutions (e.g., the randomly built initial solution $\mathcal{R}_o$ in KLS), we conduct a set of independent runs for each method, and take as result the best value found. However, both the ACO and BRKGA meta-heuristics require some additional parameter tuning. After performing some preliminary experiments, we set the parameters of the BRKGA meta-heuristic to the values summarized in Table 3.5. Due to both the fact that ACO requires the tuning of a rather large set of parameters and that these may require a different set-up in each network topology, we perform a large set of experiments considering a number of different values for each parameter. Constant parameters σ and k are set to 0.1 and 1 respectively. Besides, we observe that the best solutions are always obtained when values of r_0 close to 1 are considered. Thus, we fix r_0 to 0.9. To obtain the rest of parameter values, we run the ACO algorithm with $GlobItr = 500$, $MaxAnts = 100$, loads of 15 and 20.8 erlangs and the values proposed in Table 3.6, thus conducting 450 experiments per network topology. Note that we assume that both decay factors have the same value. We observe that the results do not report any significant dependence on the network load scenario considered. The parameter values selected are shown in Table 3.7.

The algorithms are run assuming a target $B^{QoT} = 10^{-3}$, and loads equal to 20.8 and 15 erlangs. First, in Table 3.8, we provide the number of regenerators as well as the optimality gaps found by CPLEX when solving MP1 with the time limit set to 1 hour. In addition, we include the number of

$\psi = \phi$	0.25, 0.75, 1.75
ϑ	0.001, 0.01, 0.1
β	0.5, 1, 2, 3, 4
α	0, 0.001, 0.005, 0.01, 0.1

Table 3.6: ACO parameter values evaluated

Network	$\psi = \phi$	ϑ	β	α
Usa-Can	0.75	0.1	4	0.1
German	0.25	0.001	4	0.01
Core	0.25	0.001	4	0.005
Basic	0.25	0.01	4	0.01
Large	0.25	0.001	4	0.005

Table 3.7: ACO parameters selected for each network topology

regenerators required when an opaque network scenario is considered. Second, Table 3.9, reports the results (amount of regenerators to be deployed) of all the RPD heuristics presented as well as those of the MP2/3 MILP resolution method. Also, Table 3.10 reports the average computational times required by each of the methods when the load is set 20.8 Erlangs. Whilst in the Core network all methods perform quite similar, in all the other topologies both the BRKGA and MP2/3 stand out as the best methods. However, BRKGA always provides the best solution to the problem and it is only slightly outperformed by MP1 in the Basic instance. Furthermore, it reaches its solutions within very short running times compared to all the other methods evaluated. Hence, BRKGA stands out as a very powerful algorithm providing a high quality trade-off between optimality and complexity.

To further study these algorithms, in Fig. 3.3, we show the results of all the heuristics in some of the considered networks and for some exemplary B^{QoT} target values. Again, it is possible to see that BRKGA always obtain the best results, though it is closely followed by MP2/3 in all the networks, except for the Usa-Can topology, where MP2/3 exhibits a very poor performance and it

Method	Usa-Can	German	Core	Basic	Large
load=20.8					
MP1	634	606	146	752	1231
GAP(%)	9.4	22.7	0	0.7	2.7
load=15					
MP1	482	486	115	581	981
GAP(%)	7.9	25.6	0	0.5	7.2
OPAQUE	3904	5632	1472	2624	3648

Table 3.8: MP1 results and optimality gaps obtained by CPLEX

77

Method	Usa-Can	German	Core	Basic	Large
load=20.8					
MP2/3	654	518	147	761	1241
BRKGA	607	511	146	756	1223
ACO	636	538	147	769	1271
KLS	708	659	148	803	1296
RG	727	585	148	870	1378
load=15					
MP2/3	498	404	116	586	951
BRKGA	465	397	115	582	940
ACO	502	426	116	595	972
KLS	563	536	116	638	1028
RG	570	467	117	678	1076

Table 3.9: RPD algorithms results evaluation

Method	Usa-Can	German	Core	Basic	Large
MP2/3	43	116	1	19	59
BRKGA	10	19	1	3	10
ACO	117	174	6	33	142
KLS	37	103	1	15	64
RG	1	2	0.5	1	1.8

Table 3.10: RPD algorithms execution time (seconds)
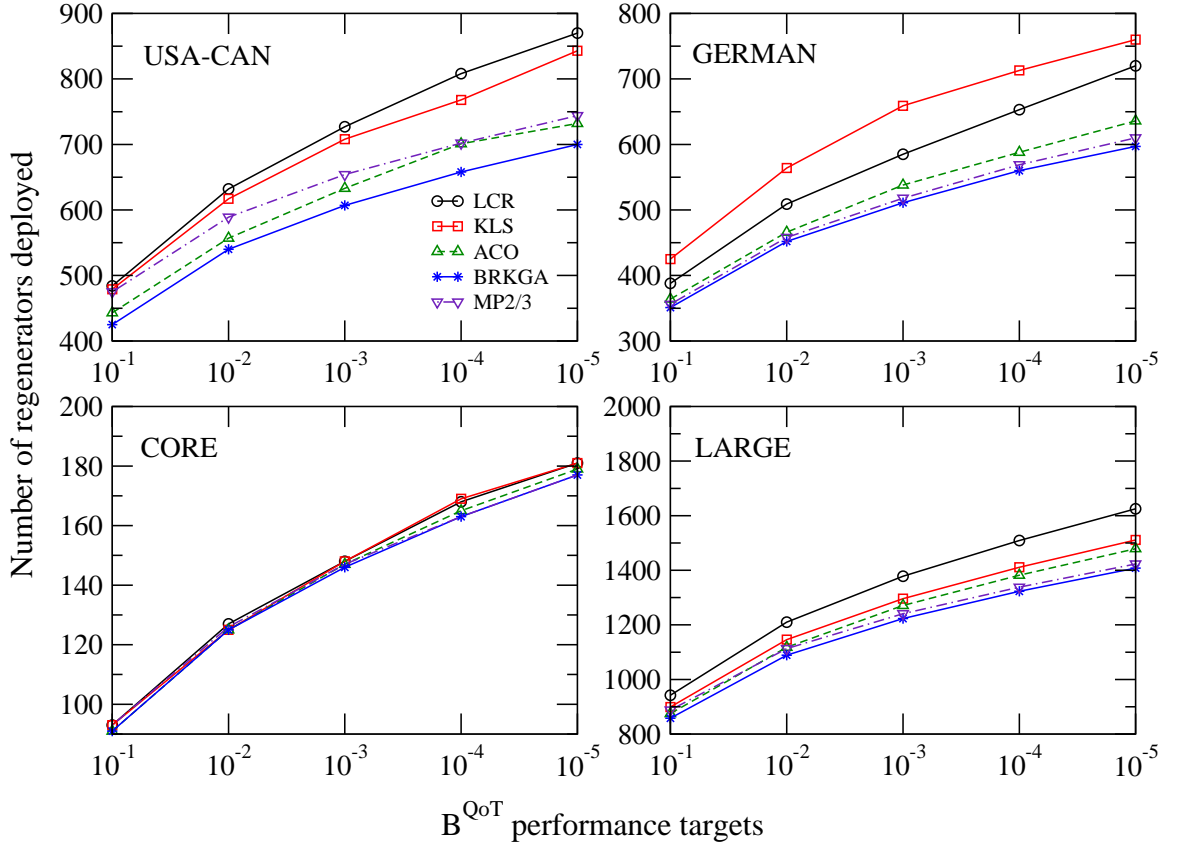
Figure 3.3: RPD algorithms performance in the Usa-Can, German, Core and Large networks under different B^{QoT} targets.

is even outperformed by ACO. In the next subsection, we evaluate the performance of some of these heuristic methods when applied to the T-OBS network architecture proposed.

3.4.3 Impact on the T-SWS network performance

The RPD heuristics proposed must ensure that burst losses due to unacceptable OSNR levels are kept under control, and thus, that the predefined target loss rate B^{QoT} is met. In order to verify that this is accomplished, we conduct a set of simulations over both the German and Large network topologies. Aiming at providing illustrative plots of the scenario in hand, we consider the best and worst RPD heuristic for each network, that is, the BRKGA as the best method in both cases, and the KLS (German) and LCR (LARGE). In addition, we include the transparent and opaque scenarios and use them as benchmark references. In both experiments, we consider B^{QoT} values equal to 10^{-3} and 10^{-5}. The results obtained are presented in Fig. 3.4(a), for the German network, and in Fig. 3.4(b), for the Large network.
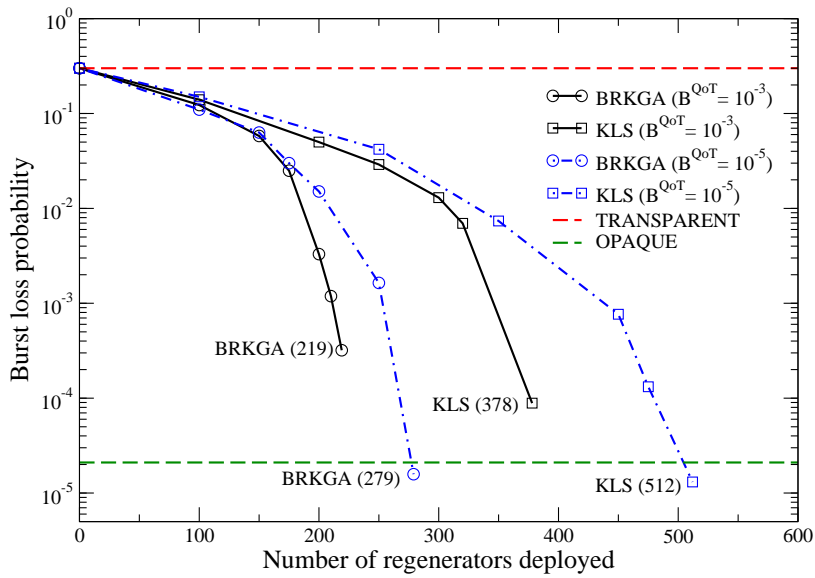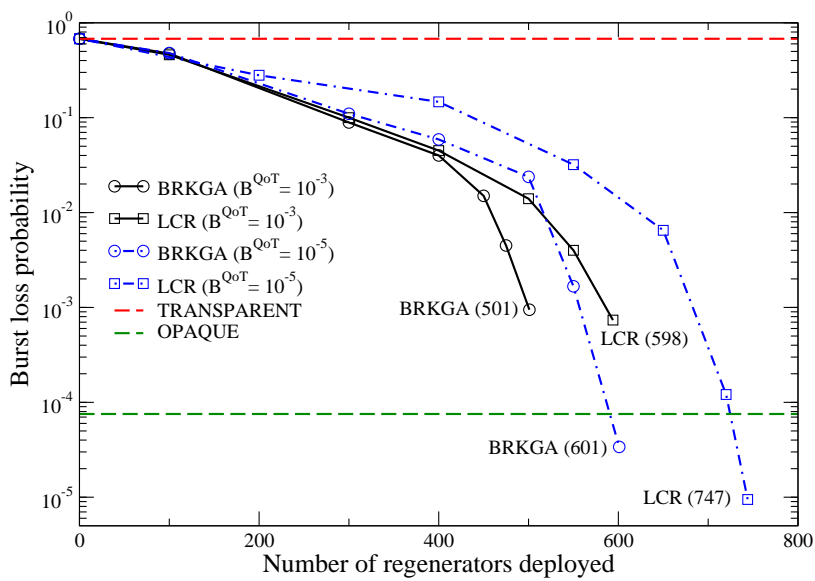
Figure 3.4: (a) BRKGA vs. KLS performance comparison in the German network, and (b) BRKGA vs. LCR performance comparison in the Large network.

Load	7	7.5	8	8.5	9	9.5	10
Contention (%)	93.7	90	88.5	84.6	80.1	73	67.1
OSNR (%)	6.3	10	11.5	15.4	19.9	27	32.9

Table 3.11: Share of burst losses for a BRKGA dimensioning in the Large network

One can note that with the progressive and even placement of regenerators (i.e., regenerators are fairly distributed among all regenerator sites) the packet loss probability (PLP) moves towards either the target performance B^{QoT} or the opaque performance. In both Fig. 3.4(a) and Fig. 3.4(b), once all the regenerators are deployed, we can observe two different situations: if B^{QoT} is set to 10^{-3}, OSNR losses are still predominant due to the low contention losses of this scenario; if B^{QoT} is set to 10^{-5}, in contrast, contention losses become predominant in the network. Note that in both of the figures provided, the PLP found in the case where contention losses are predominant slightly improves that of the opaque case. This is due to the differences in node architectures between the opaque and translucent networks: whilst the opaque network relies on in-line regenerators as in [72], our translucent architecture operates in the feed-back mode as shown in Chapter 2, and hence, packets remain in the electrical buffer until a free wavelength is found at the desired output link.

In the next experiment, and due to the fact that we are addressing an offline planning/dimensioning of the network, we evaluate the impact that load variations have on both losses due to contention in network links and losses resulting from unacceptable OSNR levels. To this end, we dimension the T-SWS network considering the Large topology, a load of 9 Erlangs and a target $B^{QoT} = 10^{-3}$. In this scenario, BRKGA provides a solution requiring 633 regenerators to be deployed. Table 3.11 reports the share of packet losses for different load values. Although we can observe that for higher loads the percentage of OSNR-based losses inevitably increases, we assume that the dimensioning of the network is made according to a worst-case scenario. Therefore, it can be concluded that our approach guarantees that OSNR losses are kept well below those caused by packet contentions in network links.

For the sake of illustration, we conduct a final experiment to report the location and exact number of regenerators per location considering both the Core and Large topologies. The results are provided in Table 3.12. The offered load per node is, respectively, 12.8 and 6.4 Erlangs for the Core and Large topologies. Note that whilst in the Core network the minimum amount of nodes equipped with regenerators is 3, in the Large network it increases up to 13.

3.5 Summary

In this chapter, we have proposed several RRPD methods for the sparse placement of regenerators in a T-SWS network. Such methods are based on an optimal MILP formulation, MILP-based and meta-heuristic techniques. Strictly speaking, we have uncoupled the routing issue from the RPD

Network	B^{QoT}	Node (Regenerators)
Core	10^{-2}	0(18),10(9),14(6)
	10^{-4}	1(19),3(13),14(16)
	10^{-3}	0(26),6(18),8(19),10(34),12(59), 14(30),17(13),18(21),22(42),23(19), 27(11),32(33),33(33)
Large	10^{-5}	0(32),6(22),8(24),10(41),12(68), 14(37),17(18),18(27),22(50),23(24), 27(15),32(28),33(40)

Table 3.12: Location and number of regenerators for both the Core and Large topologies under two different B^{QoT} scenarios

problem, and eventually solved the so-called R+RPD problem. We have presented a link congestion-reduction unsplittable routing strategy which is based on a MILP formulation aimed at reducing congestion in bottleneck network links. The routing solution obtained has then been used as input for the RPD problem. The RPD scheme presented relies on the piecewise linear approximations of the inverse of the Erlang B-loss formula. Since such formulation corresponds to the complex DCMCF problem, we have also developed heuristic MILP and meta-heuristic methods to help solve the RPD problem (i.e., RP+D heuristics). We have evaluated and compared these methods by considering the trade-off between optimality and complexity they provide. After assessing their performance over a range of network topologies, we have found that, among the MILP methods, the heuristic RPD methods proposed, that is, MP2/3 and R-MP1, provide the best trade-offs. Then, we have thoroughly evaluated and compared the performance of the meta-heuristic RPD methods proposed with that of the optimal MP1 and heuristic MP2/3 algorithm. The results have shown that BRKGA is, among all the methods evaluated, the one providing the best trade-off between optimality and complexity.

Finally, we have conducted a series of simulations in the T-SWS network and concluded that both the architecture and RRPD models proposed in this thesis ensure that, according to a pre-specified target QoT performance, losses caused by OSNR signal degradation are kept satisfactorily under control and do not impact negatively the overall T-SWS network performance.

As it has been mentioned in this chapter as well as in Chapter 2, the study presented so far relies on the off-line estimation of the PLIs, a fact which dictates the need for setting up a penalty on the $OSNR_{th}$ in order to ensure the feasibility of each connection established in the network. As it will explained in the next chapter, this results in an over-provisioning, and consequently, overuse of the costly, power-consuming regenerators. To tackle this issue, we propose a new networking model which enables the SWS network to deal, real-time, with time-varying PLIs. The direct consequence of this dynamic network are improvements in both energy efficiency and packet loss performance.

Furthermore, given the complexity found when both the MILP formulations and the meta-heuristic algorithms are run to solve RRPD in backbone scale networks such as those shown in Appendix A, in Chapter 8 in Part II of this thesis, we propose several complex, hybridized meta-heuristics to efficiently solve RRPD. Then, aiming at positioning some of the algorithms as compelling network planning algorithms for the future T-SWS networks, we compare their results with those of the optimal and heuristic MILP-based methods presented. This time, however, experiments specifically focus on solution optimization and involve performing a set of intensive, long-lasting experiments.

Chapter 4

Cost Feasibility Analysis of Translucent Optical Networks with Shared Wavelength Converters

4.1 Introduction

To deal with PLIs in SWS networks, in Chapter 2, we modeled a translucent SWS fabric configured following the tune-and-select scheme. This photonic switch is based on SOA technology to ensure the provisioning of high-speed all-optical switching in an asynchronous fashion. Given the lack of optical buffers, in this architecture, contention resolution is achieved through all-optical wavelength converters (WCs) [99, 100]. As shown in Fig. 2.2 in Chapter 2, a dedicated full-range fixed-input, tunable-output wavelength converter (FITO-WCs) is available per wavelength and input port.

However, full-range wavelength tunability results in very complex, power-consuming and lossy WC devices [101, 102, 103]. Indeed, current techniques to achieve conversion between any given combination of input/output wavelengths involve cascading a set of limited range WCs, thereby leading to very expensive devices [104]. For these very reasons, there has been significant research effort to devise photonic switch architectures which exploit WC-sharing [105], and, by this means, minimize the number of WCs required to meet a target loss performance. In these node architectures, packet loss is not only caused by the lack of a free wavelength at the selected output port, but also due to the lack of a free WC. The most well-known instance is the shared-per-node (SPN) configuration [105], which represents the perfect sharing scheme, as a pool of WCs is fairly shared among all wavelengths from all input ports. In SPN, WCs are required to be tunable-input, tunable-output (TITO-WCs), which are assumed to be the most complex and expensive type of WCs

[106]. TITO-WCs are also used in the shared-per-link (SPL) architecture [107], in which a bank of WCs is dedicated to each output fiber. SPL, however, is not considered in this study as it suffers from inefficient WC-sharing, particularly under unbalanced traffic conditions [108, 107]. More recently, in [106, 108], two alternative WC-sharing configurations were proposed that use less complex WCs. Specifically, the shared-per-input-wavelength (SPIW), and the shared-per-output-wavelength (SPOW) switching fabrics. Whilst SPIW relies on FITO-WCs as the DWC node, SPOW requires tunable-input, fixed-output WCs (TIFO-WCs), which are considered to be the less complex, and therefore, cheaper WCs [108, 109].

The consideration of WC-sharing switching fabrics has nevertheless important implications on the optical signal degradation along its way from source to destination. Indeed, the higher power penalties paid at passive devices (splitters/combiners) as well as the higher number of active components (SOA gates inducing higher ASE noise levels) that the signal traverses increase the impact of PLIs, thereby limiting the size and capacity of nodes [72, 110]. In addition, stronger degradation due to PLIs shortens optical reach, and thus, a network based on WC-sharing switching fabrics will require more regenerators to be deployed. Summarizing, when compared to the DWC node, WC-sharing architectures minimize the number of WCs, but at the same time require more complex switching fabrics (more optical gates) and increase the impact of PLIs (more regenerators). It is clear, then, that the interest of WC-sharing switches with respect to DWC-based architectures depends on the quality of the above mentioned cost trade-off.

For this reason, in this chapter, we carry out a thorough cost feasibility analysis for translucent SWS networks based on WC-sharing node architectures. To this end, we first model and assess the performance of a set of translucent WC-sharing switching fabrics and, considering a realistic node configuration for OTNs, we select one of the WC-sharing nodes to perform an adequate power-budget and noise analysis. Then, considering an optical-signal-to-noise ratio (OSNR)-based QoT model and an RRPD algorithm [18, 20], a translucent SWS network based on WC-sharing nodes is equipped with the required pools of regenerators. Through simulation, we approximate the exact amount of WCs that are required at each node to meet the loss performance of the DWC case. Finally, we consider relative cost values and state-of-the-art technology for optical gates, WCs and regenerators, to analyze, over a broad range of large-scale topologies, the viability of WC-sharing schemes for next-generation translucent SWS-based OTNs.
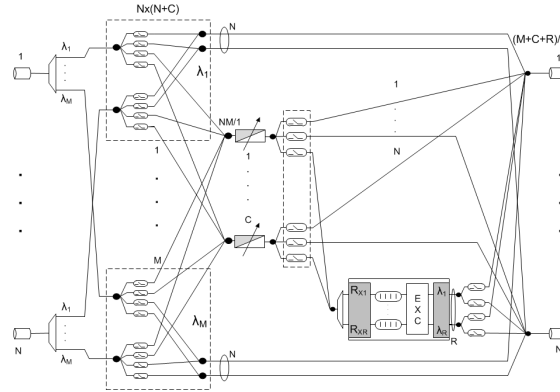
Figure 4.1: Translucent shared-per-node (SPN) architecture. TITO-WCs are used.
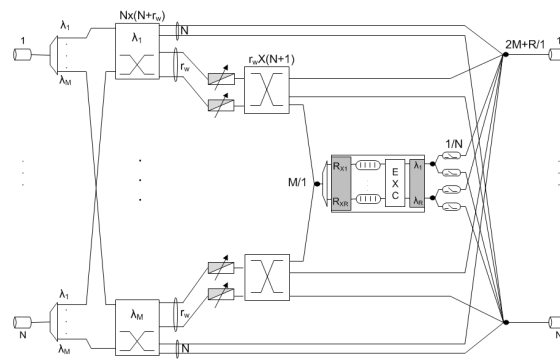
Figure 4.2: Translucent shared-per-input-wavelength (SPIW) architecture. FITO-WCs are used.
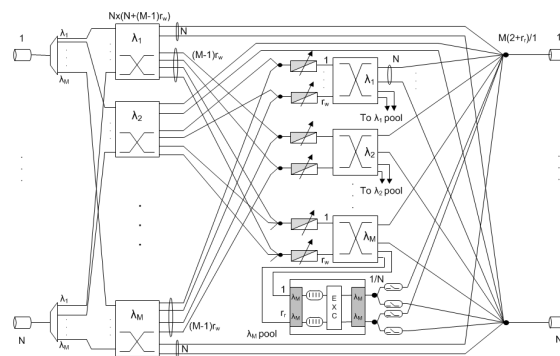
Figure 4.3: Translucent shared-per-output-wavelength (SPOW) architecture. TIFO-WCs are used.

Table 4.1: Number of WCs and SOA gates required in the translucent DWC, SPN, SPIW and SPOW architectures

Scheme	Device	Quantity
DWC	FITO-WCs	$N \cdot M$
	SOA gates	$N \cdot M \cdot (N + 1) + R \cdot N$
SPN	TITO-WCs	C
	SOA gates	$M \cdot N \cdot (N + C) + C \cdot (N + 1) + R \cdot N$
SPIW	FITO-WCs	$M \cdot r_w$
	SOA gates	$M \cdot N \cdot (N + r_w) + M \cdot r_w \cdot (N + 1) + R \cdot N$
SPOW	TIFO-WCs	$M \cdot r_w$
	SOA gates	$M \cdot N \cdot (N + r_w \cdot (M - 1)) + M \cdot r_w \cdot (N + r_r) + M \cdot r_r \cdot N$

4.2 Translucent WC-sharing architectures

We assume photonic switches with N input/output mono-fiber links, each carrying M wavelength channels (i.e., $\lambda_1 \ldots \lambda_M$) and that perform asynchronous packet switching. Figure 4.1, depicts the SPN switching fabric including a pool of R regenerators that is used to mitigate the impact of PLIs. Since in these schemes WCs are a scarce resource, an initial splitting stage, which consists of a bank of high speed switching SOA gates, can transfer the signal either directly to the selected output fiber (in case no wavelength conversion is needed) or to a bank of C TITO-WCs, which is perfectly shared among all wavelengths from all input ports. After wavelength conversion is performed, a second SOA gating stage grants access either to the selected output port or the pool of regenerators. It is worth noticing that thanks to the tunability of the output wavelength at WCs, a fair access to the regenerator pool is also provided with this architecture.

In an attempt to improve the trade-off proposed by the SPN scheme, research focused on WC-sharing schemes that could use simpler, less expensive WCs. In [106, 108], authors present the SPIW (also known as shared-per-wavelength (SPW)) and SPOW architectures.

Figure 4.2, presents the translucent SPIW switch. In this case, WCs are arranged in small banks of size r_w and dedicated to each input wavelength. Hence, if there is a packet arriving in λ_1 requiring wavelength conversion, whatever the input port is, it will only have access to the bank of WCs dedicated to λ_1. Again, thanks to the output wavelength tunability of the WC device in SPIW, a common pool of regenerators can be fairly shared. Note that for both SPIW and SPOW (see Fig. 4.3), the space switching stages follow the same SOA-based structure as shown in Fig. 4.1, for the SPN node.

Finally, Fig. 4.3 illustrates the SPOW switching fabric, where WCs are arranged in small banks of size r_w, one per output wavelength. In this case, however, since the less expensive TIFO-WCs are

used, the WC output is fixed to a different wavelength in each bank. In SPOW, an arriving packet in λ_1 has more chances to find a free WC than in the SPIW configuration, as it can try any bank of WCs except for the one where the output wavelength is set to λ_1. As to the regenerator pool configuration, and in order to maximize the sharing of regenerators, it has to be arranged in small banks, each consisting of a set of r_r regenerators for the same wavelength (fixed by the output of each FITO-WC). Finally, the complexity of the presented translucent node architectures in terms of the number of both WCs and SOA gates is reported in Table 4.1.

The efficiency in minimizing the number of WCs required to meet a target loss performance of these switching fabrics has been extensively studied under both synchronous and asynchronous scenarios, balanced and unbalanced traffic, and mono/multi-fiber schemes (see e.g., [105, 108, 106, 107, 111] and references therein). As discussed in the last section, in order to carry out the cost comparison between the DWC and WC-sharing architectures, in this study we focus on a mono-fiber, asynchronous scenario. To this end, our next objective is to select one of the WC-sharing architectures presented to continue with the cost study. In [108], a loss performance analysis is carried out under asynchronous operation, and it is shown that SPOW can provide WC savings very close to those obtained by SPN while slightly increasing the number of both SOA gates and WCs (which however are less expensive). The evaluation is nevertheless conducted considering $N =$ 16 and 32, numbers that are too high for core networks, which are our objective in this chapter. Indeed, in realistic backbone networks such as the ones considered in this thesis (see Appendix A for details), the highest node degree (N) is rather small, typically around 4 [112, 113] (5 in our instances).

Under these circumstances, and assuming Poisson traffic arrivals, we expect the arrangement of WCs in small banks in both SPIW and SPOW to have a serious adverse effect on the packet loss performance, which may lead to inefficient WC-sharing. Another drawback of the SPOW scheme that must be mentioned is the fact that regenerators are also arranged in small banks. Given the Erlang-based dimensioning function used in RRPD [18], which favors the grouping of regenerators, the SPOW set up is highly likely to require a higher number of regenerators to meet a given target loss performance in the access to these pools.

4.2.1 WC-sharing architectures evaluation in an isolated node

To analyze the performance of the different schemes, we conduct a series of simulations considering an isolated node with $N = 2$ and 5, that is, the two extreme values for a typical node degree in core OTNs (see Appendix A for more simulation details). In addition, for this experiment we neglect the impact of PLIs, and hence, no regenerators are considered (i.e., $R, r_r = 0$). We analyze the packet loss probability (PLP) as a function of the wavelength conversion ratio (ψ), which is equal to $\frac{\mathcal{C}}{NM}(\mathcal{C} = 0 \ldots NM)$ for SPN, and $\frac{r_w}{N}(r_w = 0 \ldots N)$ for SPIW and SPOW. We note that the
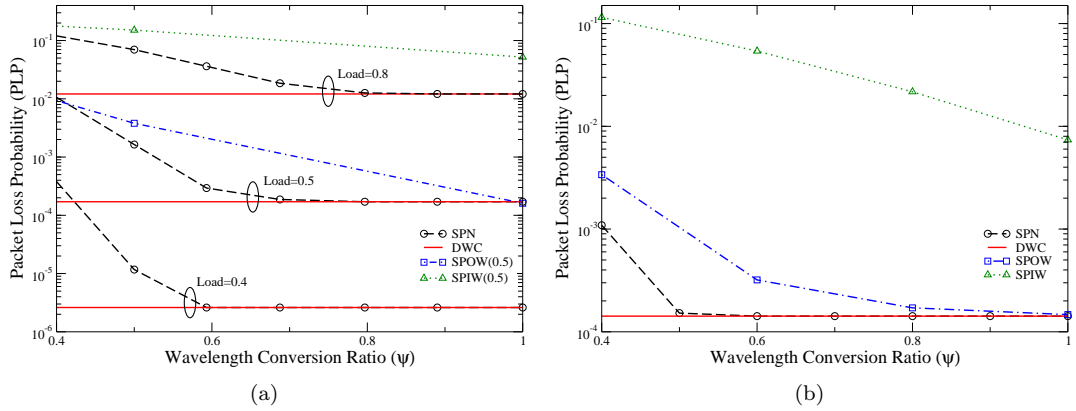
Figure 4.4: Performance evaluation of the different WC-sharing architectures proposed in an isolated node. Packet loss probability as a function of the wavelength conversion ratio with a) $N = 2$; b) $N = 5$. $M = 32$ wavelengths per link each at 10 Gbps.

scheduling algorithms considered in this chapter are the ones as described in [108].

Figures 4.4(a) and 4.4(b), provide the results obtained, respectively, for the $N = 2$ and $N = 5$ nodes. In Fig. 4.4(a), we consider three different load (ρ) values (i.e., 0.4, 0.5 and 0.8) for the SPN and DWC nodes. As expected, SPN at lower loads requires less WCs (lower ψ) to meet the performance of the DWC node. We also simulate SPIW and SPOW for the intermediate load case ($\rho = 0.5$). In the $N = 2$ node, only three possible ψ values exist for SPIW and SPOW (i.e., 0, 0.5 and 1). One can observe the poor performance of SPIW, and that SPOW requires as many WCs as DWC to meet the target performance, thus not providing any WC reduction. In Fig. 4.4(b), where $\rho = 0.5$ is assumed, whilst the higher value of N, enabling more ψ values in both SPIW and SPOW, allows the latter to slightly improve its performance, SPIW still results in a very inefficient scheme. Approximately, $\psi = 0.675$ and 1 for SPN and SPOW in the $N = 2$ node and 0.5 and 0.8 for the $N = 5$ node. Using these values, the hardware requirements for these architectures are reported in Table 4.2. Although SPOW uses WCs that are expected to be cheaper, in comparison to SPN it requires more WCs and a significantly higher amount SOA gates.

Taking into account these results and the fact that the average node degree in core OTNs is much closer to 2 than 5 (see Appendix A), we believe the SPN architecture is the best candidate to conduct the cost feasibility analysis for translucent OTNs based on WC-sharing. Finally, it is important noticing that incoming packets requiring regeneration (i.e., access to the regenerator pool) will require the use of a WC, as regenerators are accessed trough the bank of WCs. Hence, nodes equipped with regenerators (translucent nodes) will require an increase of ψ in order to meet the target loss performance. This issue, however, will be analyzed in more detail in the next section.

Table 4.2: Number of WCs and SOA gates required in an isolated node configured as DWC, SPN and SPOW switch.

Scheme	N	WCs	SOA gates
DWC	2	64	192
	5	160	960
SPN	2	44	3076
	5	80	14080
SPOW	2	64 ($r_w = 2$)	4224
	5	128 ($r_w = 4$)	21280
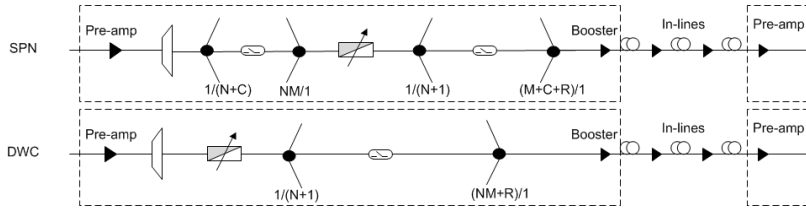
Figure 4.5: Characteristic signal path between two translucent SWS nodes configured either as DWC or SPN.

4.3 Translucent SWS network design

To design the translucent SWS network we follow the approach presented in [18, 20]. Specifically, we first consider a QoT model based on the off-line estimation of the OSNR contributions of both nodes and links in the end-to-end signal path. Hence, in this study we refer to the system QoT_{th} as $OSNR_{th}$. We also point out that there may exist strong signal degradation due to inaccuracies in these estimations, non-linear impairments arising from the high-speed ON-OFF switching nature of the traffic as well as from amplifier dynamics [114]. Due to these non-desirable impacts, it is necessary to consider a penalty margin (e.g., 2 dB extra) when determining an adequate $OSNR_{th}$ [77].

4.3.1 Power budget and noise analysis

In order to adequately tune and setup the components building both the DWC and SPN nodes, we consider the characteristic path that an optical signal follows between two neighboring nodes (see Fig. 4.5). We can anticipate that SPN, due to the more complex configuration, will suffer from higher PLI impact.

We consider the power budget and analysis model as well as sub-systems and components provided in Chapter 2. Note that with all the information we have so far, we can obtain, for a DWC-based network, the set of paths ($\mathcal{Q}$) that require regeneration at some point (i.e., whose OSNR

level at the receiving end is below $OSNR_{th}$), and thus, that are input to the RRPD algorithm. In SPN, however, we must first obtain the number of WCs C that are available at each node in order to compute the actual splitting and coupling losses in the node. In the next section, this issue is tackled by means of an iterative simulation algorithm.

4.3.2   Translucent SPN Network Dimensioning

It is obvious that the key issue when dimensioning the SPN network is to find out the minimum amount of WCs required (per node) so that the performance of the DWC architecture is matched. To approximate the exact number of WCs required at each node, we implement an iterative algorithm based on network simulation. The pseudo-code is shown in Procedure 6. We denote the set of nodes in the network as $\mathcal{V}$ and the set of nodes equipped with regenerators (translucent nodes) with $\mathcal{H} \subseteq \mathcal{V}$.

As explained in Section 4.2, this analysis is dependent on the network load assumed (ρ), and hence, this is an input parameter to be taken into account. Procedure 6, first runs a simulation considering an opaque network (i.e., no PLI impact) using the DWC switch in order to obtain the target PLP for each node of the network. Then, the loop between lines 1 and 17, is responsible for obtaining the minimum amount of WCs (C_v, $\forall v \in \mathcal{V}$) that ensures that each node in the SPN network matches the performance of its DWC counterpart. Next, the power budget and noise analysis is performed and the set of paths $\mathcal{Q}$ is obtained. Using $\mathcal{Q}$, the RRPD algorithm is run and the required regenerator pools are deployed across the network. Note that RRPD requires as parameter the target loss performance in the access to these pools (B^{QoT}). As previously mentioned, however, the fact that regenerator pools lie behind the shared bank of WCs leads to degraded loss performance in translucent nodes. For this reason, these nodes will require more WCs to meet the target DWC performance. To this end, between lines 18-29, the algorithm runs a second loop until the target PLP for every node is achieved. Note that since routing paths are computed at the very beginning of the algorithm and do not vary, this second loop does not affect the WC requirements at nodes $v \notin \mathcal{H}$. PLP values are obtained by averaging 10 independent runs of the simulation. Each run lasts enough simulation steps so that very accurate values are obtained (i.e., reporting negligible confidence intervals). Once Procedure 6 finishes, we have available the total amount of WCs, regenerators and SOA switches required by the translucent SWS network based on SPN switching fabrics.

In the next section, we dimension each of the translucent topologies considering both the DWC and SPN architectures, and finally, using relative cost values and current state-of-the-art technology for WCs, SOA gates and regenerators, we analyze the viability of deploying future SWS OTNs based on WC-sharing architectures.

Procedure 6 Translucent SPN network dimensioning

INPUT: $\mathcal{V}$, ρ;

OUTPUT: Translucent SPN network dimensioned;

  1: $C_v = 0$, $\forall v \in \mathcal{V}$;

  2: Simulate-network(DWC,ρ);

  3: Obtain $PLP(v,\text{DWC})$, $\forall v \in \mathcal{V}$;

  4: **repeat**

  5:     Simulate-network(SPN,ρ);

  6:     **for all** node $v \in \mathcal{V}$ **do**

  7:       **if** $PLP(v,\text{SPN}) > PLP(v,\text{DWC})$ **then**

  8:         $C_v \leftarrow C_v + 1$;

  9:       **else**

10:         Node v meets target $PLP(v,\text{DWC})$;

11:       **end if**

12:     **end for**

13: **until** all node $v \in \mathcal{V}$ meet target $PLP(v,\text{DWC})$

14: Perform power budget and noise analysis and obtain $\mathcal{Q}$;

15: Run RRPD($\mathcal{Q}$,ρ,B^{QoT});

16: **repeat**

17:     Simulate-network(SPN,ρ);

18:     **for all** node $v \in \mathcal{H}$ **do**

19:       **if** $PLP(v,\text{SPN}) > PLP(v,\text{DWC})$ **then**

20:         $C_v \leftarrow C_v + 1$;

21:       **else**

22:         Node v meets target $PLP(v,\text{DWC})$;

23:       **end if**

24:     **end for**

25: **until** all node $v \in \mathcal{H}$ meet target $PLP(v,\text{DWC})$

Table 4.3: Network simulation setup

Network	ρ	PLP_{opaque}	B^{QoT}	DWC WCs
Core	0.45	$2.64 \cdot 10^{-3}$	$5 \cdot 10^{-4}$	1472
Basic	0.27	$2.88 \cdot 10^{-3}$	$5 \cdot 10^{-4}$	2624
Usa-Can	0.2	$9.71 \cdot 10^{-4}$	$1 \cdot 10^{-4}$	3904
Large	0.125	$1.35 \cdot 10^{-3}$	$1 \cdot 10^{-4}$	3744

4.4 Cost comparison of translucent SWS networks based on DWC and SPN photonic switches

In this section, in order to analyze the cost implications of the SPN switching fabric and compare it against the DWC one, we dimension 4 translucent SWS network topologies (see Appendix A) following the approach presented in Section 4.3. Note that for the DWC network it is enough to first use the OSNR model to obtain the set of paths requiring regeneration, and second, execute an RRPD algorithm to deploy regenerators. It should be mentioned that the aim of the RRPD formulation is to minimize the number of regenerators deployed in the network whilst, at the same time, guaranteeing that losses caused by QoT signal degradation (optical signals whose OSNR is below OSNR_{th}) are kept well below those caused by contentions in network links. Hence, once dimensioned, a translucent network must show an overall PLP similar to that of an opaque network, where PLIs are perfectly mitigated.

Taking these details into account, in Table 4.3, we report the simulation scenario for each of the network topologies. Since the typical operation range for SWS networks is for overall PLPs in the order of 10^{-3} and lower, we select for each network a load value (ρ) which could be considered as a worst-case scenario network dimensioning. These loads allow us to obtain the PLP of the opaque network (PLP_{opaque}), which is the target PLP performance to be met by the translucent networks. Since PLP_{opaque} in both the Usa-Can and Large networks is slightly lower, we also reduce the maximum contention allowed in the access to regenerator pools (B^{QoT}). Finally, for illustration purposes, the number of WCs required in the DWC network are also provided in Table 4.3. Note that the number of WCs in a DWC network corresponds to the number of regenerators used in an opaque network (i.e., one per channel and input port).

Using the OSNR model detailed in Section 4.3, and assuming an $\text{OSNR}_{th} = 21$ dB (2 dB penalty [20]), we show in Fig. 4.6, the percentage of paths that require regeneration at some intermediate node for both the DWC and SPN architectures. We consider the optical end-to-end paths of the 4 continental scale network topologies provided in Appendix A. Routing paths are obtained using the optimization approach detailed in [20]. One can observe the higher PLI impact in SPN, a fact which will increase the number of regenerators required to meet the target QoT. These paths are therefore
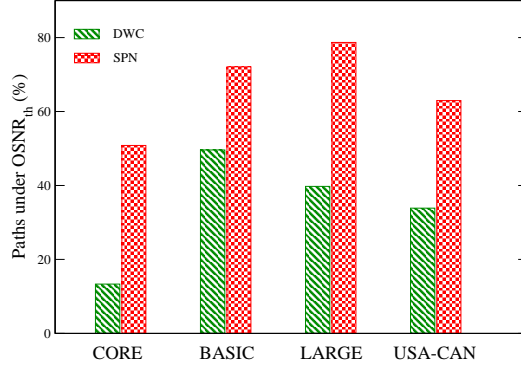
Figure 4.6: Percentage of end-to-end optical paths that do not meet the OSNR requirements for both the DWC and SPN architectures.

the input data required to run an RRPD algorithm, which will be in charge of deciding regenerator pool locations and their size. To solve RRPD, in this analysis we make use of the load-based mixed integer linear programming (LB-MILP) formulation proposed in [20]. LB-MILP is a two-step MILP formulation which focuses on grouping regenerators in as few nodes as possible in order to minimize regeneator locations/sites and the overall network load requiring regeneration.

Figures 4.7(a), and 4.7(b), provide the difference in hardware requirements between the translucent SPN and DWC networks. As expected, Fig. 4.7(a) reports the significant gain (improving with network size) in terms of the number of WCs that can be achieved with the SPN switch, and that this improvement comes at the expense of an increase in the number of regenerators to compensate the higher degradation due to PLIs. However, we can also note in Fig. 4.7(b), that due to the more complex switching fabric, SPN requires a much larger number of optical SOA gates, a fact which inevitably leads to a substantial increase in both hardware cost and power consumption.

To analyze the feasibility of the SPN node, we now consider relative cost values for the WCs (C_{WC}), SOA gates (C_{Gate}) and regenerators (C_{3R}), and compute the network CAPEX considering the complexity formulas presented in Table 4.1. Since both architectures use different WCs, we define the cost of a WC in the SPN network as $C_{WC-SPN} = \gamma C_{WC-DWC}$, where γ is defined as:

$$\gamma = \frac{C_{TITO-WC}}{C_{FITO-WC}}. \tag{4.1}$$

Finally, we define the following two relative parameters to analyze the results of both network scenarios.

$$\alpha = \frac{C_{WC}}{C_{Gate}}, \tag{4.2}$$
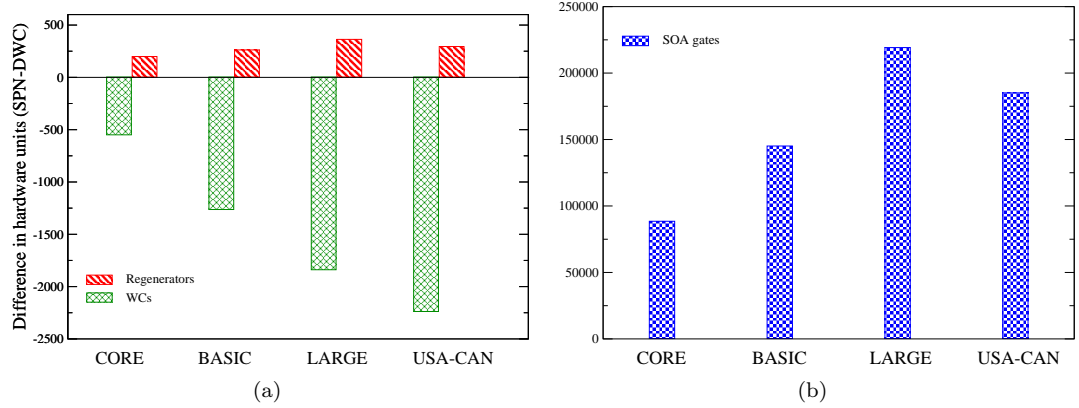
Figure 4.7: Hardware requirements difference between the SPN and DWC network architectures in terms of a) WCs and regenerators, and b) SOA gates. Note that negative values mean SPN requires less units than DWC.

$$\beta = \frac{C_{3R}}{C_{WC}}. \tag{4.3}$$

Figure 4.8, provides the results for the 4 network topologies. The y-axis represents the cost difference (in percentage) between the SWC and DWC networks. Hence, negative y-axis values mean that SPN results in a cheaper network. This cost is evaluated as a function of β, which deals with the relative cost difference between WCs and regenerators. The curves in the plots represent 4 different values for α considering $\gamma = 1$, that is, that the WCs of both architectures have the same cost. In addition, an additional curve is shown to illustrate the effect of assuming a 10 % ($\gamma = 1.1$) cost difference between both WCs for $\alpha = 200$.

Considering $\gamma = 1$, one can observe that, for the SPN network to become cost-effective, on the one hand, α has to be at least 200 in the smaller networks (Core, Basic), slightly more than 100 in the Large, and 100 for Usa-Can. Thus, SPN requires two orders of magnitude difference between a WC and a gate. This is a clear consequence of the much larger number of SOA gates required in SPN. Also, the benefits of SPN improve with network size, as more nodes allow for larger reductions in the number of WCs in the network. On the other hand, we can also observe that by increasing β, the network cost becomes dominated by $C_{Regen.}$. Since SPN requires more regenerators than DWC to mitigate PLIs, it will require β to be as low as possible. To be precise, considering $\alpha = 200$, we can estimate that for SPN to improve upon DWC, β should be ≤ 1 in both the Core and Basic networks, an approximately ≤ 2 and 5, respectively in the Large and Usa-Can topologies. Furthermore, we can notice that if a relatively small γ exists (e.g., 10-15 %), SPN will only result beneficial in large networks (e.g. Large, Usa-Can).

We have now analyzed the cost implications of the SPN switching fabric by using relative values
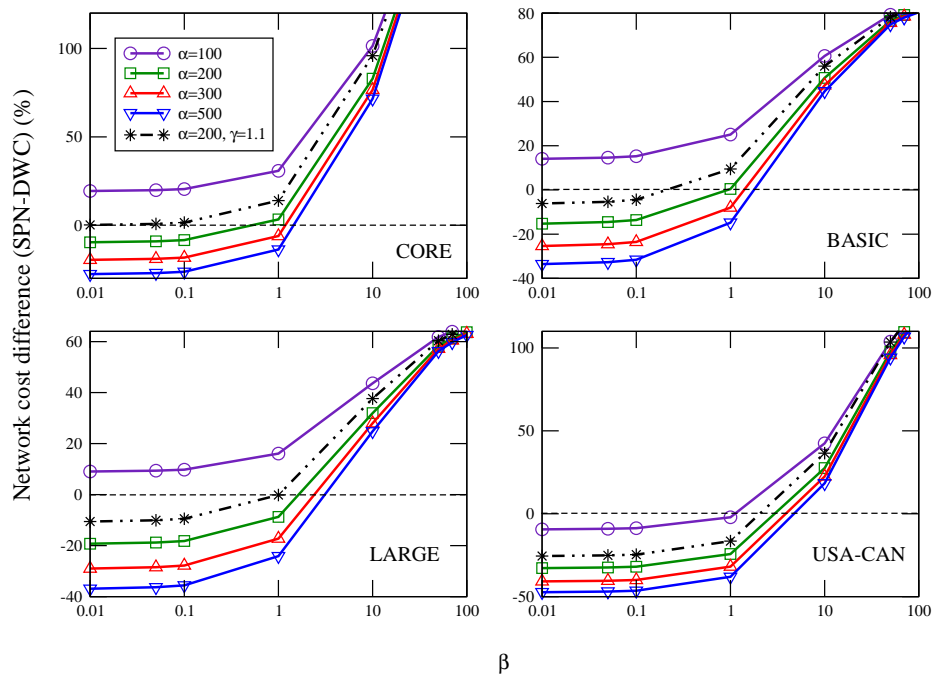
Figure 4.8: Cost difference between the SPN and DWC translucent networks as a function of α, β. Parameter γ is fixed to 1 except for one curve, where it is set to 1.1. Note that negative values mean that SPN results in a less expensive network.

for the different devices, and discussed the values of α, β and γ, where SPN results in a cost-effective network architecture. We devote the next section to discuss and forecast the feasibility of these results by considering state-of-the-art components and their respective market prices.

4.4.1 SPN outlook using state-of-the-art components

In order to assess the feasibility of the SPN architecture, we first estimate the costs of the three main elements considering commercially available devices. Note that we only take into consideration the main components, and that the additional electronic circuitry required is not accounted for.

To begin with, the cost of a commercially available high-speed SOA switch is around $C_{Gate} = $1,685$ [115]. To model the regenerator, and according to the architecture proposed in Section 4.2, we consider tunable 10 Gbps transceivers (see e.g., [116, 117]) based on mature technology, which provides both the optical-electrical (O-E) and electrical-optical (E-O) stages. The cost of these 10 Gbps transceivers is around $C_{3R} = $6k$. It should be mentioned, however, that the cost for such device increases up to > $20k for 40 Gbps [118]. Finally, to model the WC, we consider the experimental design presented in [119], where a two-stage monolithically integrated all-optical WC is shown to be able to provide TITO operation at 10 Gbps. The main components of this WC are: (a) 2 sampled-grating distributed Bragg reflector (SG-DBR) tunable lasers [120]; (b) 4 non-linear SOAs [121] (2 for a parallel cross-gain modulated (XGM) SOA structure, and 2 for a SOA-based Mach-Zehnder interferometer (SOA-MZI) which relies on cross-phase modulation (XPM)); and (c) 3 SOA booster amplifiers [122] that are placed at the output of the two SG-DBR lasers for amplification and power balancing purposes. An estimation of the current market price for all these devices is around $C_{WC} = $16k$. However, given both the difficulty in creating the control circuitry to operate these devices at high speed, and the challenge of integrating these components into a single stand-alone sub-system to be used in OTNs, we envisage the cost of a future all-optical TITO WC to be substantially higher.

According to these estimations, it seems possible to motivate the region of interest for β values, where the cost of a regenerator is similar or lower than the cost of a WC. Although 3R regenerators are power-consuming (with high impact on OPEX costs), WCs requiring such complex designs involving various processes such as XPM and XGM, are also expected to consume a significant amount of power [101]. Furthermore, experimental WC designs have shown interesting $2R$ capabilities, which in the future are expected to improve optical reach, and as a result, expand the transparent network regions without employing re-timing processes [123]. For the α region, that is, values of α which make SPN attractive from the cost point of view, we have estimated a difference of around an order of magnitude. However, we have found that at least two are required between the gate and WC cost. In favor of SPN, we have two facts: (1) the optical gate is already a technologically mature device; (2) the number of gates required in the SPN network is more than two orders of magnitude

higher than the number of WCs (e.g., in the Large network 237,377 gates vs. 1905 WCs). Whilst (1) can foster mass production of gates, (2) may lead to substantial discounts due to bulk purchasing, and therefore, we may envisage future scenarios where the requirements for α are fulfilled. Finally, regarding γ, it must be mentioned that the cost difference between TITO and FITO WCs will depend on the technology considered to implement the WC [124], and that we have observed that only small percentages could be afforded in large size networks.

Summarizing, given the more complex architecture, and hence, higher number of SOA gates, it is crucial for the success of WC-sharing architectures that the cost and power consumption of all-optical WCs is as high as possible in comparison to that of the gates. Although in this study we have focused on CAPEX costs (i.e., power-consumption has not been analyzed), our findings are in line with those presented in [101], where authors compare the power consumption of DWC and WC-sharing nodes, and conclude that for WC-sharing architectures to consume less energy than DWC, WCs have to be high energy consuming devices. All in all, we believe this study allows us to predict a bleak future for the deployment of OTNs based on WC-sharing architectures.

4.5 Summary

This chapter addressed the feasibility of deploying future translucent SWS OTNs based on WC-sharing photonic switches. To this end, we have first modeled a set of translucent WC-sharing node architectures by equipping nodes with limited size pools of electrical 3R regenerators. Assuming an isolated node scenario, we have assessed the performance of these candidate switches and found that the shared-per-node (SPN) switching fabric is the most appropriate for core transport networks. Afterwards, we have performed a comprehensive cost feasibility study of translucent SWS networks based on SPN switches. For this purpose, we compared its hardware requirements (WCs, optical gates and electrical 3R regenerators) with those of a network with dedicated WCs (DWC), that is, one WC is available per wavelength and input port. Using an iterative simulation algorithm, we have dimensioned a set of continental-scale translucent SWS networks using both SPN and DWC nodes. To analyze the cost of these networks, we have first used relative costs for the main components, and finally, discussed the feasibility of deploying WC-sharing switches by using state-of-the-art components. The main conclusion is that for translucent networks based on WC-sharing switches to become cost-effective, the cost of a WC has to be at least two orders of magnitude higher than that of the optical gate, and similar or lower than that of an electrical 3R regenerator.

Chapter 5

Cross-layer enabled translucent optical network

The rapid advances on relevant optical functions allowing for longer transmission distances, higher bit-rates, and more closely spaced wavelength channels, have dramatically increased the sensitivity to physical layer impairments (PLIs), which accumulate during the signal end-to-end transmission [66]. As commented in Chapters 2 and 3, this issue has positioned translucent architectures as potential candidates to bridge the gap between the opaque and transparent networks, and therefore, to reduce costs and energy consumption in optical transport networks (OTN)s [33]. Chapters 2 and 3 of this thesis present the existing dimensioning strategy for translucent architectures applied to the context of sub-wavelength switching (SWS) networks. Specifically, the current approach relies on the offline estimation of PLIs to strategically deploy a limited number of signal regenerators, which ensure that a target quality of transmission (QoT) network performance is met (see e.g., [125]). However, such an approach results in both over-provisioning and overuse of regenerators due to inaccuracies in these estimations [126]. Furthermore, the lack of real-time access to physical layer performance metrics prevents the network from efficiently adapting to dynamically changing PLIs, and consequently, network performance can be adversely affected [66], [76].

The goal of this chapter is to show that the introduction of real-time impairment aware routing in a translucent SWS (T-SWS) network through the novel Cross-Layer Optical Network Element (CLONE) concept [127], leads not only to significant energy savings by optimizing the usage of regeneration resources, but also to network performance improvement as CLONE-enabled networks can effectively react to time-varying PLIs.

5.1 Existing approach to PLI-awareness in OTNs

In order to meet a target QoT network performance, translucent architectures require a limited number of regenerators to be sparsely deployed across the network. This is done using a routing and regenerator placement (RRP) algorithm [125] in wavelength-routed networks, and a RRP and dimensioning (RRPD) algorithm in SWS networks as explained in the previous two chapters. Then, using a QoT estimator and a pre-specified minimum signal QoT performance (QoT_{th}), below which the signal is considered beyond the receiver's sensitivity, these algorithms can determine the impact that PLIs will have on the optical signal, and eventually, the feasibility of establishing a connection between two network points [128]. Recall from Chapter 2 that we assume the OSNR as the main signal QoT performance indicator, and hence, we refer to QoT_{th} as $OSNR_{th}$.

The adverse effect that PLIs (e.g., amplified spontaneous emission noise (ASE), polarization dependent loss (PDL), chromatic dispersion (CD), polarization mode dispersion (PMD), cross-phase modulation (XPM), self-phase modulation (SPM) and four wave mixing (FWM)) have on DWDM systems due to fiber loss, dispersion and non-linearity, drives research to develop analytical models to accurately predict their impact [129]. However, these models are still not mature enough (in terms of both accuracy and computational efficiency), and hence, it is necessary to consider a penalty margin (e.g., $OSNR_{pen} = 2dB$) when determining an adequate $OSNR_{th}$ [77]. Since a tight adjustment of $OSNR_{pen}$ may cause a number of connections to be over-estimated (i.e., establishment of unfeasible connections), network operators wishing to guarantee stringent OSNR levels have to set higher $OSNR_{pen}$ values; this in turn leads to a high number of under-estimations, and hence, to an over-provisioning of regenerators [126]. Under these circumstances, the lack of real-time feedback from the physical layer results in an overuse of costly, power-consuming regenerators. Moreover, a fixed penalty margin may still result in strong network performance degradation, as many PLIs are time-varying and can be affected by a wide range of higher-order time scale phenomena such as temperature variations, voltage drifts, component degradations and network maintenance activities [130], [131].

Therefore, in order to ensure efficient and robust operation in future dynamic OTNs, it is necessary to perform reliable and cost-effective optical performance monitoring (OPM), and, by this means, gain real-time access to the main physical layer parameters such as the OSNR and PMD [76]. In fact, this area has already received great attention in the context of wavelength-routed networks, where innovative proposals include, for example, real-time OPM coupled with path computation element (PCE)-based control planes (CP) to support dynamic management of either wavelength-switched optical networks (WSONs) [132] or the more recent elastic optical networks (EONs) [131].

However, no work as of yet has addressed the challenges of introducing real-time impairment awareness in a T-SWS scenario, which, due to its statistical multiplexing nature, requires dedicated OPM and CP solutions to optimize the use of the available (over-dimensioned) regenerators as well as to adapt to time-varying PLIs. To this end, in this chapter we introduce the novel CLONE approach

to support the dynamic management of PLIs. Assuming a pre-deployed T-SWS network, we perform a series of simulation experiments to compare the performance of the existing network approach (hereinafter referred to as STATIC network), where no real-time OPM is available, with that of a network of CLONEs using realistic time-varying PLI models. Through real-time access to OSNR measurements and a dynamic, distributed CP to efficiently disseminate this data, CLONEs optimize the use of regeneration devices, thus greatly improving energy efficiency. Moreover, we also show that the network of CLONES can dynamically adapt to time-varying PLIs and take decisions on-the-fly to re-route, drop or regenerate optical packet flows, resulting in improved network performance.

5.2 Problem framework

5.2.1 Notation

We use $\mathcal{G} = (\mathcal{V}, \mathcal{E})$ to denote the graph of a SWS network; the set of nodes is denoted as $\mathcal{V}$, and the set of bidirectional links is denoted as $\mathcal{E}$. Let $f(s{\rightarrow}d)$, denote a packet flow between source s and destination d nodes, $s, d \in \mathcal{V}$. Adequately, let $\mathcal{V}_{x-d}$ denote the ordered set of nodes that define the path that $f(s{\rightarrow}d)$ has to follow from node x to d, $x, d \in \mathcal{V}$. Let also $\mathcal{R} \subseteq \mathcal{V}$ denote the subset of nodes that are equipped with a pool of regenerators. Finally, let $\mathcal{K}_{x-d}$ denote a set of pre-computed shortest-path routes from node x to d, $x \in \mathcal{V}_{s-d} \backslash \{d\}$.

5.2.2 RRPD and OSNR models

To perform the evaluation of the CLONE network, we make use of the MILP load-based formulation presented in Chapter 3, that is, the MP2/3 RRPD algorithm. As explained, the routing and the regenerator placement and the RPD subproblems are solved sequentially so as to reduce complexity and improve network performance. As to the OSNR model, we assume the method described in Chapter 2. Recall that to estimate the OSNR level for an optical path traversing k links (P_{osnr}), this model requires the OSNR contributions of both links (L_{osnr}) and nodes (N_{osnr}) on such path. Then, P_{osnr} can be computed as detailed in Eq (2.2).

Hence, once the routing problem is solved, all paths whose estimated P_{osnr} (in dB) is lower than OSNR_{th} are considered as input data for the RPD algorithm, as regeneration is required at some intermediate node. At this point, a T-SWS network can be dimensioned through the use of both the RRPD and OSNR models.

Regarding the OSNR model, we have shown in Chapter 2 that a static value for both L_{osnr} and N_{osnr} can be estimated offline by performing an adequate system power budget and noise analysis. However, as mentioned in Chapter 2, network operators have to add a penalty margin on OSNR_{th} (i.e., $\text{OSNR}_{th} = \text{OSNR}_{min} + \text{OSNR}_{pen}$) that accounts for OSNR penalties due to maximum tolerable PMD, residual CD, and all the other non-linearities. In addition, due to a range of higher order

time-scale phenomena, both L_{osnr} and N_{osnr} are not static but time-varying contributions, making the penalty margin an even more critical parameter to deal with.

In this context, the lack of real-time OPM leads to a T-SWS infrastructure which is not able to dynamically adapt to changing PLI conditions even though it relies on an overuse of regeneration resources. As previously mentioned, we refer to this infrastructure as STATIC network.

To address these issues, we first propose to model both L_{osnr} and N_{osnr} as Gaussian random-variable functions. In the context of EONs, authors in [131] assume OSNR variations in a network link on the order of 1 dB every 30 seconds. Therefore, no abrupt/substantial changes in OSNR are expected at smaller time-scales (e.g., ms). For each node and link in the network, we denote such random function as $N(\mu[\text{dB}], \sigma[\text{dB}])$, where μ is the mean of the series and corresponds to the OSNR level estimated offline (link or node), and σ is a certain standard deviation. Under these conditions, we propose the CLONE concept to provide an efficient solution for the dynamic management of PLIs in the network.

In the next subsections, we first detail the main drawbacks of the STATIC network, and then, provide the features of the CLONE architecture.

5.2.3 The STATIC network

The RRPD algorithm disseminates both the routing and regeneration information to all network nodes so that they are able to determine, for each incoming flow of packets, the corresponding output port and whether such flow has to be regenerated. For instance, once RRPD determines that $f(s{\rightarrow}d)$ requires regeneration at some node $x \in \mathcal{V}_{s-d}\backslash\{s, d\}$, then $f(s{\rightarrow}d)$ will always be regenerated at x independently of the actual PLI conditions.

Therefore, due to the lack of real-time OSNR monitoring, the STATIC network approach exhibits the following operational issues:

- Packet flows which might not need regeneration as they have high OSNR (well above OSNR_{th}), are always regenerated in accordance to the RPD algorithm decision. Thus, they unnecessarily consume regeneration resources.

- Packet flows whose OSNR level has dropped below OSNR_{th} cannot be detected, and therefore, continue their trip until the egress node consuming network resources. Note that these flows consume unnecessarily both regeneration (if RPD determined so) and capacity resources.

- Finally, since L_{osnr} and N_{osnr} are in fact time-varying functions, a certain route in the network can become unfeasible during any given time period. This issue cannot be detected either, leading to significant increases in packet loss.
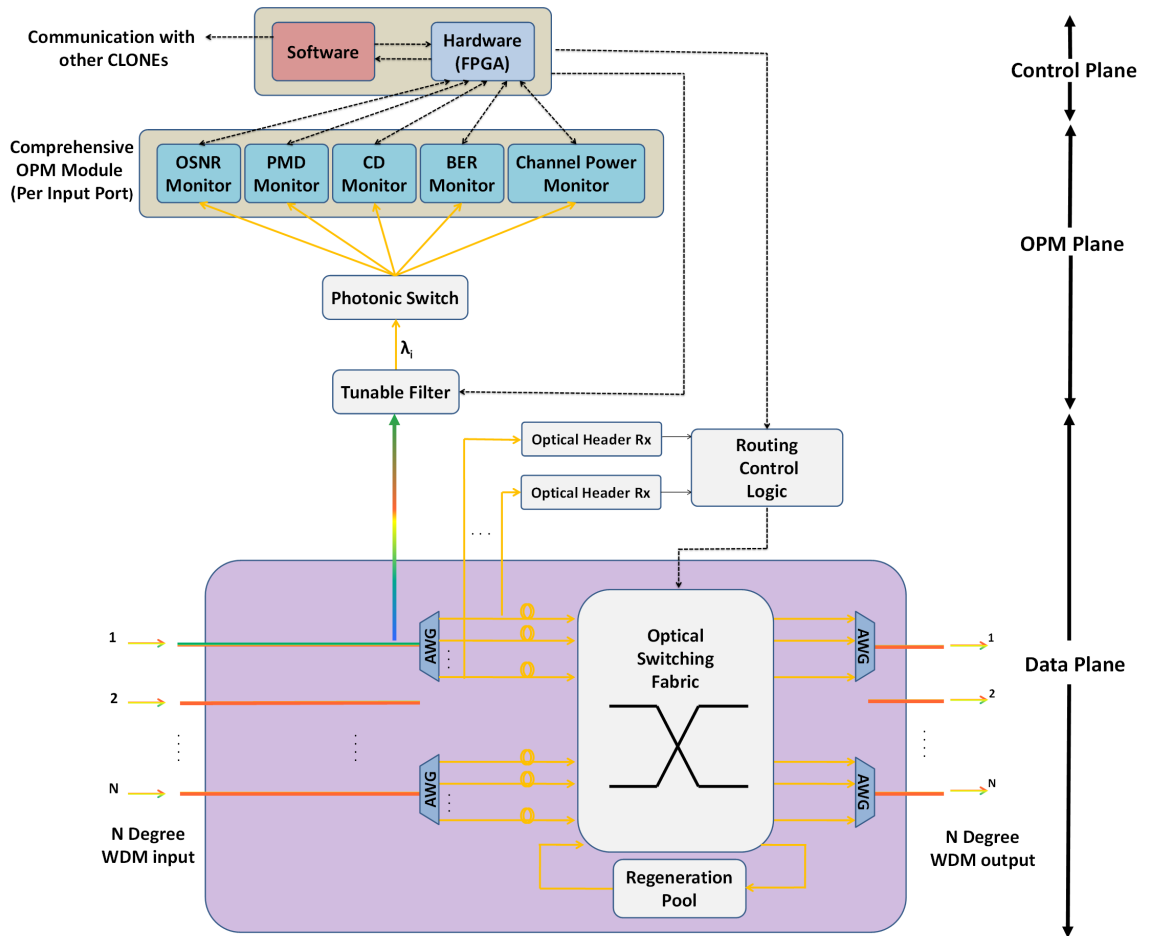
Figure 5.1: Packet-switched CLONE: A system level description indicating the bidirectional information flow between the control, OPM and data planes.

5.2.4 The CLONE enabled network

The CLONE concept arises as a result of the ever growing traffic demand and rising challenges of controlling it, which dictate the need for the development of innovative architectures able to provide dynamic, intelligent interaction between network layers [13]. We envision the CLONE network model as a promising, integrated platform that leverages emerging physical layer technologies and systems to allow for introspective access to the optical layer. Hence, CLONE-enabled networks will facilitate the retrieval of real-time OPM measurements which can then be used to achieve greater energy efficiency and optimized network performance [133].

CLONE architecture

Figure 6.1, depicts a modular, generalized description of a CLONE. Featuring a bidirectional cross-layer signaling scheme between the data, OPM, and CP planes, the CLONE enables real-time physical layer measurements affect, for example, re-routing, dropping or regeneration decisions on a per packet flow basis. Furthermore, thanks to a distributed, high-speed field-programmable gate array (FPGA)-based optical CP, which allows CLONEs to communicate with each other, local OPM metrics can be efficiently disseminated across the network of CLONEs.

As to the OPM plane, we propose a dedicated OPM device per input port, embedded directly within the optical layer. OPM is performed (in-band) over one of the channels carrying actual packet-rate data. Since future integrated OSNR monitors are expected to allow for ultra-fast measurements (e.g., hundreds of ns [127]), we envision OPM systems able to monitor ultra-fast, packet-rate channels. In fact, a proof-of-concept packet-rate OSNR monitor supporting 18 ms packet lengths has already been experimentally demonstrated [127]. Note that although in this work only OSNR is considered, we aim for OPM planes consisting of a set of sub-systems able to monitor a comprehensive range of PLIs such as OSNR, PMD and CD. In fact, PMD is also random and time-varying, and hence, PMD monitoring is crucial to manage highly reliable, ultra-high speed OTNs. For example, in [134], authors experimentally investigate an OPM technique that extracts PMD-induced signal degradation from the sum including degradations induced by others (e.g., OSNR, CD and XPM) in high speed optical links.

Finally, at the data plane, we assume the T-SWS node architecture presented in Chapter 2. It must be noted, however, that regenerator pools are only available at selected CLONEs in the network, and that their location and size is determined by the RRPD algorithm.

Real-time impairment aware routing

This section details the real-time impairment aware routing algorithm that allows for the network of CLONEs to manage both regenerations and time-varying PLIs. The implemented algorithm relies on a distributed CP to efficiently disseminate the OSNR measurements, which allows it to compute the physical layer parameters L_{osnr} and N_{osnr}. Using the embedded OPM modules, these two attributes can be computed as explained in [77]. The algorithm is executed at source nodes $s \in \mathcal{V}$ and intermediate nodes $v \in \mathcal{R}$. Such nodes do not operate with full network information (i.e., each CLONE does not need to be aware of L_{osnr} and N_{osnr} for all nodes and links in the network) but they are restricted to the transparent region they belong to and the physical layer parameters of nodes and links therein. Specifically, CLONEs take forwarding/dropping decisions based on whether $f(s{\to}d)$ can reach the next regeneration node (or d) in its path. However, since packet flows may traverse a transparent region without undergoing regeneration, communication between nodes $v \in \mathcal{R}$, which delimit transparent regions, is needed to flood the OSNR history of each $f(s{\to}d)$. To this end, we use the term $OSNR_{s-d,i}$ to denote the OSNR value of $f(s{\to}d)$ at the last regeneration node or

---

Procedure 7 Real-time impairment aware routing algorithm

INPUT: Current node x, $f(s \to d)$, $OSNR_{s-d,i}$, $\mathcal{V}_{x-d}$
OUTPUT: Forwarding or dropping decision
 1: $v^* \leftarrow$ next node $v \in \mathcal{V}_{x-d} : \{v \in \mathcal{R} || v = d\}$;
 2: $OSNR_{v^*} \leftarrow$ compute OSNR at v^*;
 3: **if** $OSNR_{v^*} > \text{OSNR}_{min}$ without regeneration **then**
 4:     Forward $f(s \to d)$ and exit; /* Exit the algorithm */
 5: **else if** $OSNR_{v^*} > \text{OSNR}_{min}$ with regeneration **then**
 6:     Regenerate and Forward $f(s \to d)$ and exit;
 7: **else**
 8:     **for all** route $k \in \mathcal{K}_{x-d}$ **do**
 9:         Re-route $f(s \to d)$ through k and generate $\mathcal{V}_{x-d}^k$;
10:         $v^* \leftarrow$ next node $v \in \mathcal{V}_{x-d}^k : \{v \in \mathcal{R} || v = d\}$;
11:         Re-compute $OSNR_{v^*}$;
12:         **if** $OSNR_{v^*} > \text{OSNR}_{min}$ without regeneration **then**
13:            Forward $f(s \to d)$ and exit;
14:         **else if** $OSNR_{v^*} > \text{OSNR}_{min}$ with regeneration **then**
15:            Regenerate and Forward $f(s \to d)$ and exit;
16:         **else**
17:            Continue;
18:         **end if**
19:     **end for**
20:     Drop $f(s \to d)$;
21: **end if**

---

source i (i.e., i can either be s or a node $v \in \mathcal{R} : \mathcal{V}_{s-d} \ni v$). For example, in Fig. 6.2, $f(26 \to 6)$ following path $\mathcal{V}_{26-6} = \{26, 15, 25, 5, 6\}$, might not need regeneration at node 25, and hence, node 25 has to send $OSNR_{26-6,25}$ to node 5 so that node 5 can determine whether the flow can eventually reach 6.

As illustrated in Procedure 7, once the algorithm is executed at node $x \in \mathcal{V}_{s-d}$, it first computes the OSNR for $f(s{\to}d)$ at the next node in the path that is either a regeneration node or d (lines 1-2). Then, computes the OSNR level at such node and decides whether $f(s{\to}d)$ can be forwarded with or without regeneration. It is worth noticing that thanks to real-time impairment awareness the threshold for decision becomes OSNR$_{min}$. In case $f(s{\to}d)$ cannot be forwarded, a set of k shortest-paths from node x to d are evaluated. If all attempts fail, $f(s{\to}d)$ is temporarily dropped at node x. Note that in Procedure 7, if node $x = s$ and $x \in \mathcal{R}$, a regeneration will never be performed as the OSNR level is already at its maximum.

5.3 Results and discussion

5.3.1 Simulation scenario

Simulations are performed considering both the Pan-European Basic (shown in Fig. 6.2, see Appendix A for further topology details) and the Usa-Can topologies. We consider 19 dB to be the
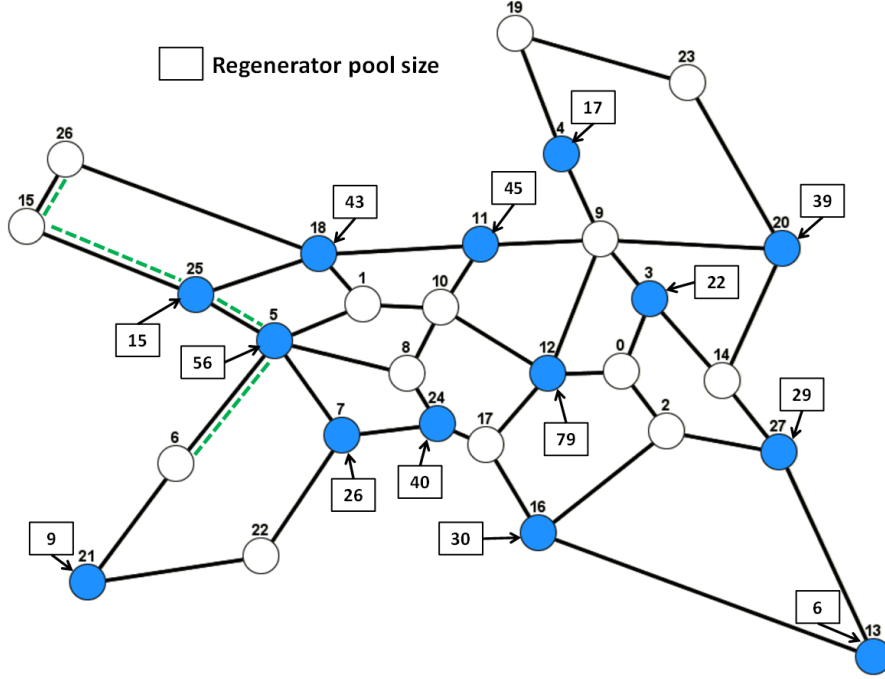
Figure 5.2: Pan-European Basic topology. Regenerator pools are sparsely deployed (blue nodes) and dimensioned according to the RRPD algorithm employed.

OSNR receiver sensitivity ($OSNR_{min}$) and a penalty $m = 2$ dB, thus $OSNR_{th} = 21$ dB. RRPD dimensions the translucent network considering a network load of 10.72 and 7.776 Erlangs, respectively, for both the Basic and Usa-Can networks. In both scenarios, we aim for a a target loss rate in the access to regenerator resources equal to $B^{QoT} = 10^{-3}$. As shown in Fig 6.2, such dimensioning results in a sparse placement of 456 signal regenerators. CLONE nodes $v \in \mathcal{R}$ monitor load at regenerator pools' access and can solve contentions at output ports using regeneration as long as target $B^{QoT} = 10^{-3}$ is met. A set of $|\mathcal{K}_{s-d}| = 3$ shortest-path routes $\forall\ s, d \in \mathcal{V}$ is pre-computed offline and available at each CLONE for re-routing purposes.

5.3.2 OSNR scenarios

We consider two different scenarios for σ:

- Scenario 1 ($Sc1$): σ is set to 0.8 dB. In this case, we have corroborated that no unexpected losses due to PLI impact occur in the network (i.e., margin m mitigates perfectly PLI impact). The objective of $Sc1$ is to exhibit the high energy-savings in terms of regenerator usage that can be achieved with the CLONE approach.

- Scenario 2 ($Sc2$): σ varies over time, and randomly can take either a very high/high value
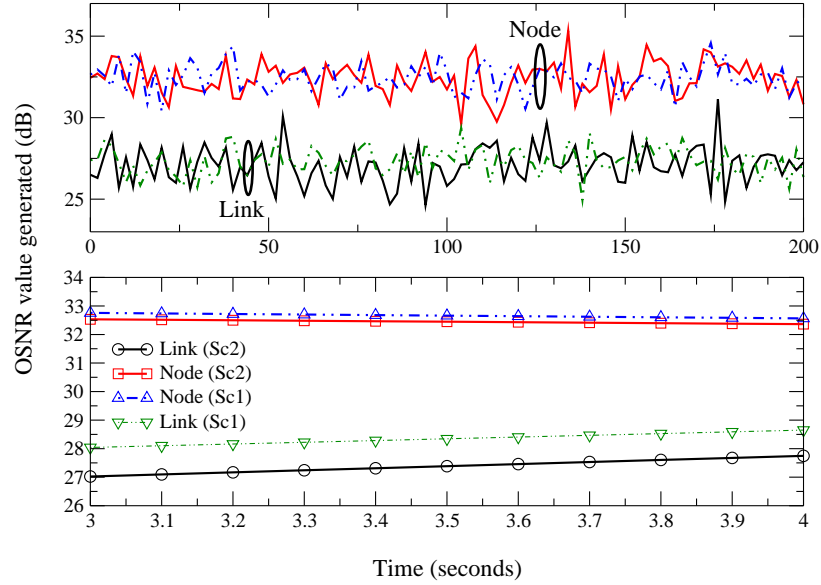
Figure 5.3: OSNR randomly-generated series for both a link and a node in the Basic topology. Values over 200 seconds (top) and 1 second (bottom) highlight that no abrupt changes in OSNR are expected at the system sampling time-scale (i.e., 100 ms).

(1.8 dB, 1.4 dB), a medium value (1.1 dB) or remain the same (0.8 dB) with probability 0.1, 0.1, 0.3 and 0.5 respectively. The goal of $Sc2$ is to generate PLI situations which cause some routes to become unfeasible for a certain amount of time, and thus, force CLONEs to react and re-route packet flows temporarily.

We assume that every 2 seconds a new OSNR value is generated. However, in order to avoid abrupt variations and smooth the curve of the series, 20 points are interpolated between two consecutive Gaussian values. Hence, we assume that OPM modules report to the CP an OSNR measurement every 100 ms. Figure 6.3, shows two randomly selected L_{osnr} and N_{osnr} from the Basic topology under the two OSNR scenarios proposed. Although variations considering a large time window (200 seconds on the top) exhibit substantial variations in the OSNR contributions, a close view to the time-scale of the CLONE system (1 second on the bottom) shows that no abrupt changes are expected at the system monitoring time-scale (i.e., 100 ms). Besides, flow forwarding/dropping decisions are taken between regeneration nodes, and hence, the largest propagation delay through the CP equals that of the largest transparent segment in the network. For the network topology considered, the worst-case delay is on the order of 7 ms. Taking this value into account as well as the smooth OSNR curve exhibited by both links and nodes at the ms time-scale allows us to assume that CLONEs take their decisions based on updated OSNR measurements.

5.3.3 Results

In Figs. 5.4(a), 5.4(b), 5.6(a) and 5.6(b), the total PLP represents the sum of losses due to contention in network links and losses due to low OSNR. OSNR loss refers to packets being lost at regenerator pools' access, dropped due to low ONSR (CLONE network) as well as packets whose OSNR at the destination node is beyond the receiver's sensitivity (STATIC network). In Figs. 5.4(a) and 5.6(a), it is possible to observe that under OSNR $Sc1$ the overall PLP (left y axis) is the same in both networks. This is because in this network scenario OSNR losses are negligible with respect to the contention ones, and hence, do not have a noticeable impact on the total PLP. However, Figs. 5.4(a) and 5.6(a), also exhibit the great optimization of regenerator resources that is achieved with the CLONE approach. Around two orders of magnitude difference in losses caused by contention at regenerator pools are achieved, which means that the CLONE network, using real-time impairment aware routing, only regenerates those flows that really need it. Furthermore, CLONE provides, regardless of the load, a reduction of more more than 60% (Basic) and almost 70% (Usa-Can) in the average per packet number of regenerations (ppr) (right y axis).

On the other hand, in Figs. 5.4(b) 5.6(b) ($Sc2$), where unexpected losses due to PLI can occur, we observe that for light-loads there exists a strong degradation in terms of the overall PLP for the STATIC approach. The CLONE network, in contrast, is aware of such PLIs and is able to re-route packets flows and, up to some extent, improve network performance. Note that this occurs within the typical operation range of SWS networks, that is, for overall PLP values of 10^{-3} and lower. Besides, the optimized management of regenerator resources is maintained as in Figs. 5.4(a) and 5.6(a). Finally, in Figures 5.5(a), 5.5(b), 5.7(a) and 5.7(b) we show the amount of regenerators that can be turned off (i.e., that are not used) during network operation under both the STATIC and CLONE approaches. Results show that the CLONE network can provide substantial energy savings as allows for a notable number of regeneration devices to be turned off during network operation.

5.4 Summary

In this chapter, we have shown that a network of CLONEs can achieve both greater energy efficiency and dynamic adaptation to time-varying PLIs. We have also proposed real-time impairment aware routing to minimize regenerator usage and to improve PLP due to the impact of time-varying PLIs. The performance of the CLONE network has been compared against the STATIC approach (see Chapters 2 and 3) which relies on offline estimations of the PLI impact. Furthermore, we have extended the CLONE network model to a test-bed and experimentally validated this novel networking concept.
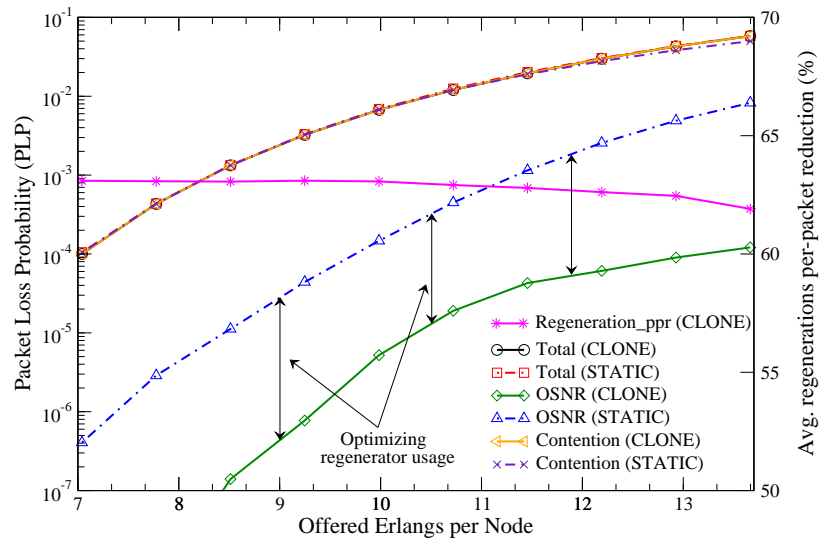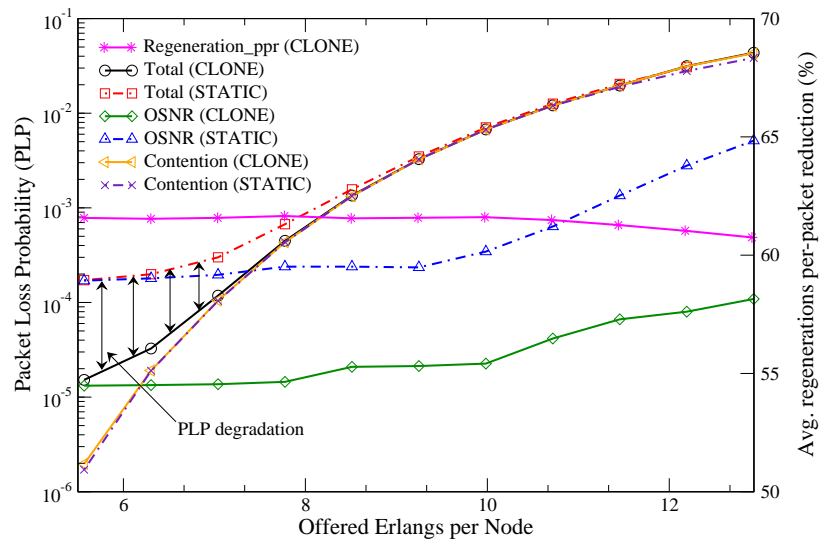
Figure 5.4: Packet loss probability (left y axis) and average regenerations per-packet reduction (ppr) (right y axis) as a function of the offered load in the Basic topology for both the CLONE and STATIC networks under a) $Sc1$, and b) $Sc2$.
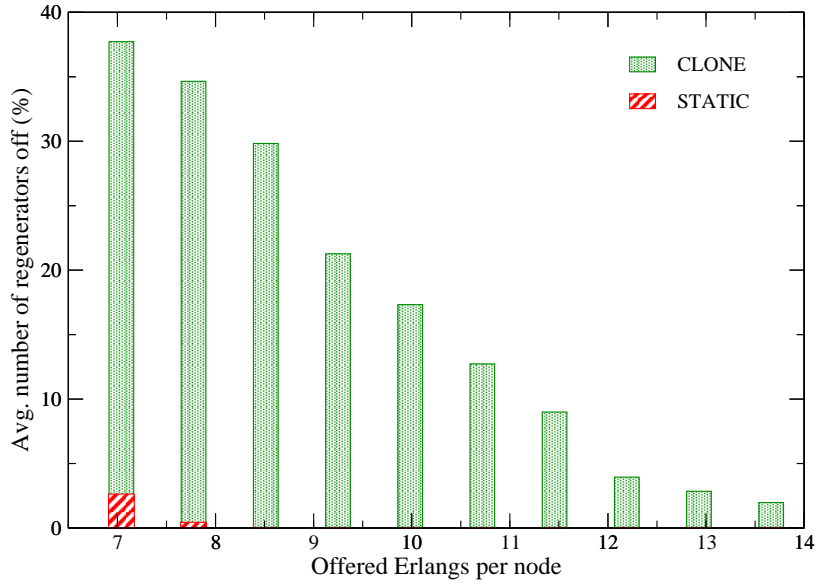
(a)
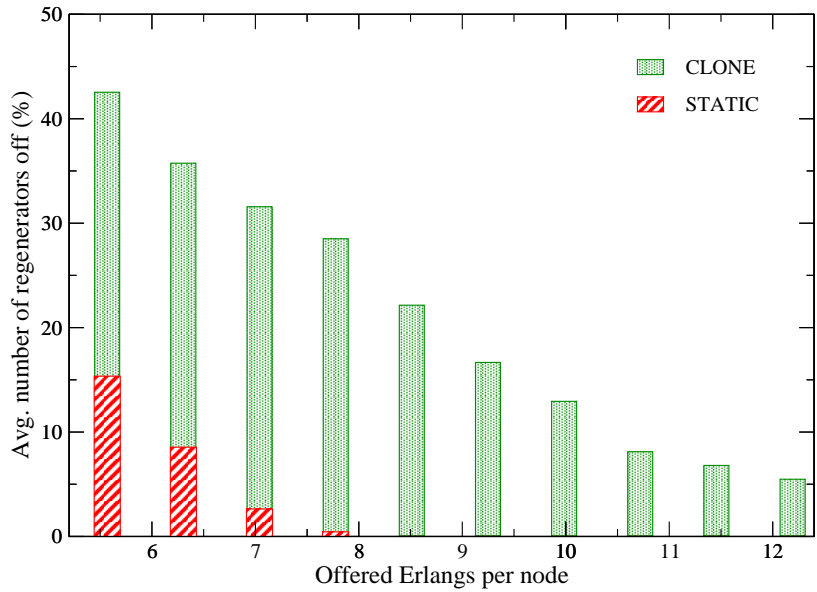
(b)

Figure 5.5: Percentage of regeneration devices turned off during network operation as a function of the offered load in the Basic topology for both the CLONE and STATIC networks under a) $Sc1$, and b) $Sc2$.
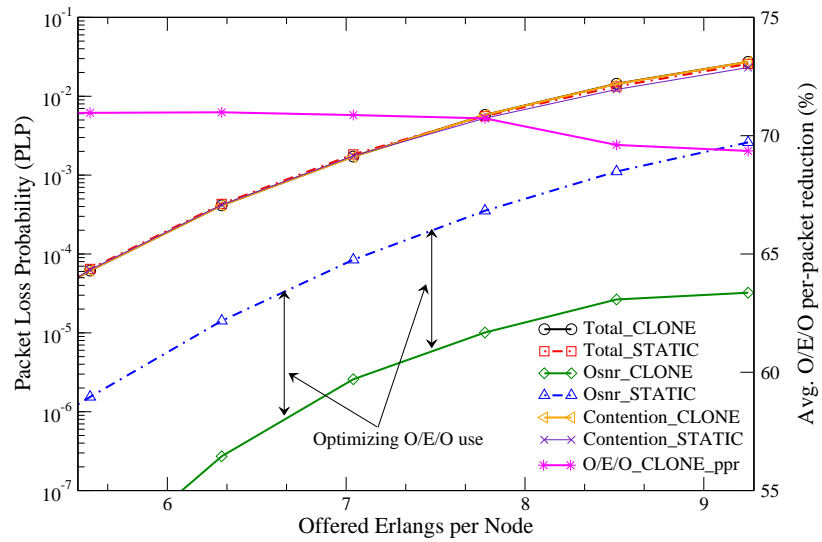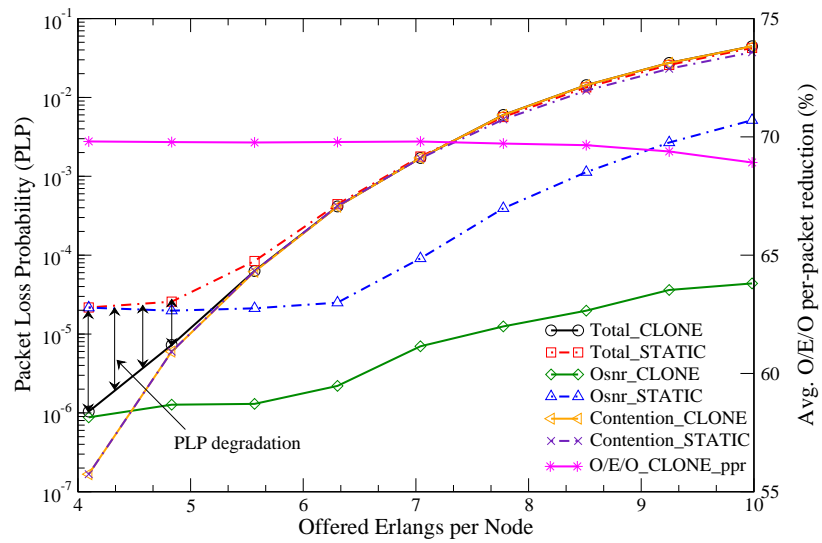
Figure 5.6: Packet loss probability (left y axis) and average regenerations per-packet reduction (ppr) (right y axis) as a function of the offered load in the Usa-Can topology for both the CLONE and STATIC networks under a) *Sc*1, and b) *Sc*2.
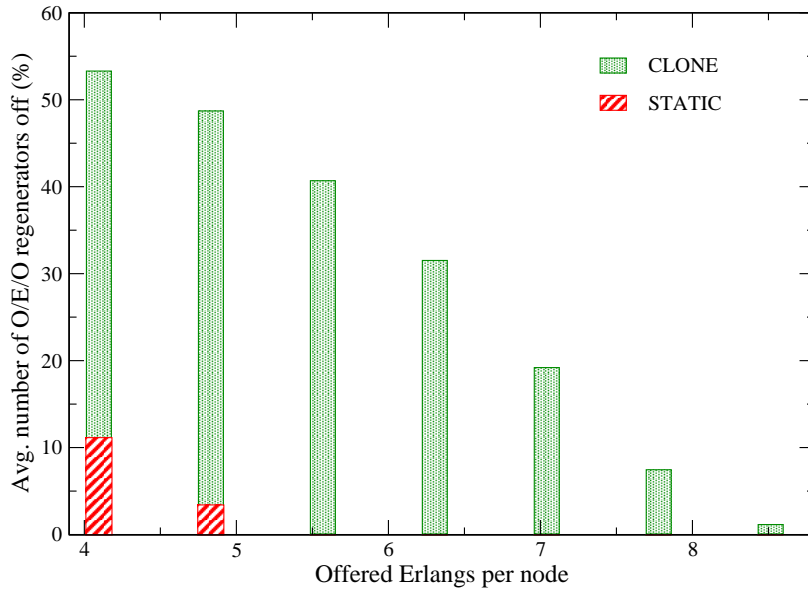
(a)
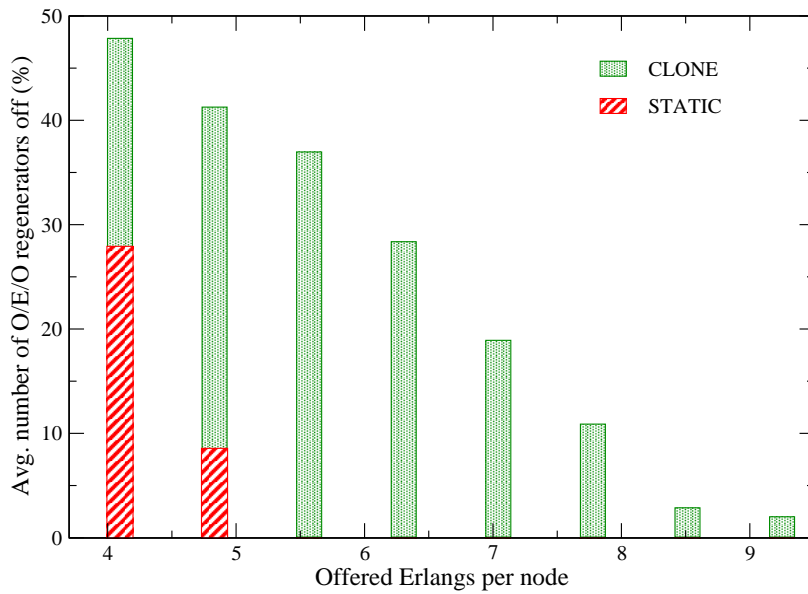
(b)

Figure 5.7: Percentage of regeneration devices turned off during network operation as a function of the offered load in the Usa-Can topology for both the CLONE and STATIC networks under a) *Sc*1, and b) *Sc*2.

Part II

Operations research for cross-layer network optimization

Introduction

Operations Research (OR) refers to a multi-disciplinary (i.e., involving mathematical, logical and analytical techniques) scientific approach to decision-making. The main focus is on the optimal allocation of scarce resources, and by this means, solve problems of cost minimization or of profit maximization or what can be termed as optimization problems. In this chapter, we apply OR to solve a variety of complex cross-layer (i.e., multi-layer) network optimization problems which are currently identified as open issues among network operators and the research community, and hence, whose solution is of great interest.

This part of the thesis is divided into three different chapters, each dealing with a different cross-layer network optimization problem. Each of the problems have been previously modeled (either within the context of this thesis or in the literature) by means of either an integer linear programming (ILP) or mixed-integer linear programming (MILP) formulation. However, once applied to real world scenarios, that is, considering real nation-wide/continental-scale backbone networks and traffic instances, the solution of both ILP and MILP formulations becomes impractical, even if commercial solvers such as CPLEX [98] are used. It is at this point where OR plays an important role by allowing researchers to obtain good near-optimal solutions to real-sized problems within practical running times. Specifically, we focus on two very well-known meta-heuristic strategies known as greedy randomized adaptive search procedure (GRASP) [135] and biased random-key genetic algorithm (BRKGA) [136]. Furthermore, and in order to enhance the GRASP and BRKGA performance, we also introduce some intensification procedures such as path relinking (PR) [137] and variable neighborhood descent (VND) [138].

These methodologies are used to solve the following problems:

- Chapter 6: Survivable multi-layer IP/MPLS-over-WSON (joint optimization of L3/L1/L0 network layers)

- Chapter 7: Multi-layer IP/MPLS-over-Flexgrid optical network (joint optimization of L3/L1/L0 network layers)

- Chapter 8: Regenerator placement and dimensioning problem in T-SWS optical networks (joint optimization of L2/L0 network layers)

Next, we provide the reader with a brief description of the main GRASP and PR features, hoping this will help to ease the subsequent reading. As to the BRKGA, we refer to Section 3.3 for a detailed description of the algorithm.

A brief GRASP overview

The GRASP procedure is an iterative two phase meta-heuristic method based on a multi-start randomized search technique with a proven effectiveness in solving hard combinatorial optimization problems. It was first presented in [135],[139], by Feo and Resende, and later formalized and given its acronym in [140], by Feo et al.. Since then, it has been used to solve a wide range of problems (see e.g.,[141], [142], [143], [144], [145] and [25]) with many and varied applications in the real life such as the design of communication networks, collection and delivery operations and computational biology. For recent and comprehensive surveys of GRASP we refer the reader to [146] and [147].

In the first phase of the multi-start GRASP procedure, a greedy randomized feasible solution of the problem is built by means of a *construction* procedure. Then, in the second phase, a *local search* technique to explore an appropriately defined neighborhood is applied in an attempt to improve the current solution. VND and approximate local search (ALS) [148] are to well-known local search algorithms. These two phases are repeated until a stopping criterion is met, and once the procedure finishes the best solution found over all GRASP iterations is returned. Note that with the basic GRASP methodology, iterations are independent from each other as previous solutions of the algorithm do not have any influence on the current iteration. One approach to include memory in the GRASP procedure is with PR, a method which was first introduced by Glover in [149], as an strategy to integrate both intensification and diversification in the context of tabu search [150]. This approach generates new solutions by exploring the trajectories connecting high-quality solutions. The path evaluated starts at a so-called *initiating* solution and moves towards a so-called *guiding* solution which is usually taken from an stored set of good quality solutions called the *elite set*.

PR was first applied in the context of GRASP by Laguna and Martí in [137] (in the so-called GRASP+PR algorithm), and widely applied ever since. Resende and Ribeiro present a wide variety of examples and applications of GRASP+PR in [146]. After a solution is output from the multi-start phase (i.e., construction plus local search), PR is applied between the current solution and a selected solution from the elite set. Then, the best solution found in this iteration is candidate for inclusion in the elite set and it is only added if a certain quality and diversity criteria is met.

Hence, PR is an intensification strategy which generates new solutions by exploring the trajectories linking two high-quality solutions (starting at an initiating solution towards the guiding one). The path connecting both solutions is generated by sequentially introducing attributes of the guiding solution into the initiating one. To ensure that PR is only applied among high-quality solutions, a set of elite solutions (ES) must be both maintained and cleverly managed during all GRASP

iterations. Note that with the attribute high-quality we are not only referring to their cost function value but also to the diversity they add to ES.

Since the PR algorithm operates on ES, its management and maintenance is, therefore, crucial to the success of the PR procedure. Previous studies such as [151], have shown that a policy to include solutions in ES only based on their individual quality does not lead to the best PR performance. Hence, to include a new solution in ES, a trade-off between quality and diversity is usually evaluated (see e.g., [152]).

Chapter 6

GRASP and PR for the Survivable IP/MPLS-over-WSON multi-layer problem

6.1 Introduction

With the advance in optics and the commercialization of enhanced devices like wavelength selective switches and tunable lasers, nowadays it is possible to remotely configure optical cross-connects (OXCs), and thus, to deploy wavelength switched optical networks (WSON). Strictly speaking, WSON extends the concept of automatically switched optical network (ASON) [153] by applying an intelligent control plane based on generalized multi-protocol label switching (GMPLS) [154]. In fact, WSONs standardization activities are currently in progress in the internet engineering task force (IETF) within the common control and measurement plane (CCAMP) working group [2]. WSONs enable to dynamically reconfigure networks, i.e. enable the automatization of the setup and tear-down of end-to-end optical connections (known as lightpaths) and the recovery of such lightpaths in case of failure. Thus, WSONs allow an efficient network operation which implies significant savings in the core transport network. Today, the optical layer (managed by a network operator) is an already deployed photonic infrastructure that provides, at the same time, different client networks with transport services such as leased lines, packet-switched networks (e.g., Internet), virtual private networks (VPNs), synchronous digital hierarchy (SDH) networks, etc. Our goal in this chapter is to further improve its benefits by applying an intelligent interworking strategy between the packet and WSON layers based on a multi-layer optimization process. Indeed, a multi-layer network can perform an optimal load balancing between these two layers optimizing both the cost of the packet layer and

the utilization of the WSON layer. Without loss of generality, we assume in this work a multi-layer network which consists of an internet protocol (IP)/ multi-protocol label switching (MPLS) packet layer over a photonic WSON transport layer, but the study herein presented is applicable to other packet technologies such as the emerging multi-protocol label switching transport profile (MPLS-TP) and provider backbone bridges traffic engineering (PBB-TE) transport alternatives.

Hence, in this chapter we tackle, for the first time to the best of our knowledge, the problem of a joint optimization of survivable non-symmetrical network layers so to provide network operators with a competitive multi-layer network planning tool which aims at minimizing the capital expenditures (CAPEX) (i.e., those costs related with purchasing and installing fixed infrastructures, such as equipments).

This multi-layer network is specifically designed to provide companies with premium *layer 1* (L1) and L2 VPN services. These services have stringent availability requirements, and therefore, ensuring network recovery in front of any kind of network component failure becomes crucial to the services' success. Indeed, in such high-capacity multi-layer network scenario, any single link or node failure would lead to tremendous losses for both network operators and clients. Thus, the concept of survivability, which allows a network to quickly recover from any kind of outage and restore the affected traffic, becomes a critical objective in the design and planning of next-generation high-speed multi-layer networks. Another advantage of the multi-layer approach is the fact that it allows the application of specifically-designed multi-layer recovery mechanisms. These procedures are able to trigger coordinated actions across both layers, thereby substantially reducing the over-dimensioning of IP/MPLS nodes when compared to the single-layer approach (i.e., separate optimization of layers) [155].

Therefore, and strictly speaking, in this work we deal with the so-called survivable IP/MPLS-over-WSON multi-layer network optimization (SIMNO) problem. To this end, and given the operator-dependent input parameters, that is, the WSON network deployed and the traffic demands to be satisfied, we design the IP/MPLS layer. It consists in the dimensioning of its nodes with the required opto-electronic (OE) interfaces and in the establishment of the virtual link connectivity at the IP/MPLS level through the given WSON layer so that every traffic demand can be successfully accommodated. Note that in the SIMNO problem, the over-dimensioning of IP/MPLS nodes required to guarantee recovery in front of any kind of network component outage is minimized thanks to the application of multi-layer optimization techniques. Therefore, we provide a solution to a real problem which is of great interest to network operators. Indeed, following the SIMNO approach, operators will be able to deploy a survivable IP/MPLS layer on top of an already deployed WSON infrastructure while minimizing their CAPEX investments. In this work, CAPEX involve the costs of both IP/MPLS nodes and OE ports installed on them, as well as the cost of using both optical ports and kilometers of optical fiber from an existing WSON network.

In order to deal with SIMNO, we present and evaluate a formal model of the problem by means

of an integer linear programming (ILP) formulation. Since the resultant model is computationally impractical, we make use of two well-known and powerful meta-heuristic models to help solve the problem, these are, a greedy randomized adaptive search procedure (GRASP) together with a path-relinking (PR) intensification method, and a biased random-key genetic algorithm (BRKGA). To evaluate both heuristics, we carry out a set of experiments using both methodologies and assess their respective performances. Furthermore, we evaluate the impact of introducing the PR intensification strategy into GRASP in the so-called GRASP with path-relinking (GRASP+PR) meta-heuristic. To conduct such experiments, we consider a set of network traffic models which are consistent with the traffic profiles foreseen in the years to come and evaluate them in three different IP/MPLS network configurations of a realistic Spanish telecommunications network.

6.2 Related work and contributions

Survivable multi-layer networks have traditionally been designed following the classical overlay approach where two redundant IP/MPLS networks are deployed over the photonic infrastructure. However, operators are now facing the challenge of dimensioning networks able to cope with the expected huge IP traffic volumes, and at the same time, keeping constant or even reducing connectivity prices. Hence, operators look for technologies providing the lowest possible network costs.

In protection and restoration schemes developed for legacy technologies, only optical links and electronic ports/interfaces have been considered as points of failure. For this reason, networks implement protection or restoration mechanisms to survive to such kind of failures. IP/MPLS nodes are not, nevertheless, as trusty as legacy telecommunication equipments. This is mainly due to the constant software and hardware upgrades they undergo ([155],[156]). To tackle this issue, backbone nodes redundancy-based schemes have been proposed for operators willing to protect their networks against IP/MPLS nodes failures [155]. However, this approach entails a substantial increase in network CAPEX, thereby clearly demonstrating that the duplicate network scheme is far away from being the optimal solution, and that the design and evaluation of novel survivable multi-layer network optimization methods such as SIMNO has gained great momentum.

In the literature, multiple recovery schemes have been specifically designed and tailored for multi-layer networks. For example, a comprehensive survey of them can be found in [156]. Another interesting study involving the evaluation of a coordinated link restoration scheme to be used in packet-over-optical networks can be found in [157]. In that work, authors illustrate a novel scheme which is cost effective compared to duplicating nodes, though it has the disadvantage of requiring the IP/MPLS and optical topologies to be symmetrical (i.e., every node has both packet and optical switching capabilities). It is worth noticing that the underlying WSON, which supports a number of heterogenous client networks and provides a range of services to residential and business customers, needs to provide different availability degrees. Hence, if symmetrical topologies are considered, the

119

IP/MPLS layer should be designed to cope with the requirements of the most constraining service, thereby highly and unnecessarily increasing network CAPEX.

Accordingly, the SIMNO approach is aimed at defining orchestrated interworking recovery actions to avoid the duplication of IP/MPLS backbone nodes. However, in this case, no symmetrical topologies are required, and hence, a number of client networks with different availability degrees can be allocated on top of the WSON. In addition, we rely on lightpath restoration, a technique which provides a finer granularity to recover selected lightpaths in very short times (e.g., on the order of hundreds of *ms* [158]), and on a novel connectivity restoration scheme to deal, not only with IP/MPLS node failures, but also with the rest of failures.

In the literature, we find a few interesting works addressing the IP/MPLS-over-WSON multi-layer network planning problem. In [159], the authors present an ILP formulation aimed at maximizing a utility function for the network operator, that is, the difference between revenues and costs, considering a scenario without failures. To this end, authors propose a Lagrangian relaxation-based method. A similar approach is not, nonetheless, applicable to the SIMNO problem owing to both its size and structure. Indeed, SIMNO includes a huge set of single failure scenarios (i.e., every IP/MPLS node, OE port and optical link in the network). For this very reason, in this work we develop and evaluate two different meta-heuristic methods to solve the SIMNO problem. Strictly speaking, an heuristic based on GRASP and PR [137],[146] and another on BRKGA [136] are proposed to find cost-effective solutions for the SIMNO problem within practical running times. As a matter of fact, previous works have already considered evolutionary genetic algorithms (GA) for the planning of optical networks. For instance, in [160] a GA-based heuristic for the single layer survivable optical network planning is presented, and in [161], a GA is applied to dimension single layer dynamic optical networks. In this study, by contrast, we consider the GRASP methodology to solve the SIMNO problem and compare its performance to that of the novel BRKGA meta-heuristic. Moreover, we evaluate the impact of the PR intensification strategy on the results obtained by GRASP, thereby illustrating one more time a successful application of this combined meta-heuristic.

6.3   Multi-layer network architecture

The multi-layer network architecture considered in this work is depicted in Fig 6.1. In this reference scenario, three types of IP/MPLS nodes can be distinguished at the packet layer (IP/MPLS), these are, *metro* nodes performing client flow aggregation, *transit* nodes providing routing flexibility, and *interconnection* nodes supporting inter-operator connection. Additionally, transport nodes (OXCs) connected by fiber links create an WSON layer. In order to minimize the overall number of OE ports in the network, metro-to-metro connections are avoided being every metro node connected to one or more transit nodes. Moreover, while it is typical that a transit node is collocated with a transport node, metro nodes are usually closer to clients, and thus, some ad-hoc connectivity is used
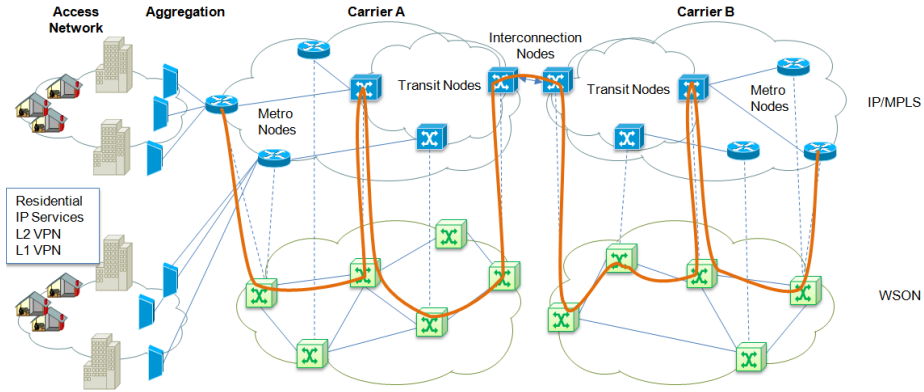
Figure 6.1: Metro and multi-layer network architecture

to connect metro to transport nodes. Figure 6.1 illustrates an exemplary end-to-end MPLS label switched path (LSP) established between two metro nodes (orange line). Note that in this example, the LSP makes use of interconnection nodes to pass from a network operated by one particular carrier to another network operated by another different carrier.

Figure 6.2 depicts an example illustrating how a multi-layer network can be designed. To be precise, Fig. 6.2a, shows a portion of the multi-layer network where each IP/MPLS metro node is connected to a transit node through virtual links, and hence, a virtual topology is created. Each virtual link is supported by a lightpath in the WSON layer. This lightpath is routed through the minimum cost path over the WSON layer. In the example, metro router M1 is connected to transit router T1 by means of only one lightpath. However, and in order to guarantee the survivability of the network, extra-capacity has already been added to every node.

In multi-layer problems, the components that may fail are optical links, OE ports and both optical and IP/MPLS nodes. We consider every component in the network as being mutually failure-independent, and thus, multiple failure scenarios are not considered in this work since their probability to happen is extremely low. Moreover, complete optical node failures are also highly unlikely and thus are also neglected in this work. This is not, however, the case with IP/MPLS nodes whose failures, mainly caused by software crashes, are a great deal more frequent.

On the one hand, in the event of an optical link failure, the multi-layer network can apply joint recovery schemes to restore the affected traffic demands. For example, when the optical link O1-O2 fails (Fig. 6.2b) recovery actions are triggered to restore the metro-to-transit (M1-T1) connectivity. Note that if a lightpath is restored at the optical layer, the connectivity at the IP/MPLS layer remains unaltered (with the corresponding CAPEX savings implications). In contrast, if no restoration is possible, a new lightpath has to be established to connect the IP/MPLS metro node to a different transit node (e.g., M1-T2), thus restoring the metro-to-transit connectivity. Note, however, that in
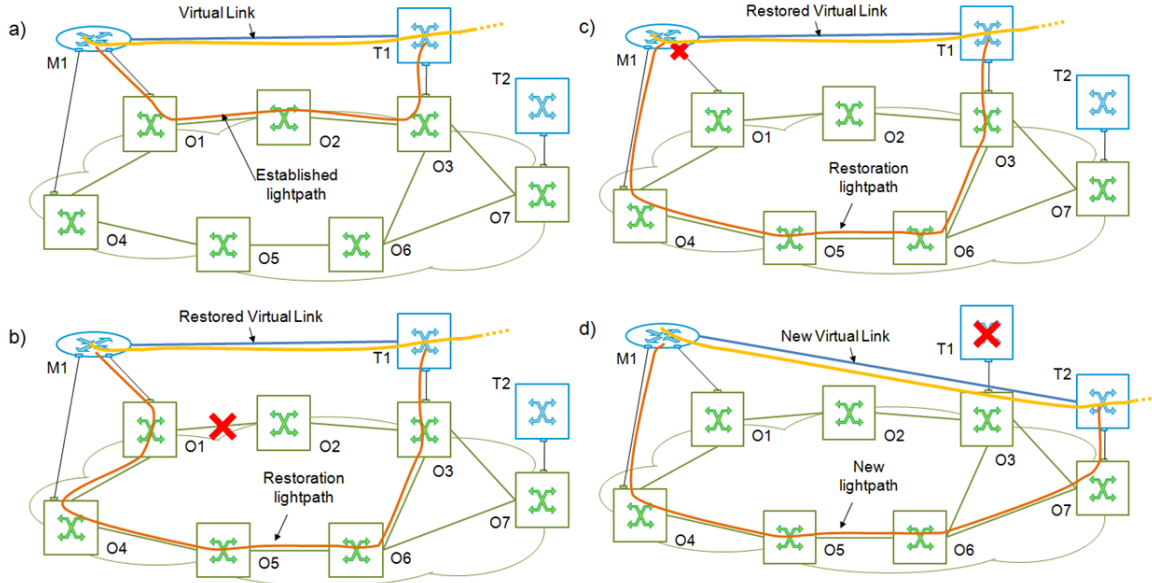
Figure 6.2: (a) Design of a multi-layer planned network portion; (b) Recovery from a link failure; (c) from a port failure, and (d) from a node failure.

this case transit node T2 must be over-dimensioned with additional OE ports to be able to cope with the requirements of this newly created lightpath. Once the connectivity is restored, the MPLS LSP can be eventually rerouted over the reconfigured virtual topology. The same actions are taken in the event of a port failure (Fig. 6.2c).

On the other hand, in the event of an IP/MPLS node failure (Fig. 6.2d), new lightpaths are established between every metro node connected to the failed node and a different transit node in order to properly restore the metro-to-transit connectivity. Therefore, in this failure scenario, setting up new virtual links is required. In the example, virtual link M1-T2 is created. After reconfiguring the virtual topology, the affected MPLS LSPs are rerouted.

6.4 SIMNO Problem statement

For the sake of clarity, the following information defines the problem input data:

- The WSON network topology consisting of both OXC nodes and fiber links;

- The correspondences between IP/MPLS nodes and OXC nodes are established beforehand;

- Each IP/MPLS node can establish a connection to each other so that all possible virtual links needed to establish a mesh virtual connectivity are predefined;

- The origin/destination (O/D) matrix and the bandwidth of each demand.

A solution to the problem must specify the configuration of each IP/MPLS node in terms of switching capability and number and bit-rate of OE ports. For each virtual link used in the optimal solution, a supporting lightpath must be established in the WSON network. Moreover, the route of the MPLS LSP over the virtual topology must be determined for every demand.

For the ILP formulation as well as the benefits of the SIMNO approach (i.e., joint layer optimization) with respect to the overlay survivability approach (i.e., redundant equipment), the reader is referred to [162].

With respect to the complexity of the problem, it is worth mentioning that even simpler versions of the survivable network planning model have been shown to be *NP*-hard [163]. For example, taking into account the instances presented in Section 8.4, the problem size raises to 10^{10} variables and 10^9 constraints, thereby making impractical its exact solution. Owing to this fact, in the next section, metaheuristic methods are proposed to provide near-optimal solutions with reasonable computational effort.

6.5 SIMNO meta-heuristic resolution methods

6.5.1 A GRASP with PR heuristic

In the next subsections we describe the different building blocks of the GRASP+PR heuristic developed to solve the SIMNO problem.

Construction procedure

Given the fact that our problem primarily consists in routing, one-by-one, a set of demands over a virtual topology, the value of the cost function, $g(\cdot)$, for any constructed solution, strictly depends on the selected set of virtual MPLS routes, $\mathcal{R} = \{r_{d_1}, ..., r_{d_i}, ..., r_{d_j}, ..., r_{d_{|\mathcal{D}|}}\}$, to be followed by each demand $d \in \mathcal{D}$. Note, however, that the selection of these routes is, for its part, strongly dependent on the ordering in which these demands are processed (i.e., ordering $\mathcal{O}_x = \{d_1, ..., d_i, ..., d_j, ..., d_{|\mathcal{D}|}\}$). Indeed, such ordering does have strong influence on resources utilization.

Let us first denote $\mathcal{C}_d$ as a set of pre-computed virtual routes available for every demand $d \in \mathcal{D}$. Then, in order to build a solution, we rely on a restricted candidate list (RCL) containing the demands $d \in \mathcal{D}$ with the best (i.e., smallest) incremental costs ($c(d)$), that is, RCL_d. To compute the incremental cost $c(d)$ for each demand $d \in \mathcal{D}$, we first evaluate the incremental cost of the virtual routes available in $\mathcal{C}_d, d \in \mathcal{D}$, and then, $c(d)$ is given the cost of the less expensive route (i.e., $c(d) = \min_{r \in \mathcal{C}_d}\{c(r)\}$). RCL_d is associated with a threshold parameter in the real interval $[0, 1]$: α. Hence, RCL_d is dynamically formed by all elements (i.e., demands) which can be inserted into the partial solution ensuring its feasibility and whose incremental cost falls within the interval defined by the threshold parameter (see Procedure 8). However, after carrying out a number of tests, we

realized that Procedure 8 becomes a really time-consuming process if real-sized, complex problem instances are considered (see Section 6.6.1). Note that to generate RCL_d, the cost $c(r)$ for all routes in $C_d, d \in D$ must be recomputed at each iteration of the *while* loop (see lines 2-9 in Procedure 8). In order to minimize this problem, we include an additional parameter (τ) which determines the maximum number of demands that can be evaluated. Hence, at each iteration, a maximum of $\tau \cdot |Q|$ candidate demands are randomly selected from set Q. As shown in Procedure 8, once the demand to be served is obtained (and added to the ordering vector), we select the route r_d with the minimum incremental cost to fill the set of selected routes R. Here it is worth noting that the selection of r_d could also have been made by means of a second RCL, in this case, however, containing the routes with the smallest incremental costs, and controlled by another threshold parameter β. In fact, in our preliminary experimentations we found that values of $\beta > 0$ always led to worst performance results (see Section 6.6.2 for further details), and hence, we do not consider this second RCL in our construction algorithm. Eventually, once the *while* loop ends, both the ordering O_x and the set of routes R for all demands are obtained. Note that to calculate $c(d)$ and build RCL_d we take into account the current state of the network (i.e., the resources already reserved by previous demands). Moreover, if a route $r_d \in C_d$ results in an unfeasible solution, its cost $c(r)$ is set to ∞, thereby avoiding its selection. Hence, at this point, a feasible solution for the network dimensioning without considering failures is obtained. The above-mentioned, is shown between lines 1 and 17 in the pseudo-code of our greedy randomized construction (GRC) algorithm in Procedure 8. The routing of demands is mainly performed over a virtual topology which is precomputed beforehand over the given optical network topology. Virtual links are created between every pair of metro and transit, transit and transit, and transit to interconnection IP/MPLS nodes satisfying that its distance is lower than a given threshold. For each virtual link, a set of routes over the optical network are computed: the shortest one and a number of restoration routes. In order to obtain C_d for each demand $d \in D$, we consider a k-shortest path algorithm. In fact, two subsets of routes are pre-computed, one over the virtual topology and another one over the optical topology, thus enabling optical by-passing. Route pre-computation is performed just once at the heuristic startup.

Due to the fact that network components such as optical links, OE ports, and IP/MPLS nodes are subject to failures, we build a set of simple failure scenarios where one component fails in each one. Then, for each failure scenario, we remove the element in failure from the network and compute the list of affected MPLS LSPs being each path subsequently rerouted. If additional OE ports need to be installed in the IP/MPLS nodes (i.e., over-dimensioning), checks are performed to ensure the feasibility of the solution. This process is illustrated between lines 18 and 29 in Procedure 8.

As it has been previously explained, in the event of an optical link failure, lightpath restoration is tried as a first option by means of the predefined set of restoration routes. If this restoration succeeds, the associated virtual link (and thus every MPLS LSP using it) is automatically restored. On the contrary, MPLS LSPs are rerouted over the new virtual topology, thereby likely increasing

---

Procedure 8 Greedy Randomized Construction Heuristic

INPUT: $\mathcal{D}, \mathcal{C}_d \ \forall \ d \in \mathcal{D}, \alpha, \tau$
OUTPUT: $\mathcal{O}_x, \mathcal{R}, g(\mathcal{O}_x, \mathcal{R})$
1: $\mathcal{R} \leftarrow \emptyset, \mathcal{O}_x \leftarrow \emptyset$
2: Initialize the candidate set: $\mathcal{Q} \leftarrow \mathcal{D}$
3: Initialize the restricted candidate set: $\mathcal{Y}$ with $\tau \cdot |\mathcal{Q}|$ demands randomly selected from $\mathcal{Q}$
4: Evaluate the incremental cost $c(d)$ for all $d \in \mathcal{Y}$
5: **while** $\mathcal{Q} \neq \emptyset$ **do**
6: $\quad c^{min} \leftarrow min\{c(d)| \ d \in \mathcal{Y}\}$
7: $\quad c^{max} \leftarrow max\{c(d)| \ d \in \mathcal{Y}\}$
8: $\quad RCL_d \leftarrow \{d \in \mathcal{Y}| \ c(d) \leq c^{min} + \alpha(c^{max} - c^{min})\}$
9: $\quad$ Select an element d from RCL_d at random
10: $\quad \mathcal{O}_x \leftarrow \mathcal{O}_x \cup \{d\}$
11: $\quad$ Take route $r_d \in \mathcal{C}_d$ such that $c(r_d) = c(d)$, and route d through r_d
12: $\quad \mathcal{R} \leftarrow \mathcal{R} \cup \{r_d\}$
13: $\quad$ Update the candidate set $\mathcal{Q}$
14: $\quad \mathcal{Y} \leftarrow$ a maximum of $\tau \cdot |\mathcal{Q}|$ demands randomly selected from $\mathcal{Q}$
15: $\quad$ Reevaluate the incremental cost $c(d)$ for all $d \in \mathcal{Y}$
16: **end while**
17: Dimension the network
18: Let $\mathcal{A}_{pf}$ denote the set of affected paths under failure scenario f
19: **for all** failure scenario $f \in \mathcal{F}$ **do**
20: $\quad \mathcal{A}_{pf} \leftarrow \emptyset$
21: $\quad \mathcal{A}_{pf} \leftarrow$ GenerateFailure(f)
22: $\quad$ **if** $\mathcal{A}_{pf} == \emptyset$ **then**
23: $\quad\quad$ Recover from failure f
24: $\quad$ **else**
25: $\quad\quad$ Reroute$(\mathcal{A}_{pf})$
26: $\quad\quad$ Increment IP/MPLS nodes capacity
27: $\quad\quad$ Recover from failure f
28: $\quad$ **end if**
29: **end for**

---

both IP/MPLS nodes switching capabilities and installed OE ports.

Therefore, a feasible solution must provide us with the set of virtual routes that are to be used to carry the amount of traffic b_d, $\forall\ d \in \mathcal{D}$ as well as with the required over-dimensioning of IP/MPLS nodes so that network survivability is guaranteed. Hence, once a set of routes $\mathcal{R}$ is obtained, cost function $g(\mathcal{O}_x, \mathcal{R})$ accounts for the CAPEX investments required to serve all traffic demands and to guarantee network recovery in front of any of the considered failures. Finally, and for the sake of clarity, hereinafter in this study, we skip the set of routes $\mathcal{R}$ from the parameters in cost function $g(\cdot)$. Note that once the order $\mathcal{O}_x$ for serving the demands is specified, the selection of routes is a pure greedy process.

Local search

Recalling that a solution to our problem can be defined by $\mathcal{O}_x$ (i.e., the ordering in which the demands are to be served), and for the purpose of neighborhood creation, we refer to a feasible solution obtained by Procedure 8 as $\mathcal{O}_x$. Due to the fact that a feasible solution $\mathcal{O}_x$ has no guarantee of being locally optimal, GRASP heuristics apply a local search procedure starting at $\mathcal{O}_x$ in the hope of finding a better solution in its neighborhood. Then, let us denote with $N_q(\mathcal{O}_x)$, the set of solutions in the *qth* neighborhood structure of $\mathcal{O}_x$. Thus, assuming an ordering of $|\mathcal{D}|$ traffic demands, $\mathcal{O}_x = \{d_1, ..., d_i, ..., d_j, ..., d_{|\mathcal{D}|}\}$, we define the neighbor of this ordering as an ordering in which d_i is interchanged with d_j. Let us denote such interchange operation in $\mathcal{O}_x$ as $I(d_i, d_j)_{\mathcal{O}_x}$. In order to generate a random neighbor in the first neighborhood (i.e., a 1-move neighbor) of $\mathcal{O}_x$ (i.e., $N_1(\mathcal{O}_x)$), we choose pivots d_i and d_j uniformly among the $|\mathcal{D}|$ demands. Hence, creating a q-move neighbor implies that this random interchange of demands is performed q times, though always ensuring that an interchange of the randomly selected pivots will bring the solution a neighborhood further.

Several approaches have been proposed in the literature to perform local search. Among them, we find techniques such as the variable neighborhood search (VNS) and variable neighborhood descent (VND), and the approximate local search (ALS) procedures (see [138],[148]). In this work, we make use the ALS procedure to implement the local search in the GRASP multi-start phase. ALS was first proposed in [148] as a trade-off between the *first-fit* and *best-fit* approaches within the N_1 and N_2 neighborhoods of a solution. As shown in the pseudo-code of Procedure 9, this technique randomly samples the 1-move and 2-move neighborhoods of $\mathcal{O}_x$. This exploration is stopped when either the set of improving solutions CS is full or a maximum of $MaxSearch$ neighbors have been explored. Then, the algorithm selects either in a greedy or a probabilistic fashion one of the solutions in CS to continue the exploration. In [148], the greedy selection outperformed the probabilistic one, and thus, in this analysis we consider the greedy choice to select a solution from CS as well as an equal probability to generate a 1-move or a 2-move neighbor. The algorithm finishes when set CS is empty and returns as output the best solution found $\mathcal{O}_B$.

Procedure 9 Approximate Local Search (ALS) heuristic

INPUT: $\mathcal{O}_x, MaxCS, MaxSearch$
OUTPUT: $\mathcal{O}_B$
 1: $\mathcal{O}_B \leftarrow \mathcal{O}_x$;
 2: **repeat**
 3:    $i \leftarrow 0, CS \leftarrow \emptyset$;
 4:    **repeat**
 5:       $\mathcal{O}_{x'} \leftarrow$ Generate-1-or-2-move-neighbor($\mathcal{O}_B$);
 6:       **if** $g(\mathcal{O}_{x'}) < g(\mathcal{O}_B)$ **then**
 7:          $CS \leftarrow CS \cup \{\mathcal{O}_{x'}\}$;
 8:       **end if**
 9:       $i \leftarrow i + 1$;
10:    **until** $|CS| \geq MaxCS$ **or** $i \geq MaxSearch$
11:    **if** $CS \neq \emptyset$ **then**
12:       Select $\mathcal{O}_x = \min_{\mathcal{O}_k \in CS}\{g(\mathcal{O}_k)\}$;
13:       $\mathcal{O}_B \leftarrow \mathcal{O}_x$;
14:    **end if**
15: **until** $CS = \emptyset$

Path-relinking

PR implementation   Several approaches on how to perform PR have been proposed and evaluated (see e.g., [164]). These techniques mainly deal with the process that is in charge of creating the path towards the guiding solution. The most usual approach consists in building the path in a greedy fashion (i.e., the most profitable or least costly move is selected). However, in this study, we have developed a specific strategy to perform PR. Two main reasons support this modeling decision. First, evaluating the cost of each possible move towards the guiding solution would entail extremely long computation times, and second, and most compelling, is the fact that in our problem instances, hundreds of demands are to be served (see Section 6.6.1), and therefore, the path connecting two high-quality solutions may easily have hundreds of moves. Thus, the use of PR would be inadvisable since it would require most of the time available, thereby drastically reducing the number of iterations performed.

Let $\mathcal{O}_1 = \{d_1, ..., d_{|\mathcal{D}|}\}$, $\mathcal{O}_2 = \{d'_1, ..., d'_{|\mathcal{D}|}\}$ be two feasible solutions interpreted as vectors (i.e., $\mathcal{O}_1(1) = d_1$, and $\mathcal{O}_2(1) = d'_1$). For the sake of this example, let us define $\mathcal{O}_1$ as the initiating solution ($\mathcal{O}_{INIT}$), and $\mathcal{O}_2$ as the guiding one ($\mathcal{O}_{GUID}$). Then, let us also denote a move from $\mathcal{O}_{INIT}$ to $\mathcal{O}_{GUID}$ as,

$$move(i)_{\mathcal{O}_{INIT}} = I(\mathcal{O}_{INIT}(i), \mathcal{O}_{GUID}(i))_{\mathcal{O}_{INIT}},$$

that is, an interchange of demand positions applied to ordering $\mathcal{O}_{INIT}$. Note that in the case that $\mathcal{O}_{INIT}(i) = \mathcal{O}_{GUID}(i)$ no move is performed. Thus, given $\mathcal{O}_{INIT}$ and $\mathcal{O}_{GUID}$, we build the path by progressively transforming $\mathcal{O}_{INIT}$ into $\mathcal{O}_{GUID}$ (i.e., by iteratively applying $move(i)$, $i = 1, ... |\mathcal{D}|$). However, as aforementioned, the size of our problem instances is really high, thus making impractical
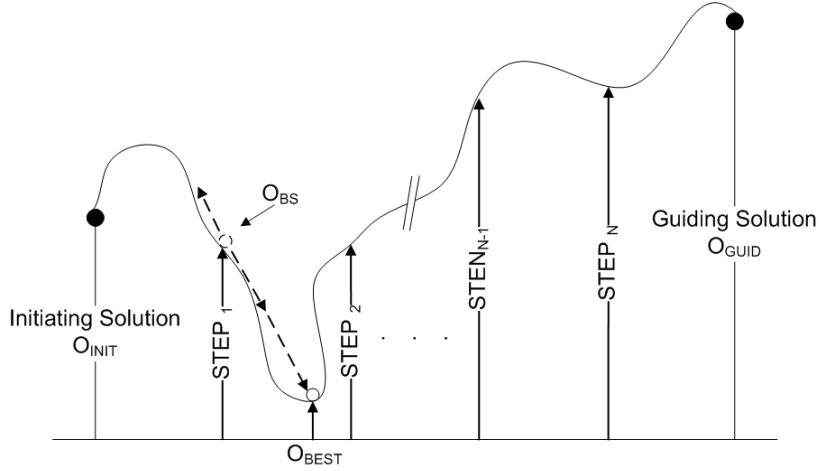
Figure 6.3: Path-Relinking heuristic implementation.

the evaluation of each solution found along the path created by PR. Hence, we propose to sample the path every T moves in the search for an improving solution, and if found, a thorough evaluation of the nearby solutions is carried out. The value of T is defined by an input parameter N_{SAMPLE} that decides into how many regions the path between both solutions must be divided. Figure 6.3 illustrates this method by showing the path being evaluated between two high quality solutions $\mathcal{O}_{INIT}$ and $\mathcal{O}_{GUID}$. We uniformly sample the path built and when $\mathcal{O}_{GUID}$ is reached the best solution found during the sampling process ($\mathcal{O}_{BS}$) is selected.

If $g(\mathcal{O}_{BS}) < \min(g(\mathcal{O}_{INIT}), g(\mathcal{O}_{GUID}))$ a move to the right and to the left of $\mathcal{O}_{BS}$ is assessed (see dotted arrows in Fig. 6.3). Then, we take the improving direction and iteratively evaluate the subsequent moves until no improvement is found. PR then returns the best solution found during this intensification step ($\mathcal{O}_{BEST}$). In this way, we have a relatively high probability of reaching the best solution in the path connecting $\mathcal{O}_{INIT}$ and $\mathcal{O}_{GUID}$. The pseudo-code for our PR implementation is illustrated in Procedure 10.

Elite set management and distance measure Initially, the elite set (ES) is empty, then, each locally optimal solution obtained and each solution resulting from a PR execution is candidate to be inserted in ES. Let us consider $\mathcal{O}_x$ as such candidate solution. If ES is not yet full, then, $\mathcal{O}_x$ is simply added to ES. Otherwise, if $\mathcal{O}_x$ improves the best solution in ES, it replaces an element of the set. In addition, if $\mathcal{O}_x$ improves upon the worst in ES and its distance to ES is larger than a pre-established threshold δ_{th}, it also replaces an element in ES. To this end, let us define $\delta_{x,y}$ as the distance between two solutions $\mathcal{O}_x$ and $\mathcal{O}_y$ (i.e., the number of moves required to reach $\mathcal{O}_y$ from $\mathcal{O}_x$). Then, the distance between a solution $\mathcal{O}_x$ and the whole ES can be defined as,

$$\delta_{x,ES} = \min_{O_i \in ES}\{\delta_{x,i}\}$$

Procedure 10 Path-Relinking Heuristic

INPUT: $\mathcal{O}_{INIT}, \mathcal{O}_{GUID}, N_{SAMPLE}$
OUTPUT: $\mathcal{O}_{BEST}$
1: $M \leftarrow$ number of moves from $\mathcal{O}_{INIT}$ to $\mathcal{O}_{GUID}$
2: $T \leftarrow \lfloor \frac{M}{N_{SAMPLE}} \rfloor$
3: $count \leftarrow 1, \mathcal{O}_{BEST} \leftarrow \emptyset, \mathcal{S} \leftarrow \emptyset$
4: $\mathcal{O}_x \leftarrow \mathcal{O}_{INIT}$
5: **for** $i \leftarrow 1, M$ **do**
6: $\quad \mathcal{O}_x \leftarrow move(i)_{\mathcal{O}_x}$
7: $\quad$ **if** $count == T$ **then**
8: $\quad\quad$ **if** $\mathcal{O}_x$ is feasible **then**
9: $\quad\quad\quad \mathcal{S} \leftarrow \mathcal{S} \cup \{\mathcal{O}_x\}$
10: $\quad\quad$ **end if**
11: $\quad\quad count \leftarrow 0$
12: $\quad$ **end if**
13: $\quad count \leftarrow count + 1$
14: **end for**
15: Select ordering $\mathcal{O}_{BS} \in \mathcal{S}$ which minimizes cost function $g(\cdot)$
16: **if** $g(\mathcal{O}_{BS}) < min(g(\mathcal{O}_{INIT}), g(\mathcal{O}_{GUID}))$ **then**
17: $\quad$ Evaluate a move to the right and to the left of $\mathcal{O}_{BS}$
18: $\quad$ Take the improving direction and iteratively move until no improvement is found
19: $\quad$ Return the best feasible solution found $\mathcal{O}_{BEST}$
20: **end if**

Hence, when ES is full, $\mathcal{O}_x$ is inserted in ES if its quality is superior to the worst in ES and $\delta_{x,ES} \geq \delta_{th}$. This threshold is empirically adjusted in Section 8.4. With the same diversity objective, and in order to maintain the size of the pool constant, whenever we add a solution to ES, another one must be removed. As usual, we remove the closest solution to $\mathcal{O}_x$, which we call $\mathcal{O}_r$, among those with a worse quality. Thus, $\mathcal{O}_r$ can be defined as follows,

$$\mathcal{O}_r = \min{}_{O_i \in ES : g(\mathcal{O}_i) > g(\mathcal{O}_x)} \{\delta_{x,i}\}.$$

Selection policy Another important aspect regarding PR is that once a solution $\mathcal{O}_x$ is output from the multi-start phase, another solution $\mathcal{O}_i$ must be selected from ES to be path-relinked with $\mathcal{O}_x$. In the literature, a common approach is to select a solution randomly from ES [146]. However, this may result in selections that are very close to $\mathcal{O}_x$, thereby reducing the probability of finding better solutions. In an attempt to minimize this issue, we adopt a biased [151] approach in which solutions are selected with probabilities proportional to their distance to $\mathcal{O}_x$. Therefore, the probability p_i of selecting a particular solution $\mathcal{O}_i \in ES$ can be computed as follows,

$$p_i = \frac{\delta_{x,i}}{\sum_{j=1}^{|ES|} \delta_{x,j}}$$

In order to perform PR, we implement the *back-and-forward* (PR$_{bf}$) strategy, which explores the path in both directions (see e.g., [151]). Once the PR finishes, if no improving solution is found, the

best of both extremes is returned as output. Finally, the pseudo-code of our GRASP+PR heuristic is shown in Procedure 11, which first executes the GRASP multi-start phase to fill ES, and then runs a pre-defined number of GRASP+PR iterations. Procedure 11 returns as output the best solution stored in ES. We point out that all input parameters required to call the construction, local search and PR methods will be adjusted in Section 8.4.

Procedure 11 GRASP+PR Heuristic

INPUT: $GlobalMaxItr, \mathcal{D}, \mathcal{C}_d \ \forall \ d \in \mathcal{D}, \alpha, \tau, MaxCS, MaxSearch, N_{SAMPLE}$
OUTPUT: $\mathcal{O}_{BEST}$
 1: $\mathcal{O}_{BEST} \leftarrow \emptyset, ES \leftarrow \emptyset$
 2: Apply GRASP (GRC followed by ALS) for $b = |ES|$ iterations to populate ES
 3: $count \leftarrow 1$
 4: **repeat**
 5: $\quad \mathcal{O}_x \leftarrow$ GRC($\mathcal{D}, \mathcal{C}_d \ \forall \ d \in \mathcal{D}, \alpha, \tau$)
 6: $\quad \mathcal{O}_{x'} \leftarrow$ LocalSearch($\mathcal{O}_x, MaxCS, MaxSearch$)
 7: $\quad$ Select elite solution $\mathcal{O}_{EL}$ from ES
 8: $\quad \mathcal{O}_B \leftarrow$ PR$_{bf}$($\mathcal{O}_{EL}, \mathcal{O}_{x'}, N_{SAMPLE}$)
 9: $\quad$ Try to insert $\mathcal{O}_B$ in ES
10: $\quad count \leftarrow count + 1$
11: **until** $count > GlobalMaxItr$
12: $\mathcal{O}_{BEST} \leftarrow \min_{\mathcal{O}_k \in ES}\{g(\mathcal{O}_k)\}$

6.5.2   A BRKGA heuristic

In this section, we describe the implementation of the BRKGA heuristic developed to solve SIMNO and which performance will be compared with that of the GRASP+PR described in the last section.

Again, the problem primarily consists in routing a set of demands over a virtual topology. In this case, we make use of one gene per virtual link and per IP/MPLS node. These genes are used to compute a metric for each element in order to perform the routing of each demand $d \in \mathcal{D}$. Besides, and recalling that the order in which the demands are served influences the goodness of the solution, additional genes are required to specify it. For this purpose, we use one additional gene per demand $d \in \mathcal{D}$. Therefore, given a virtual network represented by graph $\mathcal{G}(\mathcal{N}, \mathcal{E})$ and the set of demands $\mathcal{D}$, each individual is represented by an array of $|\mathcal{N}| + |\mathcal{E}| + |\mathcal{D}|$ genes.

Here it is worth noticing that both BRKGA and GRASP+PR (see Section 6.5.1) have the same goal (minimize network CAPEX) and that this is achieved both by minimizing routing costs (i.e., using the cheapest links and nodes), and by grooming the demands so as to minimize the use of resources. On the one hand, BRKGA uses the metrics and the ordering encoded in the chromosome. Metrics are used as a means to stimulate or penalize the use of individual links and nodes so that those resources minimizing the cost of the network are selected. Ordering, however, is used to improve the grooming of demands, thus making the most of the network resources. On the other hand, GRASP+PR relies on the ordering of demands not only to improve grooming, as in BRKGA, but to minimize the cost of the network too. Since the GRASP construction algorithm deals directly

with CAPEX incremental costs, its complexity is greater than that required to decode a chromosome in BRKGA, however this comes at the benefit of solution quality. Finally, note that fast cost function evaluations are crucial to a BRKGA algorithm, and so the differences among both heuristics when it comes to solution encoding.

To decode chromosomes into feasible solutions, the metric of IP/MPLS nodes and virtual links is initialized using the assigned gene of the input chromosome, and the order in which each demand will be routed is given by the rest of genes. After initializing every element, the network is dimensioned through the routing of the whole set of demands $\mathcal{D}$. A solution to the network dimensioning without considering failures is obtained at this step. To include failures, we use the steps already illustrated in the GRASP construction algorithm (i.e., between lines 18 and 29 in Procedure 8 in Section 8.2.1).

Additionally, in this work, a multi-population strategy where a number of populations are evolved independently has been implemented [165]. The algorithm was designed and implemented as a multi-thread application, where each population runs in a single thread. Populations exchange elite individuals after a pre-determined number of generations. In an initial phase, a data structure representing the network graph is created. At this step, the network graph only contains IP/MPLS and optical nodes and optical links. Afterwards, the virtual topology is generated; virtual links between metro and transit and between transit and transit IP/MPLS nodes are created. Demands pre-routing computation is then performed. To be precise, a set of $k = 100$ routes is pre-computed for each demand. During the decoder process, route metric re-computation is performed ensuring that the shortest route (in terms of that metric) is chosen at each step. The parameters considered for the BRKGA algorithm are provided in the next section.

6.6 Computational experiments

This section describes the computational experiments carried out to both evaluate and compare the efficiency and performance of the GRASP+PR and BRKGA heuristics proposed in this chapter to solve the SIMNO problem. All methodologies have been implemented in Java SE 1.6.0_17 using a sequential approach (though we consider parallel populations in BRKGA), and all experiments have been conducted on Intel Core 2 Quad 2.67GHz based computers running Windows 7 Professional Edition (64 bits) with 8 GB of RAM.

6.6.1 Problem instances

The performance of the proposed meta-heuristic algorithms has been compared over the realistic 21-node Spanish national optical network topology shown in Fig. 6.4. In order to have a representative range of multi-layer networks, we have considered three different IP/MPLS topologies which consist of 40 metro nodes and a different number of transit and interconnection nodes. Table 6.1 specifies the location of transit and interconnection nodes (identified by the associated OXC location) of

each multi-layer network. Moreover, for each multi-layer network, the spatial position of metro nodes is characterized by a uniform coverage degree (CD) based on the p-value of the uniformity Kolmogorov-Smirnov test [166]. Note that whilst values close to 100 % indicate that metro nodes are uniformly located on a $2D$ map, low values denote the presence of areas with high density of metro nodes. Table 6.1 also contains the CD of the three network instances under study. For the traffic, we assume two types of demands: *national* where both end metro nodes belong to the network, and *interconnection,* where one of the end metro nodes is outside of the network (i.e., either the source or the destination node of the demand is the virtual metro node as defined in Section 6.4). The mix of national and interconnection traffic is also detailed in Table 6.1. Therefore, three different multi-layer network scenarios can be identified, from the unbalanced network A, where 70 % of the total is interconnection traffic with only 3 interconnection nodes and several high density metro areas, to the well-balanced network C, with 50 % of interconnection traffic, 5 interconnection nodes and nearly uniform metro areas. Network B is in between of networks A and C. In fact, a brief analysis of the proposed instances identifies differences on the complexity of the problems. For instance, note that the size of virtual topology is 326, 361, and 408 virtual links for networks 1, 2, and 3 respectively. Thus, the mean number of feasible routes for a given demand significantly increases from network A to network C, and consequently differences in the results can be anticipated for each network instance.

Each multi-layer network has been planned taking into consideration several increasing traffic loads, starting from an initial load of 4 Gb/s per metro node and with increments of 45 % at each step (roughly representing a year-over-year traffic increase). However, since the complexity of the problems strongly depends on the number of demands to be served, this number should not be increased sharply. Instead, the average requested bandwidth in each demand is increased at each step. Aiming at providing accuracy, each traffic load has been executed three times with randomly generated demands following the above characteristics. This has resulted in a set of 21 traffic instances for each of the networks, that is, $RA_{1...21}$, $RB_{1...21}$, $RC_{1...21}$, for networks A, B and C respectively. Each of these sets, in blocks of three, represents the same traffic load but with three independent randomly generated representations. Hence, traffic profiles are represented in 7 different blocks in increasing order (e.g., $RA_{1..3}$ and $RA_{4..6}$ belong to blocks 1 and 2 respectively). Note that the higher the index of the block, the higher the complexity of the problem. These traffic instances have a minimum number of 120 demands and a maximum of 360. The bandwidth requested per demand can be either 1, 10, 40 or 100 (Gb/s), this last being the minimum amount required to perform optical by-passing. Hence, 100 Gb/s demands are the only ones allowed to perform optical bypass. We assume the availability of 80 wavelengths at every optical link in the WSON network, a maximum allowed lightpath length of 1000 kilometers, and that each metro node is connected to every interconnection node and a maximum of 4 transit nodes (the nearest 4 transits). Moreover, we fill set $\mathcal{C}_d$ with a maximum of 100 top shortest paths computed over the virtual topology for
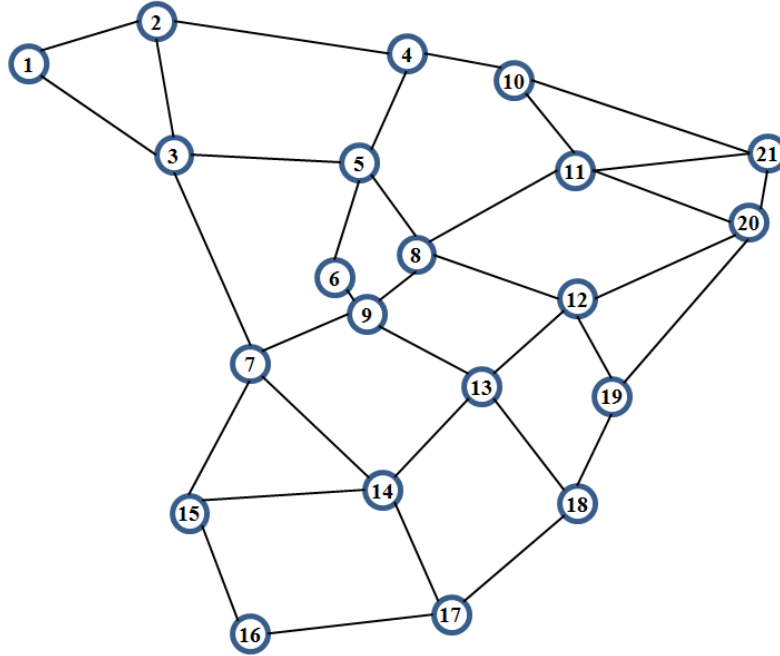
Figure 6.4: A realistic Spanish optical core transport network topology.

each demand $d \in \mathcal{D}$. As mentioned in Section 6.5.1, a set of k routes at the optical level is also pre-computed. In particular, the shortest-path route plus a restoration route per optical hop (note that a number of hops may share the same restoration route). To compute the k-shortest paths we make use of Yen's algorithm implemented as in [167]. Aiming at accurately computing the network CAPEX, we consider an adaptation of the equipment costs proposed in [168] to provide meaningful values to the ILP formulation presented in [162]. The costs of IP/MPLS nodes and OE ports are provided in Tables 6.2 and 7.4 respectively. In addition, we consider a cost per kilometer of restorable lightpath equal to 1 cost unit (c.u.).

6.6.2 Tuning of GRASP+PR and BRKGA parameters

Recently, in [169], an interesting way to solve the problem of parameter tuning for GRASP+PR heuristics has been proposed. This technique makes use of a BRKGA algorithm to explore the GRASP+PR parameter space. In this case, and for each chromosome, a random-key solution vector encodes the set of GRASP+PR parameters that we aim to tune. Then, to obtain the fitness for each chromosome, a set of V independent runs of the GRASP+PR must be executed, each lasting for U iterations. The fitness is calculated as the average objective function $g(\cdot)$ value found in these V executions.

Network	Transit	Interconnection	Metro CD	Traffic Mix National/Interconnection
A	3,4,9,11,14, 15,19,21	6,8,20	0.1 %	30/70(%)
B	1,9,10,12, 14,16,20	7,13,15,19	30 %	40/60(%)
C	3,4,5,8,9, 14,19,21	6,7,10,13,20	90 %	50/50(%)

Table 6.1: Network topologies and traffic parameters considered

Nodes	Class 1	Class 2	Class 3	Class 4	Class 5
Aggregated switching capacity (Gb/s)	160	320	640	1280	2560
Max. number of ports	4	8	16	32	64
Cost (c.u.)	3	4.5	6.5	22.5	50.19

Table 6.2: IP/MPLS Nodes features and costs

In our problem, however, given the complexity of the real-sized problems studied (i.e., multi-layer network size and traffic instances), we make use of the automatic tuning only for the parameters used in the multi-start phase of GRASP, that is, those parameters required in Procedures 8 and 9 (GRC and ALS). To perform this study, we consider a different set of 10 traffic instances per network. These instances are generated as described in Section 6.6.1, with increasing load intensities and with the number of demands limited to 40 so as to reduce complexity. The GRASP parameters that are to be tuned and their respective allowed values are: (i) Construction Procedure: $\alpha = \{0.0,0.1,0.2,0.3,0.4,0.5\}$, $\tau = \{0.1,0.2,0.3,0.4,0.5\}$, $\beta = \{0.0,0.1,0.2\}$ (recall from section 8.2.1 that although β is not shown in Procedure 8, it represents the threshold parameter for a hypothetical second RCL used to select the route for each demand). (ii) Local Search: $MaxCLS = \{5,10,20\}$, $MaxSearch = \{10,20,40\}$. Our chromosome is therefore defined by these 5 parameters of the GRASP multi-start phase. In contrast to the BRKGA defined in Section 6.5.2, here BRKGA does not make use of parallel populations. In Table 6.4, we provide the set of fixed BRKGA parameters that will be used by both BRKGAs (i.e., automatic tuning of GRASP parameters and the resolution of SIMNO). In addition, to define the BRKGA for the automatic tuning of GRASP parameters, we consider a population size equal to $p = 20$. The process is run for 10 generations. To obtain the fitness of each chromosome we perform $V = 10$ independent GRASP (GRC+ALS) executions with the time limit set to 2 hours. BRKGA tuning is applied to each of the networks (using the 10

OE Ports	1Gb	10Gb	40Gb	100Gb
Cost (c.u.)	0.45	1.5	8.125	24.625

Table 6.3: OE ports features and costs

p_e	p_m	ρ_e
0.2	0.2	0.7

Table 6.4: Fixed BRKGA parameter values

Network	α	τ	β	$MaxCS$	$MaxSearch$
A	0.4	0.1	0.0	5	20
B	0.2	0.5	0.0	5	20
C	0.2	0.2	0.0	5	20

Table 6.5: GRASP automatically tuned parameters

different traffic instances), thus resulting in a specific combination of parameters for each network. Table 6.5 reports, for each parameter and network, the values with higher frequencies of occurrence among the 10 traffic instances. It is worth highlighting that the automatic tuning always reports a value of β equal to 0, thereby eliminating the need for using an additional RCL to manage the selection of routes.

Next, we focus on the tuning of the parameters required to specify the PR method, namely the minimum distance to enter ES (δ_{th}) and the sampling parameter N_{SAMPLE}. In this work, we consider an elite set size ($|ES|$) equal to 6. Hereinafter in this chapter, and in order to quantitatively evaluate and compare the results of each experiment, we provide the performance metrics proposed in [164]. Specifically, we provide the number of times ($\#Best$) that each method is able to obtain the overall best solution value ($BestVal$) found among all methods being tested. Moreover, for each method, we compute the relative percentage deviation ($Dev(\%)$) between the best solution value obtained by that particular method and $BestVal$ for that instance. Finally, we report the statistic called $Score$ [164], [170]. In short, the $Score$ parameter counts, for a particular method M_x and for each problem instance, the number of methods that are able to find better solutions than M_x. Hence, the lower the $Score$, the better the method.

In this experiment, we consider 4 different traffic instances per network, though this time with the number of demands limited to 80. We increase the number of demands so as to obtain more accurate values to execute GRASP+PR with the real-sized traffic instances described in Section 6.6.1. Since the maximum distance between two solutions depends on the size of the demands set $\mathcal{D}$, we evaluate percentages of this figure as possible δ_{th} values. Moreover, we also test the impact of 4 different values for N_{SAMPLE}, thus resulting in 16 different parameter combinations for PR. For each traffic instance, we run 10 independent executions with the time limit set to 4 hours. The results provided in Table 6.6 clearly report that the best values for δth and N_{SAMPLE} are $0.1 \cdot |\mathcal{D}|$ and 10 respectively. Indeed, these values lead to results for the three statistics considered which compare favorably with the other values tested.

Finally, to specify the parameters of the BRKGA developed to solve SIMNO, we decided to

δ_{th}	$\frac{5}{100}\lvert\mathcal{D}\rvert$				$\frac{10}{100}\lvert\mathcal{D}\rvert$				$\frac{15}{100}\lvert\mathcal{D}\rvert$				$\frac{20}{100}\lvert\mathcal{D}\rvert$			
N_{SAMPLE}	1	10	15	20	1	10	15	20	1	10	15	20	1	10	15	20
$Dev(\%)$	2.6	2.7	2.4	2.7	2.7	**1.8**	2.5	2.7	2.1	2.6	2.8	3	3.4	3.1	2.6	3.1
$\#Best$	0	0	0	0	2	**3**	0	0	3	2	1	1	1	1	0	0
$Score$	102	86	86	94	77	**55**	96	97	69	91	85	100	105	93	88	101

Table 6.6: PR parameters evaluation.

perform a manual tuning. To this end, we conducted a set of preliminary experiments using several traffic instances for each of the networks evaluated, and took (after testing several combinations) the combination of parameters, that is, $(p, p_e, p_m, \rho_e, n_p, i_e)$, that in average led to the best solutions in all scenarios. The manually tuned parameter values found are those shown in Table 6.4 as well as a number $n_p = 3$ of parallel populations, an inter-population elite exchange $i_e = 2$ and a chromosome length as described in Section 6.5.2. Here, it is worth highlighting that we use a reduced population size ($p = 20$). As a consequence of the size of the problems, the length of the chromosome was higher than 300 genes and the decoder algorithm took more than 50 ms to build a single solution from a chromosome, that is, more than 15 seconds to build one generation when $p = n_g$ was used. Then, the BRKGA heuristic required extremely long times to reach convergence. Reducing the size of the population, the convergence time was reduced to acceptable values. As it has been mentioned, 3 populations were evolved in parallel and local elite individuals exchange was allowed every 15 generations.

6.6.3 BRKGA vs. GRASP vs. GRASP+PR performance comparison

Having tuned the parameters, we now carry out a performance analysis of the two meta-heuristic models proposed to solve the SIMNO problem, that is, BRKGA and GRASP+PR. Moreover, in order to highlight the benefits of PR, we include in the tests the results obtained by the basic GRASP heuristic (i.e., construction followed by local search). Here it is worth mentioning that the performance of both GRASP+PR and BRKGA was compared against the optimal solution obtained by solving the ILP described in Section 6.4 over a small multi-layer topology (not included in this chapter). In all the tests conducted, the optimal solution was found within running times of some seconds, in contrast to several hours needed to find the optimal solution using the ILP model.

To evaluate the three different variants, we make use of the 21 traffic instances per network as defined in Section 6.6.1. For each instance, we run 5 independent executions with the time limit set to 10 hours. The results are reported in Tables 6.7, 6.8 and 6.9, respectively for networks A, B and C.

As it can be observed, basic GRASP outperforms BRKGA in all networks, though more notably in the most complex instances (i.e., networks B,C). Note that the performance of BRKGA gradually decreases from network A to C, with higher complexity resulting in BRKGA finding convergence at very high CAPEX values when compared to both GRASP and GRASP+PR. In fact, in preliminary

Method	BRKGA	GRASP	GRASP+PR
$Dev(\%)$	7.79	6.35	2.04
$Score$	28	25	10
$\#Best$	10	4	15

Table 6.7: Results for traffic instances $RA_{1\ldots21}$

Method	BRKGA	GRASP	GRASP+PR
$Dev(\%)$	10.91	4.22	0.88
$Score$	33	22	8
$\#Best$	6	5	18

Table 6.8: Results for traffic instances $RB_{1\ldots21}$

experiments with smaller problem instances, we noticed that BKRGA obtains very good results in very short running times, outperforming GRASP in the trade-off between optimality and complexity. However, in the complex instances considered in this study, it is very difficult for BRKGA to converge to good quality solutions in short times. To illustrate this behavior, in Fig. 6.5, we plot the search profile of both BRKGA and GRASP+PR in a 10 hours execution using traffic instance RC_{10}. It is easy to observe that due to the complexity of the problem, BRKGA finds it very difficult to converge at good quality CAPEX values, whereas in GRASP+PR early results are already of good quality, thereby showing that the use of GRASP+PR does really pay off when real-sized, complex instances are considered.

Finally, GRASP+PR stands out as the best method providing in all networks the best results for all three metrics considered, a fact which clearly highlights the impact that introducing PR has in the meta-heuristic performance results. In order to graphically illustrate the performance difference between GRASP and GRASP+PR, in Fig. 6.6, we plot the search profile of 3 independent runs of both the GRASP and GRASP+PR algorithms considering traffic instance RC_5. Note that in the x-axis times are given in multiples of the average time it takes to perform a basic GRASP iteration (i.e., construction followed by local search), and hence, are shown as relative time units. The results provided claim to show the effectiveness and ability of PR to find regions of the space of solutions that, with the basic GRASP methodology, are highly unlikely to be found. Indeed, in Fig. 6.6, remarkable differences among the curves displayed by GRASP and GRASP+PR can be observed.

Method	BRKGA	GRASP	GRASP+PR
$Dev(\%)$	22.14	3.12	0.55
$Score$	42	16	5
$\#Best$	0	9	21

Table 6.9: Results for traffic instances $RC_{1\ldots21}$

Whilst the basic GRASP, after a few initial improvements, presents a rather flat profile, GRASP+PR clearly shows a more successful and thorough exploration of the space of solutions. Therefore, we consider that this study visibly shows to what extent can PR improve the results obtained by a basic GRASP heuristic, and more important, in which problems/scenarios the application of PR is really advisable. In the matter in hand, the application of GRASP+PR will definitely result in significant savings for network operators.

6.7 Summary

The objective of this study has been the development of heuristic algorithms aimed at minimizing the CAPEX investments required to plan a survivable IP/MPLS-over-WSON multi-layer network. For this purpose, we proposed a novel multi-layer optimization scheme, and hence, eventually tackled the so-called SIMNO problem. The resolution of this problem is indeed of great interest to network operators. To deal with SIMNO, we have first detailed the multi-layer network architecture under consideration as well as the novel recovery schemes proposed. Then, we have formalized the SIMNO problem by means of an ILP formulation which provided an insight into the complexity of managing the problem in hand. Finally, two powerful meta-heuristic models have been developed to help solve the SIMNO problem within practical running times. To be precise, a BRKGA and a GRASP+PR heuristic have been considered. After performing a set of exhaustive experiments, we have illustrated the difficulty that the BRKGA heuristic has in finding good quality convergence values, particularly when the problem instances are complex. At the same time, we have also shown the efficiency of the GRASP meta-heuristic specifically designed for solving SIMNO, even without the use of PR. However, the main outcome of this study has been the possibility to verify how powerful the PR intensification strategy is. Indeed, GRASP+PR has achieved significant improvements with respect to GRASP, particularly in the more complex network scenarios. In this chapter, GRASP+PR has helped to solve a current issue for network operators considering real-sized, complex network and traffic scenarios. Hence, we have illustrated one more time, a successful application of the combined GRASP+PR meta-heuristic.
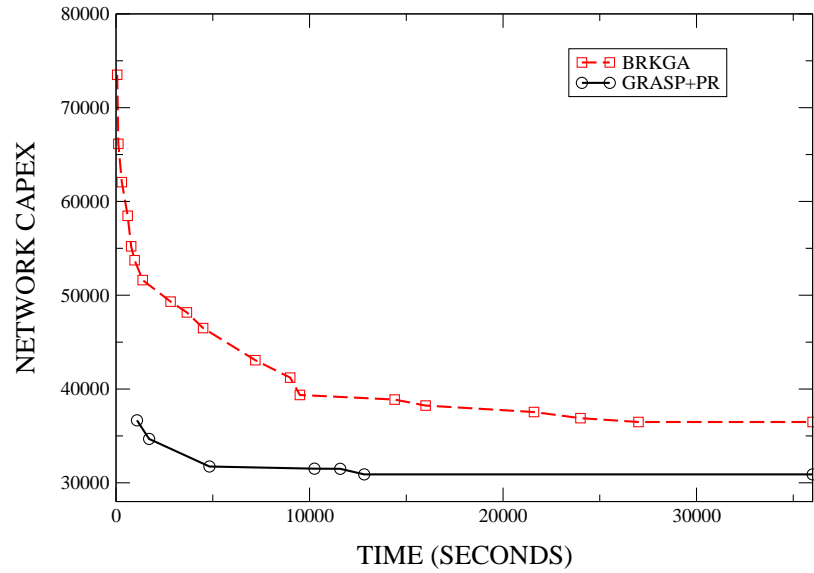
Figure 6.5: GRASP+PR vs. BRKGA performance comparison in a 10 hours execution (RC_{10}).
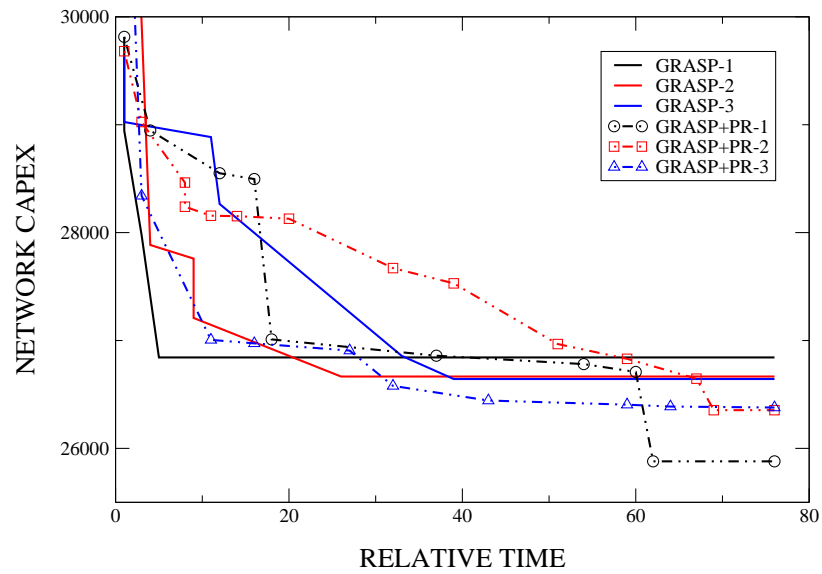
Figure 6.6: GRASP vs. GRASP+PR performance comparison using instance RC_5.

Chapter 7

GRASP and VND for the IP/MPLS-over-FlexGrid multi-layer problem

7.1 Introduction

The dramatic increase in the use of new disruptive bandwidth intensive services and applications has led to a huge surge of IP traffic which, ultimately, has brought to light the clear granularity mismatch between the client layer and current wavelength-routed dense wavelength division multiplexing (DWDM)-based optical layer. This issue results in a highly inefficient use of the network capacity, and consequently, in multi-layer networks requiring a large amount of highly expensive, power-consuming IP/MPLS equipments to be installed for aggregation (at the edge) and grooming (at the intermediate nodes) purposes.

In this context, the flexgrid technology [6], [7], provides higher spectrum efficiency and flexibility in comparison to traditional wavelength switched optical networks (WSON). By leveraging key advances in optical multi-level modulation techniques and the design of both bandwidth-variable transponders (BV-Ts) and bandwidth-variable wavelength selective switches (BV-WSSs), the main component enabling the design of bandwidth-variable wavelength cross-connects (BV-WXCs), flexgrid optical networks are able to provide both sub- and super-wavelength traffic accommodation. Whilst BV-Ts may work under both single- and multi-carrier advanced modulation formats such as QPSK, QAM, and O-OFDM [7], BV-WXCs can be assembled using existing devices like the WaveShaper programmable optical processor [171]. Thanks to this flexible technology, a flexgrid optical network can adjust to varying traffic conditions over time, space and bandwidth, thereby

creating a network scenario where wavelength channels are both switched and dimensioned (bit-rate/reach/signal bandwidth) according to temporary traffic requirements.

To this end, flexgrid optical networks divide the available optical spectrum into a set of frequency slots (FSs) of a fixed finer spectral width in comparison to the current ITU-T DWDM rigid frequency grid (50GHz) [5]. Current proposals for the slot size are 25GHz, 12.5GHz and 6.25GHz, the latter two being mentioned in the industry as potential minimum bandwidth granularities. Therefore, traffic demands are assigned a given number of FSs according to their requested bit-rate, the selected modulation technique and the considered frequency grid (i.e., the slot width) [7].

Consequently, in this flexible and dynamic network scenario, the classic constraints found in wavelength-routed networks, which are dealt with routing and wavelength assignment algorithms, are not applicable anymore. Specifically, in flexgrid optical networks emerge the so-called routing and spectrum assignment (RSA) problem where spectrum continuity along the links in the route of a given path (i.e., the same slots must be used in all the links of the path) as well as spectrum contiguity (i.e., the slots must be contiguous in the spectrum) must be guaranteed [172]. This problem poses new challenges for the design of future flexgrid optical networks, and thus, has rapidly aroused great interest within the research community. For instance, some recent works tackle the RSA problem for either the static/off-line (traffic demands are known a priori) [172], [173], [174] or the dynamic/on-line (connection requests are provisioned upon their arrival) network scenario [175], [176]. The study and development of complex RSA models and algorithms is nevertheless out of the scope of this work. In fact, here we make use of both a simplified RSA integer linear programming (ILP) model proposed in [174], which removes spectrum contiguity constraints by pre-computing demand-tailored channels (sets of spectrum contiguous slots), and an efficient RSA strategy similar to the fixed-alternate and first-fit frequency allocation algorithm proposed in [7] and evaluated in [177].

Our goal in this paper is, by contrast, to analyze for a number of candidate slot widths, the capital expenditures (CAPEX) needed to deploy a multi-layer IP/MPLS-over-Flexgrid architecture. To this end, we model the multi-layer IP/MPLS-over-Flexgrid optimization problem (hereinafter referred to as the MIFO problem) by means of both an ILP formulation and a greedy randomized adaptive search procedure (GRASP) algorithm, and solve it considering a range of real-sized network and traffic instances.

It is clear that finer grids will allow for more efficient spectrum utilization, and as a result, favor grooming data directly at the optical layer instead of requiring costly IP/MPLS equipment for such functionality. Thus, given the fact that the network CAPEX, that is, those costs related to purchasing and installing fixed infrastructures, is a figure network operators are always striving to reduce, the introduction of flexgrid technology is of paramount importance for future multi-layer networks [178]. However, it must be noted that while reducing the need for grooming at the IP/MPLS layer, this more advanced optical technology will also imply higher costs at the optical layer

given the highly demanding (grid-dependent) filtering characteristics that BV-WSSs are required to have. In addition, due to the increased spectrum fragmentation (particularly for the 12.5 GHz and 6.25 GHz grids), more complex network management, and therefore, more advanced control planes will be required, thereby leading to cost increases. Since exact costs for such components are still not available, in this study we consider a relative cost value to approximately quantify both these additional costs and, by this means, effectively determine which frequency grid will better address network operator's needs for cost-effective, spectrum-efficient network architectures.

7.2 Multi-layer IP/MPLS-over-Flexgrid optimization problem

In the literature, the multilayer network optimization problem has been tackled with a variety of objectives (see e.g., [179], [180], [181], [162] and [182]). In fact, each time a novel optical transport technology emerges such a problem has to be redefined. For example, in [182], authors propose heuristics to minimize CAPEX for a multi-layer network based on synchronous digital hierarchy over static point-to-point DWDM. More recently, in [162], authors deal with the survivable multi-layer IP/MPLS-over-wavelength switched optical network (WSON) optimization problem. Nowadays, the innovation is the replacement of the WSON technology with the emerging flexgrid paradigm. The aim of the MIFO problem is to effectively exploit network resources while, at the same time, minimizing CAPEX investments. This fact inevitably sets our focus on the size of the costly electronic layer, and hence, on the reduction of IP/MPLS equipment.

As aforementioned, flexgrid optical networks divide the available optical spectrum into a set of FSs. Then, the number of FSs each traffic demand is assigned depends on the network slot width (sw), the demand bit-rate (b_d), and the number of bits/symbol that the modulation format is able to carry (B_{mod}). Note that B_{mod} determines both the spectral efficiency of the modulation format (bits/s/Hz) and the symbol rate, and consequently, the spectral bandwidth required to transmit the signal [7]. Hence, at a given, fixed data rate, spectral savings can be obtained by reducing the symbol rate (i.e., increasing B_{mod}). For example, under good channel conditions, an advanced modulation format such as 64-QAM ($B_{mod} = 6$), would only require 1/3 of the spectral bandwidth used if QPSK ($B_{mod} = 2$) was used instead. However, these improvements come at the cost of reducing optical path lengths, as higher B_{mod} implies higher signal to noise ratio penalties and worse receiver sensitivity [7].

In order to estimate the number of FSs (n_d) (i.e., spectral bandwidth) that each traffic demand will require, we suggest using the following formula, which is in line with [7]:

$$n_d = \left\lceil \frac{b_d}{sw \cdot B_{mod}} \right\rceil \tag{7.1}$$

Demand(Gb/s)	10	40	100	400
$sw = 50$ GHz	1	1	1	4
$sw = 25$ GHz	1	1	2	8
$sw = 12.5$ GHz	1	2	4	16
$sw = 6.25$ GHz	1	4	8	32

Table 7.1: FSs required per demand under each frequency grid.

It must be mentioned that Eq. (7.1) tends to under-estimate the number of FSs required, as it assumes that bd consists only of payload data. However, in general, this is not the case, as different overhead data (e.g., around 10% extra) may be required. Such overhead may vary according to the modulation format selected. For instance, in OFDM-based systems, overhead symbols are required to avoid inter-symbol interference. Additionally, the selection of the modulation format may depend on each particular demand bit-rate. These issues, however, are left out of the scope of this work.

Specifically, in this analysis we consider QPSK ($B_{mod} = 2$) as the modulation format for all traffic demands, which are assumed to be of 10, 40, 100 or 400 Gb/s each. This way, the focus is set on the evaluation of the CAPEX savings that can be achieved through the use of narrower slot widths. Using (7.1), Table 7.1 reports the number of FSs that each demand requires under the different slot widths evaluated. One can observe that under the 50 GHz grid 10, 40 and 100 Gb/s demands will require the same amount of FSs, that is, one. However, under a 6.25 GHz grid, the same set of demands would need, respectively, 1, 4 and 8 FSs, thereby clearly illustrating the spectrum efficiency that can be obtained using finer BV-WSSs at the optical layer.

Note also that the demand to FS mapping shown in 7.1, not only has impact on the spectral efficiency achieved, but also on the number and type of BV-Ts deployed. In this work, the grooming of demands into lightpaths aims at minimizing the number of FSs used. Hence, considering the type and BV-T costs provided in Section V.A, two demands of 10 Gb/s, following the same path, would be groomed into a 40 Gb/s lightpath (requiring one 40Gb/s BV-T at each end) in both the 50 GHz and 25 Ghz grids. On the other hand, in both the 12.5 GHz and 6.25 GHz grids, two 10Gb/s lightpaths (two 10 Gb/s BV-Ts at each end) would be set up. Note that in the 12.5 GHz grid the tie in the number of FSs is broken by selecting the cheapest option, which in this case is two 10 Gb/s BV-Ts. According to this discussion, it can be anticipated that networks using finer slot widths would feature a larger number of BV-Ts but with a considerably lower average bit-rate.

In order to tackle MIFO, we assume that a network topology representing a set of geographical locations as well as the interconnectivity among them (i.e. the fibers are already deployed) is given in advance. In these sites, network equipment can be installed if necessary (see Fig. 7.1). Moreover, we assume that only a limited number of locations can be source/destination of IP/MPLS demands (blue locations). As required, nodes are equipped with BV-Ts so as to provide connectivity between the electronic and optical layer. The remaining locations (intermediate locations) are candidate
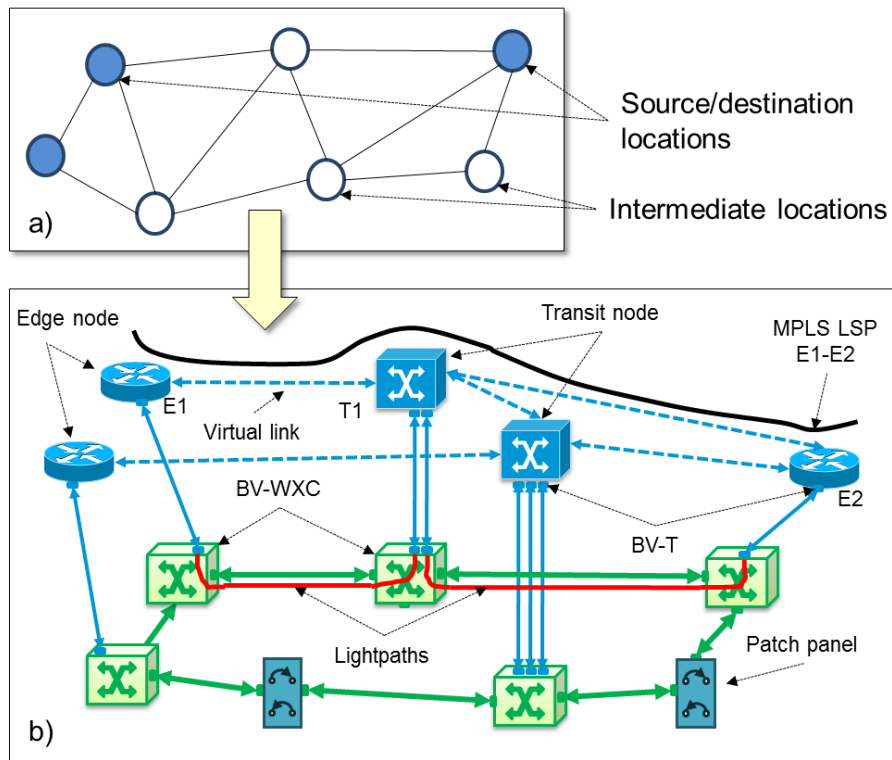
Figure 7.1: a) Geographical distribution for network topology locations. In blue, nodes that are source/destination of IP/MPLS traffic demands. White circles represent candidate locations where network equipment can be installed if necessary. b) A multi-layer network illustrating a possible solution for the MIFO problem.

spots where network equipment is installed according to the functionality required. Specifically, and given a set of traffic demands to be accommodated, intermediate locations can be either: (1) a multi-layer node with both IP/MPLS and BV-WXC functionality; (2) a BV-WXC node if no IP/MPLS operation is required; (3) a patch panel connecting optical fibers if neither IP/MPLS nor BV-WXC is required at such location; or (4) an empty location if no demand traverses such location. In Fig. 7.1(b), a multi-layer network exemplifying a possible solution to the MIFO problem applied to the topology of Fig. 7.1(a) is shown. One can observe locations that are equipped with multi-layer nodes providing either client flow aggregation (edge nodes) or routing flexibility (transit nodes). Other locations, however, only operate as patch panels for fiber connectivity purposes, thereby minimizing network CAPEX.

As an example, Fig. 7.1(b), illustrates one of the MPLS label switched paths (LSP) established in the network, that is, LSP E1-E2. In this case, this LSP entails tearing up two lightpaths to support virtual links E1-T1 and T1-E2. Recall that one lightpath, which is associated to two BV-Ts (one at each end), can be used to transport several traffic demands, and, by this means, provide the grooming functionality required to optimize the use of network resources. It is worth pointing out that the solution obtained by solving the MIFO problem (i.e., the location, type and quantity of network equipment deployed) will vary in accordance to the input traffic demands considered.

For the mathematical ILP formulation of the MIFO problem, the reader is referred to [27]. Although the ILP can be solved for small instances (see Section 7.3), its exact solving becomes impractical for realistic backbone multi-layer networks (under appreciable load) such as those described in Section 7.4, even using commercial solvers such as CPLEX [98]. Thus, aiming at providing near-optimal solutions within reasonable computational effort, our contribution in this chapter is the development of a metaheuristic method to solve the MIFO problem.

7.3 GRASP heuristic algorithm

In this Section, we provide a detailed description of GRASP heuristic algorithm that we have developed so as to efficiently solve the MIFO problem.

7.3.1 Construction algorithm

The resolution of the MIFO problem primarily consists in routing, one-by-one, a set of demands over a virtual topology. For clarity, let us denote with $g(\cdot)$ the function that computes the CAPEX required to deploy the multi-layer network. The CAPEX is computed using Eq. (2) in [27], and the specific network equipment cost values provided in Section V. The construction algorithm developed aims at generating demand orderings, $O_x = \{d_1, d_{|D|}\}$, that lead to the lowest possible CAPEX values. Considering the given physical network topology and a full mesh virtual network computed

on top, each demand $d \in D$, is associated to a sufficiently large set of pre-computed k_v shortest-path virtual routes, $R_d = \{r_1,, r_k\}$; each route $r \in R_d$ is in turn associated to a set of k_o optical routes. Thus, in order to progressively generate an ordering vector, the incremental CAPEX cost $(c_d^* = \min\{c_d(r)\}, \forall r \in R_d)$ of routing each demand is computed so that the demand leading to the smallest incremental cost $d^* = \min_{d \in D}\{c_d(r)\}$ is added to O_x. Note that $c_d(r)$ corresponds to the incremental cost of routing demand d through the cheapest route $r^* \in R_d$. For the sake of clarity, in the GRASP-specific pseudo-codes shown in Procedures 12, 14, and 15, we assume that function $g(\cdot)$ is able to compute CAPEX only receiving as input parameter ordering O_x. A detailed explanation of the CAPEX computation is provided in Procedure 13.

Procedure 12 Sample Greedy Construction

INPUT: $D, R_d, \forall\, d \in D, \tau$
OUTPUT: $O_x, g(O_x)$
 1: Initialize $O_x \leftarrow \emptyset$ and candidate set: $Q \leftarrow D$
 2: **while** $\mathcal{Q} \neq \emptyset$ **do**
 3:     Randomly sample $\min\{\tau \cdot D, Q\}$ elements from Q and put them in RCL;
 4:     Evaluate the minimum incremental cost $c_d^*, \forall\, d \in RCL$;
 5:     Select $d^* = argmin\{c_d^* : d \in RCL\}$;
 6:     $O_x \leftarrow O_x \cup \{d^*\}$;
 7:     $Q \leftarrow Q \backslash \{d^*\}$;
 8: **end while**
 9: Compute $g(O_x)$;

In this work, given both the fact that computing $c_d(r), \forall\, , r \in R_d, \forall\, d \in D$, is a time consuming task and that the size of the real-sized traffic and network instances is usually really large, we have implemented the sample-greedy (SG) construction method [147]. In this alternative construction algorithm, the greedy and randomization rules are balanced in an attempt to lower the worst case complexity of the common greedy randomized (GR) construction [147], which in order to fill the restricted candidate list (RCL) evaluates at each step all possible candidates. In contrast, as illustrated by the pseudo-code in Procedure 12, SG only samples a subset of the candidates at each iteration, and then, the element providing the best incremental cost (d^*) is added to the current solution. The percentage of elements evaluated to fill the RCL is controlled by the input parameter $\tau \in [0, 1]$. Note that parameter τ here is used to balance between greediness and randomness in the construction, with larger τ values leading to greedier solutions and higher time consumption.

To evaluate cost c_d (i.e., CAPEX) for routing each demand d through any virtual route $r \in R_d$, the heuristic algorithm proposed aims at determining the type of node to be deployed at each location as well as the type and number of BV-Ts to be installed. To this end, the steps detailed in Procedure 13 are executed. First, in line 1, demand d is added to all virtual links belonging to virtual route r. Then, for each virtual link e in the network, the loop in lines 2-6, determines the number and type (Gb/s) of candidate lightpaths (CLs) that have to be established between each pair of locations in the network. The term CL here is used emphasize that it is not until the node type to be installed

---

Procedure 13 Construct multi-layer network

INPUT: V, E, d, r
OUTPUT: Multi-layer network infrastructure
1: Associate d to all virtual links $e \in E$
2: **for all** $e \in E$ **do**
3:    Take set of demands D_e using e (if any)
4:    Groom demands in D_e and determine the number and type of candidate lightpaths (CL) required
5:    Associate CL to both $v \in V(e)$
6: **end for**
7: **for all** $v \in V$ **do**
8:    According to the CLs ending or originating at v and the demands they groom, determine the type of ndoe to be installed (IP/MPLS, BV-WXC, Patch-panel or Empty) and type and number of BV-Ts required
9: **end for**
10: Compute $COST_{FO}$ according to the installed BV-Ts, which determine the lightpaths actually established in the network
11: Compute CAPEX using $g(V, COST_{FO})$

---

at each location is known that the lightpaths are actually established. After grooming the demands into CLs, the number of contiguous FSs required by each CL is obtained. Then, an efficient first-fit RSA algorithm is run in order to allocate spectrum resources along all optical links in route $k_o = 1$ supporting e. Specifically, we model optical links as binary vectors $(x[i])$, where each position represents one FS ($x[i] = 1$ (used) or 0 (free)). Hence, given the number of contiguous FSs required, a logic and operation considering all optical links supporting e is computed to find all the candidate set of contiguous FSs where the groomed demand can be allocated. Among them, we select the set of FSs to be used in a first-fit basis. If no candidate set of FSs is found, then $k_o = 2$ is attempted. As mentioned in Section 7.1, this strategy is similar to the fixed-alternate and first-fit frequency allocation algorithm (see e.g., [177]). The main difference lies in the fact that in this work the order in which these demands are served is controlled by the proposed GRASP methodology.

The subsequent *for* loop determines the equipment to be installed at each location. Finally, according to the BV-Ts deployed, the algorithm is able to determine the actual lightpaths established and the associated cost for using the fiber ($COST_{FO}$). Hence, in line 10, CAPEX can be easily computed by applying $g(\cdot)$. Note that once the cheapest route r^* is found (and hence so is d^*), d^* is routed through r^* and the set of virtual links is updated accordingly to keep track of the demands already served. As the loop in Procedure 12 progresses, the number of demands supported by the set of virtual links E (input for the algorithm in Procedure 13) increases, and so does the size and CAPEX of the multi-layer network.

In line 8 in Procedure 13), given the CLs ending or originating at node $v \in V$, the functionality required at v can be determined. For instance, let us assume that v has only one originating (l_o) and one ending lightpath (l_e), none of the demands groomed in such lightpaths is originating or ending at v, and both lightpaths groom exactly the same demands, it means that a patch-panel can be placed at v, as only fiber connectivity is required. In contrast, assuming that another lightpath ($l_{e'}$)

147

is also ending at v through the same input port as l_e, none of the demands it supports ends at v, and $l_{e'}$ has its exact replica in one of the output ports (i.e., carrying the same groomed demands and using the same FSs (same channel)), then a BV-WXC needs to be installed, as only optical switching functionality is required. Finally, if any of the demands in such lightpaths ends or originates at v, or if any of the ending lightpaths has not its exact replica in an originating one, then IP/MPLS equipment needs to be installed, as electronic processing of the signals is required. Note that if no lightpaths end or originate at v, the location is left empty.

7.3.2 Local search algorithm

Since a feasible solution to the problem (O_x) output by Procedure 12 has no guarantee of being locally optimal, let us denote with $N_q(O_x)$, the set of solutions in the q_{th} neighborhood structure of O_x. Thus, assuming an order $O_x = \{d_1, , d_i, , d_j, , d_{|D|}\}$, we define the neighbor of this ordering as an ordering in which d_i swaps its position with d_j. In order to generate a random neighbor in the first neighborhood of O_x (i.e., $N_1(O_x)$), we choose pivots d_i and d_j uniformly among the $|D|$ demands. Hence, creating a N_q neighbor implies that this random swap of demands is performed q times. In this work, we have adopted the variable neighborhood descent (VND) [138] algorithm to perform the local search within the GRASP methodology. Specifically, VND explores a limited number of neighborhood structures ($mxStr$), by uniformly sampling a number of neighbors ($mxSam$) in each of them. Starting with N_1, VND performs local search until no further improvement is found. The VND pseudo-code is shown in Procedure 14.

Procedure 14 Variable neighborhood descent

INPUT: $O_x, mxStr, mxSam$
OUTPUT: $O_{BEST}, g(O_{BEST})$
 1: Initialize $O_y \leftarrow O_x$, $O_{BEST} \leftarrow O_x$ and $k \leftarrow 1$
 2: **while** $k < mxStr$ **do**
 3:     Randomly sample $mxSam$ elements in $N_k(O_x)$ and let O'_y be the best solution obtained
 4:     **if** $g(O_{y'}) < g(O_x)$ **then**
 5:         $O_{BEST} \leftarrow O'_y$
 6:         $O_y \leftarrow O'_y$
 7:         $k \leftarrow 1$
 8:     **else**
 9:         $k \leftarrow k + 1$
10:     **end if**
11: **end while**

7.3.3 GRASP algorithm

Finally, the pseudo-code for the GRASP algorithm is illustrated in Procedure 15, where it is possible to observe that the multi-start phase (i.e., SG followed by VND) is executed for mxIter iterations. The performance of the proposed GRASP methodology has been compared against the ILP model

described in [27]. To be able to solve the ILP model, however, we had to consider a size-constrained multi-layer network (e.g., limiting the size of the virtual topology) and a very small amount of demands for each experiment. In all the experiments performed, the GRASP heuristic was able to provide a much better trade-off between optimality and computation time due to the high difficulty in solving the model. Although for these preliminary experiments the input GRASP parameters were manually tuned, for the realistic network scenarios considered in this study a more advanced approach is employed as explained in Section 7.4.

Procedure 15 GRASP algorithm

INPUT: $D, R_d, \forall\, d \in D, \tau, mxStr, mxSam, mxIter$
OUTPUT: $O_{BEST}, g(O_{BEST})$
1: Initialize $O_{BEST} \leftarrow \emptyset$, $i \leftarrow 0$
2: **while** $i < mxIter$ **do**
3:    $O_x \leftarrow SG(D, R_d, \forall\, d \in D, \tau)$
4:    $O'_x \leftarrow VND(O_x, mxStr, mxSam)$
5:    **if** $g(O_{x'}) < g(O_{BEST})$ **then**
6:       $O_{BEST} \leftarrow O_{x'}$
7:    **end if**
8:    $i \leftarrow i + 1$
9: **end while**

7.4 Illustrative numerical results

In this section, we first present the network scenarios that we consider in order to carry out our experiments. Second, we perform the tuning of the input parameters required to execute the GRASP heuristic, and finally, solve the MIFO problem considering a set of realistic traffic instances.

7.4.1 Network scenario

In order to conduct all the experiments, we consider the three optical network topologies shown in Fig. 7.2. In these networks, we assume that $V_v = V$, that is, that any location can host an IP/MPLS node. Besides, only those locations in blue in Fig. 7.2, can be source or destination of IP/MPLS demands (as explained in Section 7.2). The remaining locations (i.e., the intermediate locations) will be equipped according to the MIFO problem solution.

As to the traffic profiles (TP) considered, we make use of three TPs as reported in Table 7.2. Although each TP injects into the network the same average amount of Tb/s, the traffic scenarios proposed feature lightly loaded demands in TP-1 (only 24.1 Gb/s on average), medium load demands (52.0 Gb/s) in TP-2, and high bit-rate demands in TP-3 (80Gb/s). Hence, the number of demands served decreases substantially from TP-1 to TP-3 in order to keep constant the total volume of Tb/s injected. These TPs are a realistic representation of the expected evolution of bandwidth necessities for the years to come in increasing order. Since our goal in this work is to evaluate the slot width
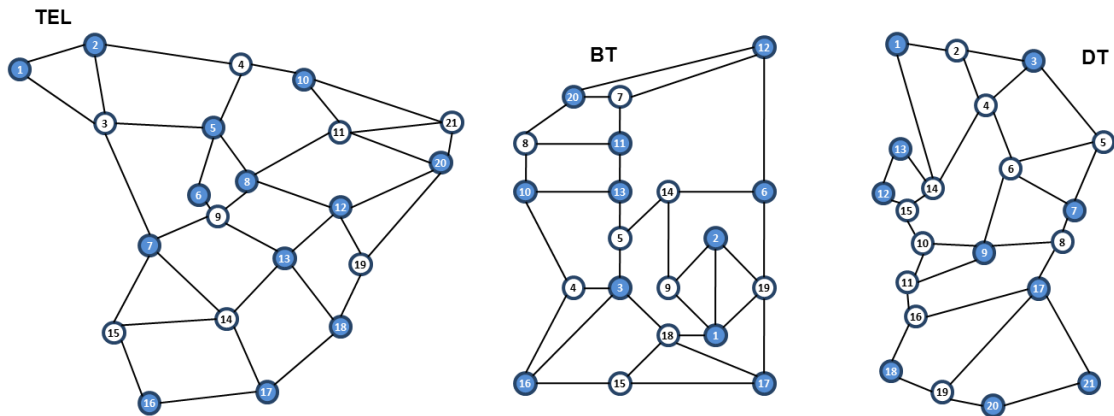
Figure 7.2: Optical network topologies considered: the 21-node Spanish Telefónica (TEL), the 20-node British Telecom (BT), and 21-node Deutsche Telecom (DT).

TP	Avg. bit-rate	Demands(%)			
	(Gb/s)	10 Gb/s	40 Gb/s	100 Gb/s	400 Gb/s
TP-1	24.1	80	13.4	5.4	1.3
TP-2	52	40	40	16	4
TP-3	80	0	66.7	26.7	6.7

Table 7.2: Traffic profiles (TPs) analyzed

Node	Class 1	Class 2	Class 3	Class 4	Class 5
Capacity (Gb/s)	160	320	640	1280	2560
Max. ports	4	8	16	32	64
Cost (c.u.)	9	13.5	19.5	67.5	150.7

Table 7.3: Cost and features of IP/MPLS nodes

BV-T	10Gb	40Gb	100Gb	400Gb
Reach (km)	2500	2000	1000	400
Cost (c.u.)	2.5	7.625	20.625	65.625

Table 7.4: Cost and reach of BV-Ts

impact on the network CAPEX, we considered a wide enough optical spectrum, taking into account the demands to be served in each TP. To be exact, using 2 THz we corroborated that for all traffic representations executed a feasible solution could be found. Table 7.3 (IP/MPLS nodes) and Table 7.4 (BV-Ts) provide the characteristics of the network equipment considered as well as their value in cost units (c.u.) that we use to compute the CAPEX. All these values have been obtained from discussions currently being held within the STRONGEST project [4].

In addition, we assume an optical amplifier cost of 5 c.u., and $C_{FO} = 0.02$, that is, the cost per km and GHz of using the already deployed optical fiber. As mentioned in Section 7.2, we consider QPSK ($B_{mod} = 2$) as modulation format. Note that considering QPSK and the network topologies shown in Fig. 7.2, it can be assumed that the number of cascaded BV-WXC traversed by a demand does not need to be limited [7]. In order to route the demands, a set of k shortest paths is pre-computed over both the physical (k_o) and virtual network topology (k_v). To this end, we implemented the Yen's algorithm as proposed in [167]. Specifically, we set respectively k_o and k_v to a maximum of 200 and 400 shortest paths.

7.4.2 GRASP parameter tuning

In order to find appropriate values for the input parameters of the GRASP procedure, we make use of the automatic biased random-key genetic algorithm (BRKGA) tuning for GRASP heuristics as proposed in [169]. The parameters that need to be adjusted are τ in the SG construction algorithm and both mxStr and mxSam for the VND local search heuristic. Thus, the chromosome used to run BRKGA is defined by these three parameters. We test the following values for each of them: $\tau = \{0.1, 0.2, 0.3, 0.4\}$, $mxStr = \{5, 10, 15\}$ and $mxSam = \{10, 15, 20\}$. To run BRKGA, we use the same approach and input parameter values as in [25]. BRKGA tuning is run considering 5 reduced-size traffic instances for each TP and network, and as a result, a combination of parameters is obtained for each of them. The parameters found to run GRASP are provided in Table 7.5.

Network	τ	$mxStr$	$mxSam$
TEL	0.2	5	15
BT	0.3	10	10
DT	0.3	5	15

Table 7.5: GRASP automatically tuned parameters

7.4.3 CAPEX using relative (grid-dependent) BV-WSS costs

In this subsection, we solve the MIFO problem with the aim of finding, given a target CAPEX investment and a set of relative cost values for the different bandwidth-variable wavelength selective switches (BV-WSSs), the maximum affordable cost for each of the (grid-dependent) BV-WSS. Although the actual cost for these enhanced optical devices (also involving higher costs due to a more complex control plane) is still not available, we assume that the finer the grid, the higher the relative cost for a BV-WSS device should be.

In Fig. 7.3, we provide for each network topology, traffic profile (TP), and frequency grid, the network CAPEX for the MIFO problem solution. Note that CAPEX here only accounts for the network equipment costs (i.e., Eq. (2) in [27]). Each of the points in the plots corresponds to an average over 10 independent runs (each lasting for 40 iterations) of the GRASP heuristic algorithm. For the sake of a comprehensive analysis, we consider two traffic scenarios for each TP, these are, a highly loaded scenario (4.5 Tb/s are injected into the network), and a medium one (3.5 Tb/s). Thus, out of the 10 runs, 5 correspond to the highly loaded scenario and 5 to the medium one.

The plots in Fig. 7.3, clearly illustrate the effectiveness of narrower grids in grooming data directly at the optical layer, thus reducing network CAPEX. Besides, such a positive effect is clearly dependent on the TP considered. For the TP-1, one can observe that the introduction of finer grids allows for the spectrum to be better exploited, and hence, to achieve further benefit. In TP-2, by contrast, the 6.25GHz grid provides the same performance as the 12.5GHz in both the TEL and DT networks, and the 25 GHz in the BT network. Eventually, in TP-3, the main benefit is obtained just by considering a 25 GHz grid.

Complementing these results, Table 7.6 reports the average number and bit-rate of the installed BV-Ts, and Table 7.7 provides the average reduction (with respect to the 50 GHz grid) in both IP/MPLS node switching capacity and actual amount of traffic switched (flow switched). As expected, these values are strongly dependent on both the frequency grid and TP evaluated. As anticipated in Section 7.2, and as long as the TP analyzed allows for it, the use of finer frequency grids entails a higher number of BV-Ts due to the more fragmented spectrum, which eventually results in a different grooming of demands into lightpaths (according to the mapping shown in Table 7.1 and the equipment costs provided this section). However, this increase comes at the benefit of having a considerably much lower average bit-rate per BV-T, a fact which leads to lower switching capacity, and therefore, to cheaper IP/MPLS equipment.
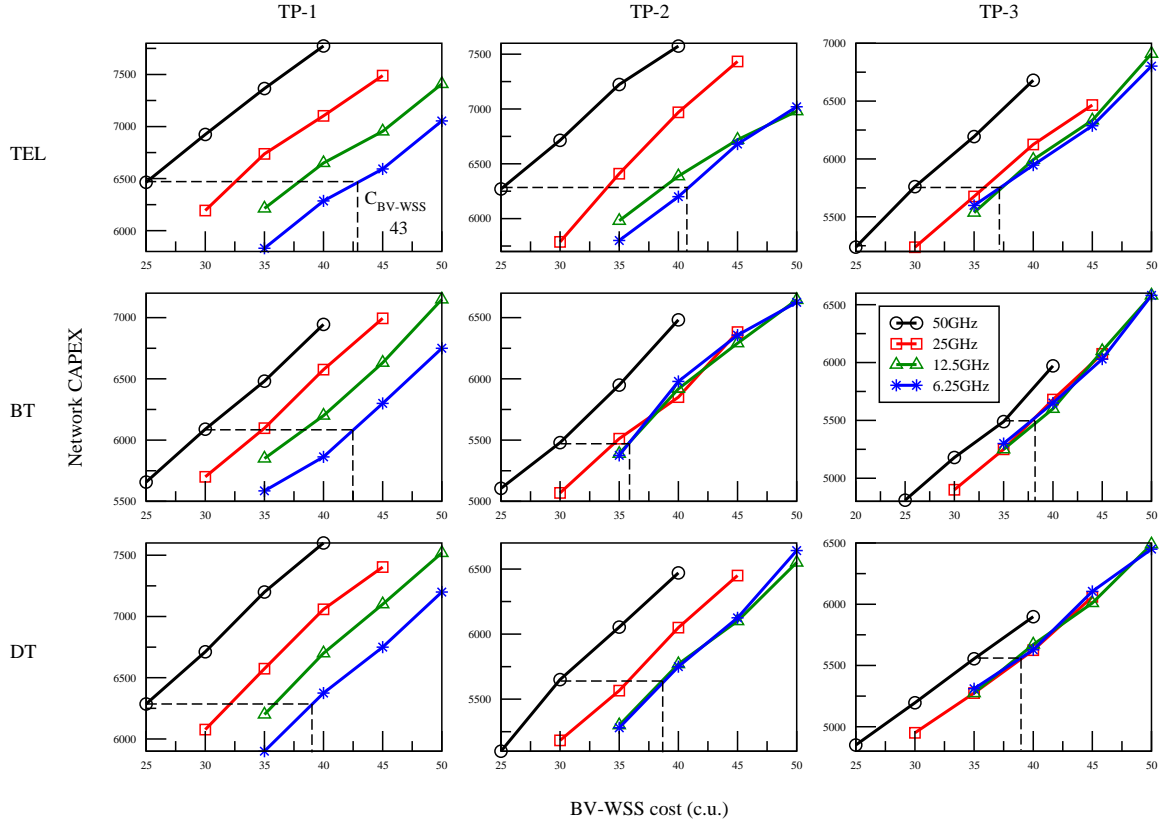
Figure 7.3: Network CAPEX (IP/MPLS and optical equipment cost) as a function of the relative cost for one BV-WSS. The three network topologies are analyzed under the four different slot widths.

Network	Grid	BV-T number			BV-T bit-rate		
		TP-1	TP-2	TP-3	TP-1	TP-2	TP-3
TEL	50	158	148	119	64	70	70
	25	190	179	118	50	49	67
	12.5	229	219	117	37	39	66
	6.25	277	260	118	30	32	66
BT	50	136	121	111	55	59	64
	25	170	150	112	42	47	63
	12.5	215	160	111	32	41	58
	6.25	255	164	110	26	39	57
DT	50	147	117	115	59	58	62
	25	183	140	117	49	50	61
	12.5	235	157	116	41	45	60
	6.25	257	170	117	31	41	61

Table 7.6: Avg. BV-T number and bit-rate (Gb/s)

Network	Grid	Capacity (%)			Flow (%)		
		TP-1	TP-2	TP-3	TP-1	TP-2	TP-3
	25	13	11	8	10	8	4
TEL	12.5	20	13	8	16	9	4
	6.25	24	13	8	24	11	4
	25	5	4	1	5	5	1
BT	12.5	8	7	2	7	7	2
	6.25	14	7	2	14	8	3
	25	4	6	1	4	12	1
DT	12.5	11	10	1	11	13	2
	6.25	17	14	1	17	14	2

Table 7.7: Avg. reduction per grid in node switching capacity and flow switched (with respect to the 50 Ghz grid)

Grid	TP-1	TP-2	TP-3
25	25.6	27.3	23.2
12.5	41.3	36.1	33.5
6.25	57.6	38.9	39.9

Table 7.8: Avg. BV-WSS affordable cost increment per frequency grid (%)

Finally, in order to estimate the maximum affordable cost increment for a BV-WSS in the 6.25 GHz grid, we use as benchmark reference a BV-WSS cost in the 50 GHz grid (see dotted lines in Fig 3). In the TEL network under TP-1, the cost of the BV-WSSs can be, for the same network CAPEX, as high as 43 c.u., that is, 72% more expensive than the one used in the 50 GHz grid (25 c.u.). However, when the on-average bit-rate of the demands increases in both TP-2 and TP-3, the cost of a BV-WSS decreases to about 41 c.u. (64%) and 37 c.u. (23%), respectively. In Table 7.8, the average BV-WSS affordable cost increment provided by each frequency grid is reported.

In light of the results shown in Table 7.8, which represent an average over the three network topologies, it is clear that from a temporal perspective given by the on-average bit-rate of demands, high cost increments can be assumed for a 6.25 GHz grid BV-WSS in the near future (57.6%). However, considering the expected traffic evolution, which for the long-term estimates a TP similar to the TP-3 analyzed in this chapter, these investments will not be profitable. Therefore, it can be concluded that investments in flexgrid optical networks using the 12.5 GHz or even the 25 GHz grid (considering the increased management complexity of the network in finer frequency grids), are cheaper in the short-term and more appropriated for medium and long-term scenarios.

7.5 Summary

This paper addressed the design of a multi-layer IP/MPLS-over-flexgrid network. To this end, an ILP formulation has been presented and, given its complexity, a GRASP meta-heuristic has been developed. Through extensive numerical experiments, we have analyzed the cost implications that the frequency grid (slot width) has on this emerging multi-layer network planning problem. For the sake of a comprehensive study, we have considered a set of realistic network topologies, equipment costs, and traffic instances.

The results have shown that the benefits that can be achieved through the use of finer slot widths are strongly dependent on the actual traffic profile (TP) under which the network is operating. Whilst investments in costly bandwidth-variable wavelength selective switches (BV-WSS) (finer grid) devices are very well motivated under traffic conditions reporting a high number of light bit-rate demands, which represent short-term traffic scenarios, they do not seem profitable in the long-term, where a reduced number of higher bit-rate demands are expected. Consequently, this study reports both the 12.5 GHz and the 25 GHz slot widths as potential candidates for the deployment of future multi-layer networks based on flexgrid technology.

Chapter 8

Meta-heuristic hybridizations for the RPD problem in T-SWS optical networks

8.1 Introduction

As explained in Chapters 2 and 3 in Part I of this thesis, in translucent sub-wavelength switching (T-SWS) networks, the routing and regenerators placement and dimensioning (RRPD) problem emerges. We have shown that the joint RRPD problem leads to a very complex formulation, and consequently, we have proposed to solve both the routing and RPD subproblems separately. To be precise, we have provided a mixed integer linear programming (MILP) model for the routing problem (minimizing congestion in network bottleneck links), and an optimal MILP formulation to solve RPD. While the routing formulations proposed are optimal and can be efficiently solved, the RPD formulation still results in a complex formulation for which only fairly small problem instances can be solved exactly. Hence, we have also provided both MILP-based and heuristic RPD algorithms and assessed their performance.

In the context of communication networks, operations research (OR) methodologies provide a means of efficiently solving real life problems which are currently identified as open issues among network operators, and consequently, their solution is of great interest. Indeed, by applying powerful metaheuristic techniques one can gain a valuable insight into the problem in hand, as they allow for the consideration of real-sized, complex network and traffic scenarios such as the ones used in this thesis. Successful applications of OR in this field are, among others, efficient heuristics for routing and wavelength assignment (RWA) in optical networks [183], optimization of network design/planning problems [145], and multicast routing algorithms for IP networks [184].

156

In this chapter, we restrict our attention to the modeling of efficient metaheuristic hybridizations to solve the complex RPD problem found in sub-wavelength switching networks. To this end, a greedy randomized adaptive search procedure (GRASP) [139] and a biased random-key genetic algorithm (BRKGA) [136] are proposed. GRASP-based heuristics have been used to solve a wide range of problems with many and varied applications in the real life such as the design of communication networks [141] and collection and delivery operations [142]. Similarly, BRKGAs, which are a particular class of genetic algorithms (GAs), have also proven to be very effective at solving complex optimization problems. Indeed, we can find very recent works which apply BRKGAs to complex communication network problems such as routing in IP networks [97], and RWA in wavelength-routed optical networks [96].

In this study, we further enhance these methodologies by introducing an adaptation of the variable neighborhood descent (VND), and the path-relinking (PR) intensification procedures. VND was proposed as a search heuristic within the framework of variable neighborhood search methods [138]. PR, by contrast, was first applied in the context of GRASP by [137], thereby developing the powerful and widely used GRASP+PR algorithm. For a wide variety of examples and applications of GRASP+PR, the reader is referred to [146]. Both VND and PR have proven to be efficient in solving real life problems. For instance, in the field of optical networks, [185] have recently applied VND to solve the RWA problem, and [25] have used GRASP+PR to tackle the complex multilayer optical network optimization problem.

Through extensive experiments, we show that BRKGA-based hybridizations outperform those based on GRASP and that the introduction of both VND and PR results in significant performance improvement for both algorithms. Further, by comparing the results of the metaheuristic hybridizations with that of MILP optimal and heuristic algorithms, this work reports yet another successful application of OR methods in the field of optical networks.

8.2 A GRASP-based RPD heuristic

The multi-start GRASP procedure basically consists of two phases. In the first phase, a greedy randomized feasible solution of the problem is built by means of a *construction* procedure. Then, in the second phase, a *local search* technique to explore an appropriately defined neighborhood is applied in an attempt to improve the current solution.

8.2.1 Construction procedure

In order to construct a solution, our problem consists in selecting, for each path $p_i \in \mathcal{P}^o = \{p_1, ..., p_{|\mathcal{P}^o|}\}$, a regeneration option $s_j \in \mathcal{S}_{p_i} = \{s_1, ..., s_{|\mathcal{S}_{p_i}|}\}$. For the sake of clarity, let us define a path instantiation u_j^i as the assignment of regeneration option $s_j \in \mathcal{S}_{p_i}$ to path $p_i \in \mathcal{P}^o$, that is, $u_i^j = < p_i, s_j >$. Moreover, let $\mathcal{U} = \bigcup_{p_i \in \mathcal{P}^o} u_i^j$ denote the complete set of path instantiations.

Note that we are dealing with an unconstrained problem, and thus, any path $p \in \mathcal{P}^o$, can take any $s \in \mathcal{S}_p$ independently of the decision taken by other paths (i.e., no path instantiation can lead to an unfeasible solution). Hence, once $\mathcal{U}$ is generated, a feasible solution to the RPD problem can be obtained. Let us denote with $g(\cdot)$ the cost function which aims at minimizing the total amount of regenerators to be deployed given a B^{QoT} target performance. Function $g(\cdot)$ makes use of Procedure 7 as defined in Section 3.1.4 to compute the number of regenerators. Note that set $\mathcal{U}$ helps determine load $\rho_v^o, v \in \mathcal{V}$, and thus, a solution to the problem can be obtained by applying $g(\mathcal{U})$. However, it must be noted that such an operation is required in every phase of the GRASP heuristic and performed a very high number of times. In addition, parameter R (see Eq. (3.11)) can be extremely high in some network scenarios. For this very reason, we use a binary search algorithm to reduce the complexity of Procedure 7 to $O(logR)$. Our approach to construct solutions takes into consideration the order in which path instantiations are performed, as in fact, due to the already deployed regenerators, such order has influence on subsequent path instantiations. Thus, we consider the order $\mathcal{O}_x = \{p_1, ..., p_{|\mathcal{P}^o|}\}$ as a guide to iteratively perform, for each path $p \in \mathcal{P}^o$, the required path instantiation and generate $\mathcal{U}$. From this point on, it will be up to the subsequent intensification strategies to improve set $\mathcal{U}$.

Specifically, the construction procedure that we consider to solve the RPD problem is the greedy randomized construction (GRC) as described in the next subsection.

Greedy randomized construction (GRC)

GRC relies on a restricted candidate list (RCL) which is made up of the paths $p \in \mathcal{P}^o$ with the best (smallest) incremental costs $c(p)$. Paths are iteratively processed, and at each step, costs $c(p)$, $p \in \mathcal{P}^o$ are recomputed to account for the paths already processed (i.e., path instantiations previously performed). All regenerative options $s \in \mathcal{S}_p$ are considered, and $c(p)$ is given the value of the option s with the lowest incremental cost (i.e., $c(p) = \min_{s \in \mathcal{S}_p} \{c(s)\}$). It is worth mentioning that costs $c(s)$ account for the increment in regenerators caused by the selection of s as regeneration option for path p. Therefore, RCL is dynamically built with all paths $p \in \mathcal{P}^o$ whose cost $c(p)$ falls within the interval defined by the real parameter $\alpha \in [0, 1]$ (see lines 5-7 in Procedure 16). Then, one of the paths in the RCL (p_i) is randomly chosen and the regeneration option $s_j \in \mathcal{S}_{p_i}$ with the lowest incremental cost is selected to perform the required path instantiation u_i^j. Once $\mathcal{Q}$ becomes an empty set, all paths in $\mathcal{P}^o$ have been processed, and hence, we can finally obtain the total number of regenerators deployed by applying $g(\mathcal{U})$. Note that costs $c(s_j)$, $s_j \in \mathcal{S}_{p_i}$, are again recomputed at each iteration in order to take into account previous path instantiations (i.e., regenerator sites already distributed in the network). In this algorithm, parameter α needs to be adjusted as shown in Section 8.4.

Procedure 16 Greedy Randomized Construction (GRC)

INPUT: $\mathcal{P}^o, \mathcal{S}_p \; \forall \; p \in \mathcal{P}^o, \alpha$
OUTPUT: $\mathcal{O}_x, \mathcal{U}_x, g(\mathcal{U}_x)$
1: $\mathcal{U}_x \leftarrow \emptyset, \mathcal{O}_x \leftarrow \emptyset$;
2: Initialize the candidate set: $\mathcal{Q} \leftarrow \mathcal{P}^o$;
3: Evaluate the incremental cost $c(p)$ for all $p \in \mathcal{Q}$;
4: **while** $\mathcal{Q} \neq \emptyset$ **do**
5:     $c^{min} \leftarrow min\{c(p) \mid p \in \mathcal{Q}\}$;
6:     $c^{max} \leftarrow max\{c(p) \mid p \in \mathcal{Q}\}$;
7:     $RCL \leftarrow \{p \in \mathcal{Q} \mid c(p) \leq c^{min} + \alpha(c^{max} - c^{min})\}$;
8:     Select an element p_i from RCL at random;
9:     $\mathcal{O}_x \leftarrow \mathcal{O}_x \cup \{p_i\}$;
10:    Take element $s_j \in \mathcal{S}_{p_i}$ such that $c(s_j) = c(p_i)$;
11:    Perform path instantiation u_i^j
12:    $\mathcal{U}_x \leftarrow \mathcal{U}_x \cup \{u_i^j\}$;
13:    Update candidate set $\mathcal{Q}$;
14:    Reevaluate the incremental cost $c(p)$ for all $p \in \mathcal{Q}$;
15: **end while**

8.2.2 Local search

In this section, we provide the details concerning neighbor generation as well as the pseudo-code and operation of the local search algorithm adopted, namely the VND technique.

Neighbor generation

Once the path instantiation set $\mathcal{U}_x$ is obtained by means of GRC, local search aims at improving such a solution by exploring its neighborhood. Note that, due to the fact that path instantiations are performed taking into account the current location and number of regenerators deployed, only the last path to be instantiated takes its decision with a whole view of the problem. Changing one regenerator selection may therefore impact on subsequent decisions and eventually provide a different solution. Neighbor generation tries to exploit this issue. To this end, random neighbors in the first neighborhood (i.e., $1 - move$ neighbor) of $\mathcal{U}_x$, that is, $N_1(\mathcal{U}_x)$, are generated by uniformly selecting a pair of pivots p_i, p_j among those in set $\mathcal{P}^o$. Then, we take their respective path instantiations (u_i^m, u_i^n) and try to improve the selection of s_m and s_n as regeneration options for paths p_i and p_j respectively. We evaluate the incremental costs of all $s_k \in \mathcal{S}_{p_i}, s_l \in \mathcal{S}_{p_j}$ so that both path instantiations are recomputed and inserted in $\mathcal{U}_x$ again. Note that a $q - move$ neighbor is generated by performing such a random pair selection and re-computation operation for q consecutive times over the same set $\mathcal{U}_x$.

Variable neighborhood descent (VND)

The pseudo-code for the VND algorithm is illustrated in Procedure 17. Starting at $\mathcal{U}_x$, VND begins the search by constructing a set of $MaxSearch$ neighbors in N_1, and if among them all, an improving

$\mathcal{U}_N$ solution is found, the algorithm moves to $\mathcal{U}_N$ and continues the search in N_1. If no improvement is found, by contrast, VND switches to N_2 and so on. Due to the fact that VND switches back to N_1 every time an improvement is found, this algorithm is able to perform an exhaustive search until the last allowed neighborhood N_{MAX} is reached. Note that the intensity of the search in each neighborhood structure depends on the number of neighbors sampled ($MaxSearch$). The best solution found ($\mathcal{U}_{BEST}$) is returned as output when neighborhood N_{MAX} is reached and no improvement is found.

Procedure 17 Variable Neighborhood Descent (VND)

INPUT: $\mathcal{U}_x, MaxSearch, N_{MAX}$;
OUTPUT: $\mathcal{U}_{BEST}$;
 1: $\mathcal{U}_B \leftarrow \mathcal{U}_x, k \leftarrow 1, \mathcal{U}_{BEST} \leftarrow \mathcal{U}_x$;
 2: **repeat**
 3:     $i \leftarrow 0, \mathcal{U}_N \leftarrow \mathcal{U}_B$;
 4:     **repeat**
 5:         $\mathcal{U}_{x'} \leftarrow$ Create-N_k-neighbor($\mathcal{U}_B$);
 6:         **if** $g(\mathcal{U}_{x'}) < g(\mathcal{U}_N)$ **then**
 7:             $\mathcal{U}_N \leftarrow \mathcal{U}_{x'}$;
 8:         **end if**
 9:         $i \leftarrow i + 1$;
10:     **until** $i \geq MaxSearch$
11:     **if** $g(\mathcal{U}_N) < g(\mathcal{U}_B)$ **then**
12:         $\mathcal{U}_B \leftarrow \mathcal{U}_N$;
13:         $k \leftarrow 1$;
14:     **else**
15:         $k \leftarrow k + 1$;
16:     **end if**
17:     **if** $g(\mathcal{U}_B) < g(\mathcal{U}_{BEST})$ **then**
18:         $\mathcal{U}_{BEST} \leftarrow \mathcal{U}_B$;
19:     **end if**
20: **until** $k \geq N_{MAX}$

8.2.3 Path relinking

PR [149] generates new solutions by exploring the trajectories connecting pairs of high-quality solutions. To ensure a proper PR operation, the management of the *elite set* (ES) has to balance between quality and diversity attributes [151].

Greedy PR (GPR)

To perform PR, we make use of the path instantiation set $\mathcal{U}$ so as to easily detect solution differences. Hence, given an initiating ($\mathcal{U}_i$) and a guiding ($\mathcal{U}_g$) solution, we obtain the set of divergences $\Psi_{i,g}$ by identifying those path instantiations in $\mathcal{U}_g$ which differ from those selected in $\mathcal{U}_i$, that is, $\Psi_{i,g} = \mathcal{U}_g \backslash \{\mathcal{U}_g \cap \mathcal{U}_i\}$. In this work, we consider the greedy PR (GPR) approach [164] to build the path from the initiating towards the guiding solution. Therefore, at each single movement we evaluate

the impact that all path instantiations in $\Psi_{i,g}$ have when introduced in $\mathcal{U}_i$. Among them, we select the one minimizing $g(\cdot)$, that is, u^*, and replace the corresponding path instantiation in $\mathcal{U}_i$. Ties in this case are broken randomly. Finally, u^* is removed from set $\Psi_{i,g}$. In this way, we progressively move towards $\mathcal{U}_g$ and until $\Psi_{i,g}$ becomes an empty set (i.e., the guiding solution has been reached). PR is implemented using the *back-and-forward* (PR_{bf}) strategy, which explores the path in both directions [151].

Moreover, the selection of a solution from ES depends on both a distance measure and a selection policy. We consider the approach presented in [151], where the authors propose to select the elite solution with probabilities proportional to their distance to the solution on which to perform PR ($\mathcal{U}_x$). Note that the maximum distance between two solutions $\mathcal{U}_x$ and $\mathcal{U}_y$, that is, $d_{x,y}$, is equal to $|\mathcal{P}^o|$. As to ES management (i.e., which solution can be inserted and which has to be removed in order to keep $|ES|$ constant), it is worth noticing that a solution whose quality is lower than the best stored in ES and higher than the worst in ES, will be added iff its distance to ES (i.e., $d_{x,ES} = \min_{\mathcal{U}_i \in ES}\{d_{x,i}\}$) is larger than a pre-established threshold d_{th}, that is, $d_{x,ES} > d_{th}$, where $d_{x,ES} = \min_{\mathcal{U}_i \in ES}\{d_{x,i}\}$.

8.2.4 GRASP+PR algorithm

The GRASP+PR algorithm design considered in this study is the evolutionary GRASP+PR (EPR) implementation [164]. Specifically, the authors propose three different hybridizations of GRASP+PR, namely static, dynamic and evolutionary GRASP+PR. Among them, the evolutionary variant displayed better performances. For this reason, in order to tackle RPD, we consider the evolutionary scheme. EPR is based on an evolutionary post-processing phase for GRASP+PR algorithms introduced by [151]. The pseudo-code for EPR is shown in Procedure 18. After set ES becomes full, the so-called dynamic GRASP+PR (DPR) algorithm is executed for *LocalItr* iterations (between lines 4 and 12 in Procedure 18). Then, the set of solutions in ES is evolved. This process is repeated for a maximum of *GlobItr* iterations and eventually the best solution in ES is returned as output.

It is worth mentioning that we use a parallel implementation of the algorithm in order to better exploit the capacity of our evaluation platform (see Section 8.4) and to both speed up the algorithm execution time and enhance its performance. A pool of k threads is generated, each of them running in parallel the inner loop of the EPR algorithm, that is, DPR. During *LocalItr* iterations all threads share a common ES which is accessed following a mutual-exclusion policy. Once all threads have finished their task, ES is evolved as dictated by the EPR method.

Procedure 18 Evolutionary GRASP+PR (EPR)

INPUT: $GlobItr$, $LocalItr$, $|ES|$;
OUTPUT: $\mathcal{U}_{BEST}$;
1: $i \leftarrow 0, j \leftarrow 0, ES \leftarrow \emptyset$;
2: Execute multi-start GRASP phase until ES is full;
3: **repeat**
4:    **repeat**
5:       $\mathcal{U}_x \leftarrow$ ConstructionProcedure;
6:       $\mathcal{U}_{x'} \leftarrow$ Local Search starting at $\mathcal{U}_x$;
7:       Randomly select $\mathcal{U}_e$ from ES;
8:       $\mathcal{U}_y \leftarrow \text{PR}_{bf}(\mathcal{U}_{x'}, \mathcal{U}_e)$;
9:       $\mathcal{U}_{y'} \leftarrow$ Local Search starting at $\mathcal{U}_y$;
10:      Try to insert $\mathcal{U}_{y'}$ in ES;
11:      $j \leftarrow j + 1$;
12:    **until** $j \geq LocalItr$
13:    Improvement $\leftarrow 1$;
14:    **while** Improvement **do**
15:       Improvement $\leftarrow 0$;
16:       Apply $\text{PR}_{bf}(\mathcal{U}_x, \mathcal{U}_{x'})$ for every pair $(\mathcal{U}_x, \mathcal{U}_{x'}) \in ES$ and let $\mathcal{U}_y$ be the best solution found;
17:       $\mathcal{U}_{y'} \leftarrow$ Local Search starting at $\mathcal{U}_y$;
18:       **if** $\mathcal{U}_{y'}$ can be inserted in ES **then**
19:          Improvement $\leftarrow 1$;
20:       **end if**
21:    **end while**
22:    $i \leftarrow i + 1$;
23: **until** $i \geq GlobalItr$
24: $\mathcal{U}_{BEST} = \min_{\mathcal{U}_k \in ES}\{g(\mathcal{U}_k)\}$;

8.3   A BRKGA-based RPD heuristic

In BRKGA, a population of p individuals is evolved over a number of generations. Each individual is represented by an array of n genes (called a chromosome), and where each gene can take any value in the real interval [0,1]. Thus, each chromosome encodes a solution of the problem and a fitness value, that is, the value of the objective function. In BRKGA, individuals of the population are divided into the elite set p_e (those individuals with the best fitness values), and a non-elite set. Whilst the majority of new individuals are generated by crossover combining two elements, one elite and another non-elite, elite individuals are copied unchanged from one generation to the next so as to keep track of good solutions. With the very same objective, in the crossover operation an inheritance probability (ρ_e) is defined as the probability that an offspring inherits the gene of its elite parent. Finally, a small number of mutant individuals are introduced to complete a population. A deterministic algorithm, named decoder, transforms any input chromosome into a feasible solution of the optimization problem and computes its fitness value.

The decoder algorithm for our BRKGA was first presented in [18], where our aim was to develop a simple and straightforward decoding algorithm, as fast cost function evaluations are crucial to BRKGAs. For completeness, the decoder pseudo-code is illustrated in Procedure 19. Each chromosome contains as many genes as nodes in the network, and each gene assigns its random value to the corresponding node (see line 2 in Procedure 19). Then, the regeneration option minimizing the sum of such node metric is selected. Hence, a very fast fitness computation can be obtained with this decoding algorithm, even if complex problem instances are considered. However, such simplicity may also hinder the possibility of approaching optimality. This is indeed an important issue to be tackled since the reduction of just one regenerator unit implies significant cost and energy savings in the network, and thus, it cannot be neglected. For this very reason, in the next section, we re-consider the implementation of BRKGA for the RPD problem, and propose an enhanced method including VND and PR as intensification strategies, namely the BVR algorithm.

8.3.1   BRKGA with VND and PR (BVR) algorithm

Although in the literature several works report successful implementations of genetic algorithms working in conjunction with PR (see e.g., [186], [187]), BVR proposes a novel algorithm implementation in which both a local search (VND) and a PR strategy are inserted into the basic BRKGA methodology. The pseudo-code for BVR is illustrated in Procedure 20. The input parameters *gens* and *GlobItr* define the maximum number of generations over which the initial population is evolved. After BRKGA is run for *gens* generations, the chromosomes belonging to the elite set (p_e) in the resulting population $\mathcal{P}_{op}$ are all candidate to be inserted in ES. Then, following the same probabilistic approach as in the GRASP+PR algorithm described in Section 8.2, a solution from ES is selected to perform both PR with $\mathcal{U}_x$ and the subsequent local search intensification. Then, the evolution of

---

Procedure 19 BRKGA decoder

INPUT: $\mathcal{N}$, *chromo*, $\mathcal{P}^o, \mathcal{S}_p \; \forall \; p \in \mathcal{P}^o$;
OUTPUT: $\mathcal{U}_x, g(\mathcal{U}_x)$;
 1: **for all** node $n \in \mathcal{N}$ **do**
 2:    $n.metric \leftarrow chromo.getGene(n)$;
 3: **end for**
 4: $\mathcal{U}_x \leftarrow \emptyset$;
 5: **for all** path $p_i \in \mathcal{P}^o$ **do**
 6:    **for all** option $s_j \in \mathcal{S}_{p_i}$ **do**
 7:       **for all** node $n \in s_j$ **do**
 8:          $c(s_j) \leftarrow c(s_j) + n.metric$;
 9:       **end for**
10:    **end for**
11:    $s^* = \min_{s_j \in \mathcal{S}_{p_i}} \{c(s_j)\}$;
12:    $\mathcal{U}_x \leftarrow \mathcal{U}_x \cup \{s^*\}$;
13: **end for**

---

the current population is resumed for another *gens* generations. Finally, the best solution stored in ES is returned as output.

Again, BVR is implemented following a parallel approach in which k threads run the algorithm separately sharing a common ES. Note that the parallel approach not only allows to reduce time complexity but also generates higher quality elite sets, as ES is concurrently fed by up to k threads. Finally, all parameters needed to set up both the BVR and EPR algorithms will be adjusted in Section 8.4.

Procedure 20 BVR algorithm

INPUT: *gens*, *GlobItr*;
OUTPUT: $\mathcal{U}_{BEST}$;
 1: $i \leftarrow 0$, $ES \leftarrow \emptyset$;
 2: init-BRKGA();
 3: **repeat**
 4:    $\mathcal{P}_{op} \leftarrow$ run-BRKGA(gens);
 5:    Take p_e from $\mathcal{P}_{op}$;
 6:    **for all** chromosome $ch \in p_e$ **do**
 7:       Take $\mathcal{U}_{ch}$ and try to insert it in ES;
 8:    **end for**
 9:    Randomly select $\mathcal{U}_e$ from ES;
10:    $\mathcal{U}_y \leftarrow \text{PR}_{bf}(\mathcal{U}_x, \mathcal{U}_e)$;
11:    $\mathcal{U}_{y'} \leftarrow$ Local Search starting at $\mathcal{U}_y$;
12:    Try to insert $\mathcal{U}_{y'}$ in ES;
13:    $i \leftarrow i + 1$;
14: **until** $i \geq GlobItr$
15: $\mathcal{U}_{BEST} = \min_{\mathcal{U}_k \in ES} \{g(\mathcal{U}_k)\}$;

8.4 Computational experiments

This section describes the computational experiments conducted so as to both evaluate and compare the performance of the MILP-based MP1 (optimal) and R-MP1 models with that of the EPR and BVR hybridized heuristic models proposed in this study. The heuristic methodologies have all been implemented in Java SE 1.6.0_17 using a parallel approach. The experiments have been conducted on an Intel(R) Core(TM) i7 CPU 950 at 3.07GHz with 4GB RAM under Windows 7 Professional Edition (64 bits). We use CPLEX (version 12.1) as the underlying MILP-solver. Note that with this processor we can make use of up to 8 parallel threads, and thus, in all our problems we set $k = 8$.

8.4.1 Problem instances

The performance of the proposed metaheuristic hybridizations as well as that of the MILP models has been compared considering the simulation scenario and the set of optical core transport networks provided in Appendix A.

8.4.2 Sub-wavelength optical network scenario

As to the QoT model, we make use of method proposed in Chapter 2 to obtain the set of paths $\mathcal{P}^o$ that do not comply with the OSNR system specifications. Aiming at performing an exhaustive evaluation of all the methods proposed, we consider a target QoT performance $B^{QoT} = 10^{-3}$ in 4 different network scenarios (see Table 8.1). These scenarios represent load values corresponding to both a medium and a highly loaded network, and thresholds corresponding to realistic values. Whilst an increase in load represents an increase in the number of regenerators required to support each independent burst flow, rising T_{osnr} implies increasing the size of set $\mathcal{P}^o$ as shown in Table 8.2. Further, Table 8.2 reports the total number of regeneration options $\mathcal{C}^*$ (i.e., $\mathcal{C}^* = \bigcup_{p \in \mathcal{P}^o} \mathcal{S}_p$) under both T_{osnr} values, thus allowing for a fair estimation of the different problem complexities. One can observe that in both the Basic and Large networks such amount of options decreases with the increase of T_{osnr}. This can happen as higher thresholds may limit reachability in the resulting transparent graph, and consequently reduce the number of regeneration options. It is also worth mentioning that in the study provided in Chapter 3, the size of set $\mathcal{C}^*$ was limited to a maximum of $|\mathcal{S}_p| = 25$, $\forall p \in \mathcal{P}^o$ so as to reduce complexity. However, such an approach hinders the possibility of approaching optimality, which is our primary objective.

In order to conduct a thorough analysis of all the RPD methods, we first obtain the results for both MP1 and R-MP1 using CPLEX as solver. These results provide us with the best known solutions for each of the scenarios evaluated. Afterwards, a set of preliminary experiments is carried out so as to obtain the best set up for both the EPR and the BVR RPD metaheuristics. Finally, we evaluate their performance in terms of solution quality and study the statistical significance of the

Table 8.1: Network scenarios evaluated

Scenario	*A*	*B*	*C*	*D*
Erlangs	15	25	15	25
$T_{osnr}[dB]$	20	20	21	21

Table 8.2: T_{osnr} impact on $|\mathcal{P}^o|$ and $|\mathcal{C}^*|$

	T_{osnr}	Usa-Can	German	Core	Basic	Large
$|\mathcal{P}^o|$	20dB	421	338	18	349	746
	21dB	657	752	55	462	919
$|\mathcal{C}^*|$	20dB	21414	22987	328	7707	16438
	21dB	23757	38615	596	6459	13616

results obtained through non-parametric tests.

8.4.3 Experimental analysis

MILP methods results

We use CPLEX to solve MP1 and R-MP1 under each network and scenario. Table 8.3 reports the minimum number of regenerators to be deployed as well as the optimality GAP (%) of the solutions provided by CPLEX. Note that the MILP optimality GAP is defined as: $GAP(\%) = \frac{best-lb}{best}$, where *best* refers to the best current solution, and *lb* to the best current lower bound found by the CPLEX branch-and-bound process.

Each execution is stopped when either the running time reaches 24 hours or the tree size grows up to 4GB. One can observe that MP1 is only able to reach optimality in the most simple problem instance, that is, the CORE network. Indeed, optimality gaps of up to 11.9% are observed in the German network. However, we can observe that with R-MP1 such gaps are brought to 0 in all cases except for scenarios *C* and *D* in the German network. As aforementioned, however, this is the consequence of introducing in MP1 two additional heuristic constraints, which definitely reduce the search space, and thus, the complexity of the problem. Whilst R-MP1 works properly in some scenarios (e.g., Basic(*A,C*)), in others, such a cut of the solution space excludes high-quality solutions, thereby hindering the possibility of approaching optimality (Usa-Can(*C,D*), Large (*B*)). The results in Table 8.3 are also in line with the different problem complexities given by the values provided in Tables 8.1 and 8.2. First, we observe that load variations, which have an effect on parameter R (see Eq(3.11)), do not have a significant impact on the results obtained, as there are no notable differences among scenarios *A-B* and *C-D*. Indeed, as shown in Section 3.1.4, it is both the number of regeneration options and the size of set $\mathcal{P}^o$ what has the greater impact on the number of variables and constraints of the problem. However, rising T_{osnr} does have a clear impact on the problem complexities. As shown in Table 8.2, in both the Basic and Large topologies, it represents an

Table 8.3: MP1 and R-MP1 results (total number of regenerators and optimality gaps).

Network	A		B		C		D	
	MP1	R-MP1	MP1	R-MP1	MP1	R-MP1	MP1	R-MP1
Core	44	44	62	62	115	115	166	166
Basic	385	384	572	574	580	579	874	873
Large	658	661	998	1139	942	937	1432	1430
Usa-Can	269	264	402	400	472	493	710	755
German	193	188	277	275	403	393	601	589
Gap (%)								
Core	0	0	0	0	0	0	0	0
Basic	1.8	0	2.1	0	0.5	0	0.8	0
Large	4.1	0	4.1	0	2.2	0	2.7	0
Usa-Can	3.7	0	3.2	0	7.0	0	6.2	0
German	11.9	0	5.42	0	8.9	4.8	7.2	5.1

increase in $\mathcal{P}^o$, but, at the same time, a substantial reduction of $|\mathcal{C}^*|$, thereby lowering the problem complexity. This issue is reflected in the optimality gaps found by MP1 in these two topologies, as they decrease from scenarios (A,B) to (C,D). In the Usa-Can and German networks, as expected, complexities and gaps increase. We note however that in the German network there is a reduction from scenario A to C. We attribute this behavior to the very high gap found in scenario A, which may be due to a specific particularity of this problem instance.

In the rest of our experiments, we exclude the Core network instance as it does not provide any way of differentiating the performance of the different methods.

EPR and BVR parameter tuning

To perform a comprehensive quantitative analysis of the results, we consider the statistics proposed in [164]. Specifically, we provide the number of times ($\#Best$) that each method is able to obtain the overall best solution value ($BestVal$) found among all methods studied. Moreover, we compute the relative percentage deviation (Dev) between the best solution value obtained by a particular method and $BestVal$ for that instance. Finally, we report the statistic called *Score* [170].

In our first preliminary experiment, our focus is on tuning α, that is, the value that controls the access into the RCL in the construction algorithm. To this end, we construct, for each α value and network scenario, 200 solutions with GRC. The results are shown in Table 8.4, where the best global value for each parameter is shown in boldface. The results report $\alpha = 0.5$ as the best method, as it provides the best value for each of the statistic parameters evaluated. Therefore, we use $GRC(\alpha = 0.5)$ in the rest of our experiments.

The next preliminary experiment is devoted to the tuning of the two parameters required to set up the VND local search algorithm, that is, $MaxSearch$ and N_{MAX}. For this experiment, we make use of the so-called BRKGA tuning as proposed in [169], where authors use a BRKGA algorithm so

Table 8.4: α performance evaluation in all networks and scenarios.

α	0.1	0.2	0.3	0.4	0.5	0.6	0.7	0.8	0.9
$\#Best$	2	0	3	1	**5**	4	1	2	3
$Score$	72	68	58	70	**32**	57	66	60	38
$Dev(\%)$	1.68	1.08	1.03	1.31	**0.43**	1.19	1.41	1.19	0.89

Table 8.5: Determination of an adequate size for set ES using the DPR algorithm.

$|ES|$	4	6	8
$\#Best$	9	**17**	4
$Score$	13	**2**	22
$Dev(\%)$	1.77	**0.42**	2.86

as to find adequate parameter values for a GRASP+PR heuristic. In this case, however, and due to the complexity of the instances considered, we only tune the VND parameters. Then, we perform a more exhaustive evaluation of the key PR parameters, namely the size of set ES and d_{th}, which manages the access to ES.

We test the following values for each parameter: (a) $N_{MAX} = \{5,8,12,15\}$; (b) $MaxSearch = \{15,25,40,50,70\}$. Therefore, a chromosome is defined by 2 parameters. BRKGA in this experiment makes use of: $p = 20$, $p_e = 0.2$, $p_m = 0.2$, $\rho_e = 0.7$. The fitness for each chromosome corresponds to the average obtained over 5 independent executions of GRC plus VND, each lasting for 56 iterations (7 iterations per thread). The automatic tuning sets parameters $N_{MAX} = 50$ and $MaxSearch = 8$ (i.e., the values with higher frequencies of occurrence).

Next, we conduct two additional preliminary experiments in order to set up the parameters corresponding to the PR procedure, namely the size of set ES, and the minimum distance d_{th}. First, we evaluate 4, 6, and 8 as candidate sizes for set ES. We note here that the size of set ES represents a trade-off between quality and diversity that needs to be evaluated. To this end, we run 20 independent executions of the DPR algorithm for all network scenarios, each lasting for 100 iterations. According to the statistics reported in Table 8.5, $|ES| = 6$ represents the best trade-off to perform PR, and hence, we consider this value for the rest of our experiments requiring the PR intensification procedure.

To analyze the impact of d_{th}, and given the fact that the maximum distance between two solutions is equal to $|\mathcal{P}^o|$, we compare the performance of three different percentages of this value as possible distance thresholds, that is, 5%, 10%, and 15%. We perform 20 independent executions of the algorithm each lasting for 200 iterations in all network scenarios. According to the statistics reported in Table 8.6, the best value is $d_{th} = 10\%$, and hence, we select it for the rest of our experiments. Note that both the VND and the PR parameters found will be used by both EPR and BVR algorithms.

Finally, to specify the parameters in BVR that deal with the evolution of the population, we consider the values that after some preliminary experimentation we successfully tested in [18]. These

Table 8.6: Study of d_{th} using the DPR algorithm.

$\mathbf{d_{th}}$	$\frac{5}{100}\mathcal{P}^o$	$\frac{10}{100}\mathcal{P}^o$	$\frac{15}{100}\mathcal{P}^o$
$\#Best$	8	**12**	6
$Score$	14	**6**	16
$Dev(\%)$	1.8	**0.52**	2.1

values are the ones used in Section 8.4.3, though in this case the population size is set to $p = |\mathcal{N}|$ and the chromosome structure as described in Section 8.3. In the next Section, we compare the performance of the metaheuristic hybridizations for the RPD problem proposed in this chapter with that of the MILP-based MP1 and R-MP1 models.

RPD methods performance comparison

In this final experiment, we compare the performances of all the RPD resolution methods proposed throughout this chapter. Specifically, the following five algorithms configurations are executed (for each method 20 independent executions are run each with 8 threads evolving in parallel):

- *BRKGA*: Run for a minimum of 1000 generations and stopped after a maximum of 200 generations without improvement.

- *BVR*: Run for 500 generations. Three different configurations for this method are tested, namely BVR(1), BVR(3) and BVR(5). The number in brackets corresponds to *GlobItr*, that is, the number of times that the evolution process is stopped so that both PR and VND can be executed. Accordingly, for each method the value of *gens* corresponds to $\lceil \frac{500}{GlobItr} \rceil$.

- *GRASP*: The GRASP multi-start phase (i.e., GRC followed by VND). Each thread performs 36 multi-start iterations.

- *DPR*: The dynamic variant of GRASP+PR, each thread is run with *LocalItr* set to 36 iterations. Note that in this case the evolutionary stage is not executed.

- *EPR*: In this algorithm, each thread is run with the parameters *LocalItr* and *GlobItr* set to 12 and 3 respectively.

The results provided in Table 8.7, report BVR(3) and BVR(5) as the best methods, thereby showing the benefits achieved by incorporating both VND and PR into the basic BRKGA procedure. Although one can observe that further iterations (BVR(5)) slightly increase $\#Best$ with respect to BVR(3), it does so at the cost of substantially increasing computation times. Further, in BVR(5), the remaining two parameters do not experience any improvement. Hence, considering that our primary objective is to approach optimality, and that in this respect both BVR(3) and BVR(5) provide the same performance, this experimental analysis reports BVR(3) as the most efficient RPD

Table 8.7: Statistic results for all RPD methods

Method	BRKGA	BVR(1)	BVR(3)	BVR(5)	GRASP	DPR	EPR	MP1	R-MP1
#*Best*	40	162	**168**	175	0	0	0	0	140
Score	62	23	**1**	1	142	115	90	102	58
Dev(%)	0.35	0.1	**0.02**	0.02	5.46	2.08	1.5	1.23	2.14
Time(s)	100.6	75.9	**88.1**	149.9	1022.3	4008.8	5138.1	24h	8236

algorithm among the ones evaluated in this chapter. Results obtained by all three GRASP variants also show the impact of introducing PR and in particular of the evolutionary stage. As expected, EPR is able to provide better performance, though requiring more computation time. For the sake of a fair comparison, if a MILP method obtains a *BestVal* for a particular instance, its counter of #*Best* is incremented by 20 units.

Next, in order to be able to numerically compare the heuristic results with those of the MILP methods, in Table 8.8, we provide the final results for the best methods in terms of the number of regenerators. In this case, the numbers shown in boldface represent the problem instances in which that particular method has not been able to at least equal the result obtained by the best of MP1 and R-MP1 for that particular instance. One can note that BVR(3) improves upon the MILP models in all cases except for the German(B) scenario, and that even EPR reports best values in some instances compared to the MILP methods. In fact, considering all the problem instances, BVR(3) using much less computation time, provides a reduction of 272 regenerators when compared with R-MP1, 106 with MP1, and of 60 if compared with the best of both MILP methods. These results also allow us to analyze the effect of the problem complexity on the performance of the best BRKGA-based algorithm (BVR(3)), and the best GRASP-based method (EPR). Using the values reported in Table 8.8, we compute the difference between the results of both heuristics (i.e., regs(EPR)-regs(BVR(3))). Whilst the total difference in the number of regenerators for scenarios (A,B) is 22, it increases up to 94 for scenarios (C,D). Further, we confirm that the difference between both algorithms does not change significantly under a load variation, as the aggregated difference is 56 and 60 respectively, for scenarios (A,C) and (B,D).

Hence, considering only solution quality, these results report that BRKGA-based heuristics are more appropriated for the RPD problem because of both their simple decoding algorithm and ability to obtain high-quality solutions in short computational times. Further, we can notice that despite the benefits generated by both VND and PR in GRASP are noticeable, they are not able to match the fast genetic evolution. The size of both $\mathcal{P}^o$ and $\mathcal{C}^*$ make it necessary to introduce memory into the process, and in this aspect, BVR clearly outperforms EPR thanks to the joint operation of the genetic evolution and PR.

Table 8.8: RPD methods results (number of regenerators deployed).

		BRKGA	BVR(1)	BVR(3)	EPR	MP1	R-MP1
	A	384	384	383	**386**	385	384
Basic	B	571	571	571	571	572	574
	C	**582**	579	579	**582**	580	579
	D	**874**	873	873	**875**	874	873
	A	655	653	652	657	658	661
Large	B	985	984	983	986	998	1139
	C	937	935	934	**940**	942	937
	D	1419	1418	1417	1423	1432	1430
	A	**265**	264	264	**265**	269	264
Usa-can	B	400	400	400	**401**	402	400
	C	465	463	462	471	472	493
	D	701	700	700	703	710	755
	A	**189**	188	188	**191**	193	188
German	B	**277**	**276**	**276**	**282**	277	275
	C	**396**	**394**	393	**419**	403	393
	D	589	587	587	**626**	601	589

8.4.4 Statistical analysis of the results

In this section, we aim at confirming the results obtained in the last section. To this end, we conduct tests to analyze whether the performance differences found among the RPD algorithms are statistically significant.

[188] tackled the issue of statistical tests for comparison of algorithms on multiple problem instances. In this thesis, we use the non-parametric Friedman Test [189], and the Nemenyi Post hoc test [190] to evaluate our $k = 9$ algorithms under the $N = 16$ different problem instances as reported in Table 8.1.

The Friedman test ranks the algorithms for each problem instance separately. By comparing the average ranks of the algorithms, the statistical significance of differences between the methods is examined. In this work, we use the enhanced version of the Friedman test developed by [191], which uses the test statistic $\mathcal{F}_F$ based on the F-distribution with degrees of freedom $((k-1),(k-1)(N-1))$. If the equivalence of the algorithms is rejected, the Nemenyi post hoc test is applied in order to perform pairwise comparisons. The average ranks are reported in Table 8.9 for each of the 9 different RPD methods. Given the ranking obtained, BVR(3) and BVR(5) represent the best performing algorithms closely followed by BVR(1). Then, we find BRKGA and R-MP1 providing quite similar performance. The next group is formed by EPR and MP1, and finally the DPR and GRASP algorithms reporting the worst results. The next step is devoted to analyzing the statistical significance of differences between these ranks. In our scenario, the $\mathcal{F}_F$ test statistic is distributed according to the F-distribution with (8,120) degrees of freedom. In this case, $\mathcal{F}_F = 44.543$, a value which is fairly greater than the critical value 2.66 obtained with the F-distribution and a

Table 8.9: Rank results and pairwise differences of the RPD algorithms. ($CD = 3.76$)

Method	BVR(3)	BVR(5)	BVR(1)	BRKGA	R-MP1	EPR	MP1	DPR	GRASP
Avg. Rank	(2.125)	(2.125)	(2.93)	(4.53)	(4.781)	(5.937)	(6.5)	(7.25)	(8.875)
BVR(3)	-	0	0.82	2.41	2.66	3.81	4.38	5.13	6.75
BVR(5)	-	-	0.82	2.41	2.66	3.81	4.38	5.13	6.75
BVR(1)	-	-	-	1.59	1.84	3	3.56	4.31	5.94
BRKGA	-	-	-	-	0.25	1.4	1.97	2.72	4.34
R-MP1	-	-	-	-	-	1.15	1.72	2.47	4.09
EPR	-	-	-	-	-	-	-	1.31	2.93
MP1	-	-	-	-	-	-	-	0.75	2.38
DPR	-	-	-	-	-	-	-	-	1.63
GRASP	-	-	-	-	-	-	-	-	-

significance level of the test $\alpha = 0.01$. Taking into account this test, a significant difference between the performance of the different RPD methods exists, and thus, the equivalence can be rejected. Hence, we can proceed with the Nemenyi Post hoc test to determine differences between the average ranks for every pair of algorithms. To this end, we compute the critical difference (CD) (see [188]) between algorithm ranks. For a significance value $\alpha = 0.01$, we have that $CD = 3.76$. Given the results provided in Table 8.9, we can clearly identify two different groups. A first group consisting of BRKGA-based methods plus R-MP1, and a second one with the remaining algorithms. Note that algorithms within a group differ from best to worst in less than CD. Hence, the Friedman and Nemenyi tests confirm the results obtained in the experimental analysis and reinforce the conclusion that BRKGA-based algorithms are effective metaheuristics for the RPD problem.

8.5 Summary

The purpose of this chapter has been the development of efficient metaheuristic methods to solve the RPD problem found in T-SWS networks. This problem deals with the minimization of the number of regenerators required to mitigate the impact of the PLIs in the network. Due to both their high cost and power-consumption, this problem is of great interest for network operators which strive for cost-effective, energy-efficient architectures. We have developed two different hybridized metaheuristics based on both GRASP and BRKGA algorithms. Moreover, we have introduced VND and PR into their basic procedures, and finally implemented the EPR and BVR algorithms to solve the RPD problem. We have compared their results with those of both an optimal and a heuristic MILP formulation using CPLEX. Among them, BVR reported the best overall results in all the scenarios evaluated except for one, thereby standing as an efficient and competitive algorithm to be taken into consideration for the planning and design of future sub-wavelength OTNs. Further, we also observed that genetic methods such as BVR are particularly recommended for the RPD problem because of their efficient decoding algorithm and fast genetic evolution.

Part III

Conclusions

Chapter 9

Conclusions and future works

Part I

This first part of the thesis has dealt with the modeling, optimization and performance analysis of next-generation cross-layer OTNs based on SWS. To this end, this thesis has taken into account the impact that L0 phenomena (i.e., PLIs) have on the optical end-to-end signal transmission (i.e., L2-L0 cross-layer optimization). A novel transmission mode, the QS, has been proposed for OBS networks. QS has been shown to be able to provide substantial improvements in terms of the BLP (wrt. the asynchronous transmission), while avoiding the hardware complexity of the pure synchronous approach. Furthermore, we have modeled a novel translucent node architecture for T-SWS networks by means of commercially available components and sub-systems. Through extensive simulation experiments, we have proved that the T-SWS is able to perfectly mitigate the adverse effect of PLIs, and therefore, that it represents a compelling model for future OTNs. Finally, we introduced real-time OPM monitoring in the T-SWS network by means of the CLONE networking model. We showed that CLONE based networks, thanks to their dynamic adaptation to time-varying PLIs, provide substantial improvements in terms of both energy efficiency and packet loss performance.

Future research within T-SWS networks should involve the development of more accurate analytical models to account for the impact of non-linear PLIs [129], as future higher bit-rates and more closely spaced channels will dramatically increase their impact. Also, the modeling of amplifier dynamics contributing to channel power excursions is a subject certainly deserving further research [192], [193].

Part II

In this part, we have presented a set of successful applications of OR methodologies in the planning/dimensioning of cross-layer OTNs. GRASP and BRKGA meta-heuristics are developed to solve complex multi-layer optimization problems such as survivability in IP/MPLS-over-WSON, planning of IP/MPLS-over-Flexgrid and RPD in T-SWS networks. By proving to be efficient in minimizing network CAPEX, whilst, at the same time, optimizing resources usage, these methodologies represent efficient and competitive tools to be taken into consideration in future research dealing with the planning/dimensioning of multi-layer Internet networks.

Appendix A

Simulation Scenario

The simulation results for Part I of this thesis as well as Chapter 8 have all been obtained by considering, if not specifically given differently, the following network scenario.

In our studies, we have used a set of backbone network topologies (see Fig. A.1): a set of Pan-European [194] networks known as: Large (a), Basic (b) and Core (c) with 37, 28 and 16 nodes and 57, 41 and 23 links respectively; the NSFNET (a US network) [195] (d), with 14 nodes and 21 links; the JANOS-US-CA [196] (e), a reference network that interconnects cities in the USA and Canada with 39 nodes and 61 links, and a German backbone topology known as GERMAN50 [196] (f), with 50 nodes and 88 links. In addition, Table A.1 summarizes, for all the networks, some interesting parameters regarding both the number of nodes (e.g., network diameter) and the distance of their respective optical end-to-end paths. In the figure caption, the average node degree for the networks evaluated in Chapter 4 are reported.

Network links are bidirectional and dimensioned with the same number of wavelengths $M = 32$. The transmission bitrate of both transmitters at edge nodes and regenerators at core nodes is set to $10Gb/s$.

We assume that the traffic is uniformly distributed between nodes and that each edge node offers

Network	Max. nodes	Avg. nodes	Max. length	Avg. length
NSFNET	6	3.22	6320	2713.79
Usa-Can	12	5.36	3297	1360.55
German	13	5.5	1037.6	421.1
Core	7	3.7	2912	1238.4
Basic	10	4.75	6505	2094.4
Large	12	5.1	7824	2410.1

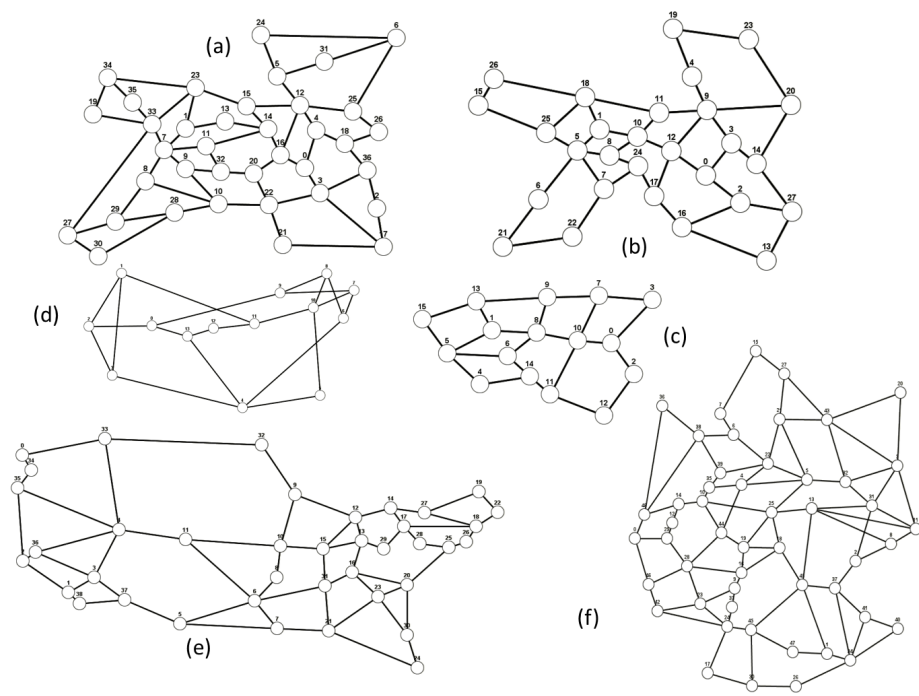Table A.1: Paths characteristics: number of nodes traversed and distance (km)

Figure A.1: a) Large (37 nodes, 3.08 avg. node degree), b) Basic (28 nodes, 2.92 avg. node degree), c) Core (16 nodes, 2.875 avg. node degree), d) NSFNET (14 nodes), e) Usa-Can (39 nodes, 3.128 avg. node degree), f) German (50 nodes).

the same amount of traffic to the network; this offered traffic is normalized to the transmission bit-rate and expressed in Erlangs. In our context, an Erlang corresponds to the amount of traffic that occupies an entire wavelength (e.g., 20 Erlangs mean that each edge nodes generates $200Gb/s$).

Packets are generated according to a Poisson arrival process and have exponentially distributed lengths. The mean duration of a burst $(1/\mu)$ is $100\mu s$ ($1Mb$). Note that due to both the Poisson assumption and the fact that we neglect both the switching and processing times of packets, the packet size does not have any impact on the results obtained [51]. In obtaining the simulation results, we have estimated 99% confidence intervals. However, since the confidence intervals found are very narrow, we do not plot them in order to improve readability.

Throughout this thesis we consider an OSNR_{min} threshold equal to 19dB. This value is commonly used as OSNR_{th} for the experimental assessment of translucent WSONs with similar network link configurations (i.e., 32 wavelengths and 10Gb/s) as well as NRZ (non-return to zero) modulation format (see e.g., [77], [82]). Note that these 19dB already account for the OSNR penalties due to the maximum acceptable PMD, residual CD, and nonlinearities degradation found in WSONs. In this thesis, due to the higher impact of both non-linear impairments and amplifier dynamics in SWS networks, we add on top of the $\text{OSNR}_{min} = 19$ dB, penalties of 1 and 2 dB to analyze the performance of our RRPD algorithms.

All simulations have been conducted on the sub-wavelength switching JAVOBS [197] network simulator on an Intel Core 2 Quad $2.67GHz$ with $4GB$ RAM. We use CPLEX (version 12.1) [98] as underlying MILP-solver for all the MILP formulations presented throughout this thesis.

Appendix B

Thesis scientific production

B.1   Journal articles

- **O. Pedrola**, D. Careglio, M. Klinkowski, L. Velasco, K. Bergman and J. Solé-Pareta, "Meta-heuristic Hybridizations for the Regenerator Placement and Dimensioning problem in sub-wavelength switching optical networks," *Elsevier European Journal of Operational Research,* in press. (DOI:10.1016/j.ejor.2012.08.011).

- **O. Pedrola**, A. Castro, L. Velasco, M. Ruiz, J. Fernández-Palacios and D. Careglio, "CAPEX study for IP/MPLS over FlexGrid optical network, "*IEEE/OSA Journal of Optical Communications and Networking,* vol. 4, no. 9, Sep. 2012.

- **O. Pedrola**, M. Ruiz, L. Velasco, D. Careglio, O. González de Dios, J. Comellas, "A GRASP with path-relinking heuristic for the survivable IP/MPLS-over-WSON multi-layer network optimization problem, "*Elsevier Journal of Computers & Operations Research,* Special Issue on GRASP and PR, in press. (DOI:10.1016/j.cor.2011.10.026).

- **O. Pedrola**, D. Careglio, M. Klinkowski and J. Solé-Pareta, "Regenerator Placement strategies for Translucent OBS networks," *IEEE/OSA Journal of Lightwave Technology,* vol. 29, no. 22, pp. 3408-3420, Nov. 2011.

- **O. Pedrola**, D. Careglio, M. Klinkowski and J. Solé-Pareta, "Offline routing and regenerator placement and dimensioning for translucent OBS networks," *IEEE/OSA Journal of Optical Communications and Networking,* vol. 3, no. 9, pp. 651-666, Sep. 2011.

- **O. Pedrola**, S. Rumley, M. Klinkowski, D. Careglio, C. Gaumier, J. Solé-Pareta, "Performance overview of the Quasi-Synchronous operation mode in OBS networks," *Elsevier Journal of Optical Switching and Networking,* vol. 8 , no. 1, pp. 32-45, Jan. 2011.

- **O. Pedrola**, S. Rumley, M. Klinkowski, D. Careglio, C. Gaumier, J. Solé-Pareta, "JAVOBS: a flexible simulator for OBS network architectures," *Academy publisher Journal of Networks,* vol. 5, no. 2, pp. 256-264, Feb. 2010.

B.2 Conference papers

- **O. Pedrola**, B. G. Bathula, M. S. Wang, A. Ahsan, D. Careglio, and K. Bergman, "Cross-Layer Enabled Translucent Optical Network with Real-time Impairment Awareness," *in Proceedings of 2012 IEEE Global Communication Conference (Globecom 2012),* Anaheim, CA, US, Dec. 2012.

- **O. Pedrola**, L. Velasco, A. Castro, D. Careglio, J. P. Fernández-Palacios, and G. Junyent, "CAPEX study for grid dependent multi-layer IP/MPLS-over-EON using relative BV-WSS costs," *in Proceedings of IEEE/OSA Optical Fiber Communication Conference and Exposition, and the National Fiber Optic Engineers Conference (OFC/NFOEC),* Los Angeles, USA, March 2012, Paper ID: NTu2J.7

- **O. Pedrola**, D. Careglio, M. Klinkowski, and J. Solé-Pareta, "Translucent OBS network architectures with Dedicated and Shared wavelength resources," *in Proceedings of the 16th European Conference on Networks and Optical Communications (NOC2011),* Newcastle upon Tyne, UK, July 20-22, 2011.

- **O. Pedrola**, D. Careglio, M. Klinkowski, and J. Solé-Pareta, "RRPD strategies for a T-OBS network architecture," *in Proceedings of IEEE International Conference on High Performance Switching and Routing (HPSR 2011),* Cartagena, Spain, July 4-6, 2011.

- **O. Pedrola**, D. Careglio, M. Klinkowski, and J. Solé-Pareta, "Modelling and performance evaluation of a translucent OBS network architecture," *in Proceedings of 2010 IEEE Global Communication Conference (Globecom 2010),* Miami, Florida, USA, December 6-10, 2010.

- **O. Pedrola**, D. Careglio, M. Klinkowski and J. Solé-Pareta, "On the physical impairments constraint in OBS networks," *in Proceedings of 12th IEEE International Conference on Transparent Optical Networks (ICTON2010),* Munich, Germany, June-July 2010.

- **O. Pedrola**, S. Rumley, D. Careglio, M. Klinkowski, P. Pedroso, J. Solé-Pareta, C. Gaumier, "A performance survey on deflection routing techniques for OBS networks," *in Proceedings of 11th IEEE International Conference on Transparent Optical Networks (ICTON2009),* Island of Sao Miguel, Azores, Portugal, June 28-July 2, 2009.

- **O. Pedrola**, S. Rumley, M. Klinkowski, D. Careglio, C. Gaumier, J. Solé-Pareta, "Flexible Simulators for OBS Network Architectures," *in Proceedings of 10th IEEE International Conference on Transparent Optical Networks (ICTON2008),* Athens, Greece, June 22-26, 2008.

B.3 Submissions under review

- **O. Pedrola**, D. Careglio, M. Klinkowski, Josep Solé-Pareta and Keren Bergman, "Cost Feasibility Analysis of Translucent Optical Networks with Shared Wavelength Converters, "under review in *IEEE/OSA Journal of Optical Communications and Networking,* July, 2012.

- **O. Pedrola**, A. Ahsan, M. S. Wang, B. G. Bathula, D. Careglio, and K. Bergman, "Simulation and Experimental Validation of a Cross-Layer Enabled Optical Transport Network with Real-time OSNR monitoring,"will be submitted by September 2012 to *IEEE/OSA Journal of Lightwave Technology.*

B.4 Other publications

- L. Velasco, M. Ruiz, A. Castro, **O. Pedrola**, M. Klinkowski, D. Careglio, and J. Comellas, "On the Performance of Flexgrid-based Optical Networks,"*in Proceedings of the 14th IEEE International Conference on Transparent Optical Networks (ICTON2012),* Coventry, UK, July 2012.

- M. Ruiz, **O. Pedrola**, L. Velasco, D. Careglio, J. Fernández-Palacios, G. Junyent, "Survivable IP/MPLS-over-WSON multi-layer network optimization,"*IEEE/OSA Journal of Optical Communications and Networking,* vol. 3, no. 8, pp. 629-640, Aug. 2011.

- S. Rumley, **O. Pedrola**, C. Gaumier, J. Solé-Pareta, "Feedback Based Load Balancing, Deflection Routing and Admission Control in OBS Networks,"*Academy publisher Journal of Networks,* vol. 5, no. 11, pp. 1290-1299, Nov. 2010.

- P. Pedroso, **O. Pedrola**, D. Papadimitriou, D. Careglio, M. Klinkowski, "AnyTraffic routing algorithm for label-based forwarding,"*in Proceedings of 2009 IEEE Global Communication Conference (Globecom 2009),* Honolulu, Hawaii, USA, November 30-December 4, 2009.

- S. Rumley, **O. Pedrola**, M. Klinkowski, P. Pedroso, C. Gaumier, D. Careglio, J. Solé-Pareta, "Adaptive burst admission and forwarding in OBS networks,"*in Proceedings of 11th IEEE International Conference on Transparent Optical Networks (ICTON2009),* Island of Sao Miguel, Azores, Portugal, June 28-July 2 , 2009.

Acronyms

ASE Amplified Spontaneous Emission

BAS Broadcast and Select

BCP Burst Control Packet

BLP Burst Loss Probability

BRKGA Biased Random-Key Genetic Algorithm

CAPEX Capital Expenditure

CD Chromatic Dispersion

CLONE Cross-Layer Optical Network Element

C-OBS Conventional Optical Burst Switching

DWDM Dense Wavelength Division Multiplexing

EDFA Erbium-Doped Fiber Amplifier

E-OBS Offset-time Emulated Optical Burst Switching

GRASP Greedy Randomized Adaptive Search Procedure

ILP Integer Linear Programming

IP Internet Protocol

LSP Label Switched Path

MILP Mixed Integer Linear Programming

MPLS Multi-Protocol Lambda Switching

OBS Optical Burst Switching

ODS Optical Data-unit Switching

O/E/O Optical/Electrical/Optical

OFS Optical Flow Switching

OPEX Operational Expenditure

OPM Optical Performance Monitoring

OPS Optical Packet Switching

OSNR Optical Signal to Noise Ratio

OTN Optical Transport Network

OXC Optical Cross-Connect

PLI Physical Layer Impairment

PLP Packet Loss Probability

PMD Polarization Mode Dispersion

PR Path Relinking

QoT Quality of Transmission

QS Quasi-Synchronous

RP Regenerator Placement

RRP Routing and Regenerator Placement

RRPD Routing and Regenerator Placement and Dimensioning

RWA Routing and Wavelength Assignment

SDH Synchronous Digital Hierarchy

SOA Semiconductor Optical Amplifier

SWS Sub-Wavelength Switching

TAS Tune and Select

TCO Total Cost of Ownership

VND Variable Neighborhood Descent

WDM Wavelength Division Multiplexing

WSON Wavelength Switched Optical Network

WXC Wavelength Cross-Connect

Bibliography

[1] C. Lange, "Energy-related aspects in backbone networks," in *Optical Communication (ECOC), 2009 35th European Conference and Exhibition on*, sept. 2009.

[2] Y. Lee, G. Bernstein, and W. Imajuku. (2011) Framework for GMPLS and path computation element (PCE) control of wavelength switched optical networks (WSONs). IETF draft. [Online]. Available: http://www.hjp.at/doc/rfc/rfc6163.html

[3] S. J. Ben Yoo, "Optical packet and burst switching technologies for the future photonic internet," *Lightwave Technology, IEEE/OSA Journal of*, vol. 24, no. 12, pp. 4468–92, 2006.

[4] STRONGEST. (2012) (Scalable, Tunable and Resilient Optical Networks Guaranteeing Extremely-high Speed Transport). [Online]. Available: http://www.ict-strongest.eu/

[5] ITU-T. (2012) G.694.1, spectral grids for WDM applications: DWDM frequency grid. standard. [Online]. Available: http://www.itu.int/rec/T-REC-G.694.1-200206-I/en

[6] M. Jinno, H. Takara, B. Kozicki, Y. Tsukishima, Y. Sone, and S. Matsuoka, "Spectrum-efficient and scalable elastic optical path network: architecture, benefits, and enabling technologies," *Communications Magazine, IEEE*, vol. 47, no. 11, pp. 66–73, 2009.

[7] M. Jinno, B. Kozicki, H. Takara, A. Watanabe, Y. Sone, T. Tanaka, and A. Hirano, "Distance-adaptive spectrum resource allocation in spectrum-sliced elastic optical path network," *Communications Magazine, IEEE*, vol. 48, no. 8, pp. 138–145, 2010.

[8] O. González de Dios, G. Bernini, G. Zervas, and M. Basham. (2011) Framework for gmpls and path computation support of sub-wavelength switching optical networks. IETF draft. [Online]. Available: http://tools.ietf.org/html/draft-gonzalezdedios-subwavelength-framework-00

[9] J. Gripp, J. E. Simsarian, J. D. LeGrange, P. G. Bernasconi, and D. T. Neilson, "Architectures, components, and subsystems for future optical packet switches," *Selected Topics in Quantum Electronics, IEEE Journal of*, vol. 16, no. 5, pp. 1394–1404, 2012.

[10] G. Zervas et al., "Multi-granular optical cross-connect: Design, analysis and demonstration," *Optical Communications and Networking, IEEE/OSA Journal of*, vol. 1, no. 1, pp. 69–84, 2009.

[11] C. P. Lai, A. Shacham, and K. Bergman, "Demonstration of asynchronous operation of a multiwavelength optical packet-switched fabric," *Photonics Technology Letters, IEEE*, vol. 22, no. 16, pp. 1223–25, Aug. 2010.

[12] D. Kilper, K. Guan, G. Atkinson, J. Llorca, and Y. Pan, "Modelling network energy reductions through dynamic wavelength functionality," in *Transparent Optical Networks (ICTON 2011), 13th Anniversary International Conference on*, june 2011.

[13] CIAN. (2012) (center for integrated access networks). [Online]. Available: http://cian-erc.org

[14] O. Pedrola, S. Rumley, D. Careglio, M. Klinkowski, P. Pedroso, C. Gaumier, and J. Solé-Pareta, "A performance survey on deflection routing techniques for obs networks," in *Transparent Optical Networks (ICTON 2009), 11th Anniversary International Conference on*, Jun. 2009.

[15] O. Pedrola, S. Rumley, M. Klinkowski, D. Careglio, C. Gaumier, and J. Solé-Pareta, *Optical Switching and Networking, Elsevier Journal of*, vol. 8, no. 1, pp. 32–45, nov. 2011.

[16] O. Pedrola, D. Careglio, M. Klinkowski, and J. Solé-Pareta, "Online physical-layer impairment-aware routing with quality of transmission constraints in translucent optical networks," in *Transparent Optical Networks (ICTON 2010), 12th Anniversary International Conference on*, jul 2011, pp. 1–4.

[17] ——, "Modelling and performance evaluation of a translucent OBS network architecture," in *Global Communications (GLOBECOM 2010), IEEE International Conference on*, dec. 2010, pp. 1–6.

[18] ——, "Offline routing and regenerator placement and dimensioning for translucent OBS networks," *Optical Communications and Networking, IEEE/OSA Journal of*, vol. 3, no. 9, pp. 651 –666, september 2011.

[19] ——, "RRPD strategies for a T-OBS network architecture," in *High Performance Switching and Routing (HPSR 2011), IEEE Conference on*, july 2011, pp. 89 –94.

[20] ——, "Regenerator placement strategies for translucent OBS networks," *Lightwave Technology, IEEE/OSA Journal of*, vol. 29, no. 22, pp. 3408 –3420, nov. 2011.

[21] ——, "Translucent OBS network architectures with Dedicated and Shared wavelength resources," in *Networks and Optical Communications (NOC), 2011 16th European Conference on*, Jul. 2011.

[22] O. Pedrola, D. Careglio, M. Klinkowski, J. Solé-Pareta, and K. Bergman, "Cost feasibility analysis of translucent optical networks with shared wavelength converters," *Optical Communications and Networking, IEEE/OSA Journal of*, submitted 2012.

[23] O. Pedrola, B. G. Bathula, M. S. Wang, A. Ahsan, D. Careglio, and K. Bergman, "Cross-layer enabled translucent optical network with real-time impairment awareness," in *Global Communications (GLOBECOM 2012), IEEE International Conference on*, Dec. 2012, pp. 1–7.

[24] O. Pedrola, A. Ahsan, M. S. Wang, B. G. Bathula, D. Careglio, and K. Bergman, "Simulation and experimental validation of a cross-layer enabled sub-wavelength switching optical network with real-time osnr monitoring," *Lightwave Technology, IEEE/OSA Journal of*, to be submitted by the end of June 2012.

[25] O. Pedrola, M. Ruiz, L. Velasco, D. Careglio, O. González de Dios, and J. Comellas, "A GRASP with path-relinking heuristic for the survivable IP/MPLS-over-WSON multi-layer network optimization problem," *Computers & Operations Research, Elsevier Journal of*. [Online]. Available: http://dx.doi.org/10.1016/j.cor.2011.10.026

[26] O. Pedrola, A. Castro, L. Velasco, D. Careglio, J. P. Fernández-Palacios, and G. Junyent, "CAPEX study for grid dependent multi-layer IP/MPLS-over-EON using relative BV-WSS costs," in *Optical Fiber Communication (OFC), collocated National Fiber Optic Engineers Conference, 2012 Conference on (OFC/NFOEC)*, Mar. 2012, p. NTu2J.7.

[27] O. Pedrola, A. Castro, L. Velasco, M. Ruiz, J. Fernandez-Palacios, and D. Careglio, "CAPEX study for multilayer IP/MPLS-over-Flexgrid optical network," *Optical Communications and Networking, IEEE/OSA Journal of*, under second review, 2012.

[28] O. Pedrola, D. Careglio, M. Klinkowski, L. Velasco, K. Bergman, and J. Solé-Pareta, "Meta-heuristic hybridizations for the regenerator placement and dimensioning problem in sub-wavelength switching optical networks," *Operational Research, Elsevier European Journal of*, under second review, 2012.

[29] P. Gambini et al., "Transparent optical packet switching: network architecture and demonstrators in the keops project," *Selected Areas in Communications, IEEE Journal on*, vol. 16, no. 7, pp. 1245 –1259, sep. 1998.

[30] G. Ellinas, J.-F. Labourdette, S. Chaudhuri, J. Walker, E. Goldstein, K. Bala, S. Chaudhuri, and L. Lin, "Network control and management challenges in opaque networks utilizing transparent optical switches," *Communications Magazine, IEEE*, vol. 42, no. 2, pp. 16 –24, feb. 2004.

[31] B. Ramamurthy, H. Feng, D. Datta, J. Heritage, and B. Mukherjee, "Transparent vs. opaque vs. translucent wavelength-routed optical networks," in *Optical Fiber Communication Conference, 1999, and the International Conference on Integrated Optics and Optical Fiber Communication. OFC/IOOC '99. Technical Digest*, vol. 1, 1999, pp. 59 –61.

[32] J. Solé-Pareta, S. Subramaniam, D. Careglio, and S. Spadaro, "Cross-layer approaches for planning and operating impairment-aware optical networks," *Proceedings of the IEEE, Special Issue on The Evolution of Optical Networks*, vol. 100, no. 5, pp. 1118–1129, May 2012.

[33] G. Shen and R. S. Tucker, "Translucent optical networks: the way forward [topics in optical communications]," *Communications Magazine, IEEE*, vol. 45, no. 2, pp. 48 –54, feb. 2007.

[34] Y. Lee, G. Bernstein, D. Li, and G. Martinelli. (2010) A framework for the control of wavelength switched optical networks (WSON) with impairments. IETF draft. [Online]. Available: http://tools.ietf.org/html/draft-ietf-ccamp-wson-impairments-08

[35] T. Rasmussen, "Next generation packet-optical systems," in *Optical Fiber Communication (OFC), collocated National Fiber Optic Engineers Conference, 2010 Conference on (OFC/NFOEC)*, Mar. 2010, pp. market watch–panel IV.

[36] V. Chan, "Optical flow switching," in *Optical Fiber Communication (OFC), collocated National Fiber Optic Engineers Conference, 2010 Conference on (OFC/NFOEC)*, Mar. 2010, p. OWI6.

[37] M. Klinkowski, D. Careglio, J. Solé-Pareta, and M. Marciniak, "Performance overview of the offset time emulated obs network architecture," *Lightwave Technology, IEEE/OSA Journal of*, vol. 27, no. 14, pp. 2751–2764, Jul 2009.

[38] J. Y. Wei and R. I. McFarland, "Just-in-time signaling for wdm optical burst switching networks," *Lightwave Technology, IEEE/OSA Journal of*, vol. 18, no. 12, pp. 2019–2037, Dec. 2000.

[39] J. S. Turner, "Terabit burst switching," *High Speed Networks, IOS Press Journal of*, vol. 8, no. 1, pp. 3–16, Mar. 1999.

[40] C. Qiao and M. Yoo, "Optical burst switching (obs)-a new paradigm for an optical internet," *High Speed Networks, IOS Press Journal of*, vol. 8, no. 1, pp. 69–84, Jan 1999.

[41] F. Kuo, "Computer networks," *Prentice-Hall*, pp. 501–518, 1973.

[42] C. Guillemot et al., "Transparent optical packet switching: the european acts keops project approach," *Lightwave Technology, IEEE/OSA Journal of*, vol. 16, no. 12, pp. 2117–2134, Dec 1998.

188

[43] O. Ozturk, E. Karasan, and N. Akar, "Performance evaluation of slotted optical burst switching systems with quality of service differentiation," *Lightwave Technology, IEEE/OSA Journal of*, vol. 27, no. 14, pp. 2621–2633, Jul 2009.

[44] Z. Zhang, L. Liu, and Y. Yang, "Slotted optical burst switching (sobs) networks," *Computer Communications, Elsevier Journal of*, vol. 30, no. 8, pp. 3471–3479, Jul 2007.

[45] J. Ramamirtham and J. Turner, "Time sliced optical burst switching," in *INFOCOM 2003, IEEE International Conference on Computer Communications 2003*, Apr. 2003, pp. 2030–2038.

[46] F. Farahmad, V. Vokkarane, and J. Jue, "Practical priority contention resolution for slotted optical burst switching networks," in *Proc. of IEEE/SPIE WOBS'03*, Sep. 2003.

[47] A. Rugsachart and R. Thompson, "An analysis of time-synchronized optical burst switching," in *High Performance Switching and Routing (HPSR 2006), IEEE Conference on*, Jun. 2006.

[48] A. Rugsachart, "Time-synchronized optical burst switching," *Ph.D dissertation*, 2007.

[49] A. Pattavina, "Architectures and performance of optical packet switching nodes for ip networks," *Lightwave Technology, IEEE/OSA Journal of*, vol. 23, no. 3, pp. 1023–1032, Mar 2005.

[50] G. A. Pratt and J. Nguyen, "Distributed synchronous clocking," *Transactions on Parallel and Distributed Systems, IEEE Journal on*, vol. 6, no. 3, pp. 314–328, Mar 1995.

[51] Z. Rosberg, H. L. Vu, M. Zukerman, and J. White, "Performance analyses of optical burst-switching networks," *Selected Areas in Communications, IEEE Journal on*, vol. 21, no. 7, pp. 1187–1197, Sep 2003.

[52] J. Teng and G. Rouskas, "A detailed analysis and performance comparison of wavelength reservation schemes for optical burst switched networks," *Photonic Network Communications, Springer Journal of*, vol. 9, no. 3, pp. 1187–1197, May 2005.

[53] S. Danielsen, B. Mikkelsen, C. Joergensen, T. Durhuus, and K. Stubkjaer, "Wdm packet switch architectures and analysis of the influence of tuneable wavelength converters on the performance," *Lightwave Technology, IEEE/OSA Journal of*, vol. 15, no. 2, pp. 219–226, Feb 1997.

[54] G. P. Agrawal, "Fiber-optic communication systems," *Wiley*, pp. 501–518, 2002.

[55] A. Rugsachart and R. Thompson, "Optimal timeslot size for synchronous optical burst switching," in *BROADNETS 2007, IEEE International Conference on Broadband Communications, Networks, and Systems 2007*, Mar. 1993, pp. 885–892.

[56] M. Klinkowski, M. Pioro, D. Careglio, M. Marciniak, and J. Solé-Pareta, "Routing optimization in optical burst switching networks," in *ONDM 2007, International Conference on Optical Network Design and Modeling 2007*, May 2007.

[57] J. Perelló, S. Spadaro, J. Comellas, and G. Junyent, "A load-based reflection routing protocol with resource pre-allocation for contention resolution in obs networks," *European Transactions on Telecommunications, Wiley Journal of*, no. 20, pp. 1–7, Feb 2009.

[58] M. Morita, H. Tode, and K. Murakami, "Reflection-based deflection routing in ops networks," *Transactions on Communications, IEICE Journal of*, vol. E91-B, no. 2, pp. 409–417, Feb 2008.

[59] S. Gjessing, "A novel method for re-routing in obs networks," in *Proc. of IEEE ISCIT'07*, Oct. 2007, pp. 22–27.

[60] C. Hsu, T. Liu, and N. Huang, "Performance analysis of deflection routing in optical burst-switched networks," in *INFOCOM 2002, IEEE International Conference on Computer Communications 2002*, Jun. 2002.

[61] S. Sygletos, I. Tomkos, and J. Leuthold, "Technological challenges on the road toward transparent networking," *J. Opt. Netw., OSA*, vol. 7, no. 4, pp. 321 –350, apr. 2008.

[62] Y. Huang et al., "Simultaneous all-optical 3R regeneration of multiple WDM channels," in *Lasers & electro optics society 18th annual meeting, IEEE LEOS 2005*, Oct. 2005, pp. 59 –61.

[63] M. Rochette, J. L. Blows, and B. J. Eggleton, "3R optical regeneration: An all-optical solution with BER improvement," *Optics Express, OSA*, vol. 14, no. 14, pp. 6414–6427, Jul 2006.

[64] P. N. Desai, A. J. Phillips, and S. Sujecki, "Modeling of burst mode 2R optical regenerator cascades for long-haul optical networks," *Optical Communications and Networking, IEEE/OSA Journal of*, vol. 4, no. 4, pp. 304 – 313, Apr. 2012.

[65] S. Azodolmolky, M. Klinkowski, E. Marín-Tordera, D. Careglio, J. Solé-Pareta, and I. Tomkos, "A survey on physical layer impairments aware routing and wavelength assignment algorithms in optical networks," *Computer Networks, Elsevier Journal of*, vol. 53, no. 7, pp. 926–944, May 2009.

[66] C. V. Saradhi and S. Subramaniam, "Physical layer impairment aware routing (PLIAR) in WDM optical networks: issues and challenges," *Communications Surveys and Tutorials, IEEE*, vol. 11, no. 4, pp. 109–130, Dec 2009.

[67] J. Simmons, "On determining the optimal optical reach for a long-haul network," *Lightwave Technology, IEEE/OSA Journal of*, vol. 23, no. 3, pp. 1039 – 1048, Mar. 2005.

[68] X. Yang and B. Ramamurthy, "Sparse regeneration in translucent wavelength-routed optical networks: Architecture, network design and wavelength routing," *Photonic Network Communications, Springer Journal of*, vol. 10, pp. 39–53, 2005.

[69] W. Zhang, J. Tang, K. Nygard, and C. Wang, "REPARE: Regenerator placement and routing establishment in translucent networks," in *Global Communications (GLOBECOM 2009), IEEE International Conference on*, Dec. 2009.

[70] R. Muñoz, R. Martínez, and R. Casellas, "Challenges for gmpls lightpath provisioning in transparent optical networks: wavelength constraints in routing and signalling," *Communications Magazine, IEEE*, vol. 47, no. 8, pp. 26–34, Aug 2009.

[71] K. Manousakis, P. Kokkinos, K. Christodoulopoulos, and E. Varvarigos, "Joint online routing, wavelength assignment and regenerator allocation in translucent optical networks," *Lightwave Technology, IEEE/OSA Journal of*, vol. 28, no. 8, pp. 1152–1163, Apr 2010.

[72] H. Buchta and E. Patzak, "Analysis of the physical impairments on maximum size and throughput of soa-based optical burst switching nodes," *Lightwave Technology, IEEE/OSA Journal of*, vol. 26, no. 16, pp. 2821–2830, Aug 2008.

[73] Y. Fan and B. Wang, "Physical impairment aware scheduling in optical burst switched networks," *Photonic Network Communications, Springer Journal of*, vol. 18, no. 2, pp. 244–254, Oct 2009.

[74] B. Bathula, R. Bikram, V. Vokkarane, and S. Talabattula, "Quality of transmission aware manycasting over optical burst-switched (obs) networks," *Optical Communications and Networking, IEEE/OSA Journal of*, vol. 2, no. 10, pp. 820–829, Oct 2010.

[75] H. Buchta, C. Gauger, and E. Patzak, "Maximum size and throughput of soa-based optical burst switching nodes with limited tuning-range wavelength converters and fdl buffers," *Lightwave Technology, IEEE/OSA Journal of*, vol. 26, no. 16, pp. 2919–2927, Aug 2008.

[76] D. Kilper et al., "Optical performance monitoring," *Lightwave Technology, IEEE/OSA Journal of*, vol. 22, no. 1, pp. 293–304, Jan 2004.

[77] R. Martínez, R. Casellas, R. Munoz, and T. Tsuritani, "Experimental translucent-oriented routing for dynamic lightpath provisioning in GMPLS-enabled wavelength switched optical networks," *Lightwave Technology, IEEE/OSA Journal of*, vol. 28, no. 8, pp. 1241–1255, Apr 2010.

[78] P. Pavon-Mariño et al., "Offline impairment aware rwa algorithms for cross-layer planning of optical networks," *Lightwave Technology, IEEE/OSA Journal of*, vol. 27, no. 12, pp. 1763–1775, Jun 2009.

[79] A. Morea, N. Brogard, F. Leplingard, J.-C. Antona, T. Zami, B. Lavigne, and D. Bayart, "QoT function and A∗ routing: an optimized combination for connection search in translucent networks," *Optical Communications and Networking, IEEE/OSA Journal of*, vol. 7, no. 1, pp. 42–61, Jan 2008.

[80] H. Pereira, D. Chaves, C. Bastos-Filho, and J. Martins-Filho, "Osnr model to consider physical layer impairments in transparent optical networks," *Photonic Network Communications, Springer Journal of*, vol. 2, no. 18, pp. 137–149, Oct 2009.

[81] M. Zannin et al., "On the benefits of optical gain-clamped amplification in optical burst switching networks," *Lightwave Technology, IEEE/OSA Journal of*, vol. 27, no. 23, pp. 5475–5482, Dec 2009.

[82] T. Tsuritani, M. Miyazawa, S. Kashihara, and T. Otani, "Optical path computation element interworking with network management system for transparent mesh networks," in *Optical Fiber Communication - incudes post deadline papers, 2008. OFC 2008. Conference on*, feb 2008, pp. 1–10.

[83] INPHENIX. (2012). [Online]. Available: http://www.inphenix.com/soa_devices.html

[84] MRV. (2012). [Online]. Available: http://www.mrv.com/product/MRV-LD-OAB

[85] M. Mestre et al., "Tuning characteristics and switching speed of a modulated grating Y structure laser for wavelength routed PONs," in *Proc. ANIC'10*, jun. 2010.

[86] M. Klinkowski et al., "An overview of routing methods in optical burst switching networks," *Optical Switching and Networking, Elsevier Journal of*, vol. 7, no. 2, pp. 41–53, Abr 2010.

[87] M. Klinkowski, M. Pióro, D. Careglio, M. Marciniak, and J. Solé-Pareta, "Non-linear optimization for multi-path source routing in OBS networks," *Communications Letters, IEEE*, vol. 11, no. 12, pp. 1016–1018, Dec 2007.

[88] R. Syski, "Introduction to congestion theory in telephone systems," *North-Holland*, 1960.

[89] M. Minoux, "Mathematical programming: Theory and algorithms," *John Wiley & Sons*, 1986.

[90] ——, "Discrete cost multicommodity network optimization problems and exact solution methods," *Annals of Operations Research*, vol. 106, no. 1, 2001.

[91] J. Kleinberg and E. Tardos, "Algorithm design," *Addison-Wesley*, pp. 661–706, 2005.

[92] M. Dorigo and C. Blum, "Ant colony optimization theory: A survey," *Theor. Comput. Sci.*, vol. 344, no. 2-3, pp. 243–278, 2005.

[93] R. Garlick and R. Barr, "Dynamic wavelength routing in wdm networks via ant colony optimization," *Lect. Notes Comput. Sc.*, vol. 2463, pp. 27–41, 2002.

[94] S. Ngo, X. Jiang, and S. Horiguchi, "An ant-based approach for dynamic rwa in optical wdm networks," *Photinc Network Communications, Springer Journal of*, vol. 11, no. 1, pp. 39–48, 2006.

[95] J. Triay and C. Cervelló-Pastor, "An ant-based algorithm for distributed routing and wavelength assignment in dynamic optical networks," *Selected Areas in Communications, IEEE Journal on*, vol. 28, no. 4, pp. 542–552, May 2010.

[96] T. Noronha, M. Resende, and C. Ribeiro, "A biased random-key genetic algorithm for routing and wavelength assignment," *J. Global. Optim.*, p. in press, Sep. 2010.

[97] R. Reis, M. Ritt, L. Buriol, and M. Resende, "A biased random-key genetic algorithm for ospf and deft routing to minimize network congestion," *International Transactions in Operational Research, Wiley Journal of*, p. in press, Aug. 2010.

[98] IBM. (2012) ILOG CPLEX. . [Online]. Available: http://www-01.ibm.com/software/integration/optimization/cplex/

[99] S. L. Danielsen, P. Hansen, and K. E. Stubkjaer, "Wavelength conversion in optical packet switching," *Lightwave Technology, IEEE/OSA Journal of*, vol. 16, no. 9, pp. 2095–2108, Dec. 1998.

[100] J. M. H. Elmirghani and H. T. Mouftah, "All-optical wavelength conversion: technologies and applications in DWDM networks," *Communications Magazine, IEEE*, vol. 38, no. 3, pp. 86–92, Dec. 2000.

[101] V. Eramo and M. Listanti, "Power consumption in bufferless optical packet switches in SOA technology," *Optical Communications and Networking, IEEE/OSA Journal of*, vol. 1, no. 3, pp. B15–B29, Aug. 2009.

[102] D. Apostolopoulos et al, "Cascadability performance evaluation of a new NRZ SOA-MZI wavelength converter," *Photonics Technology Letters, IEEE*, vol. 21, no. 18, pp. 1341–1343, Sep. 2009.

[103] M. Spyropoulou et al., "40 Gb/s NRZ wavelength conversion using a differentially-biased SOA-MZI: Theory and experiment," *Lightwave Technology, IEEE/OSA Journal of*, vol. 29, no. 10, pp. 1489–1499, May 2011.

[104] V. Eramo, M. Listanti, and M. Spaziani, "Resource sharing in optical packet switches with limited-range wavelength converters," *Lightwave Technology, IEEE/OSA Journal of*, vol. 23, no. 2, pp. 671–687, Feb. 2005.

[105] V. Eramo, M. Listanti, and P. Pacifici, "A comparison study on the number of wavelength converters needed in synchronous and asynchronous all-optical switching architectures," *Lightwave Technology, IEEE/OSA Journal of*, vol. 21, no. 2, pp. 340–355, Feb. 2003.

[106] V. Eramo, A. Germoni, C. Raffaelli, and M. Savi, "Packet loss analysis of shared-per-wavelength multi-fiber all-optical switch with parallel scheduling," *Computer Networks, Elsevier Journal of*, vol. 53, no. 2, pp. 202–216, Feb. 2009.

[107] N. Akar, E. Karasan, and K. Dogan, "Wavelength converter sharing in asynchronous optical packet/burst switching: An exact blocking analysis for markovian arrivals," *Selected Areas in Communications, IEEE Journal of*, vol. 24, no. 12, pp. 69–80, Dec. 2006.

[108] N. Akar, C. Raffaelli, M. Savi, and E. Karasan, "Shared-per-wavelength asynchronous optical packet switching: a comparative analysis," *Computer Networks, Elsevier Journal of*, vol. 54, no. 13, pp. 2166–2181, Sep. 2010.

[109] Y. Fukushima, H. Harai, S. Arakawa, and M. Murata, "Design of wavelength-convertible edge nodes in wavelength-routed networks," *Optical Networking, OSA Journal of*, vol. 5, no. 3, pp. 196–209, Mar. 2006.

[110] C. Raffaelli, M. Savi, G. Tartarini, and D. Visani, "Physical path analysis in photonic switches with shared wavelength converters," in *Transparent Optical Networks (ICTON 2010), 12th Anniversary International Conference on*, vol. 1, june 2010, p. Mo.C1.5.

[111] C. Raffaelli, M. Savi, and A. Stavdas, "Multistage shared-per-wavelength optical packet switch: Heuristic scheduling algorithm and performance," *Lightwave Technology, IEEE/OSA Journal of*, vol. 27, no. 5, pp. 538–551, Mar. 2009.

[112] J. M. Simmons, "Analysis of wavelength conversion in all-optical express backbone networks," in *Optical Fiber Communication (OFC), collocated National Fiber Optic Engineers Conference, 2002 Conference on (OFC/NFOEC)*, Mar. 2002, p. TuG2.

[113] O. Gerstel, R. Ramaswami, and S. Foster, "Merits of hybrid optical networking," in *Optical Fiber Communication (OFC), collocated National Fiber Optic Engineers Conference, 2002 Conference on (OFC/NFOEC)*, Mar. 2002, p. TuG1.

[114] J. Junio, D. C. Kilper, and V. W. S. Chan, "Channel power excursions from single-step channel provisioning," *Optical Communications and Networking, IEEE/OSA Journal of*, vol. 4, no. 9, pp. A1–A7, Sep. 2012.

[115] Thorlabs. (2012) High-speed soa switch: Mod. soa1013sxs. online. [Online]. Available: http://www.thorlabs.us/thorProduct.cfm?partNumber=SOA1013S

[116] Menara. (2012) Tunable OTN XFP DWDM 11.1 Gb/s transceiver with integrated G.709 and E-FEC. online. [Online]. Available: http://www.menaranet.com/downloads/187-04001-$00_O TN_T UNABLE_X FP_1 0Gb.pdf$

[117] Finisar. (2012) Tunable XFP (T-XFP) transceiver. online. [Online]. Available: http://www.finisar.com/products/optical-modules/xfp/FTLX4213xxxxxx

[118] ——. (2012) 40Gbps-OTU3 DWDM tunable very long reach transponder. online. [Online]. Available: http://www.finisar.com/products/optical-modules/300-pin/53DPAAU4JBLCB

[119] J. A. Summers, M. L. Masanovic, V. Lal, and D. J. Blumenthal, "Monolithically integrated multi-stage all-optical 10gbps push-pull wavelength converter," in *Optical Fiber Communication (OFC), collocated National Fiber Optic Engineers Conference, 2007 Conference on (OFC/NFOEC)*, Mar. 2007, p. OthT2.

[120] JDSU. (2012) SG-DBR tunable laser source. online. [Online]. Available: http://www.acronymeo.com/jdsgtulaso24.html

[121] CIP-Technologies. (2012) Non-linear SOA: Mod. SOA-XN-OEC-1550. online. [Online]. Available: http://www.ciphotonics.com/download/datasheet/soa/SOA-XN-C-14-FCA$_A$.pdf

[122] Thorlabs. (2012) Booster soa: Mod. boa1004s. online. [Online]. Available: www.thorlabs.us/thorProduct.cfm?partNumber=BOA1004S

[123] D. Apostolopoulos, K. Vyrsokinos, P. Zakynthinos, N. Pleros, and H. Avramopoulos, "An SOA-MZI NRZ wavelength conversion scheme with enhanced 2R regeneration characteristics," *Photonics Technology Letters, IEEE*, vol. 21, no. 19, pp. 1363–1365, Oct. 2009.

[124] V. Eramo, A. Germoni, A. Cianfrani, M. Listanti, and C. Raffaelli, "Evaluation of power consumption in low spatial complexity optical switching fabrics," *Selected Topics in Quantum Electronics, IEEE Journal of*, vol. 17, no. 2, pp. 396–405, Mar/Apr. 2011.

[125] B. Garcia-Manrubia, P. Pavon-Marino, R. Aparicio-Pardo, M. Klinkowski, and D. Careglio, "Off-line impairment-aware RWA and regenerator placement in translucent optical networks," *Lightwave Technology, IEEE/OSA Journal of*, vol. 29, no. 3, pp. 265–277, Feb 2011.

[126] F. Leplingard, T. Zami, A. Morea, N. Brogard, and D. Bayart, "Determination of the impact of a quality of transmission estimator margin on the dimensioning of an optical network," in *Optical Fiber Communication (OFC), collocated National Fiber Optic Engineers Conference, 2008 Conference on (OFC/NFOEC)*, Mar. 208, p. OWA6.

[127] C. P. Lai et al., "Experimental demonstration of packet-rate 10-gb/s ook osnr monitoring for qos-aware cross-layer packet protection," *Optics Express, OSA*, vol. 19, no. 16, pp. 14 871–82, aug 2011.

[128] B. Lavigne et al., "Method for the determination of a quality-of-transmission estimator along the lightpaths of partially transparent networks," in *Optical Communication, 2007. ECOC '07. 33th European Conference on*, vol. 3, 2007, pp. 287–8.

[129] H. Song and M. Brandt-Pearce, "Range of influence of physical impairments in wavelength-division multiplexed systems," in *Global Communications (GLOBECOM 2011), IEEE International Conference on*, Nov. 2011.

[130] F. Leplingard, A. Morea, T. Zami, and N. Brogard, "Interest of an adaptive margin for the quality of transmission estimation for lightpath establishment," in *Optical Fiber Communication (OFC), collocated National Fiber Optic Engineers Conference, 2009 Conference on (OFC/NFOEC)*, Mar. 2009, p. OWI6.

[131] D. Geisler et al., "Experimental demonstration of flexible bandwidth networking with real-time impairment awareness," *Optics Express, OSA*, vol. 19, no. 26, pp. B736–45, Dec 2011.

[132] L. Liu et al., "Field and lab trials of pce-based onsr-aware dynamic restoration in multi-domain gmpls-enabled translucent wson," *Optics Express, OSA*, vol. 19, no. 27, p. 2656877, Dec 2011.

[133] C. P. Lai et al., "Demonstration of qos-aware packet protection via cross-layer osnr signaling," in *Optical Fiber Communication (OFC), collocated National Fiber Optic Engineers Conference, 2010 Conference on (OFC/NFOEC)*, Mar. 2010, p. OTuM2.

[134] H. Takeshita, K. Fukuchi, S. Shioiri, and E. L. T. de Gabory, "In-service monitoring of pmd induced optical signal degradation using sop vector trajectory on the poincare sphere for high-speed reconfigurable optical networks," in *Optical Communication, 2009. ECOC '09. 35th European Conference on*, Sep. 2009.

[135] T. A. Feo and M. G. C. Resende, "A probabilistic heuristic for a computationally difficult set covering problem," *Operations Research Letters, Elsevier*, vol. 8, no. 12, pp. 67–71, Dec. 1989.

[136] J. Gonçalves and M. Resende, "Biased random-key genetic algorithms for combinatorial optimization," *Heuristics, Springer Journal of*, vol. 17, no. 5, pp. 487–525, 2010.

[137] M. Laguna and R. Martí, "Grasp and path relinking for 2-layer straight line crossing minimization." *Computing, INFORMS Journal on*, vol. 11, pp. 44–52, 1999.

[138] P. Hansen and N. Mladenovic, "Variable neighborhood search: principles and applications." *Operational Research, Elsevier European Journal of*, vol. 130, no. 3, pp. 449–467, May 2001.

[139] T. Feo and M. Resende, "Greedy randomized adaptive search procedures," *Global Optimization, Springer Journal of*, vol. 6, pp. 109–133, 1995.

[140] T. A. Feo, M. G. C. Resende, and S. H. Smith, "A greedy randomized adaptive search procedure for maximum independent set," *Operations Research*, vol. 42, no. 12, pp. 860–878, Dec. 1994.

[141] F. Palmieri, U. Fiore, and S. Ricciardi, "A grasp-based network re-optimization strategy for improving rwa in multi-constrained optical transport infrastructures," *Computer Communications, Elsevier Journal of*, vol. 33, no. 15, pp. 1809–1822, 2010.

[142] J. G. Villegasa, C. Prinsa, C. Prodhona, A. L. Medaglia, and N. Velasco, "A grasp with evolutionary path relinking for the truck and trailer routing problem," *Computers & Operations Research, Elsevier Journal of*, vol. 38, no. 9, pp. 1319–1334, 2011.

[143] L. S. Pessoa, M. G. C. Resende, and C. C. Ribeiro, "A hybrid lagrangean heuristic with grasp and path relinking for set k-covering," *AT&T Labs Research Technical Report*, 2010.

[144] J. Santamara, O. Cordn, S. Damas, R. Martí, and R. Palma, "GRASP and path relinking hybridizations for the point matching-based image registration problem," *Heuristics, Springer Journal of*, vol. 18, no. 1, pp. 169–192, 2012.

[145] H. Höller, B. Melián, and S. Voß, "Applying the pilot method to improve VNS and GRASP metaheuristics for the design of SDH/WDM networks," *Operational Research, Elsevier European Journal of*, vol. 191, no. 3, pp. 691–704, Dec 2008.

[146] M. Resende and C. Ribeiro, "Grasp with path-relinking: Recent advances and applications," *In T. Ibaraki, K. Nonobe & M. Yagiura (Eds.), Metaheuristics: Progress as Real Problem Solvers*, pp. 29–63, 2005.

[147] ——, "Greedy randomized adaptive search procedures: Advances and applications," *In M. Gendreau & J.Y Potvin (Eds.), Handbook of Metaheuristics. 2nd edn.*, pp. 29–63, 2010.

[148] G. Mateus, M. G. C. Resende, and R. Silva, "Grasp with path-relinking for the generalized quadratic assignment problem," *Journal of Heuristics, Springer Journal of*, vol. 17, no. 5, pp. 527–565, 2011.

[149] F. Glover, "Tabu search and adaptive memory programing: Advances, applications and challenges," *In R.S. Barr, R.V. Helgason, & J.L. Kennington (Eds.), Interfaces in Computer Science and Operations Research*, pp. 1–75, 1996.

[150] F. Glover and M. Laguna, "Tabu search," *Kluwer Academic Publishers*, 1997.

[151] M. Resende and R. Werneck, "A hybrid heuristic for the p-median problem," *Heuristics, Springer Journal of.*, vol. 10, pp. 59–88, 2004.

[152] A. Duarte, R. Martí, M. G. C. Resende, and R. M. A. Silva, "Grasp with path relinking heuristics for the antibandwidth problem," *Networks, Wiley Journal of*, vol. 58, no. 3, pp. 171–189, 2011.

[153] O. Aboul-Magd et al. (2002) Automatic switched optical network (ASON) architecture and its related protocols. IETF draft. [Online]. Available: http://tools.ietf.org/html/draft-ietf-ipo-ason-02

[154] E. Mannie. (2004) Generalized multi-protocol label switching (gmpls) architecture. RFC-3945. [Online]. Available: http://www.ietf.org/rfc/rfc3945.txt

[155] A. Chiu and J. Strand, "Joint ip/optical layer restoration after a router failure," in *Optical Fiber Communications Conference, 2001. OFC 2001*, Mar. 2001, pp. 1–3.

[156] P. Cholda and A. Jajszczyk, "Recovery and its quality in multilayer networks," *Lightwave Technology, IEEE/OSA Journal of*, vol. 28, pp. 372–389, 2010.

[157] C. Chigan, G. W. Atkinson, and R. Nagarajan, "Cost effectiveness of joint multilayer protection in packet-over-optical networks," *Lightwave Technology, IEEE/OSA Journal of*, vol. 21, pp. 2694–2704, 2003.

[158] L. Velasco et al., "Gmpls-based multi-domain restoration: Analysis, strategies, policies and experimental assessment," *Optical Communications and Networking, IEEE/OSA Journal of*, vol. 2, pp. 427–441, 2010.

[159] X. Zhang, F. Shen, L. Wang, S. Wang, L. Li, and H. Luo, "Two-layer mesh network optimization based on inter-layer decomposition," *Photonic Network Communications, Springer Journal of*, vol. 21, no. 3, pp. 310–320, 2011.

[160] R. Morais, C. Pavan, A. Pinto, and C. Requejo, "Genetic algorithm for the topological design of survivable optical transport networks," *Optical Communications and Networking, IEEE/OSA Journal of*, vol. 3, pp. 17–26, Mar. 2011.

[161] I. de Miguel, R. Vallejos, A. Beghelli, and R. Durán, "Genetic algorithm for joint routing and dimensioning of dynamic wdm networks," *Optical Communications and Networking, IEEE/OSA Journal of*, vol. 1, no. 7, pp. 608–621, Mar. 2009.

[162] M. Ruiz, O. Pedrola, L. Velasco, D. Careglio, J. Fernández-Palacios, and G. Junyent, "Survivable IP/MPLS-over-WSON multi-layer network optimization," *Optical Communications Networking, IEEE/OSA Journal of*, vol. 3, no. 8, pp. 629–640, 2011.

[163] M. Pióro and D. Medhi, "Routing, flow, and capacity design in communication and computer networks," *Morgan Kaufmann Publishers*, 2004.

[164] M. Resende, R. Martí, M. Gallego, and A. Duarte, "Grasp and path relinking for the max-min diversity problem," *Computers & Operations Research, Elsevier Journal of*, vol. 37, pp. 498–508, 2010.

198

[165] J. Gonçalves and M. G. C. Resende, "A parallel multi-population genetic algorithm for a constrained two-dimensional orthogonal packing problem," *Combinatorial Optimization, Springer Journal of*, vol. 22, no. 2, pp. 180–201, 2011.

[166] C. P. Robert and G. Casella, "Monte carlo statistical methods," *Springer*, vol. 37, 2004.

[167] E. Martins and M. Pascoal, "A new implementation of Yen's ranking loopless paths algorithm," *Operations Research, 4OR: A Quarterly Journal of*, vol. 1, no. 2, pp. 121–133, 2003.

[168] R. Huelsermann, M. Gunkel, C. Meusburger, and D. A. Schupke, "Cost modelling and evaluation of capital expenditures in optical multilayer networks," *Optical Networking, OSA Journal of*, vol. 7, no. 9, pp. 814–833, 2008.

[169] P. Festa, J. F. Gonçalves, M. Resende, and R. Silva, "Automatic tuning of GRASP with path-relinking heuristics with a biased random-key genetic algorithm," *Computer Science, Springer Lecture Notes in*, vol. 6049, pp. 338–349, 2010.

[170] C. Ribeiro, E. Uchoa, and R. Werneck, "A hybrid grasp with perturbations for the steiner problem in graphs," *Computing, INFORMS Journal on*, vol. 14, pp. 228–246, 2002.

[171] Finisar. (2011) Programmable narrow-band filtering using the WaveShaper 1000E and WaveShaper 4000E. white paper. [Online]. Available: http://www.finisar.com

[172] K. Christodoulopoulos, I. Tomkos, and E. Varvarigos, "Elastic bandwidth allocation in flexible OFDM based optical networks," *Lightwave Technology, IEEE/OSA Journal of*, vol. 29, no. 9, pp. 1354–1366, May 2011.

[173] Y. Wang, X. Cao, and Y. Pan, "A study of the routing and spectrum allocation in spectrum-sliced elastic optical path networks," in *INFOCOM 2011, IEEE International Conference on Computer Communications 2011*, Apr 2011.

[174] L. Velasco, M. Klinkowski, M. Ruiz, and J. Comellas, "Modeling the routing and spectrum allocation problem for future elastic optical networks," *Photonic Network Communications, Springer Journal of*, p. in press, 2012. [Online]. Available: http://dx.doi.org/10.1007/s11107-012-0378-7

[175] X. Wan, L. Wang, N. Hua, H. Zhang, and X. Zheng, "Dynamic routing and spectrum assignment in flexible optical path networks," in *Optical Fiber Communication (OFC), collocated National Fiber Optic Engineers Conference, 2011 Conference on (OFC/NFOEC)*, Mar. 2011, p. JWA55.

[176] K. Christodoulopoulos, I. Tomkos, and E. Varvarigos, "Dynamic bandwidth allocation in flexible OFDM-based networks," in *Optical Fiber Communication (OFC), collocated National Fiber Optic Engineers Conference, 2011 Conference on (OFC/NFOEC)*, Mar. 2011, p. OTuI5.

[177] M. Klinkowski and K. Walkowiak, "Routing and spectrum assignment in spectrum sliced elastic optical path network," *Communications Letters, IEEE*, vol. 15, no. 8, pp. 884–886, Dec 2011.

[178] O. Ribal and A. Morea, "Cost-efficiency of mixed 10-40-100Gb/s networks and elastic optical networks," in *Optical Fiber Communication (OFC), collocated National Fiber Optic Engineers Conference, 2011 Conference on (OFC/NFOEC)*, Mar. 2011, p. OTuI4.

[179] S. Koo, G. Sahin, and S. Subramaniam, "Dynamic LSP routing in IP/MPLS-over-WDM networks," *Selected Areas in Communications, IEEE Journal of*, vol. 24, no. 12, pp. 45–55, Dec. 2006.

[180] B. Chen, G. Rouskas, and R. Dutta, "Clustering methods for hierarchical traffic grooming in large-scale mesh WDM networks," *Optical Communications Networking, IEEE/OSA Journal of*, vol. 2, no. 8, pp. 502–514, Aug 2010.

[181] K. Zhu and B. Mukherjee, "Traffic grooming in an optical WDM mesh network," *Selected Areas in Communications, IEEE Journal of*, vol. 20, no. 1, pp. 122–133, Jan 2002.

[182] H. Höller and S. Voß, "A heuristic approach for combined equipment-planningand routing in multi-layer SDH/WDM networks," *Operational Research, Elsevier European Journal of*, vol. 171, no. 3, pp. 787–796, Jun 2006.

[183] N. Skorin-Kapov, "Routing and wavelength assignment in optical networks using bin packing based algorithms," *Operational Research, Elsevier European Journal of*, vol. 177, pp. 1167–1179, 2007.

[184] Z. Liang, W. A. Chaovalitwongse, M. Cha, and S. Moon, "Redundant multicast routing in multilayer networks with shared risk resource groups: Complexity, models and algorithms," *Computers & Operations Research, Elsevier Journal of*, vol. 37, pp. 1731–1739, 2010.

[185] A. X. Martins et al., "Variable neighborhood descent with iterated local search for routing and wavelength assignment," *Computers & Operations Research, Elsevier Journal of*, vol. 39, no. 9, pp. 2133–2141, 2012.

[186] C. Reeves and T. Yamada, "Genetic algorithms, path relinking and the flowshop sequencing problem," *Evolutionary Computation, MIT Press Journal of*, vol. 6, pp. 230–234, 1998.

[187] G. Zhang and K. Lai, "Combining path relinking and genetic algorithms for the multiple-level warehouse layout problem," *Operational Research, Elsevier European Journal of*, vol. 169, pp. 413–425, 2006.

[188] J. Demsar, "Statistical comparison of classifiers over multiple data sets," *Machine Learning Research, MIT Press Journal of*, vol. 7, pp. 1–30, 2006.

[189] F. Friedman, "A comparison of alternative tests of significance for the problem of m rankings," *The Annals of Mathematical Statistics, Institute of Mathematical Statistics Journal on*, vol. 11, no. 1, pp. 86–92, 1940.

[190] P. Nemenyi, "Distribution-free multiple comparisons," Ph.D. dissertation, Princeton University, New Jersey, USA, 1963.

[191] R. Iman and J. Davenport, "Approximations of the critical region of the friedman statistic," *Communications in Statistics-Theory and Methods, Taylor & Francis Journal of*, vol. 9, pp. 571–595, 1980.

[192] Y. Pan, D. Kilper, and G. Atkinson, "Persistent channel power deviations in constant gain amplified long-chain roadm networks," in *Optical Fiber Communication (OFC), collocated National Fiber Optic Engineers Conference, 2011 Conference on (OFC/NFOEC)*, Mar. 2011, p. JWA10.

[193] Y. Pan, D. Kilper, A. Morea, J. Junio, and V. Chan, "Channel power excursions in gmpls end-to-end optical restoration with single-step wavelength tuning," in *Optical Fiber Communication (OFC), collocated National Fiber Optic Engineers Conference, 2012 Conference on (OFC/NFOEC)*, Mar. 2011, p. JTh2A.

[194] S. De Maesschalck et al., "Pan-european optical transport networks: An availability-based comparison," *Photonic Network Communications, Springer Journal of*, vol. 5, no. 3, pp. 203–225, May 2003.

[195] K. Claffy, G. Polyzos, and H. Braun, "Traffic characteristics of the t1 nsfnet backbone," in *INFOCOM 1993, IEEE International Conference on Computer Communications 1993*, Mar. 1993, pp. 885–892.

[196] S. Orlowski, M. Pióro, A. Tomaszewski, and R. Wessäly, "Sndlib 1.0survivable network design library," in *Proc. INOC'07*, 2007.

[197] O. Pedrola, S. Rumley, M. Klinkowski, D. Careglio, C. Gaumier, and J. Solé-Pareta, "JAVOBS: a flexible simulator for OBS network architectures," *Networks, Academy publisher Journal of*, vol. 5, no. 2, pp. 256–264, Feb 2010.